UNIVERSITY OF LEEDS

CHARACTERISING MEMBRANE PROTEIN–SURFACTANT COMPLEXES USING MASS SPECTROMETRY METHODS

Thomas Geoffrey Watkinson

Submitted in accordance with the requirements for the degree of Doctor of Philosophy

The University of Leeds

Astbury Centre for Structural Molecular Biology

September 2016

The candidate confirms that the submitted work is his own, except where work which has formed part of jointly-authored publications has been included. The contribution of the candidate and the other authors to this work has been explicitly indicated overleaf. The candidate confirms the appropriate credit has been given within the thesis where reference has been made to the work of others. This copy has been supplied on the understanding that it is copyright material and that no quotation from this thesis may be published without proper acknowledgement.

Jointly Authored Publications

Throughout this thesis the work directly attributable to the candidate is as follows:

(i) Literature research and compilation of the manuscript stated above.

(ii) The candidate performed all the experimental work and data analysis unless otherwise stated.

Details of jointly authored publications and the contributions of other authors to these manuscripts:

Chapter 3 contains work from the following manuscripts submitted for publication:

- CALABRESE, A. N.; WATKINSON, T. G.; HENDERSON, P. J. F.; RADFORD, S. E.; ASHCROFT, A. E., Amphipols outperform dodecylmaltoside micelles in stabilising membrane protein structure in the gas phase. *Analytical Chemistry* 2015, *87* (2), 1118-1126.

In this work, I carried out all experimental work and data analysis referring to $OmpT_{HT}$. ANC carried out all experimental work and data analysis referring to PagP, Mhp1 and GalP.

- WATKINSON, T. G.; CALABRESE, A. N.; GIUSTI, F.; ZOONENS, M.; RADFORD, S. E.; ASHCROFT, A. E., Systematic analysis of the use of amphipathic polymers for studies of outer membrane proteins using mass spectrometry. *International Journal of Mass Spectrometry* 2015, *391*, 54-61.

In this work, PagP expression and purification was carried out by ANC and all APols (except A8-35) were provided by Dr Manuela Zoonens and her collaborators (described in detail in Section 2.1). All remaining experimental work and data analysis was carried out by me.

Chapter 4 contains work from the following manuscripts submitted for publication:

- WATKINSON, T. G.; CALABRESE, A. N.; AULT, J. R.; RADFORD, S. E.; ASHCROFT, A. E., FPOP-LC-MS/MS Suggests Differences in Interaction Sites of Amphipols and Detergents with Outer Membrane Proteins. *Journal of the American Society for Mass Spectrometry* 2016, 35-40.

In this work, I carried out all experimental work and data analysis. Installation and setting up of necessary FPOP instrumentation was carried out by ANC and JRA.

Acknowledgements

My time in Leeds has been the most spectacular time in my life, both rewarding and entertaining. I owe this to the people that I have met whilst being here and those who have helped me get here.

Firstly, I would like to thank **Prof. Alison Ashcroft** and **Prof. Sheena Radford**. Without their desire for success in their own endeavours and those of the people who work with them, my time in Leeds could have been very different.

I must also thank a number of collaborators. Thanks to **Dr. Rachel Garlish**, **Dr. Richard Taylor** and **Dr. Rebecca Rose** of UCB for continuing to help with my work here in Leeds, even if our combined projects were not always the easiest. Thanks go to **Prof. Jean-Luc Popot, Dr. Manuela Zoonens** and the people of the extended Amphipol network, who provided their much appreciated materials and expertise and gave me the opportunity to give back to them at their excellent workshops across the world.

I need to thank every member of the Ashcroft and Radford groups since my arrival. I owe special thanks to **Dr. Anton Calabrese**, who worked with me on the project and always made sure I was prepared, focused and going in the right direction (and there was always milk in the fridge!). I do not think there will ever be a way to repay him. Thank you to **Dr. Aneika Leney** and **Dr. Lindsay McMorran** for walking me through the early days of my PhD and setting me up for the remainder of my time in Leeds. I need to thank **Nasir Khan** and **Dr. James Ault** for keeping everything running smoothly and making sure everyone is full of biscuits! Thank you to **Bob Schiffrin** and all other members of the Radford "OMPire" for long winded hallway conversations about OMPs, which I fear often ended in more questions than answers and a great deal of confusion. The same goes to the entire mass-spec group, keeping everyone going even when there is a heatwave, the air-con is broken and there are no windows.

Thank you to the Monday Night Gaming Crew (all hail our glorious leader **Patrick Knight**, Lord of the Hall of Nerd-dom!) and all other members of the Ashcroft, Radford and Berry groups for being the greatest of friends, the FAB trips, the chest-bumps, the transfer tattoos, the felt-tip whiskers, the wintery weekend in the

wilderness and a list of other amazing memories that would far exceed my page limit. No more dragons needed!

Finally, I would like to thank all members of my family. I am eternally grateful for everything they have done for me, even if I am guilty of forgetting to show it too often. My parents **Colin** and **Julie** have been tremendous throughout my life in getting me where I need to go and my brother **Jack** always had my back, cheering me along. I would not be here without the help of my grandparents, they have always helped to push me on and none of this would be possible without the help they gave me in getting to Cardiff to start on my Masters.

Thank you every one for everything…….Pub?

Table of Contents

List of Figures

List of Tables

List of Equations

List of Abbreviations

ABC	ATP Binding Cassette
APol	Amphipol
ATD	Arrival Time Distribution
AUC	Analytical Ultracentrifugation
β_2AR	β_2-adrenergic GPCR
BAM	β-barrel Assembly Machinery
BR	Bacteriorhodopsin
CEM	Chain Ejection Model
CFTR	Cystic Fibrosis Transmembrane Conductance Regulator
CCS	Collision Cross Section
CD	Circular Dichroism
CI	Chemical Ionisation
CID	Collision Induced Dissociation
CIU	Collision Induced Unfolding
CRM	Charged Residue Model
cmc	Critical Micelle Concentration
DAGK	Diacyl Glycerol Kinase
DDA	Data-Dependent Acquisition
DDM	n-Dodecyl β-D-maltoside
EHSS	Exact Hard Sphere Scattering
EI	Electron Impact
EM	Electron Microscopy

ESI	Electrospray Ionisation
ECD	Electron Capture Dissociation
ETD	Electron Transfer Dissociation
FPOP	Fast Photochemical Oxidation of Proteins
FRET	Forster Resonance Energy Transfer
GF	Glycerol Facilitator
GPCR	G-Protein Coupled Receptors
HDX	Hydrogen Deuterium Exchange
IEM	Ion Ejection Model
IMS	Ion Mobility Spectrometry
IPTG	Isopropyl-β-D-1-thiogalactopyranoside
LB	Lysogeny Broth
LC	Liquid Chromatography
LDAO	lauryl-Dimethylamine-N-Oxide
LHC	Light Harvesting Complex
LPS	Lipopolysaccharide
LUV	Large Unilamellar Vesicles
MALDI	Matrix Assisted Laser Desorption Ionisation
MCP	Multi Channel Plate
MD	Molecular Dynamics
MGST1	Microsomal Glutathione Transferase-1
MP	Membrane Protein

MS	Mass Spectrometry
MS/MS	Tandem Mass Spectrometry
m/z	Mass-to-Charge Ratio
NAPol	Nonionic APol
nESI	Nanoelectrospray Ionisation
NMR	Nuclear Magnetic Resonance
nAChR	Nicotinic Acetylcholine Receptor
OM	Outer Membrane
OMP	Outer Membrane Protein
OTG	Octyl Thioglucoside
PA	Projection Approximation
PC-APol	Phosphocholine APol
PMSF	Phenylmethylsulphonyl Fluoride
POTRA	Polypeptide-Transport Associated domains
PSA	Projection Superposition Approximation
PTM	Post Translational Modification
RF	Radio Frequency
RP-HPLC	Reverse Phase High Performance Liquid Chromatography
SAPol	Sulphonated APol
SAXS	Small Angle X-ray Scattering
SANS	Small Angle Neutron Scattering
SDS	Sodium Dodecyl Sulphate

SDS-PAGE	SDS-Polyacrylamide Gel Electrophoresis
SEC	Size Exclusion Chromatography
Tm	Trajectory Method
TM	Transmembrane
ToF	Time of Flight
TWIMS	Travelling Wave Ion mobility Spectrometry
UV	Ultraviolet

Abstract

Membrane proteins (MPs) facilitate a large number of essential physiological functions and are the targets for greater than 50 % of licensed pharmaceuticals. MPs, however, are difficult to study *in vitro* as a result of their inherent properties, such as their insolubility in aqueous solution without the presence of a suitable surfactant to maintain the native-like state. For this reason, high resolution structural data of MPs are lacking relative to their water soluble counterparts. This has inspired a need for improvement in methods of solubilisation and analysis of MPs.

Amphipols (APols), are a class of novel surfactants for solubilisation of MPs in a native-like state. APols provide a means for solubilisation of MPs with very high kinetic stability using materials and an approach that can be applied, possibly indiscriminately, to any MP.

Mass spectrometry (MS) is a multi-faceted technique used in structural biology. Native-MS, which emerged following the development of "soft" ionisation methods such as electrospray ionisation (ESI), has been used extensively to deliver proteins in to the gas phase for analysis of protein ion *m/z*, whilst maintaining their native state and non-covalent interactions. The combination of native-MS and ion mobility spectrometry (IMS) allows simultaneous measurement of the collision cross section (CCS) and *m/z* of protein ions. This can be used to study the conformational state of proteins and protein complexes.

Native MS is being used more frequently for the study of MPs. Collisional activation of MP:surfactants allows for liberation of MPs and MP complexes, and determination of CCS values using IMS-MS to evaluate the conformational state and investigate the topology and stability of MP complexes.

In addition to native-MS, structural proteomics is a growing field for MS-based study of MP structural biology. In work shown here, Fast Photochemical Oxidation of Proteins (FPOP) and Hydrogen-Deuterium Exchange (HDX) coupled to liquid chromatography (LC)-MS allow for observation of solvent accessible regions of the bacterial outer membrane protein (OMP) OmpT in detergent micelles and APols.

Work presented here in three experimental chapters shows APols to improve on detergent micelles in the ability to observe the most native-like forms of MPs in the gas phase, finding that the MPs OmpT, Mhp1 and GalP are only observed in the most lowly charged and, hence, more native-like states by nESI-IMS-MS when released from A8-35 and not from DDM micelles. Certain properties of APols (such as molecular weight and charge density) further benefit or hinder delivery of OMPs in to the gas phase. OmpT, tOmpA and PagP are less readily observed by nESI-IMS-MS when solubilised in the largest and most-negatively charged APols. Following from this, FPOP-LC-MS data suggest that this protective effect of APols is mediated through extra contacts with the non-transmembrane regions of MPs, preventing unfolding and protecting MPs from excess charging during ionisation (as evidenced by a decreased degree of oxidation of reactive residue side chains near the boundaries of the transmembrane domain of OmpT). This same degree of protection is not observed using HDX-MS. In fact, data suggests that NAPol (a non-ionic APol with significantly different chemical composition than the previously described A8-35-like APols) promotes greater flexibility of OmpT in the extramembrane regions relative to solubilisation in DDM micelles, despite it being thought to provide the most native-like environment for MPs.

Altogether, this thesis shows the power of A8-35-like APols as a solubilisation tool for studying MP structure and function using MS-based techniques. Data shown here also informs on the nature of APol interactions with MPs and how this may manifest in the improved stability of MPs in solution.

1 Introduction

1.1 Membrane Proteins

Membrane proteins (MPs) are a subset of proteins found embedded in the lipid membranes of cells and subcellular compartments. They are uniquely different from water soluble proteins, in that they display a large proportion of outward facing hydrophobic residues that would normally be buried in a water-soluble protein's "hydrophobic core". Instead, these side chains are outwardly presented in MPs and associated with the highly hydrophobic environment of the lipid bilayer membrane[1-2].

MPs operate a large number of functions in many organisms. Their location at the surface of cells and subcellular compartments makes them very well suited for functions such as receptors (e.g. G-protein coupled receptors (GPCRs)), transporters, pores and ion channels[3-7]. They can also function as membrane localised enzymes, structural proteins and sites for invasion or attack from viral and bacterial species[8].

As well as their broad range of functions, MPs can adopt distinct structures. Among the most commonly observed are the α-helical bundles (7-transmembrane (TM) receptors, 12 TM transporters, multimeric ion channels)[3-4, 9-10], β-barrels (such as those found in the outer membranes of bacteria, mitochondria and chloroplasts)[11-14] and monotopic single pass MPs (these use a single hydrophobic helix to pass, or embed, into a lipid membrane)[15] (Figure 1-1). In addition to monomeric MPs, MPs can often be found in complexes with other membrane-embedded proteins (multimeric ion channels) or associated with water-soluble subunits or lipoproteins (ATPases or β-barrel assembly machinery (BAM) complex)[16-19].

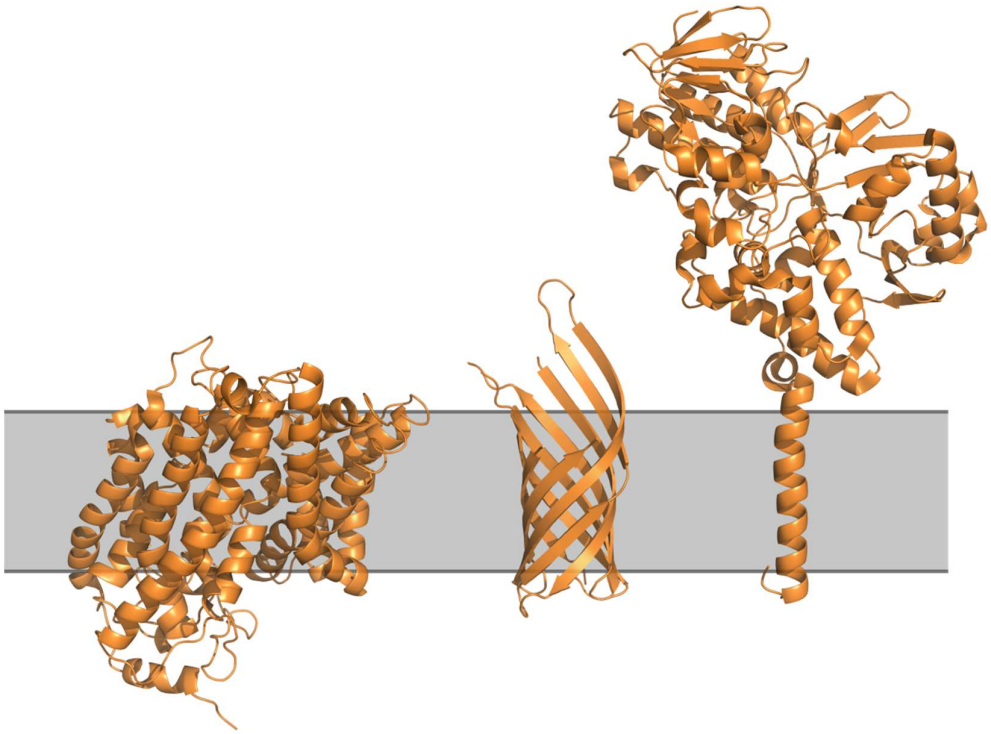

Figure 1-1 - Representative structures of common MP topologies. Mhp1 (left) is a 12-TM α-helical transporter from the bacterial inner membrane (PDB no. 2X79)[7], tOmpA (centre), the transmembrane (TM) domain of OmpA, is an 8-stranded β-barrel porin from the bacterial outer membrane (PDB no. 1QJP)[20] and Monoamine Oxidase A (MAO-A, right) is an enzyme that degrades amine neurotransmitters in humans and is tethered to the membrane by a single membrane spanning helix (PDB no. 2Z5X)[15].

MPs present an interesting quandary in the scope of structural biology. Despite their wide range of essential functions, significance in the human genome (25-30 %)[21] and the high number of currently approved pharmaceuticals that target them (~50 %)[22-23], high resolution structural data for MPs falls greatly behind that of their water soluble counterparts[1]. There are ~120,000 solved structures from nuclear magnetic resonance (NMR), X-ray crystallography or electron microscopy (EM) in the protein databank (PDB). Within these, only ~2000 uploaded co-ordinate files are for MPs.

This deficit stems mostly from the inherent properties of MPs that make them difficult to study. The previously mentioned presentation of hydrophobic residues on the surface of MPs means they are insoluble in aqueous solutions without the presence of a suitable surfactant. MPs are also unstable in aqueous solution, are often expressed in low quantities and can be difficult to purify, making it difficult

to acquire sufficient (often mg) quantities needed for structural studies[1-2, 24]. Those interested in MP structural biology are always looking to develop new methods to solubilise and study MPs[1, 25-26].

1.2 Outer Membrane Proteins

Outer membrane proteins (OMPs)[11, 27] are a family of β-barrel membrane proteins found in the outer membranes of bacteria, mitochondria and chloroplasts. β-barrel MPs are formed of even numbers of β-strands (between 8 and 24) arranged in a closed barrel, with both termini on the periplasmic side of the membrane. These strands are tilted between 30^{o} and 60^{o} perpendicular to the membrane and are connected by periplasmic and extracellular loops[11]. OMPs have a broad array of functions including enzymes (PagP, OmpT)[28-30], porins (OmpA, trimeric OmpF)[8, 20, 31], channels (mechano-sensitive BtuB)[32] and insertases (BamA in BAM complex)[18-19] (Figure 1-2).

OMP β-barrels are known for their high stability and their improved ability to unfold and refold relative to many α-helical proteins[27]. These properties make OMPs more manageable experimentally, enabling detailed studies into the mechanisms of their folding and insertion into a membrane[1-2, 25, 27]. Work presented in this thesis is carried out almost exclusively on OMPs, more specifically, OmpT, PagP and tOmpA (TM domain of OmpA) (Figure 1-2a,b,c).

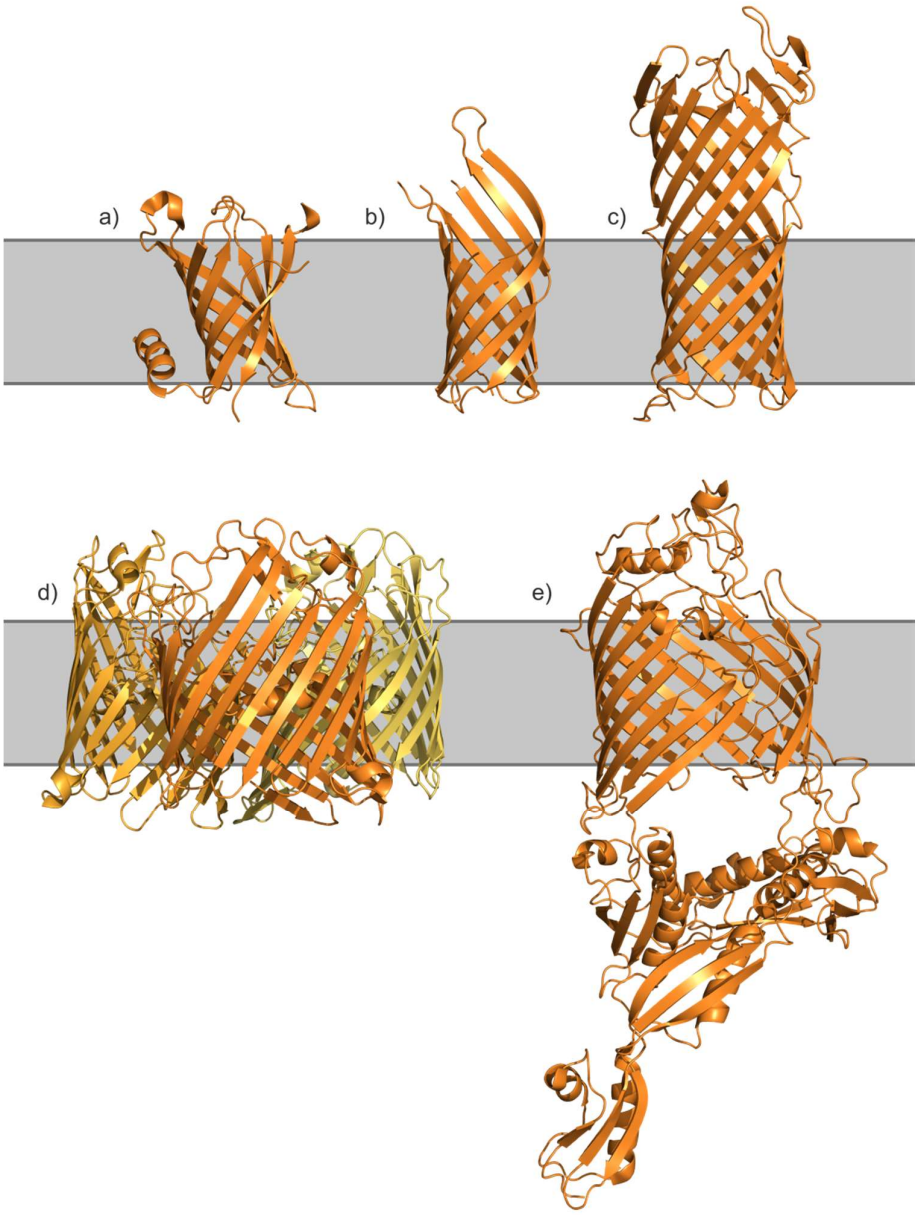

Figure 1-2 – Structures of bacterial β-barrel OMPs vary greatly. a) PagP is an 8-stranded β-barrel palmitoyl transferase with an N-terminal membrane-embedded helix (PDB 1THQ)[28], b) tOmpA is the TM domain of OmpA, an 8-stranded β-barrel porin with an unresolved periplasmic domain involved in dimerization (PDB 1QJP)[20], c) OmpT is a 10-stranded β-barrel endopeptidase with ~50% of the barrel protruding from the extracellular face of the membrane (PDB 1I78)[30], d) OmpF is a homotrimer of 16-stranded β-barrels that functions as a porin (PDB 3O0E)[31], e) BamA is 16-stranded β-barrel membrane-embedded component of the BAM complex involved in insertion of OMPs into the outer membrane (OM) of bacteria, BamA has 5 homlogous polypeptide transport associated (POTRA) domains in the periplasmic space that are involved in OMP substrate recognition and association of other BAM complex components (PDB 5D0O)[18].

1.2.1 OmpT

OmpT, is a 10-stranded (~33 kDa) endopeptidase enzyme[30]. OmpT falls into a family of protease enzymes known as omptins and is thought to have a serine protease-like mechanism of cleavage, evidenced by its sensitivity to serine protease inhibitors despite the structure of OmpT (Figure 1-2c) showing no typical serine protease catalytic triad[30]. Ser99 and His212 residues (previously thought to form a serine protease-like triad) are too far apart (~9 Å) in the solved structure to act as a functional protease. OmpT proteolytic activity is highly sensitive (~500 fold reduction) to alanine mutations of Asp83, Asp85, Asp 210 and His 212. Asp83-Asp85 and Asp210-His212 pairs are separated by ~5 Å and represent the catalytic site of aspartic acid proteases and the His-Asp pair in serine protease, respectively. The high activity of OmpT in high pH suggests the involvement of a His residue but with no clear nucleophile close to the Asp210-His212 pair, it has been proposed that a water molecule may be activated by the pair and be responsible for the nucleophilic attack on the peptide bond[33].

OmpT enzymatic function is dependent on binding of lipopolysaccharide (LPS), the major constituent of the outer leaflet of the outer membrane of bacteria[34]. LPS binding to other proteins, such as FhuA[35-36], is shown to be co-ordinated by four basic residues. Of these four residues involved in FhuA-LPS, three (Arg 138, Arg 172 and Arg 226) exist in OmpT in a similar arrangement[30], located just above the extracellular boundary of the TM domain of OmpT, resulting in a prime positioning for orientation of the LPS headgroup (Figure 1-3 and Figure 1-5).

OmpT differs from the majority of other OMPs, in that it has a large proportion of its barrel (~50 %) protruding from the extracellular side of the membrane[11, 30, 37]. OmpT has a defined aromatic girdle at the boundaries of the TM region formed of belts of large hydrophobic residues[30] (Figure 1-3).

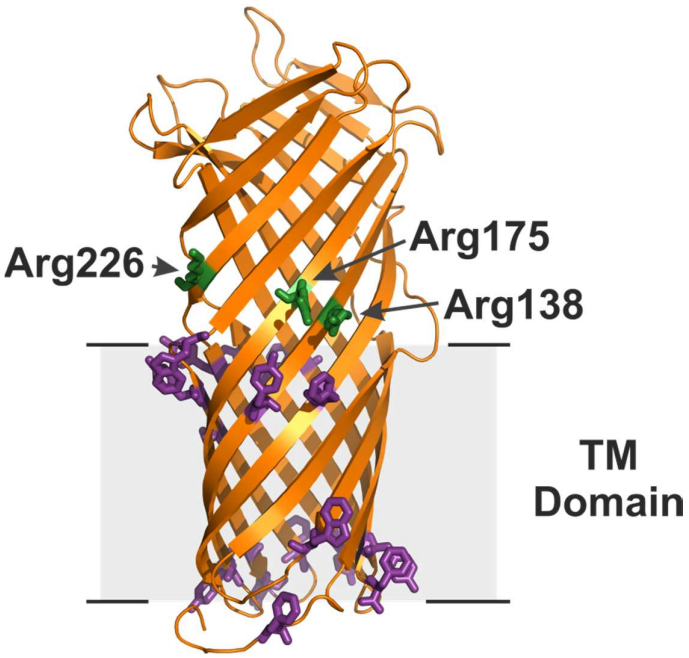

Figure 1-3 – Aromatic girdle and LPS coordinating residues of OmpT. Aromatic girdle of OmpT is formed by clustering of aromatic residues to the top and bottom of the TM domain and a cluster of basic residues mediate the LPS headgroup interaction. Aromatic residues (purple) are focused at the limits of the TM domain of OmpT, forming the aromatic girdle that mediates the association of lipid chains to the TM domain. Arg 138, Arg 175 and Arg 226 mediate the interaction of the headgroup of LPS (required for OmpT activity) to OmpT and represent 3 residues of a structural motif present in the LPS-binding protein FhuA[30].

OmpT cleaves selectively between consecutive basic residues (Lys/Arg, with a preference for Arg in the P1 position) (Figure 1-4) which is supported by a large density of acidic residues in the cleft in the inner face of the extramembrane region (Figure 1-5). Residues upstream and downstream of the cut site contribute to the substrate specificity of OmpT. There is a high prevalence of small non-polar residues (Val/Ala) at the P2' position of OmpT substrates and Arg and Trp in the P3 and P4 positions (Figure 1-4)[38].

$$H_2N - - - P_4 - P_3 - P_2 - P_1 \,|\, P_1' - P_2' - P_3' - P_4' - - - CO_2H$$

Figure 1-4 – OmpT substrate cut-site nomenclature. OmpT cleaves between consecutive basic residues at the P_1 and P_1' positions. Substrates commonly have preference for substrates with Val or Ala at the P_2' position and Arg and Trp at the P_3 and P_4 position.

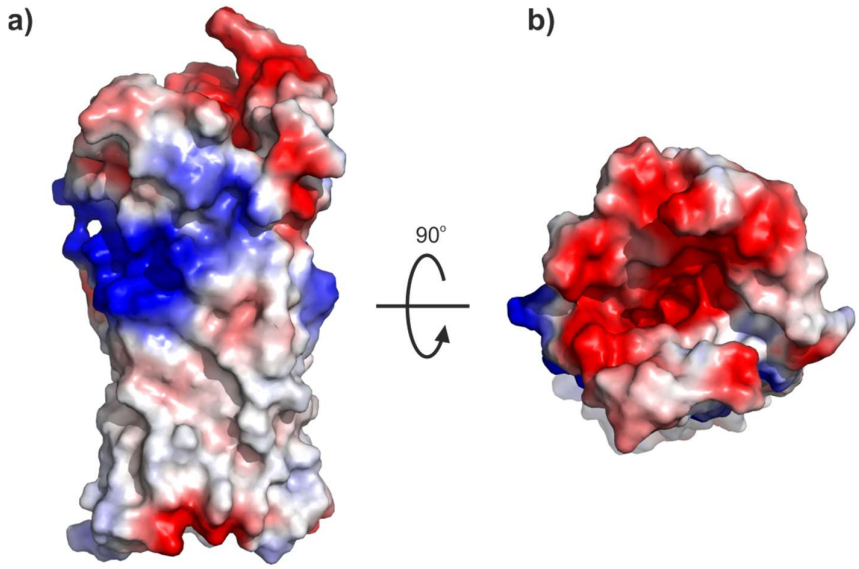

Figure 1-5 – Partial charge representation of OmpT shows a density of basic residues on the outer surface of the extramembrane domain and a large density of acidic residues on the inner face of the barrel. a) Side view of OmpT shows a density of positive charge (blue) on the outer surface of the extramembrane domain of OmpT that correlate with the location of previously described Arg residues that mediate the interaction with LPS headgroups. b) Top view of OmpT shows a density of negative charge (red) on the inner face of the barrel which mediates the binding and cleavage of substrate peptides and proteins.

1.2.2 PagP

PagP is an 8-stranded barrel (~20 kDa) with a N-terminal helix that is membrane embedded (Figure 1-2a). PagP functions as a palmitoyl transferase enzyme, that transfers palmitate fatty acid chains onto lipid A headgroups, functioning as a mechanism for antimicrobial peptide resistance[39]. The crystal structure of PagP shows a palmitate chain bound to the "hydrocarbon ruler" (substrate recognition pocket) in the outer region of the inner face of the barrel[28]. PagP has been extensively studied as model for mechanisms of folding and unfolding of OMPs[40-41].

1.2.3 tOmpA

tOmpA is the TM domain of the highly expressed OmpA. OmpA (~35 kDa) is an 8-stranded β-barrel[20] with a periplasmic soluble domain and is the most highly expressed OMP in the outer membrane of *E. coli*, with ~ 100,000 copies per cell[42]. The function of OmpA is disputed and it appears to serve numerous functions[8, 42]. The crystal structure of OmpA (Figure 1-2b) shows small solvent filled pockets but

does not allow for free conductance[20]. However, NMR and molecular dynamics simulations (MD) show that the flexibility of OmpA can result in expansion of the pore (in a lowly populated conformation) and support previous theories about ion and water channel function[8]. Others have speculated on the possibility of OmpA interacting with the peptidoglycan layer in the periplasm[8]. OmpA also appears to have numerous roles in the virulence of *E. coli,* bacterial survival under immune attack and biofilm formation[8].

1.3 Solubilising media for native membrane proteins

1.3.1 Detergent Micelles

MPs must be solubilised in an appropriate media in order to be maintained in solution in a native state, commonly in detergent micelles. Detergent molecules can form micelles when added to aqueous solutions above their critical micelle concentration (cmc)[43]. Hydrophobic tails of detergent molecules come together in the centre of a spherical micelle with the charged or polar headgroups forming a hydrophilic "shell" around the perimeter (Figure 1-6a)[43]. MPs can sit in this hydrophobic environment and be maintained in a native state[1-2, 43]. These micelles are often highly uniform, for example, n-dodecyl-β-D-maltoside (DDM) micelles have a homogenous mass of ~60 kDa[43]. Detergents can vary in strength (ability to denature solutes), with detergents such as sodium dodecyl-sulphate (SDS) being more likely to maintain proteins in a denatured or semi-native state and DDM being used to solubilise the native states of MPs (and is often used for extraction of MPs from membranes in their native state)[28].

Despite being commonly used, detergent micelles have properties that make them less than ideal for maintaining the native state of MPs for *in vitro* studies. Their spherical structure can perturb the native structure of MPs and their dynamic nature makes MPs prone to dilapidation, where MPs undergo unfolding and aggregation[44-45]. For this reason, other methods of MP solubilisation that maintain MPs in a more native-like state are also being developed.

1.3.2 Liposomes

Large unilamellar vesicles (LUVs) are large spherical structures (~100 nm) formed of bilayer lipids. Liposomes provide a native-like environment for MPs and can be varied by changing the lipid composition (changing chain length and headgroup) to yield more suitable conditions for chosen MPs[46-47].

1.3.3 Bicelles and Nanodiscs

Bicelles and nanodiscs are novel solubilisation media that form lipid bilayer discs encapsulated by detergent or amphipathic protein helices, respectively (Figure 1-6b,c). These methods provide the positive features of the native-like lipid bilayer of liposomes and their size (~100 Å diameter)[48-50] makes their use in techniques such as X-ray crystallography, NMR, MS, EM, small-angle X-ray scattering (SAXS) and size exclusion chromatography (SEC) possible[49-57]. Like detergent micelles, bicelle and nanodisc compositions must be screened and optimised for each MP[43-44].

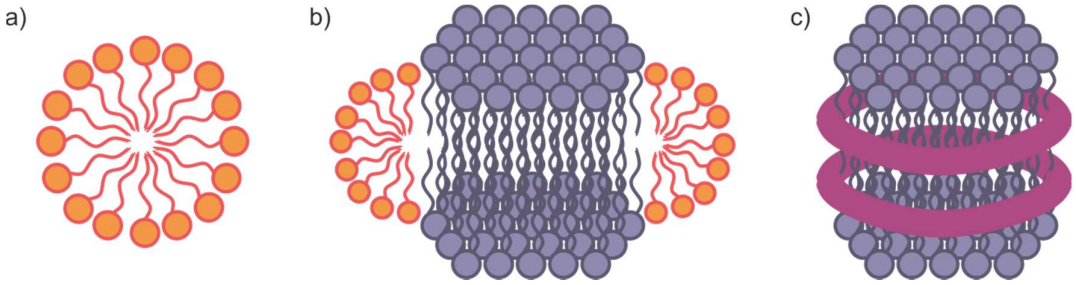

Figure 1-6 – Solubilising methods for native-like MPs. a) Detergents added above their cmc form spherical micelles that can accommodate the TM region of a MP. b) Bicelles and c) nanodiscs are formed of lipid bilayer discs encapsulated with detergent or amphipathic helical proteins, respectively, in order to provide a more native-like environment for MPs.

1.4 Amphipols

Amphipols, or amphipathic polymers, (APols) are a novel form of surfactant for solubilisation of MPs in a native state[58-59]. It has been shown that APols stabilise the folded state of β-barrels, OmpA and FomA, that are resistant to SDS-induced unfolding as demonstrated by cold-SDS-PAGE (SDS-polyacrylamide gel electrophoresis)[60], improved activity of diacyl glycerol kinase (DAGK) in PMAL-B-100, a zwitterionic APol[61], and native-like fluorescence of bacteriorhodopsin (BR)-bound retinal in A8-35 (Figure 1-7a) comparable to that in octyl-thioglucoside (OTG) detergent micelles[62]. APols have been used to stabilise the native state of a number of types of MPs including the previously mentioned OmpA and FomA β-barrels, nicotinic acetylcholine receptor (nAChR) channel, the SERCA1 Ca^{2+}-dependent ATPase, the SecYEG translocon of the bacterial inner membrane, a number of GPCRs and even a number of larger MP complexes such as cytochrome bc_1 and b_6f[58, 60, 63-64].

APol complexes with MPs are highly stable. BR in complex with OTG detergent micelles is 100 % unfolded after 18 days (as shown by loss of native like fluorescence of retinal) but is mostly unchanged in A8-35 APol[65]. Stability of these complexes is attributed to a high kinetic stability[60]. Despite OmpA having a greater thermodynamic stability in A8-35 versus lauryl-dimethylamine-N-oxide (LDAO) detergent micelles, OmpA in complex with A8-35 is highly stable, remaining folded in excess of 52 days[60].

A8-35, the most used and well characterised APol[58-59], is synthesised by grafting of isopropyl- and octyl-amines onto a polyacrylic acid precursor (Figure 1-7a). Solubility of A8-35 and its complexes with MPs are dictated by the free acid groups, while the grafting of isopropyl and octyl groups provide the hydrophobic environment for MP stabilisation[58-59]. A8-35 was presumed to have an average mass of ~8 kDa (this has now been shown to be ~4.5 kDa by MS and other methods)[33, 58, 66], ~35 % of free acid groups ungrafted and ~ 40 % and 25 % of acid groups grafted with isopropyl and octyl groups, respectively[58, 66]. Due to the nature of the synthesis of A8-35, it is highly heterogenous, varying in both its mass (500 Da – 20 kDa) and degree of grafting. Despite the heterogeneity of individual molecules of A8-35, in solution, A8-35 forms homogenous particles of ~40 kDa[67]. A

number of A8-35-like APols have been developed, the name being indicative of the properties of the APol. In A8-35, 8 and 35 represent the average mass of the polymer and the proportion of acid groups left unmodified, respectively. A8-75 is synthesised from the same polyacrylic acid precursor as A8-35 (and hence will have a similar mass distribution) but without the isopropyl grafting, resulting in a larger extent (~75 %) of free acid groups. A34-35 and A34-75 are the counterparts of A8-35 and A8-75 synthesised from larger polyacrylic acid precursors with similar grafting densities (Figure 1-7a)[58-59].

The solubility of these APols (and their complexes with MPs) is dependent on the free acid groups and so is highly sensitive to pH and divalent salt concentration. A8-35 is insoluble at pH values less than 7 and Ca^{2+} concentrations above 5 mM[58-59]. For this reason, other APols have been developed to expand their range of potential applications. Sulphonated APol (SAPol) (Figure 1-7b) was developed to allow solubilisation of MPs in low pH conditions for use in NMR studies, this was achieved by grafting of taurine in place of the isopropyl amine, which provides a charged group that is less sensitive to pH[58-59]. Phosphocholine APol (PC-APol) (Figure 1-7d) uses further grafting of zwitterionic phosphocholine groups in place of the remaining free acid groups to provide permanent charge[58-59]. In addition to these highly ionic APols, a non-ionic APol (NAPol) that uses glucose-based moieties to maintain solubility has been developed (Figure 1-7c)[58-59]. NAPol is credited for providing the most native environment for MPs and is uniquely capable of allowing cell-free expression of folded MPs in the absence of detergent or lipid[68].

1.5 Other Polymer-based surfactants

In addition to APols, there are a number of emerging polymer-based surfactants for the solubilisation of MPs. Styrene-maleic acid lipid particles (SMALPs) can be used to excise MPs from native membranes and have a morphology comparable to that of nanodiscs with upside from potential ease-of-use and wide applicability[69-70]. Polymersomes are vesicle-like structures formed from amphiphilic block copolymers added above a critical micelle concentration, with great promise in their tuneable membrane properties and potential in drug delivery[71-72].

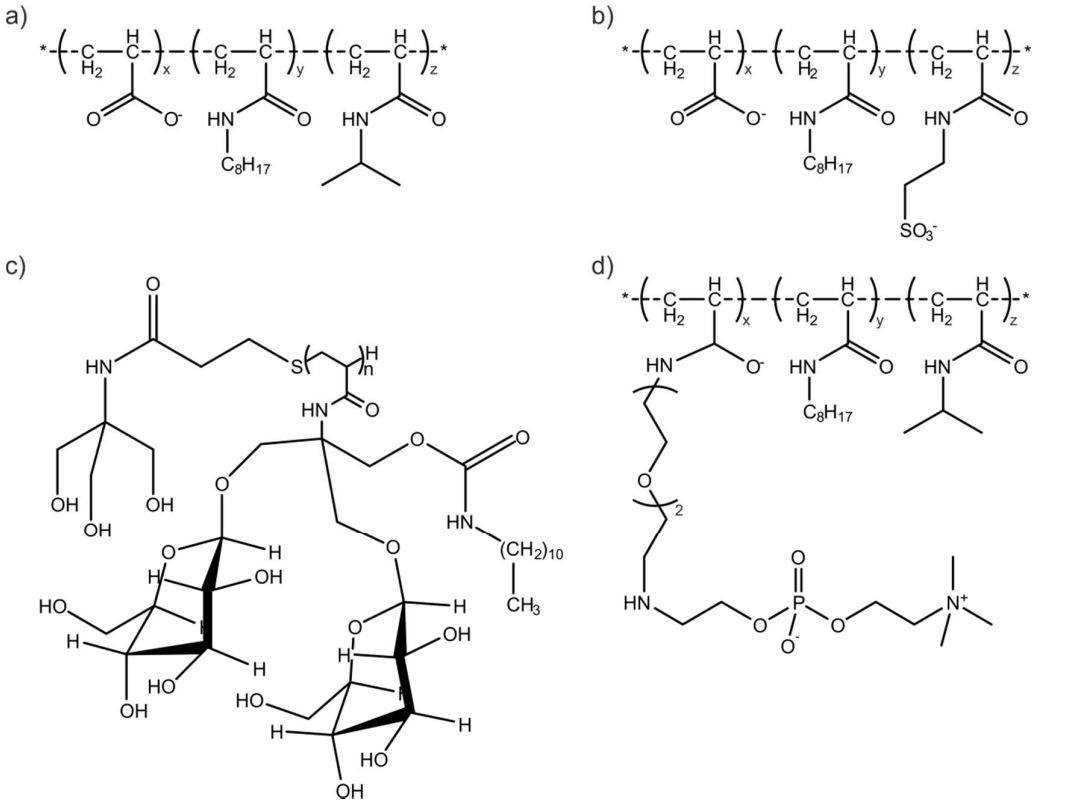

Figure 1-7 – Different APols with a range of functional groups. a) A8-35 is the most well characterised APol, water solubility is provided by free acid (x) and hydrophobicity provided by octyl (y) and isopropyl (z) grafting. b) Sulphonated APol (SAPol) has taurine (z) grafting in place of isopropyl to allow solubility in low pH conditions. c) Non-ionic APol (NAPol) is a homomeric APol that uses polar glucose-based moieties to maintain solubility. d) Phosphocholine APols (PCAPols) have a phosphocholine (x) grafting of the free acid to maintain the solubility[33, 58]*.*

APols have been shown to be useful surfactants for stabilization of native-like state of MPs, having been adopted for use by many techniques, including NMR, MS, EM, SEC, SANS, analytical ultracentrifugation (AUC) and Forster resonance energy transfer (FRET)[62, 73-80].

1.6 Mass Spectrometry

Mass spectrometry involves the analysis of gas phase ions by means of measuring their mass-to-charge ratio (m/z), and therefore requires analytes to be ionised prior to analysis. Harsh methods such as electron impact (EI) and chemical ionisation (CI) require the analytes to be vaporised prior to ionisation by an electron beam or gas-reaction with ionising substrates in EI and CI, respectively[81]. The need for prior evaporation and, in the case of EI, the high risk of fragmentation upon ionisation means that these methods of ionisation are not feasible for proteins or large peptides. As such, "soft" ionisation methods have been developed that allow for ionisation of peptides and proteins.

1.6.1 Ionisation

1.6.1.1Matrix Assisted Laser Desorption Ionisation (MALDI)

Matrix-assisted laser desorption ionisation (MALDI) is a commonly used "soft" ionisation method for ionising proteins, first introduced by Karas and Hillenkamp in 1987[82-83]. The analyte is mixed with an organic photosensitive matrix (commonly, 3,5-dimethoxy-4-hydroxycinnamic (Sinapinic) or 4-hydroxy-3-methoxycinnamic (Ferulic) acid) and dried onto a metal target plate, which is then introduced into the vacuum of the mass spectrometer. The sample is irradiated using a Neodinium:Yttrite laser, which evaporates the sample-mixture and activates the matrix. Activation of the matrix results in transfer of a proton onto the analyte (Figure 1-8). This method generates predominantly singly charged analyte ions that subsequently enter the mass spectrometer[81, 84-85].

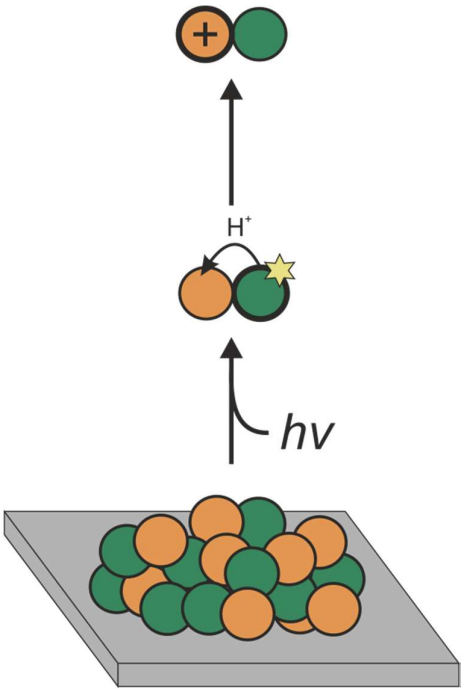

Figure 1-8 – Matrix-Assisted Laser Desorption Ionisation (MALDI). Analyte (orange) is mixed with an excess of a matrix agent (green) and allowed to dry on a metal plate. This plate is then inserted into the ionization chamber (under the vacuum of the mass spectrometer). Irradiation of the analyte-matrix mixture results in desorption of both analyte and matrix from the surface and activation of the matrix molecule. Activated matrix molecules transfer a proton to the analyte, and the analytes enter the analyser of the mass spectrometer.

1.6.1.2 Electrospray Ionisation

Electrospray ionisation (ESI) was first used in conjunction with mass spectrometry for the analysis of polymer macromolecules by Dole et al. in 1968[86] and further developed for efficient ionisation of biomolecules by Fenn et al. in 1989[87]. Analytes are dissolved in a solvent and passed through a narrow capillary (which is subjected to a high voltage) under atmospheric conditions. Analytes are ionised in charged droplets and migrate towards the entrance of the mass spectrometer, attracted by a potential gradient. There are a number of models for the means of desolvation and ionisation by ESI that have been suggested to be used concurrently, and are likely dependent on the particular analyte[88].

The ion ejection model (IEM)[88] (Figure 1-9a) involves the analyte adopting a charge whilst evaporating from a charged droplet. This model is best suited to small analytes such as small molecules and peptides, as the large displacement of

solvent and charge by a protein is highly unfavourable. The chain ejection model (CEM)[88] (Figure 1-9b) describes the gradual ejection of long chain polymers (including unfolded proteins) from the droplet with charges being picked up as these chains exit the droplet. The charged residue model (CRM)[88-89] (Figure 1-9c) is the preferred model for large compact analytes (folded proteins). Charged droplets reduce in size until Coloumbic repulsion exceeds the surface tension of the droplet (Rayleigh Limit) and the droplets split into a number of smaller charged droplets. Through a number of rounds of evaporation and fission, remaining charges are deposited on the surface of the analyte.

Classical ESI involves passing samples through a metal capillary, with flow rates of 1-20 $\mu l.min^{-1}$, with the application of high voltages and temperatures to bring about the ionisation and desolvation[86]. nanoESI (nESI)[90] involves applying a voltage to sample-loaded capillary with a narrow opening. Sample flow is generated by capillary action with a flow rate of ~20 $nl.min^{-1}$ (considerably lower than standard ESI) and generates smaller droplets (~200 nm in diameter). The reduced flow rates and droplet size result in greater sensitivity, greater ionisation efficiency (~500-fold increase), reduced sample consumption (as little as 1 µl at 1 µM), improved tolerance of salts (up to 0.1 M) and the use of disposable single loading capillaries prevents cross-contamination[90].

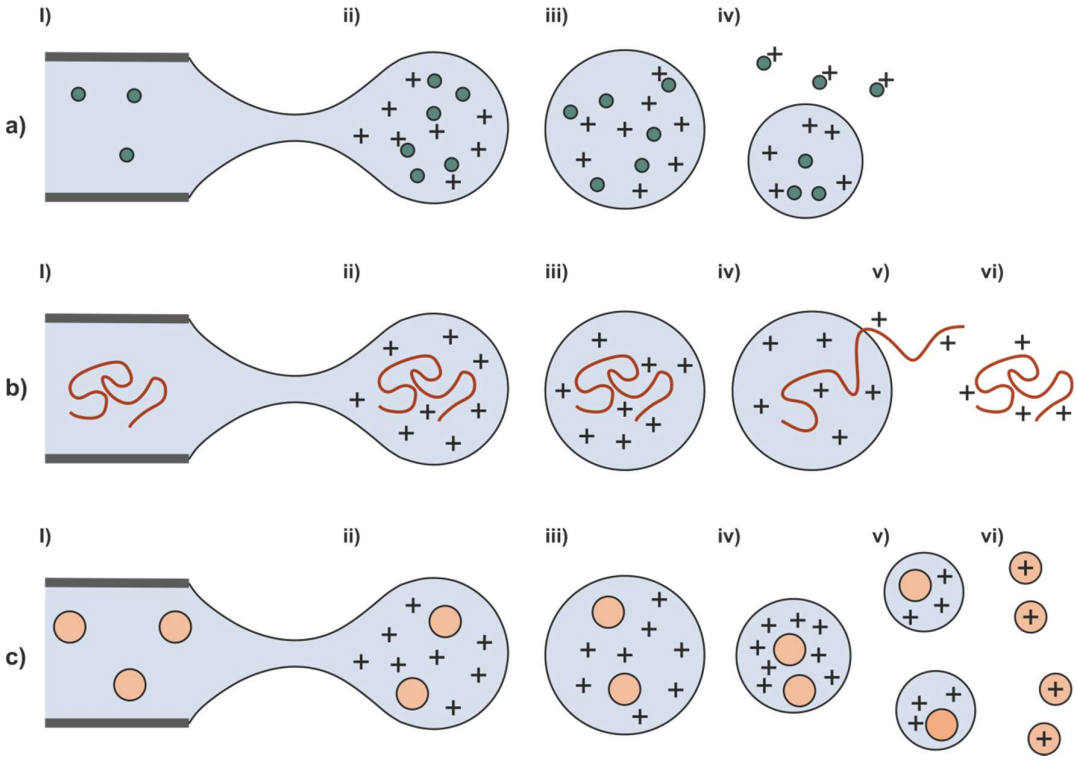

Figure 1-9 – Schematic for the mechanisms of electrospray ionization (ESI). In all models, application of a voltage to the capillary (i) results in an increase in charge density, the formation of a Taylor cone (ii) and analyte containing charged droplets being ejected from the Taylor cone (iii). a) The ion ejection model (IEM)[88] results in small analytes evaporating from the droplet and adopting charge as they adduct protons during ejection (iv). b) The chain ejection model (CEM)[88] describes gradual ejection of an extended protein or polymer analyte from the droplet (iv) with charges being picked up periodically as it is ejected (v) until a fully desolvated charged analyte is formed (vi). c) The charged residue model (CRM)[88-89] does not allow for ejection of large analytes from the droplet. The analyte containing droplet goes through rounds of solvent evaporation (iv) and fission as the charge density exceeds surface tension (v) until residual charge is deposited on the analyte following desolvation (vi).

ESI provides some immediate advantages over MALDI for ionisation of native proteins. Using ESI, native proteins are ionized from a more native-like aqueous solution, whereas ions from MALDI are more likely to be denatured by the more organic and acidic medium in which they are dissolved. Where MALDI generates predominantly singly charged ions, ESI generates ions with multiple charges and ions with an array of different charge states. Multiply charged ions have a lower mass-to-charge ratio (*m/z*) and can be observed on instruments with lower *m/z* ranges, avoiding unnecessary development of mass spectrometers with larger *m/z* ranges. Charge state distributions can be used to inform on the folded state of ions,

with more unfolded proteins having a larger surface area, picking up more charges and being observed at a lower *m/z* (Figure 1-10)[91].

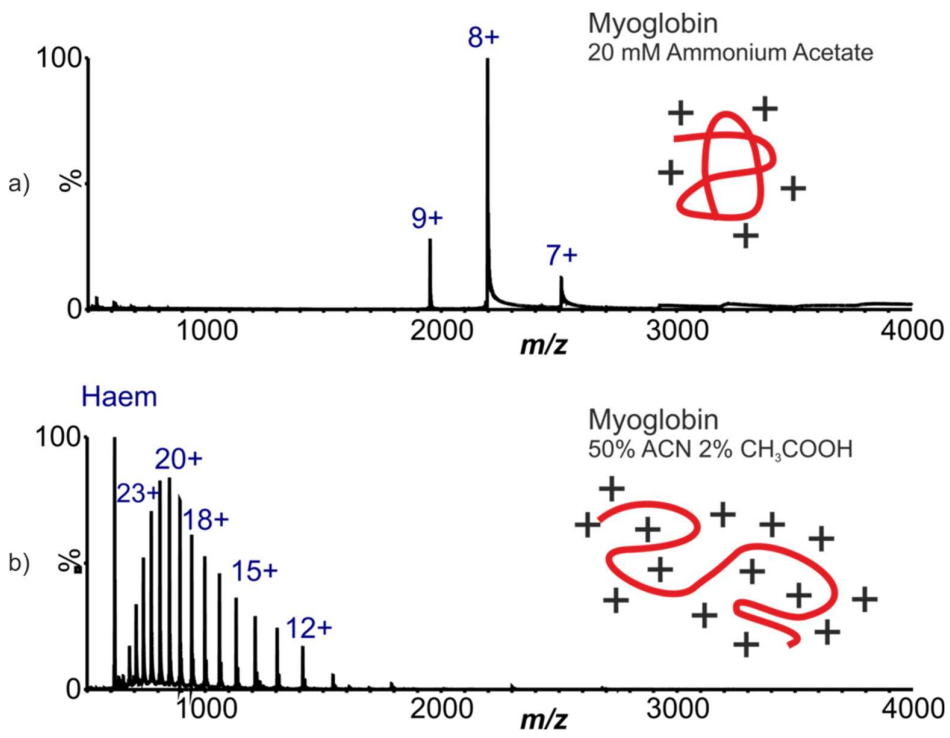

Figure 1-10 – Myoglobin analysed by nESI-MS under native and denaturing conditions. a) Native holo-Myoglobin (with non-covalently bound haem) analysed from 20 mM ammonium acetate populates more lowly charged states (7-9⁺), indicative of a compact conformation with lower surface area. b) Myoglobin analysed from 50 % acetonitrile, 2 % acetic acid is denatured and populates more highly charged states (11-25⁺) with the non-covalently bound haem group now unbound.

It has been shown that protein structure *in vacuo* is representative of that *in vitro* by the calculation of collision cross-section (CCS) values by IMS-MS (described below)[92-93], observation of comparable secondary structure of amyloid proteins by solution- and gas-phase infrared spectroscopy[94-95] and observation of native forms of viral capsid protein from soft-landing MS (a technique that captures ions for EM analysis following analysis by MS)[96].

1.6.2 Mass Analysis

All native MS work shown in this thesis was performed on a Waters Synapt G1 HDMS (Waters, Wilmslow, UK), FPOP-LC-MS work was performed on a Waters Synapt G2Si HDMS (Waters, Wilmslow, UK) and HDX-MS was performed on a Waters Xevo Q-ToF instrument (Waters, Wilmslow, UK). Figure 1-11 shows a schematic of a Synapt G1 instrument, which possesses a drift cell between a quadrupole and a Time-of-Flight (ToF) mass analyser (all parts described later). The Synapt G2Si has a step-wave ion guide in place of the primary ion guide, which improves sensitivity by filtering of neutral particles. The Xevo instrument is similar in composition to the Synapt G2Si instrument but with a collision cell in place of the drift cell (used for TWIMS analysis).

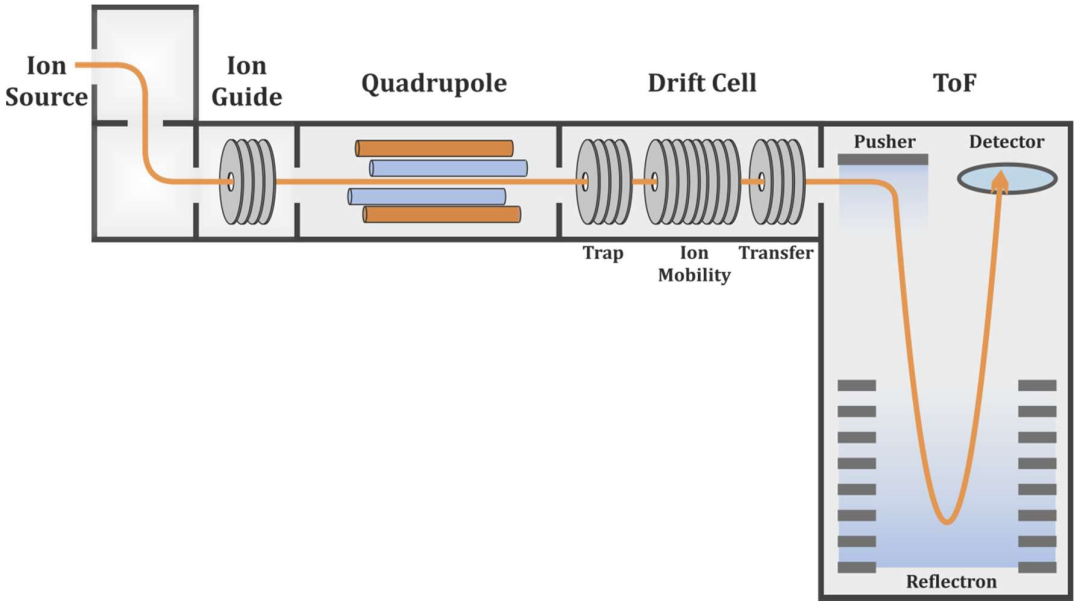

Figure 1-11 – Schematic of a Waters Synapt G1 HDMS. After introduction into the mass spectrometer, ions are focused by an ion guide and directed into the quadrupole, an analyser that can select ions of specific m/z. Subsequently ions enter the drift cell for TWIMS analysis and the ToF analyser for m/z analysis.

1.6.2.1 Time of Flight (ToF)

The first ToF analyser was a linear ToF presented in 1955 by Wiley and McLaren[97]. ToF mass analysers measure the *m/z* of ions based on the time taken for the ions to traverse a known distance after acceleration into a field-free region of the instrument (Equation 1-1, Equation 1-2 and Equation 1-3).

$$E_k = \frac{m.v^2}{2} = z.e.V$$

Equation 1-1 – Kinetic energy of an ion after acceleration (E_k) is related to the charge of the ion (z) and the strength of the accelerating voltage (V). This kinetic energy is proportional to the square of the resultant velocity of the ion (v) and to the ion's mass (m). This assumes all potential energy of the ion is translated to kinetic energy.

$$v = \frac{d}{t}$$

Equation 1-2 – the velocity of an ion in a field free region (v) relates the time taken (t) to traverse a known distance (d).

$$m = \frac{2.E_k.t^2}{d^2} = \frac{2V.e.z.t^2}{d^2}$$

$$\frac{m}{z} = \frac{2V.e.t^2}{d^2}$$

Equation 1-3 – With acceleration voltage (V) and distance (d) known, the mass-to-charge ratio of an ion (m/z) is proportional to the square of the time taken to traverse the ToF chamber (t).

Resolution of early ToF analysers was limited by the spread of kinetic energy of ions. Advancements in ToF technology (such as delayed pulse extraction[98] and the reflectron[99]) have improved this.

When introduced, MALDI was readily interfaced with ToF mass analysers, as the pulsed ionization by MALDI generated 'packets' of ions which are periodically analysed by the ToF mass analyser. Delayed pulse extraction in linear ToF instruments reduces the spread of ion energy. Ions of higher energy (greater velocity) entering the ToF chamber migrate further prior to the pulse. As a result of remaining closer to the pusher, the delayed pulse results in the ions of

previously lower energy being accelerated more than those of higher energy and thus compensating for small energy differences between ions, ensuring that ions of the same *m/z* arrive at the detector simultaneously[81, 98].

The reflectron is a stacked ring electrode that reflects ions with a reversing field and was first implemented with linear MALDI-TOF instruments[99]. The reflectron alleviates loss of resolution from spread of ion energy as a result of ions with greater kinetic energy penetrating the field further, effectively travelling a greater distance to the detector and arriving at the detector at the same time as lower energy ions of the same *m/z*[81, 99].

Where the linear ToF instruments measures the drift time of ions pushed in a direction parallel to the ion path into the ToF chamber, ions are pushed perpendicular to the ion path in the orthogonal ToF (Figure 1-12)[100]. Ions are collected into 'packets' and pushed perpendicular to the entry path of ions into the ToF and directed back to the detector by the reflectron. The orthogonal ToF mass analyser allowed ToF analysers to be interfaced with ESI sources that have a continuous ion generation[100].

ToF analysers with longer drift distances allow for a theoretically infinite *m/z* range and greater *m/z* resolution. Waters Synapt instruments are fitted with a two reflectrons opposite from one another to allow ions travel in a W-shaped path as opposed to a V-shaped path. This allows increased resolution (due to greater distance travelled by ions) but at the cost of sensitivity (as a result of slower push cycles).

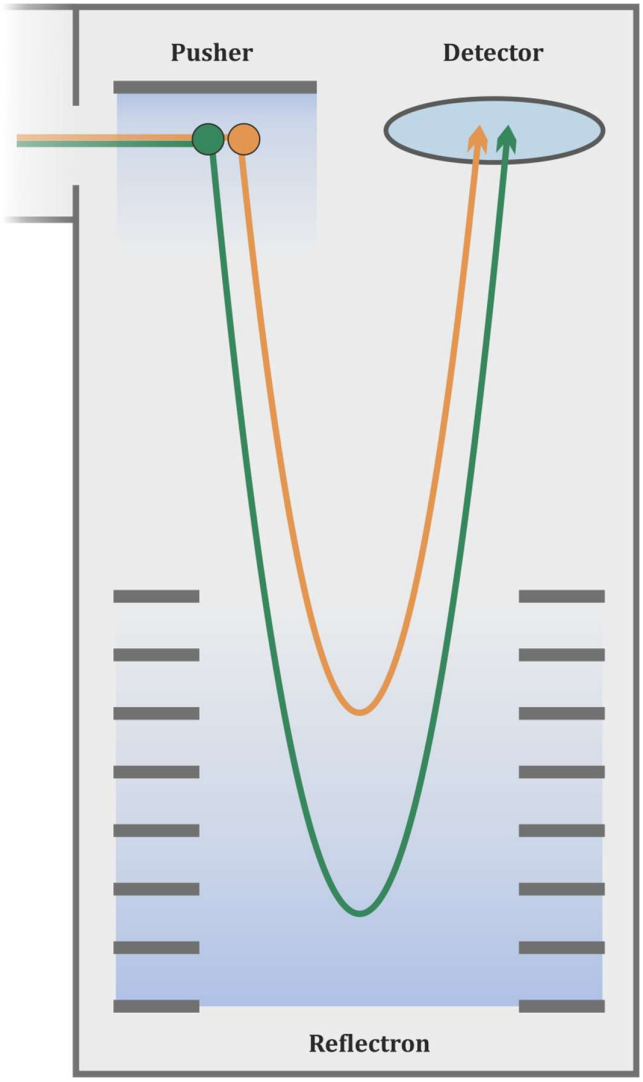

Figure 1-12 – Reflectron Time of Flight (ToF) mass analyser. ToF mass analysis calculates the m/z of ions based on the time for ions to traverse a fixed distance. Linear ToF analysers (ions travel parallel to the ion beam on entering the ToF chamber) have limitations on resolution as a result of ions of same m/z with differing kinetic energies traversing the ToF chamber at different rates. Introduction of the orthogonal pusher allows for cooling prior to pushing to reduce the spread of kinetic energy. Ions are accelerated toward the reflectron, a reversing field that directs ions toward the detector. The reflectron reduces loss of resolution by spread of kinetic energy, as ions with greater kinetic energy penetrate into the reversing field further effectively increasing the distance travelled and directing ions of the same m/z to the detector in time with one another.

In the previously mentioned Synapt G1 HDMS (Figure 1-11) and other Q-ToF instruments, this analyser is found at the back end of the instrument and is used for *m/z* analysis.

1.6.2.2 Quadrupole

Whilst ToF analysers allow the analysis of multiple *m/z* species simultaneously, quadrupoles use interacting oscillating electric fields to allow the stable transmission of a single *m/z* species[81, 101-102]. The quadrupole consists of four rods arranged symmetrically, parallel to the ion path. Each of the rods is electrically connected to the rod opposite. Ions are directed through the chamber with a potential gradient in the absence of fields generated by the four rods. Within each of the two pairs of rods, both rods are positively or negatively charged, depending on the phase of the oscillation of the radio frequency (RF) field. Positive ions are repelled toward the centre when the rods are positively charged and drawn towards the rods when negatively charged. The RF field from a single pair of rods would act as a high pass *m/z* filter, with ions of low *m/z* being drawn to the rods when they are negatively charged and being eliminated, where high *m/z* ions are drawn by the constant field. Each pair of rods is generating RF fields that are out of phase with one another. The interaction of the fields, only allows for stable trajectory of ions of a particular *m/z* (Figure 1-13) (or range of *m/z* values)[81, 102].

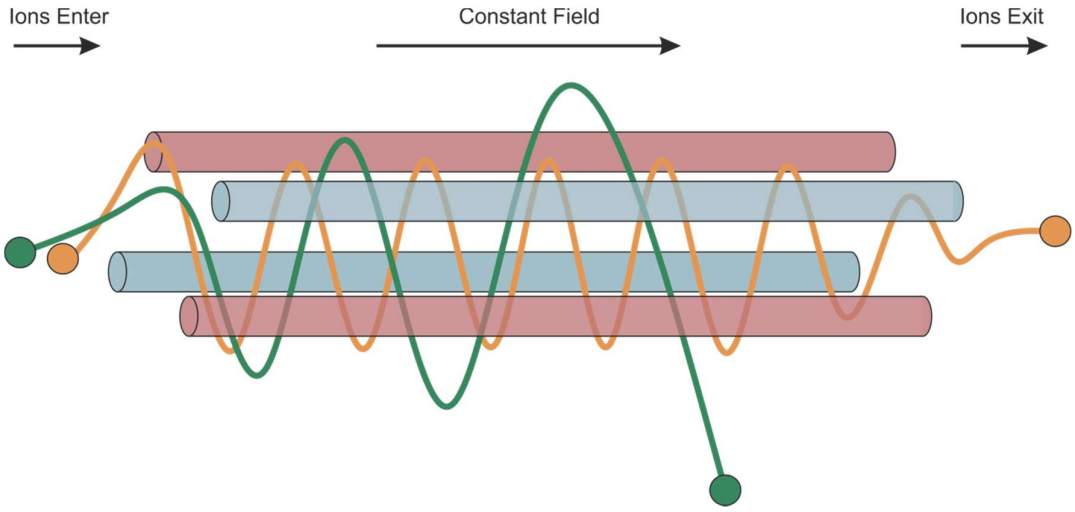

Figure 1-13 – Quadrupole mass analyser. Quadrupoles use interacting RF electric fields to allow transmission of ions of a particular m/z. Ions are accelerated through the quadrupole by a constant field. Each pair of rods (red and blue) generates an RF field that radially focuses ions. Interaction of the fields results in the stable trajectory of ions of a specific m/z and all others ions to be lost.

Quadrupoles mass analysers are commonly used for quantitative analyses of targeted species or selecting specific gas phase ions for subsequent gas-phase analyses, such as in Tandem MS (MS/MS) experiments or collision-induced-dissociation/unfolding (CID/CIU)[81, 103]. In the Waters Synapt G1 HDMS (Figure 1-11), the quadrupole is situated prior to the drift cell and ToF analyser, performing mass selection and allowing TWIMS and *m/z* analysis of specific ions and their products following collisional activation.

1.6.3 Detectors

Most detectors are a form of electron multiplier or photomultiplier, for example, a multi-channel plate (MCP) is formed of a plate with many wells kept under high voltage (Figure 1-14). Ion collisions with the surface of the wells begin an electron generation cascade. The electrons are funnelled along the well until they reach a central rail and generate an amplified current that can be detected and recorded by an attached computer as both time (used to derive the *m/z*) and intensity (Figure 1-14)[81, 104].

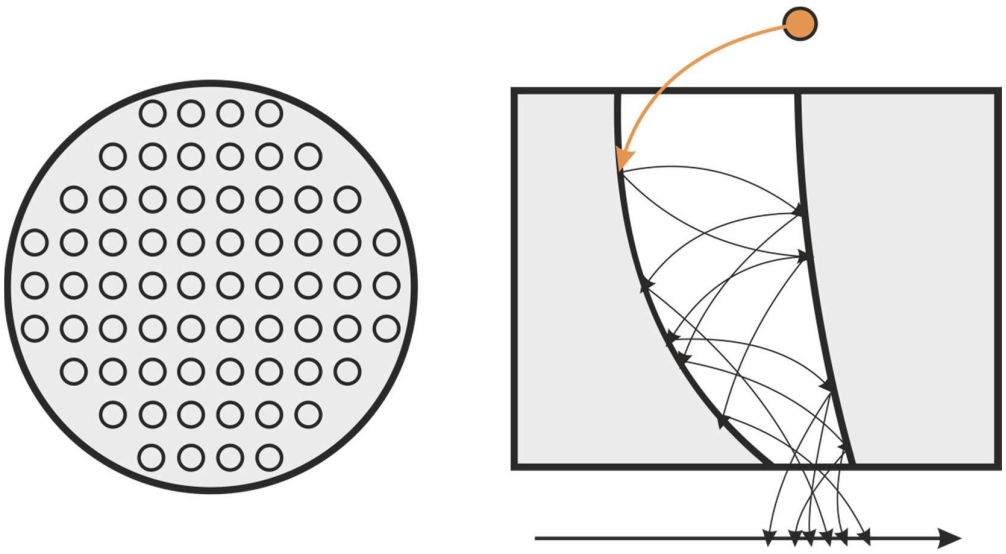

Figure 1-14 – Multi Channel Plate (MCP) detector. The MCP is formed by a plate with numerous openings with high voltage applied (left). Impact of an ion with the surface of one of the wells commences an electron cascade (right). Electrons are funneled along the well and directed towards a rail that feeds into a recording computer.

1.6.4 Ion Mobility Spectrometry (IMS)

Ion mobility spectrometry (IMS) is a gas phase technique commonly used in conjunction with MS[92-93, 105-107], both are gas phase ion techniques that provide complementary information on ion structure. IMS separates ions based on their size, shape, mass and charge by accelerating ions through a region of low vacuum. IMS is a valuable technique for determining the conformational state of a protein ion, as the drift time of an ion is related to the collision cross section (CCS)[106]. Larger (or more expanded) ions experience more collisions with a neutral buffer gas in a drift chamber and traverse more slowly (Figure 1-15)

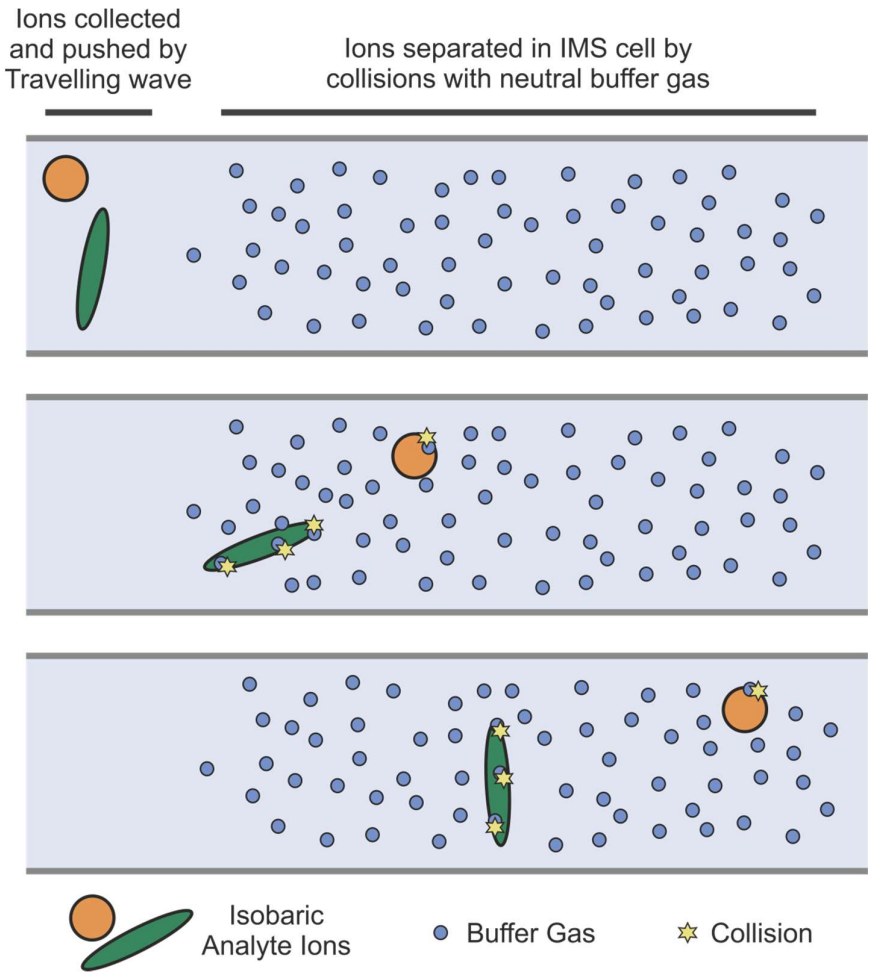

Figure 1-15 – Ion Mobility Spectrometry (IMS) separates ions based on their size, shape, mass and charge. Isobaric ions (ions of the same m/z) pushed into the ion mobility region are separated based on their structure and charge. Ions with a greater surface area (green) experience a greater number of collisions with the neutral buffer gas than more compact ions (orange) and travel the drift cell with a longer arrival time.

Using a linear drift tube (which employs a constant field to accelerate ions through the drift cell), drift time is directly related to the CCS of an ion when the mass and charge are known and the temperature, pressure and field strength are controlled[107-108] (Equation 1-4). However, linear drift tubes are limited by low sensitivity, with only approximately 1 % of ions being fully transmitted[107]. Travelling-wave IMS (TWIMS)[92, 105, 107, 109-110] employs a field that migrates along the stacked rings of the drift tube to allow for improved transmission of ions. In the case of TWIMS, where the interaction of the field with gas phase ions is non-uniform (Equation 1-5)[92], a calibration approach is required to determine CCS values of ions[93, 106, 111]. Concurrent analysis of denatured or native ions of known CCS allows determination of CCS values of analyte ions, where values relating drift time and CCS are determined from drift times of calibrant ions (Equation 1-7)[92, 106, 111].

$$\Omega = \frac{(18\pi)^{1/2}}{16} \cdot \frac{ze}{(k_B.T)^{1/2}} \cdot \left[\frac{1}{m_l} + \frac{1}{m_n}\right]^{1/2} \cdot \frac{760}{P} \cdot \frac{T}{273.2} \cdot \frac{1}{N} \cdot \frac{t_D.E}{L}$$

Equation 1-4 – CCS (Ω) is calculated from drift time (t_D) through a linear drift tube. The relationship between t_D and Ω is dependent on charge of the ion (z), temperature (T), the field strength (E) and tube length (L). It is also dependent on the reciprocal of the reduced mass of the ion (highlighted in grey, Equation 1-6), which is a function of the mass of the ion (m_I) and the neutral buffer (m_n).

$$\Omega = \frac{(18\pi)^{1/2}}{16} \cdot \frac{ze}{(k_B.T)^{1/2}} \cdot \left[\frac{1}{m_l} + \frac{1}{m_n}\right]^{1/2} \cdot \frac{760}{P} \cdot \frac{T}{273.2} \cdot \frac{1}{N} \cdot A{t_D}^B$$

Equation 1-5 – The relationship between t_D and Ω is not linear when using TWIMS. Terms referring to the field strength and tube length in Equation 1-4, have been replaced by constants A and B that are dependent on experimental wave parameters.

$$\mu = \frac{1}{\left[\frac{1}{m_l} + \frac{1}{m_n}\right]}$$

Equation 1-6 – Reduced mass (μ) represents the significance of an impact between two particles. It is a function of the masses of the two colliding particles (m_I and m_n).

$$\Omega = A' {t_D}^B$$

Equation 1-7 – Simplified equation relating ion drift time to CCS when using TWIMS. Calibration approach with ions of known Ω values allows for elimination of T and P values (assuming they are constant) and correction of the drift time value for mass and charge.

Measured CCS values of gas phase ions can be compared to theoretical values calculated from known structures, such as those from X-ray crystallography or NMR for proteins and protein complexes. There are a number of methods that can be used to calculate theoretical values, that can vary in accuracy and demand for computational power[92, 112-115]. The trajectory method (Tm)[113] determines the CCS of ions by simulating the approach of neutral buffer gas and analyte molecules. The Tm is the most accurate method for calculating theoretical CCS values but is highly computationally demanding.

Projection Approximation (PA)[115] values, such as that calculated using MOBCAL[113-114], are calculated by projecting "a shadow" of the analyte from numerous orientations and determining the average area of the projection. PA is much less demanding of computational power but is less accurate and known to underestimate contributions of concave structures. However, the application of an adjustment factor generates CCS values that correlate with Tm values. This new value is known as the Projection Superposition Approximation (PSA)[112]. The exact hard sphere scattering (EHSS) method simulates the interactions of buffer gas molecules with the analyte, which is represented with a hard sphere in the position of each atom[114].

In Waters Synapt instruments (Figure 1-11), TWIMS analysis is carried out in the ion mobility region of the drift cell, situated after the quadrupole and the Trap region of the drift cell. Quadrupole selection allows TWIMS analysis of selected ions, collisional activation in the Trap region allows TWIMS analysis of fragments of all or selected ions and collisional activation in the Transfer region allows post-TWIMS *m/z* analysis of ion fragments (which can be used for studying specific conformers of protein ions).

1.6.5 Tandem Mass Spectrometry (MS/MS)

MS/MS experiments allow instruments with two mass analysers to perform more complex analyses on a sample. These experiments often involve some form of ion selection (by a quadrupole or ion trap) and activation or fragmentation of the selected ion. These methods underpin a large number of proteomic, peptide mapping and post-translational modification (PTM) identification experiments.

1.6.6 MS/MS Experiments

Product Ion Scan involves sequentially selecting precursor ions, fragmenting the precursor and analysing all product ions (Figure 1-16a)[81]. This method is commonly used for *de novo* peptide sequencing and small molecule identification[116-117]. This method can also be used in native mass spectrometry to select and disassemble protein-protein and protein-ligand complexes to determine stoichiometry and stability[17, 118].

Precursor Ion Scan fragments precursor ions, in the same way as Product Ion Scan. However, the second mass analyser selects only those products with a specific *m/z* (Figure 1-16b)[81, 119]. This approach can be used for identification of specific components of a complex mixture e.g. ligands, PTMs.

Neutral Loss Scan sequentially selects precursor ions, fragments and then selects product ions with a targeted mass difference (Figure 1-16c)[81]. Where in Precursor Ion Scan the target product is fixed, the selected product *m/z* in Neutral Loss Scan is dependent on the *m/z* of the selected precursor.

Selected Reaction Monitoring selects a specific precursor *m/z*, fragments and selects a specific product *m/z* (Figure 1-16d)[81]. This approach is used for highly targeted proteomic methods, such as those identifying very specific components from a complex mixture[117, 120]. Multiple Reaction Monitoring is similar to Selected Reaction Monitoring and can be used to identify one or more specific products from a specific precursor. This is useful if the precursor can dissociate by more than one pathway.

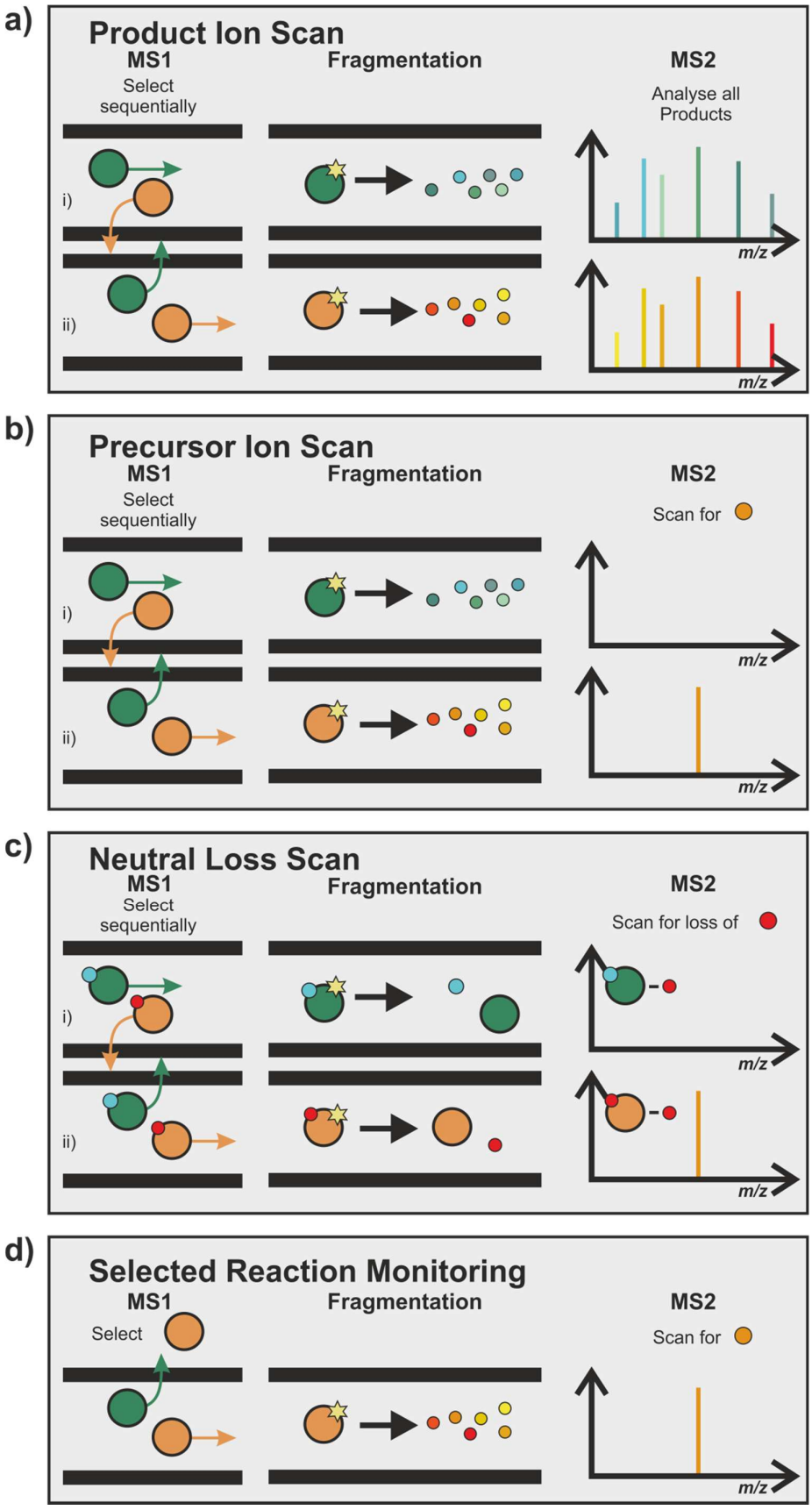
a)
Product Ion Scan
MS1
Select sequentially
Fragmentation
MS2
Analyse all Products
i)
ii)
m/z
m/z
b)
Precursor Ion Scan
MS1
Select sequentially
Fragmentation
MS2
Scan for
i)
ii)
m/z
m/z
c)
Neutral Loss Scan
MS1
Select sequentially
Fragmentation
MS2
Scan for loss of
i)
ii)
m/z
m/z
d)
Selected Reaction Monitoring
MS1
Select
Fragmentation
MS2
Scan for
m/z

Figure 1-16 – Tandem MS (MS/MS) methods. a) Product ion scan selects each precursor sequentially, fragments and analyses all products. This method is commonly used for de novo identification of peptides and small molecules. b) Precursor ion scan selects each precursor sequentially, fragments and selects a specific fragment ion. This method is commonly used for identification of precursors with a specific group or PTM. c) Neutral loss scan selects each precursor, fragments and then selects the fragment with m/z equal to the precursor with a loss of a specific mass. Like the precursor ion scan, this method is commonly used for identification of precursors with a specific group or PTM. d) Selected reaction monitoring selects a specific precursor, fragments and selects a specific fragment. This method is commonly used for targeted identification of a specific species in a complex mixture, such as in quantitative proteomic experiments.

These methods described above and displayed below (Figure 1-16) are designed for use in triple-quadrupole instruments[121-122], which feature three consecutive quadrupole mass analysers and are commonly used in MS/MS experiments on small molecules and peptides using the middle quadrupole as a collision cell[121-122]. Q-ToF instruments such as the Waters Synapt (Figure 1-11) instruments are capable of performing such experiments. These instruments are used in work shown in this thesis to perform bottom-up sequencing of purified proteins using a product-ion scan method (Chapter 4) and by others elsewhere for the same and for targeted proteomic analysis of complex mixtures of biomolecules[123-125].

These methods can be used in conjunction with chromatography methods (such as liquid chromatography (LC), described later) for further separation of components of a complex mixture.

1.6.6.1 Fragmentation Methods

Gas phase fragmentation of analyte ions has many uses in MS experiments, as described previously. Two commonly used methods for peptide fragmentation are collision induced dissociation (CID) and electron transfer/capture dissociation (ETD/ECD). CID[81, 126-127] involves accelerating analyte ions into a gas filled region of the instrument. Collisions with the neutral buffer gas (e.g. Argon, Helium, N_2) result in an exchange of the ion's kinetic energy into internal thermal and vibrational energy. CID fragmentation is an ergodic process, allowing dissipation of internal energy across the molecule and breakage of the weakest bonds. For peptides, this the amide bond of the peptide backbone, cleavage of which results in the generation of *b* and *y* ions (Figure 1-17). CID is commonly employed as a fragmentation method due its well-understood fragmentation pathways and relative simplicity in instrumentation. There are, however, drawbacks in using CID as a fragmentation method for protein and peptide sequencing. The ergodic nature of CID results in an effective upper limit in mass of analyte ions that can be fragmented. Also, activation of peptides results in a disruption of the random distribution of charge across the peptide backbone, meaning charge drawing groups (such as phosphorylated Serine or Threonine or consecutive basic residues) disrupt peptide backbone fragmentation at their positions[119, 128]. In addition, CID results in "scrambling" in deuterium labelled peptides[129-130], where labile hydrogen atoms of the peptide backbone are able to exchange in the gas phase and limit hydrogen-deuterium-exchange (HDX)-MS analyses to the peptide level.

ETD/ECD fragments peptides and proteins by collision of the analyte with a reactive species[131-133]. Fragmentation by ETD/ECD is a non-ergodic process, resulting in fragmentation at the point of collision, fragmenting the peptide backbone at N-C_α bonds, generating *c* and *z* ions (Figure 1-17). Fragmentation is independent of analyte size and is highly useful in top-down proteomic experiments looking at surface exposed regions of whole proteins[134-137]. The nature of fragmentation by ETD/ECD allows sequencing of peptides without "scrambling" and is a useful technique for residue-level HDX-MS analyses of proteins[134, 138-139]. However, ETD/ECD fragments peptides at the position of a

charge, resulting in the elimination of this charge. As a result ETD/ECD can only be performed on multiply charged analytes[131-132].

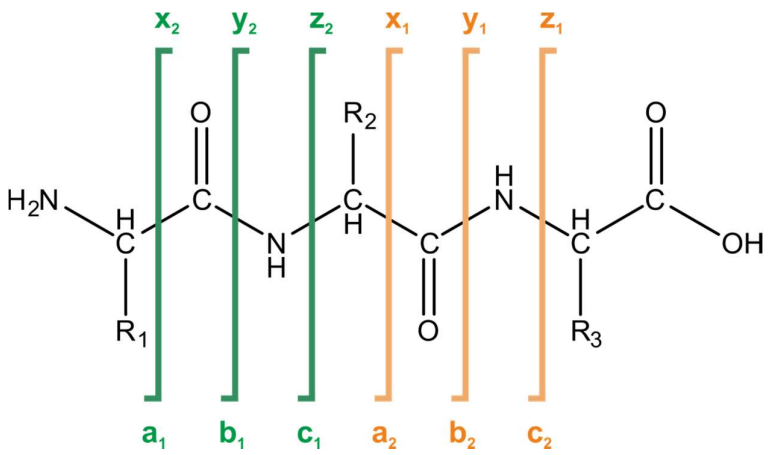

Figure 1-17 – Peptide fragment ion nomenclature. Following gas phase fragmentation, peptides can be broken at many positions on the peptide backbone. x, y and z ions represent charge retentions on the C-terminal fragments of peptides broken at the C-C_α, C-N and C_α-N bonds, respectively. a, b and c ions represent charge retention on the N-terminal counterparts to x, y and z ions, respectively. Fragmentation by CID and ETD typically produce b/y and c/z fragments, respectively.

1.6.7 Collisional activation to liberate MPs in the gas phase

MS analyses of native MPs are limited by the need to liberate MPs from surfactants in the gas phase before they can be observed. MPs in complex with detergent micelles or APols are highly disperse and result in observation of broad unresolved peaks in the mass spectrum. These complexes must be collisionally activated in the gas phase to mediate release of free MP prior to mass analysis (Figure 1-18)[140-142].

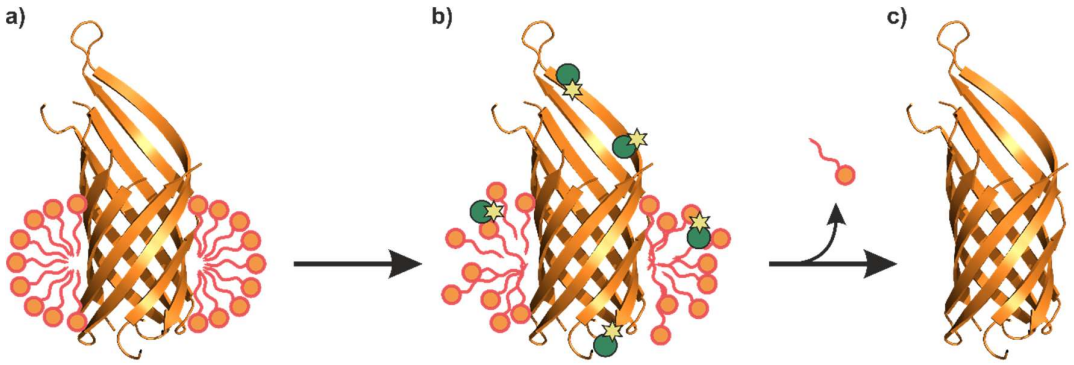

Figure 1-18 – Detergent-bound MPs must be liberated in the gas phase by collisional activation prior to observation. a) MP:detergent complexes are b) collisionally activated, resulting in an increase in internal energy and dissociation of detergent as a means of evaporative cooling. c) Liberated MPs can now be observed using MS.

In native MS work shown in this thesis, this is carried out in the Trap region of the drift cell of a Synapt G1 HDMS, prior to TWIMS analysis in the ion mobility region of the drift cell and *m/z* analysis by the ToF analyser.

1.6.8 Application of Native MS methods to MPs

Since the first analyses of native proteins by MS using ESI[87, 91], delivering native water-soluble proteins into the gas phase has become fairly routine with the development of nESI and MS instruments with increasing *m/z* range and resolution. MS (particularly in combination with IMS) can be used routinely to study protein structure (including MPs) and resolve the conformation(s) of proteins, identify oligomeric states of proteins and the presence and impact of non-covalent protein-protein and protein-ligand interactions[92-93, 106-107, 109, 111, 143-145]. Observation of native MPs by MS has also developed since the first native MS experiments of water-soluble proteins, although at a slower pace as a result of the

conditions required for solubilisation of MPs and the need for liberation of MPs from complexes with surfactant in a native-like state.

Despite this, a number of native MPs and MP complexes have been observed using MS. Detergent micelles have been the gold-standard for delivering MPs in the gas phase and have yielded a great deal of success[140, 146-147]. Early native MS experiments with detergent-solubilised MPs yielded mass spectra of a homotrimer of microsomal glutathione transferase-1 (MGST1) and monomeric EmrE bound to detergent and ligand molecules at low charge states[146, 148]. This continued with observation of heteromeric MP complexes such as $BtuC_2D_2$[140] and large ATPase complexes[16-17]. Determination of topology has also been achieved by ejection of subunits with further collisional activation by CID[16-17], observation of MacB and LmrCD ABC transporter complexes and trimeric MexB[149] and observation of cross-linked stabilised $BtuC_2D_2$ using MALDI[84]. nESI-IMS-MS allowed determination of CCS values of MP complexes $KirBac_{3.1}$ and $BtuC_2D_2$[150] and identified mechanisms of partial opening of a mechanosensitive pore protein, MscL[151]. In this particular instance, heteropentamers of Cys mutants of MscL were treated with the bulky thiol-reactive MTSET and found to have graded opening and distinct CCS values by IMS that correlate to incorporation of more MTSET labelled monomers[151]. Specific binding of lipids has been shown to modulate and stabilise MP complexes[152-155].

MD and nESI-IMS-MS have been used to prove the nature of MP:detergent complexes and how interaction and dissociation of detergent molecules impacts the gas phase structure of MPs[118, 156-158]. Under high temperature conditions, MD shows DPC and DHPC detergents undergo micelle inversion and mediate destabilisation of MP structure where DDM micelles maintain their orientation and protect MPs[158]. Dissociation of detergent molecules from PagP in the gas phase was found to exhibit a form of evaporative cooling on MP structure resulting in better stabilisation of PagP in the gas phase[118].

Detergent micelles have proven highly useful for delivering native-like MPs and MP complexes into the gas phase but others have begun to explore the possibility of solubilising media that may provide a more native like environment, such as bicelles, nanodiscs and APols[53, 75, 159]. A comparative analysis of DgkA trimer from a

number of solubilising media, showed that this MP was readily observed by nESI-MS from DHPC-DMPC bicelles and DMPC nanodiscs, partially from A8-35 APol and not at all from DDM micelles, showing that methods of solubilising MPs for MS, other than detergent micelles, can achieve good results[159]. APols have been shown in a number of instances to reliably deliver native MPs instances to the gas phase as shown by observation of BR from NAPol and intact cytochrome b_6f from A8-35 using MALDI-ToF analysis[63]. A8-35 APol was also used to observe native conformations of β-barrel OMPs, OmpT and PagP, and validate their native state using nESI-IMS-MS to calculate CCS values correlating with theoretical vales calculated from crystal structures[75].

1.6.9 Liquid Chromatography-MS (LC-MS)

Liquid Chromatography (LC) is commonly used for separation, identification and quantification of components in a complex solution[81]. This is achieved by passing a sample over an adsorbent solid material (packed into an analytical column, known as the stationary phase) at high pressure. By running an appropriate solvent (known as the mobile phase) over the column (often over a gradient), sample components are separated by their relative affinity to the adsorbent material[81, 160].

Reverse-phase High Performance Liqiud Chromatography (RP-HPLC) is most common for separation of proteins and peptides prior to MS analysis. RP-HPLC commonly requires running samples over a non-polar stationary phase (often silicon-bound alkyl chains) and elution from the column using a H_2O:acetonitrile (ACN) gradient (with formic or trifluoroacetic acid) mobile phase. This results in the most non-polar components being retained on the column longer, being the last eluted and analysed[160].

The eluent from LC instruments can be interfaced directly with a mass spectrometer using ESI. Low flow rate HPLC instruments such as the Waters nanoAcquity UPLC can be fitted to a nESI source[81].

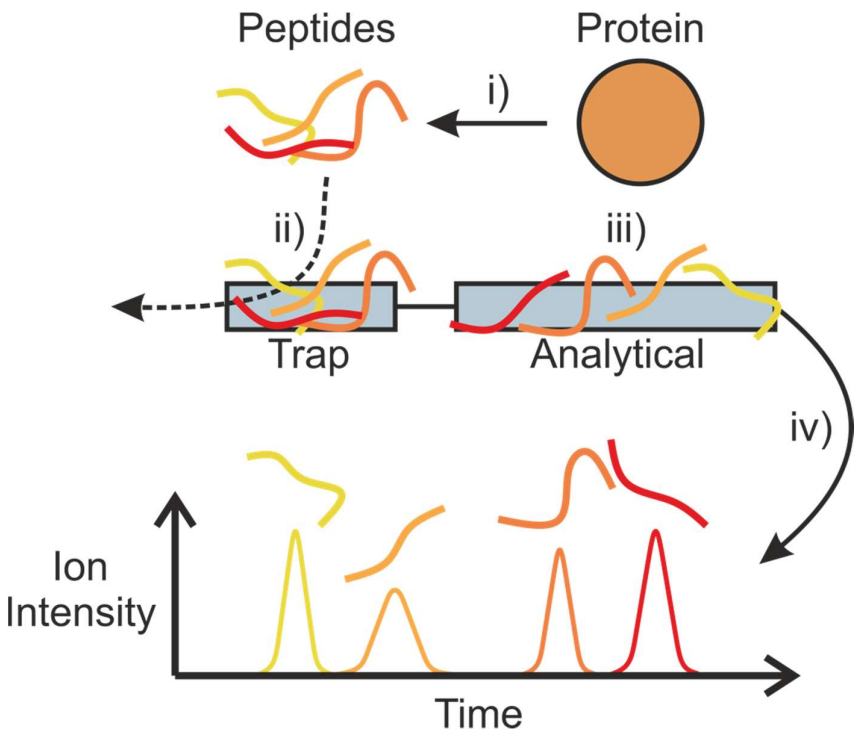

Figure 1-19 – Protein digest analysis by RP-HPLC-MS. i) Protein is enzymatically digested (commonly trypsin or pepsin) to generate a range of peptides. ii) Peptides are washed over a Trap column in a low-organic solvent for desalting and aligning for analytical separation. iii) Trap and Analytical columns (grey boxes) are aligned and mobile phase elutes peptides over the analytical column. This is achieved by an increasing organic mobile phase (H_2O:ACN gradient), resulting in the elution of the least non-polar peptides (yellow) first and the most non-polar peptides (red) last. iv) HPLC feeds eluent directly into a mass spectrometer using ESI for subsequent MS or MS/MS analysis.

Two methods of LC-MS/MS analysis have been used in work shown here. Data-dependent acquisition (DDA)[161] uses a Product Ion Scan in combination with RP-HPLC to provide high quality protein sequencing, peptide mapping and identification of chemical modifications. On a Waters Synapt instrument, the most intense ions in each precursor scan are selected sequentially using the quadrupole, fragmented in the Trap and the products are analysed using the ToF analyser. Peptide fragment spectra can be analysed to determine the sequence and the location of modifications. MS/MS method parameters can be tuned to select ions of specific charge states, include/exclude specific *m/z*, set threshold intensities for selection and set dynamic exclusions times (after selection and analysis of a particular *m/z*, the instrument will not select it again for a determined period of time). This method provides high quality qualitative data informing on the protein

sequence and location of chemical modification but is limited in its quantitative power as a result of non-continuous acquisition.

MS^{e}[162] is an alternate method of LC-MS/MS analysis used in work shown here (Figure 1-20). Rather than selecting precursors, all eluting precursors are analysed simultaneously. The instrument constantly switches between a low and high energy setting. In high energy setting, all eluting species are activated, fragmented and analysed. This allows for more reliable quantitation as a result of the continuous acquisition of the precursor, but results in much more complex data. MS^{e} data analysis requires product ions to be assigned to their respective precursor ion using their respective elution profiles.

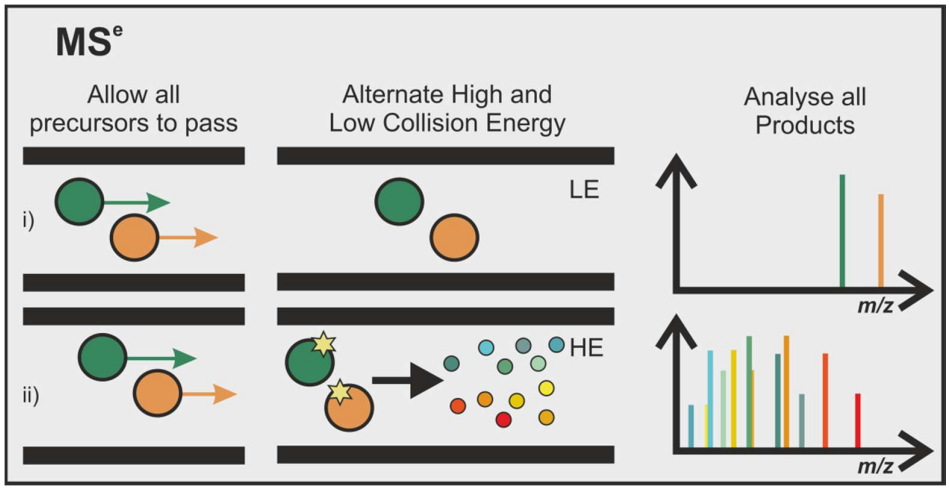

Figure 1-20 – MS^{e} MS/MS method. Precursors are all transmitted and fragmented simultaneously and all product ions are analysed. The instrument switches between a i) low and ii) high energy conditions, resulting in precursor and product spectra, respectively. Product ions are aligned with and assigned to their respective precursor, based on their retention time.

1.7 Fast Photochemical Oxidation of Proteins (FPOP)

To investigate changes at an amino acid residue level, chemical labelling techniques are now being used. FPOP[163-166] is a novel method for labelling reactive amino acid side chains in solvent accessible regions of proteins. Proteins are labelled by hydroxyl radicals generated by photolysis of H_2O_2. Protein is irradiated by a pulsed laser (248 nm) in the presence of H_2O_2 and an excess of a scavenger molecule (normally Gln or His) whilst flowing through a capillary (Figure 1-21). Laser pulse frequency and duration, width of the irradiation window and capillary flow rate are controlled to ensure each bolus of protein containing solution receives a single exposure to UV irradiation, whilst the presence of excess scavenger limits the lifetime of generated OH radicals to ~1 μs[166]. The short lifetime of OH radicals results in labelling faster than protein folding/unfolding events and does not allow diffusion to dynamic or less-solvent accessible regions of a protein[164, 166].

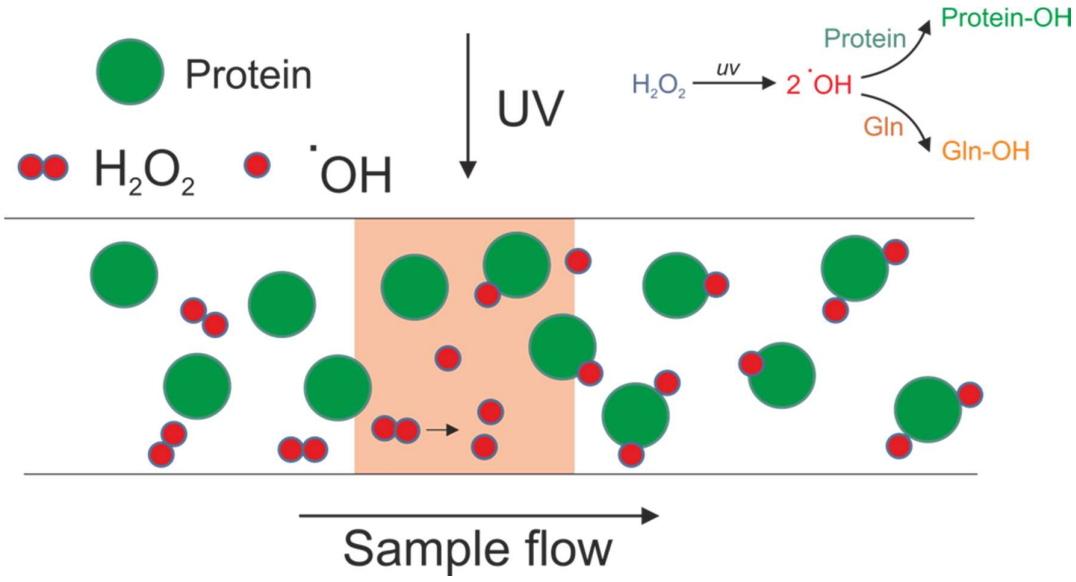

Figure 1-21 – Fast Photochemical Oxidation of Proteins (FPOP). Protein sample is flowed through a capillary in the presence of H_2O_2 and a radical scavenger (often Gln or His). UV irradiation results in photolysis of H_2O_2, generating OH radicals, which react with solvent accessible side chains. In the presence of an excess of radical scavenger, the lifetime of OH radicals is ~1 μs. Control of sample flow rate, capillary dimensions, UV pulse rate, UV pulse duration and irradiation window width means the sample is only exposed to a single dose of OH radicals.

FPOP results in covalent modifications that are readily detected by MS and MS/MS methods[163-164, 167-168]. The irreversible nature of the modification allows for rigorous and varied workup for MS and MS/MS analyses, where other labelling methods such as HDX require very specific analysis conditions. Using MS/MS, modifications can be localised to the peptide or residue level by observation of characteristic mass additions, of which +16 Da is the most common[164-166, 169]. Figure 1-22 shows representative spectra of a peptide (Angiotensin II, AngII) before and after treatment by FPOP and the addition of up to three hydroxyl oxidative modifications. These mass additions can be localised to any residue side chain but there is a spread in the degree of reactivity of different side chains with OH radicals, with sulphur-containing (Cys and Met) and aromatic (Trp, Tyr, Phe and His) residues reacting more readily[165].

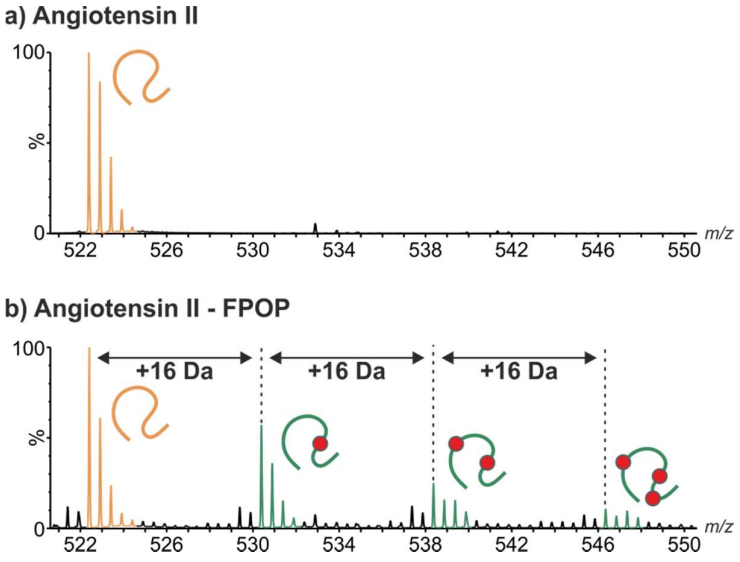

Figure 1-22 – Observation of FPOP oxidation by MS. MS is particularly suited to observation of oxidation by FPOP, as evidenced by observation of one or many additions of 16 Da. a) Prior to FPOP, angiotensin II is observed as a single species (orange, $AngII^{2+}$, m/z of 522.3). b) After FPOP, then unmodified angiotensin II (orange, m/z of 522.3) is observed, as well as a series of peaks representing the addition of 16 Da (difference of 8 m/z represents a 16 Da mass difference in a doubly charged peptide).

1.7.1 Applications of FPOP

FPOP is dependent on specific instrumentation and, as a result, studies using FPOP have been exploring the potential applications and improving methods. This has included details about OH radical dosimetry[170], radical lifetime[164, 171], labelling of

proteins *in vivo*[172], mixing methods[168, 173] and data analysis and quantitation[163, 174]. FPOP has been used to identify interaction sites in protein-protein interactions[167, 175] and protein folding intermediates[169, 176].

With respect to MPs, application of FPOP has been used to map regions of solvent accessibility as evidenced by labelling of Cys and Met residues, including structural transitions in BR and the Glycerol Facilitator (GF)[177-178] and with improved accuracy in the region of interest using site-directed mutagenesis[179]. More recently, FPOP has been used as a method for quantifying the folded state of the Cystic Fibrosis Transmembrane Conductance Regulator (CFTR) *in vivo* by observing loss in oxidation intensity in structural marker peptides[174] and mapping the topology of the Light Harvesting Complex (LHC) reconstituted into a lipid nanodisc[180].

1.8 Hydrogen Deuterium Exchange (HDX) – Mass Spectrometry

Hydrogen Deuterium Exchange (HDX) is a labelling technique commonly used in conjunction with mass spectrometry. HDX with MS is comparatively new compared with its use with infrared and UV-spectroscopy, neutron scattering and NMR, with HDX-MS shortly following the first use of ESI to analyse the conformational state of proteins[181-184]. HDX-MS provides a number of benefits over other HDX techniques including low detection limits (as a result of the large dynamic range of MS), reduced sample consumption and the study of complex mixtures[181].

Solution phase HDX experiments are commonly used to probe the structural and dynamic properties of proteins[136, 181-183, 185-186]. They measure the degree and rate of incorporation of deuterons into the peptide backbone at amide N atoms following immersion in a D_2O solvent environment. Before hydrogens can exchange, the peptide backbone must be in a solvent-exposed and "unfolded-like" state and hence deuterium incorporation is related to dynamics of the protein backbone. When in an unprotected state, incorporation is dependent on the intrinsic rate of exchange (k_2, Equation 1-8), which is dependent on the residues either side of the peptide bond. In folded proteins, observed exchange rates (k_{ex}) of

peptide backbone hydrogens are reduced as a result of hydrogen bonding and the burial of residues within protein structure excluding them from solvent exposure[181, 183, 185-186],. In this instance, the rate of exchange is dependent on the both the intrinsic exchange rate (k_2) and folding and unfolding rates (k_{-1} and k_1, respectively, Equation 1-8).

$$F_H \underset{k_{-1}}{\overset{k_1}{\rightleftharpoons}} U_H \xrightarrow{k_2} U_D \underset{k_1}{\overset{k_{-1}}{\rightleftharpoons}} F_D$$

Equation 1-8 – Rate of hydrogen exchange at the peptide backbone from an unfolded state is dependent on the rate constants of folding (k_{-1}), unfolding (k_1) and intrinsic rate of hydrogen exchange (k_2). F_H and U_H represent the folded and unfolded states of the hydrogenated forms of a protein, respectively , and F_D and U_D represent the folded and unfolded states of the deuterated form of a protein, respectively.

HDX occurs through one of two mechanisms, EX1 and EX2[181-183]. EX1 kinetics describe exchange when the rate constant of exchange is much faster than the rate constant of folding ($k_2 >> k_{-1}$, Equation 1-9), and results in complete exchange following unfolding and is observed in regions of the peptide backbone that undergo slow, large scale movements and in fully unfolded proteins.

$$k_{ex} = k_1$$

Equation 1-9 –EX1 exchange kinetics. When the rate of exchange (k_2) is much faster than the rate of folding (k_{-1}), rate of exchange (k_{ex}) is dependent only on the rate constant of unfolding (k_1).

EX2 exchange kinetics are observed in regions where small, transient fluctuations in protein structure occur, where the rate consant of exchange is slower than the rate constant of return to a protected, hydrogen bonded state. In folded proteins, EX2 kinetics are more commonly observed than EX1 kinetics[181, 183, 186].

$$k_{ex} = \frac{k_1}{k_{-1}} k_2 = K_{unf} k_2$$

Equation 1-10 – EX2 exchange kinetics. When the rate of exchange (k_2) is much slower than the rate of folding (k_{-1}), the rate of exchange (k_{ex}) is dependent on the equilibrium constant of protein folding (K_{unf}) and intrinsic exchange rate (k_2).

Native exchange rates of amide hydrogens are pH sensitive. At neutral pH, exchange occurs primarily through a base catalysed exchange mechanism, where OD^- abstracts a proton from the amide nitrogen and then the basic amide abstracts a deuteron from D_3O^+ [183, 185, 187-188]. As a result of this, the rate of hydrogen exchange is reduced with decreasing pH (therefore reduced [OD^-]) until a pH-exchange rate minimum. At this point, a further decrease in pH (and increased [H^+]) drives an acid-catalysed exchange mechanism (Equation 1-11, Figure 1-23)[181, 183, 185]. The pH-exchange rate minimum value is typically between pH 3-5 and is dependent on the protein/peptide primary structure and buffer components (Figure 1-23)[189-191]. For this reason HDX experiments are quenched by reducing the pH, to a point where the intrinsic exchange rates are lowest, in order to prevent back-exchange during the analysis.

$$A - H + OD^- \longrightarrow A^- + H - OD$$
$$A^- + D_3O^+ \longrightarrow A - D + D_2O$$

Equation 1-11 – Base-dependent hydrogen exchange at amides. Deuteroxide (OD^-) abstracts a protein from the protonated amide (A-H) forming a basic amide N (A^-) and H-OD. The basic amide now abstracts a deuteron from deuteronium (D_3O^+) to form a deuterated amide and D_2O.

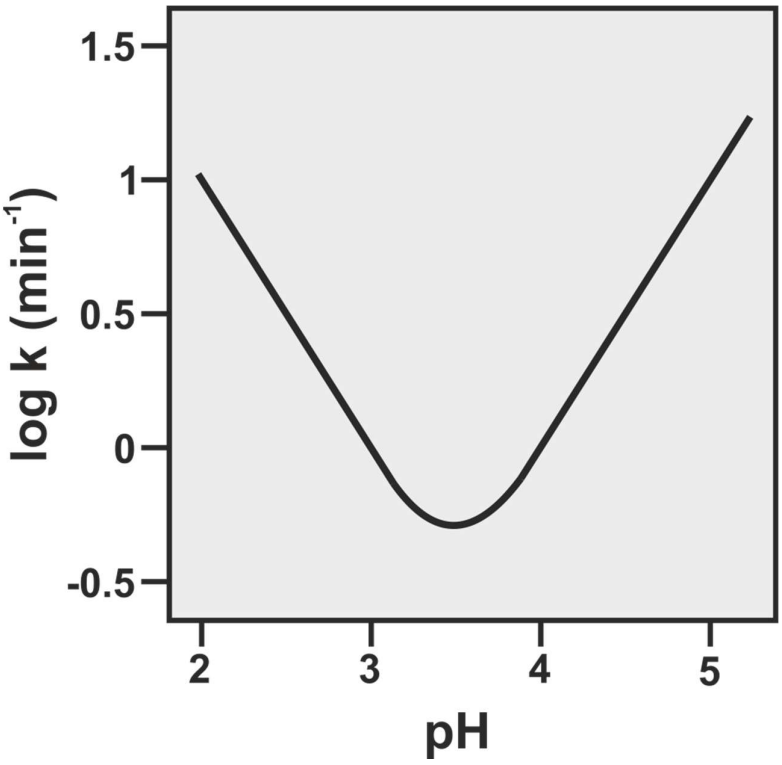

Figure 1-23 - Intrinsic rate of exchange of any labile proton/deuteron is dependent on pH. Minimum rate of exchange is at ~pH 3 with increasing rate of exchange toward neutral and strongly acidic pH. pH-logk relationship is linear, as exchange is dependent on [H⁺]. This graph shows representative data based on data show in the thesis of J.P.Hodkinson, University of Leeds, 2009.

Regions of a protein that undergo HDX by EX1 and EX2 kinetics can be distinguished by peptides with distinctive spectra when analysed by MS (Figure 1-24). ESI mass spectra of peptides that undergo exchange by EX1 kinetics have a bimodal distribution as a result of full exchange when a region has become solvent accessible (Figure 1-24a). Peptides that undergo exchange by EX2 kinetics are only partially exchanged between unfolding and folding events and the resultant mass spectra have a more continuous distribution (Figure 1-24b).

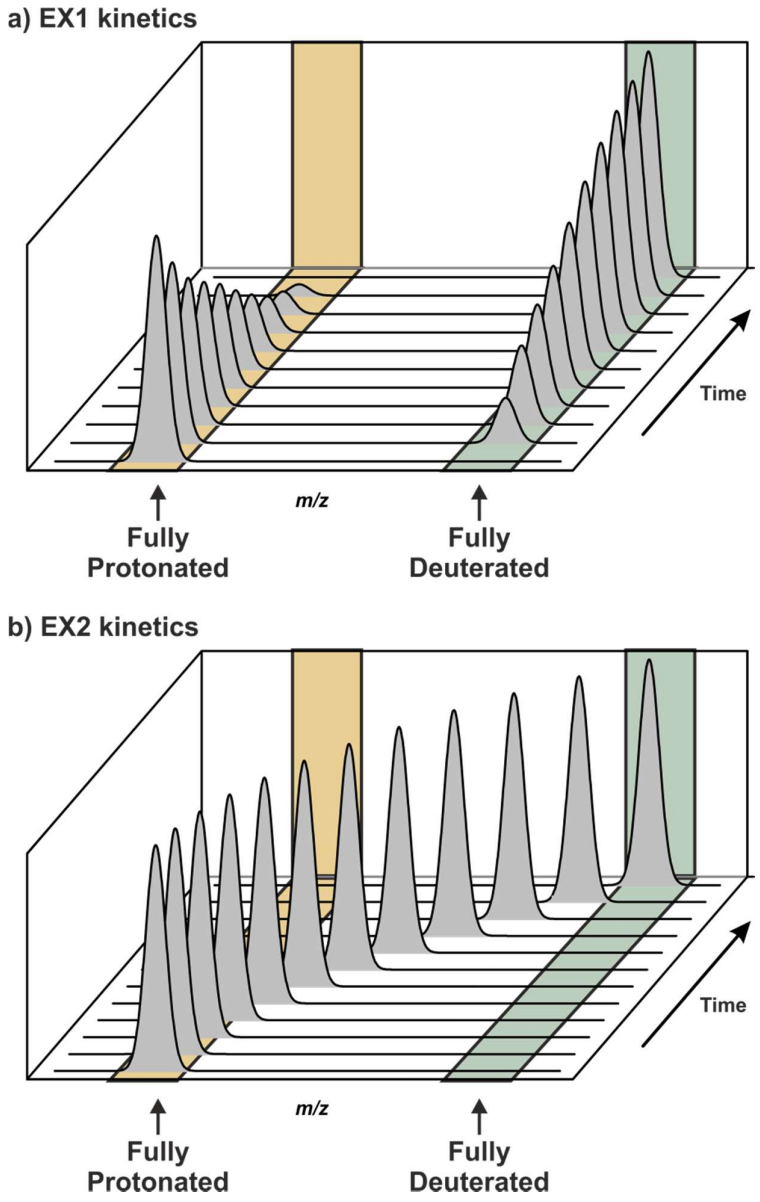

Figure 1-24 – Regions of a protein undergo hydrogen exchange through either a) EX1 or b) EX2 kinetics. a) Protons in regions that undergo slow folding events (rate of exchange is far greater folding rate) are fully exchanged following an unfolding/opening event (EX1) and result in bimodal mass spectra that represent the proportion of peptides that have populated the unfolded/open conformation. b) Protons in regions of proteins that undergo fast folding events (similar to or faster than the rate of exchange) are only partially exchanged following an unfolding/opening event (EX2) and result in mass spectra that show a continuum of m/z peaks. Fully protonated (orange) and deuterated (green) states are indicated below each of the spectra.

Two different methods of HDX-MS can be used[183, 186]. Pulsed labelling experiments (Figure 1-25a) involve periodically labelling a refolding or unfolding protein with D_2O for a short time to observe the degree of uptake of deuterium at different

points along the folding/unfolding timecourse[186]. Continuous labelling (Figure 1-25b) experiments involve dilution of a protein in equilibrium into D_2O for a range of incubation times and observing the rate of deuterium uptake[181]. Both of these methods allow for global (intact protein) and local (digested protein) analyses and can be used to inform on the rates and mechanisms of folding pathways and the equilibrium dynamics, respectively.

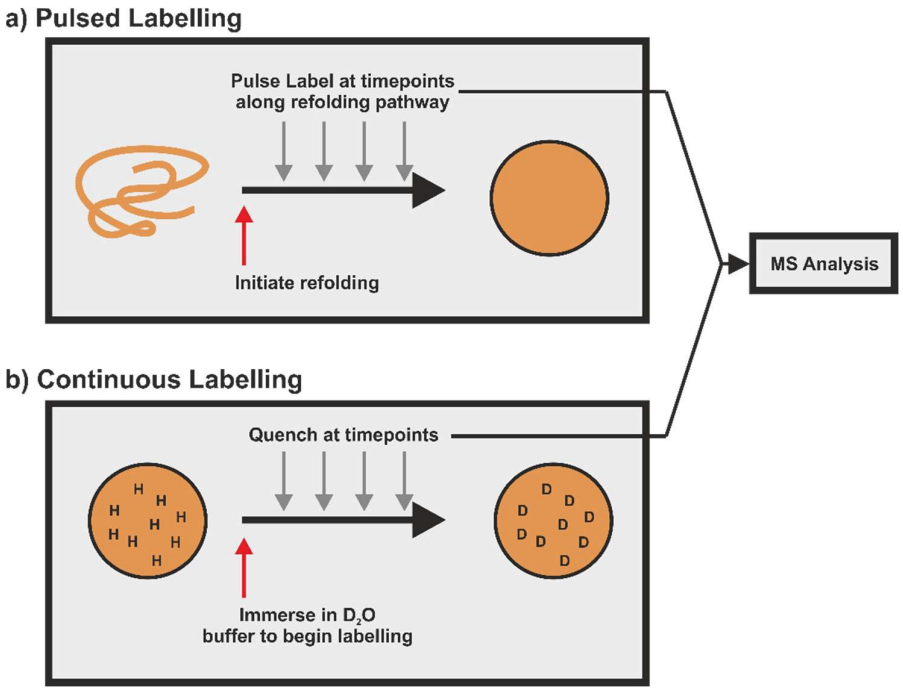

Figure 1-25 – a) Pulsed and b) continuous labelling HDX experiments allow for observation of the exchange kinetics of a refolding/unfolding protein or a protein in equilibrium, respectively. a) Pulsed labelling entails initiating the refolding or unfolding of a protein and at various timepoints, labelling with a short D_2O pulse (often 12 µs) and immediately quenching and analysing the extent of exchange using MS analysis. b) Continuous labelling begins with D_2O labelling and quenching the exchange at various timepoints and analysing.

Analysis by HDX-MS is dependent on certain conditions as a result of the necessity for rapid analysis in low pH conditions. Labelled proteins are kept on ice after low pH quenching and digested using acid-stable pepsin before LC-MS/MS analysis using low pH mobile phase[181-183, 192]. Modern instrumentation now allows for HDX analysis with on-line pepsin digests and temperature controlled chromatography in order to minimise back exchange[181, 192].

HDX-MS/MS allows analysis of protein structure and dynamics to a peptide level with the use of CID for peptide sequencing[182-183, 186]. Residue-level resolution is limited due to the previously mentioned "scrambling" effect redistributing amide hydrogen/deuterons across the backbone[129]. A pseudo-residue level analysis can be afforded by analysis of overlapping, redundant peptides resulting from the non-specific pepsin digest. Recently, HDX-MS/MS using ETD has been able to analyse HDX-labelled proteins to the residue level[134, 138].

1.8.1 Studies on MPs using HDX-MS

When applied to MPs, HDX-MS is used primarily to determine the dynamics of proteins to a peptide level in their "resting" state and the influence of the MP's environment and interacting partners on dynamics and solvent exposure. The GF is shown to have a highly flexible TM helix and loop region that harbours residues involved in the selectivity filter[178]. Deuterium uptake in many peptides of BR occurs at a greater rate and to a greater extent when in its more flexible, active light–treated form[193]. BmrA shows a significant decrease in the degree of deuterium uptake in the cavity formed by the extended intracellular domains when in a closed conformation (maintained by a specific mutation in the intracellular domain) that greatly reduces solvent exposure of the cavity[194].

HDX-MS has been used to identify pH-dependent conformations of Diptheria T toxin. At neutral pH, the toxin is in its native state, at pH 6 it begins to unfold with the N- and C-terminal domains separating and exposing a hydrophobic hairpin. At pH 5.5, the hairpin is fully exposed, preparing it for embedding in to the membrane[195].

Retinal binding to rhodopsin was shown to decrease the half-life of deuterium uptake in extracellular facing His residues and increase uptake half-life in cytoplasmic facing His residues[196]. ADP/ATP carrier protein was shown to have differential uptake in the deeper regions of the cavity following binding of inhibitors that have been used to maintain different conformations of the protein in crystal structures, with observations in both detergent micelles[197] and in mitochondrial membranes[198]. Binding of partial agonist carazolol to $\beta_2$adrenergic

GPCR (β_2AR) resulted in increased uptake in a number of regions of the protein as a result of increased flexibility[199].

HDX-MS has also been used to explore the refolding mechanism of BR and identify that a large number of secondary structure elements are formed relatively late on in the refolding pathway as evidenced by lack of protection during pulse labelling experiments and that retinal is mediating a shift in the core of the protein after formation of late intermediate[200].

To date, only one study on β_2AR has compared the effect of solubilising media on MPs using HDX-MS and found no significant differences in the properties when solubilised in bicelles or detergent micelles. Although, they do not directly compare MP structure and dynamics in different native-like solubilising media, the previously mentioned studies on the ADP/ATP carrier protein described similar behaviour in both detergent micelles and in mitochondrial membranes[197-198].

1.9 Aim of the Thesis

Given the interest in MP structure and the inherent difficulties in studying these hydrophobic proteins, new methods are needed, with respect to instrumentation and technical methods and regarding methods for solubilising MPs in a stable native state.

It has been shown above that native MS has promise for observing native MPs in the gas phase but predominantly from detergent micelles, which are known to destabilise MP structure during the ionisation and release processes. Introduction of new surfactants such as bicelles, nanodiscs and APols have presented opportunities to improve on detergent micelles and this work explores the use of APols for MS-based study of MPs, furthering on work of Leney at al. and definitively verifying the delivery of native-like MPs into the gas phase by APols[75].

In addition to studying the structure and function of MPs at the intact protein level, FPOP and HDX-MS have been used to probe MP structure, dynamics and identification of interaction sites at the residue and peptide level. This makes them valuable techniques for work probing the nature of interaction of MPs with APols and detergent micelles, which have been posited to mediate differences in

structure and stability of MPs[33, 58, 60], which can also subsequently be observed using native MS, FPOP and HDX-MS.

This thesis aims to explore the optimum conditions for solubilisation of MPs using APols, investigate the potential of APols for delivering native-like MPs into the gas phase for nESI-IMS-MS analysis and how the properties of a range of APols can benefit or hinder these analyses (Chapter 3). In addition to this, FPOP-LC-MS (Chapter 4) and HDX-MS (Chapter 5) are used to probe the mechanism by which APols protect MPs from aggregation and unfolding.

2 Materials and Methods

2.1 Materials

A8-35, LDAO, DDM and β-octyl-glucoside (β-OG) were purchased from Anatrace/Generon Ltd., Herts., UK). A8-75 and SAPol were provided by Prof Jean-Luc Popot and Dr. Manuela Zoonens (Institut de Biologie Physico-Chimique, CNRS/Université Paris, France), A34-35 and A34-75 were provided by Professor Christophe Tribet (Ecole Normale Supérieure de Paris, Départment de Chimie, France) and NAPol was provided by Professor Grégory Durand (Université d'Avignon et des Pays du Vaucluse, France). Unless stated otherwise, all other materials were purchased from Sigma-Aldrich Company Ltd., Dorset, UK.

tOmpA expression plasmid was kindly provided by Prof Karen Fleming (John Hopkins University, Baltimore, MD, USA). All other OMP expression vectors were developed in-house by Dr Alice Bartlett and Dr Lindsay McMorran, University of Leeds.

2.2 OMP expression and purification

2.2.1 Constructs

Two OmpT constructs are used in the following work. Both are lacking the outer membrane targeting signal sequence. Untagged OmpT (Table 2-1) is used for all experiments involving direct refold into A8-35 (data shown under headings 3.1.1 – 3.1.3). N-terminally His-tagged OmpT ($OmpT_{HT}$) (Table 2-1) is used for all subsequent work, involving refolding into detergent micelles and subsequent exchange into APols (data shown under headings 3.1.4 and onwards).

tOmpA (Table 2-1) is the N-terminal β-barrel region (residues 1-171) of the full length OmpA protein, lacking the outer membrane signal sequence. PagP (Table 2-1) has a C-terminal His_6-tag and lacks the outer membrane signal sequence.

Protein	Vector	Residues (Incl. Met)	M_W (Incl. Met) (Da)	Extinction Coefficient ($M^{-1}.cm^{-1}$)
OmpT	pET11a	298	33609	78270
$OmpT_{HT}$	pET11a	311	35284	76790
PagP	pET11a	168	19933	82390
tOmpA	pET11a	172	18875	46870

Table 2-1 – Residue numbers, molecular weights, extinction coefficients and expression vectors for constructs used in work presented in this thesis.

2.2.2 Overexpression of OMPs as inclusion bodies

1 µl (100ng) of the appropriate pET11a expression vector containing the respective OMP gene was transformed into 50 µl of BL21 (DE3) competent cells (New England Biolabs, Herts., UK) by incubation on ice for 30 mins followed by a 45 sec heat shock at 42 ^oC. After addition of 450µl sterile LB media (25 $g.L^{-1}$ lysogeny broth (LB) (Millipore, Abingdon, UK)), transformed cells were incubated at 37 ^oC for 1 hour and then loaded onto LB-agar plates (25 $g.L^{-1}$ LB and 15 $g.L^{-1}$ agar) supplemented with 100 $\mu g.ml^{-1}$ carbenicillin (Formedium, Norfolk, UK) and further incubated at 37 ^oC for 16 hours. Single colonies were used to innoculate 5 ml sterile LB cultures grown overnight with shaking at 37 ^oC. Overnight cultures were added to 500 ml of prewarmed (37 ^oC) LB media with 100 $\mu g.ml^{-1}$ carbenicillin and grown to an OD_{600} of 0.6, at which point 1mM isopropyl-β-D-1-thiogalactopyranoside (IPTG) was added to induce OMP expression as inclusion bodies. After 4 hours, cells were pelleted by centrifugation at 5,000 x *g* at 4^oC for 20 mins, collected and stored at -20^oC until required.

2.2.3 Isolation of inclusion bodies

Pelleted cells were resuspended in 20 ml of 25 mM tris.HCl pH 8.0 containing 1 mM phenylmethylsulphonyl fluoride (PMSF) and 2 mM benzamidine and lysed by 6 rounds of 1 min sonication (on ice) with 1 min rest. Lysate was pelleted (20 mins, 25,000 x *g*, 4 ^{o}C) and resuspended in 25 mM tris.HCl pH 8.0 containing 2% (*w/v*) Triton X-100 (Calbiochem, UK) and pelleted (as previously) to retain soluble protein and remove residual membrane components. Inclusion bodies were washed by 2 rounds of resuspension in 25 mM tris.HCl pH 8.0 and pelleting (as previously).

2.2.4 Purification of denatured OMPs

2.2.4.1 Ni^{2+}-affinity purification of $OmpT_{HT}$ and PagP

$OmpT_{HT}$ and PagP (His_6-tagged) were resolubilised in 25 mM tris.HCl pH 8.0 containing 6M guanidine.HCl and loaded onto a 5 ml HisTrap column (GE Healthcare, Amersham, Bucks., UK). The column was washed with 25 mM tris.HCl pH 8.0 containing 6M guanidine.HCl and 20mM imidazole before the protein was eluted with a linear imidazole gradient (20-250 mM over 50 ml). Ni^{2+}-affinity purified $OmpT_{HT}$ and PagP were further purified by SEC (see below).

2.2.4.2 Size exclusion chromatography (SEC) purification of OMPs

OMPs solubilised in 25 mM tris.HCl pH 8.0 containing 6M guanidine.HCl were filtered using a 0.45 μm syringe filter (Millipore, Abingdon, UK) and loaded onto a 26/300 Superdex75 gel filtration column (pre-equilibrated with 2 column volumes of 25 mM tris.HCl pH 8.0 containing 6M guanidine.HCl) (GE Healthcare, Amersham, Bucks., UK). Protein was eluted at a flow rate of 2 ml.min^{-1} and 2.5 ml fractions were collected after the 90 ml void volume. OMP-containing fractions (determined using SDS-PAGE) were pooled, concentrated (to ~600 μM) and stored at -80 ^{o}C.

Data below (Figure 2-1) shows OMPs to be pure and ready for refolding.

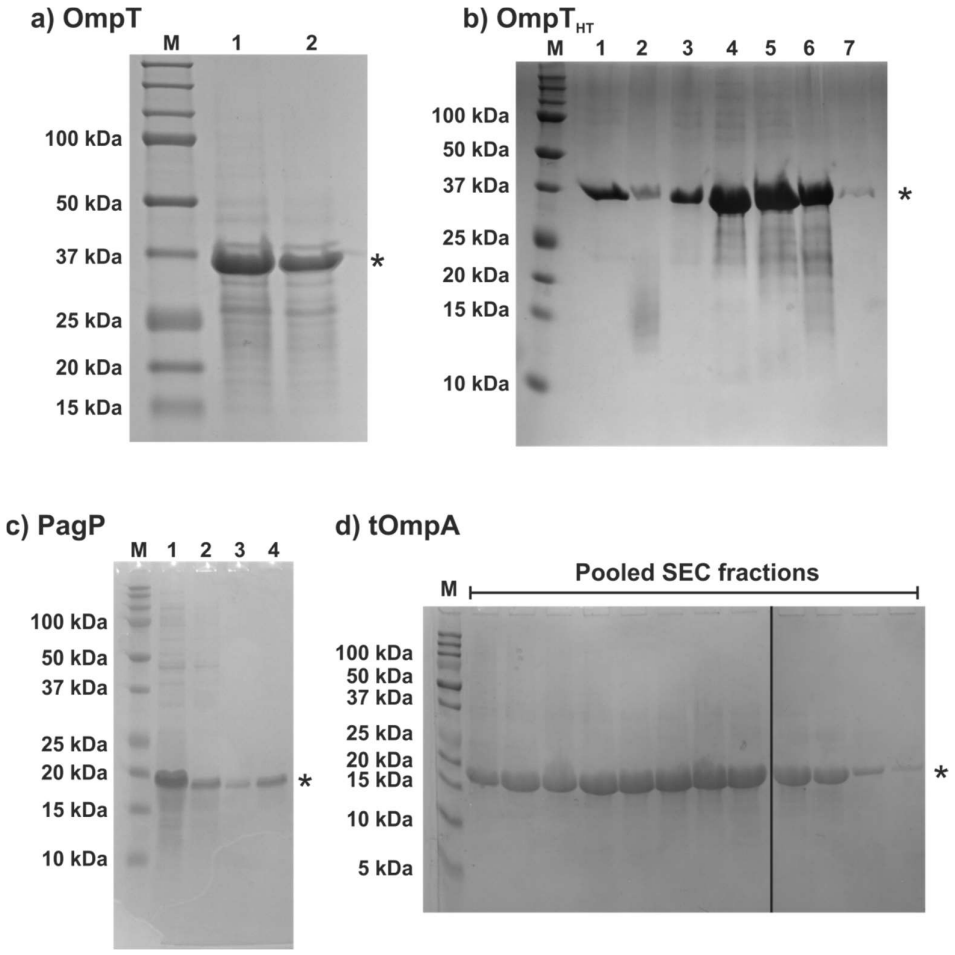

Figure 2-1 – SDS-PAGE shows high purity of a) OmpT b) OmpT$_{HT}$, c) PagP and d) tOmpA. In all instances, target proteins are indicated by an asterisk (*) and protein mass marker lanes are labelled (M). a) OmpT lanes marked 1 and 2 represent OmpT following inclusion body isolation and SEC, respectively. b) OmpT$_{HT}$ was purified using Ni^{2+} affinity purification and SEC purification. HisTrap column eluent is shown in lane 1 and pooled SEC fractions are shown in lanes 2-7. c) PagP lanes show inclusion bodies as isolated (1), and loaded onto a HisTrap column with some material remaining unbound (2), some material being eluted in a low imidazole (20 mM) wash step (3) and pure PagP being over a linear imidazole gradient (20-250 mM) (4). PagP was subsequently further purified using SEC (data not shown). d) Each lane represents a fraction of tOmpA eluted using SEC that was subsequently pooled. The black line represents joining of two concurrently stained PAGE gels.

2.3 OMP Refolding

2.3.1 Direct refolding of OmpT into A8-35 APol

50 µl of 100 mg.ml^{-1} A8-35 APol (5 mg) was added to 1 ml of OmpT (1 mg.ml^{-1}) solubilised in 100 mM ammonium bicarbonate pH 7.8 containing 8 M urea (MP Biomedicals via Fisher Scientific, Loughborough, UK). After 30 mins incubation, OmpT:A8-35 was dialysed against urea-free 100 mM ammonium bicarbonate pH 7.8 at 4 ^{o}C (Figure 2-2).

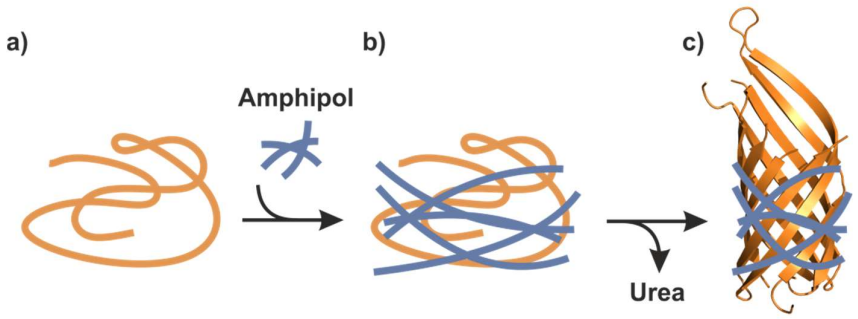

Figure 2-2 – OMPs can be folded directly into APol from a urea-denatured state. a) OMPs denatured in 8 M urea. b) Addition of A8-35 APol in a 1:5 OMP:APol ratio (w/w) results in the formation of a complex. c) Dialysis against a urea-free buffer (such as 100 mM ammonium bicarbonate pH 7.8) results in removal of urea and spontaneous refolding of OMPs into APol.

2.3.2 Refolding of OmpT and PagP into DDM micelles via LDAO micelles

1 ml of OmpT or PagP (5 mg.ml^{-1} in 25 mM tris.HCl pH 8.0 containing 6M guanidine.HCl) was added dropwise to 20 ml of 25 mM tris.HCl pH 8.0 containing 0.5 % (w/v) LDAO with rapid stirring and incubated overnight at 4 ^{o}C. LDAO-solubilised OMPs were loaded onto a 1 ml HisTrap column (GE Healthcare, Amersham, Bucks., UK), equilibrated 25 mM tris.HCl pH 8.0 containing 0.1 % (*w/v*) LDAO. 0.1 % (*w/v*) LDAO was then exchanged for 0.02% (*w/v*) DDM by a stepwise gradient (5 ml of LDAO (0.1 %):DDM (0.02 %) in a 80:20, 50:50, 20:80 and 0:100 ratio) and eluted with 25 mM tris.HCl pH 8.0 containing 0.02 % (*w/v*) DDM 250 mM imidazole. The final protein concentration (0.85-0.95 mg.ml^{-1}) was determined by measurement of absorbance at 280 nm following dilution into 25 mM tris.HCl pH 8.0 containing 6M guanidine.HCl (extinction coefficients in Table 2-1).

2.3.3 Refolding of tOmpA into β-OG micelles using heat shock

tOmpA (200 μM) in 25 mM tris.HCl pH 8.0 containing 6M guanidine.HCl was diluted 20-fold into 25 mM tris.HCl pH 8.0 containing 2.9 % (*w/v*) β-OG and incubated on ice for 30 mins. Refolding was initiated by heatshock (2 mins at 70 ^{o}C) and then the sample put on ice for 2 mins. Final protein concentration (0.85-0.95 mg.ml^{-1}) was determined by measurement of absorbance at 280 nm following dilution into 25 mM tris.HCl pH 8.0 containing 6M Guanidine.HCl (extinction coefficients in Table 2-1).

2.3.4 Exchanging detergent solubilised OMPs into APol

APol was added to detergent-solubilised OMPs in a 1:5 (*w/w*) OMP:APol ratio and incubated for 1 hour at 4 ^{o}C. Detergent was then removed by addition of BioBeads (BioRad, Hemel Hempstead, Herts., UK) and incubated overnight at 4 ^{o}C with gentle agitation (rocking table or mixing wheel) (Figure 2-3). Final protein concentration (0.85-0.95 mg.ml^{-1}) was determined by measurement of the absorbance at 280 nm following dilution into 25 mM tris.HCl pH 8.0 containing 6M guanidine.HCl (extinction coefficients in Table 2-1).

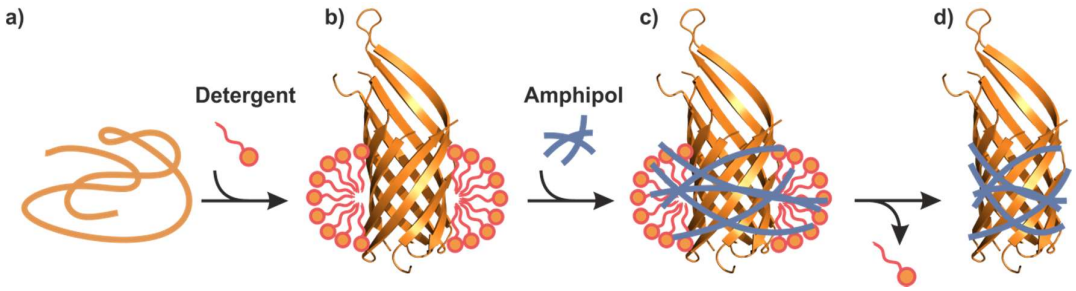

Figure 2-3 – OMPs can be folded into detergent micelles and subsequently exchanged into APol. a) OMPs are denatured in 8 M urea or 6 M guanidine.HCl. b) OMPs can be spontaneously refolded into detergent micelles (may be specific to OMP). c) Addition of APol in a 1:5 OMP:APol (w/w) results in formation of a complex. d) Treatment with BioBeads removes detergent and allows for exchange of folded OMPs in to the APol.

2.4 OMP folding assays

2.4.1 Cold-SDS-PAGE

Samples were diluted 2-fold with 2 x SDS-PAGE loading buffer (50 mM tris.HCl pH 6.8, 100 mM DTT, 2 % (w/v) SDS, 0.1 % (w/v) bromophenol blue, 10 % (v/v) glycerol). Samples were loaded onto a 12.5 % SDS-polyacrylamide gel loaded into a cassette with cathode buffer (100 mM tris, 100 mM tricine, 0.1 % SDS, pH 8.3) in the inner reservoir and anode buffer in the outer reservoir (100 mM tris.HCl, pH 8.9). Proteins were stacked by a constant current of 35 mA until the dye-front reached the resolving gel and electrophoresed by applying a constant current of 70 mA until the dye front reached the bottom of the gel. Protein mass markers (Precision Plus Protein™ Dual Xtra Standards (Bio-Rad, UK)) were loaded in a separate lane. Gels were stained using InstantBlue (Expedeon, UK).

2.4.2 Circular Dichroism

Protein samples (refolded in or exchanged into 100 mM ammonium bicarbonate pH 7.8 +/- 0.02 % (*w/v*) DDM) were diluted to 0.2 $mg.ml^{-1}$ and loaded into a 0.1 mm path length slide cuvette (Hellma UK, Essex, UK). Circular Dichroism data were collected from 200 – 260 nm in 1 nm steps (0.75 seconds per step) and averaged over 5 scans. Circular dichroism spectra were acquired for each samples respective buffer (i.e. 100 mM ammonium bicarbonate pH 7.8 +/- 0.02 % (*w/v*) DDM or 1 $mg.ml^{-1}$ A8-35) and subtracted from spectra of all the samples. All recordings were performed on a Chirascan circular dichroism spectrometer (Applied Photophysics Ltd., UK).

2.4.3 Activity Assays

2.4.3.1 OmpT cleavage of a self-quenching fluorogenic peptide

The self-quenching fluorogenic peptide Abz-ARRAY-NO_2[29] (25 μM) (Peptide Protein Research, Hampshire, UK) (Figure 2-4) was added to a range of OmpT concentrations (125 nM – 7.5 μM) in 25 mM tris·HCl, pH 8.0 containing 0.02 % (*w/v*) DDM or 1:5 (w/w OmpT:APol). OmpT was incubated with 1 $mg.ml^{-1}$ LPS (Sigma Aldrich, Gillingham, Dorset, UK) for 1 hour prior to the assay. Cleavage of Abz-ARRAY-NO_2 was monitored by observing an increase in emission at 430 nm

following excitation at 325 nm using a fluorimeter (Photon Technology International, Ford, West Sussex, UK) for 300 sec. Specific activity was calculated for OmpT in each solubilising medium using the OmpT/peptide concentration, initial rate of fluorescence change and endpoint fluorescence (Equation 2-1). Specific activity was calculated for each concentration of OmpT and mean value of 12 results (3 repeats of 4 concentrations) and standard error of the mean are reported.

$$Specific\ Activity \quad \frac{initial\ rate}{endpoint\ fluoresence} \ x \ \frac{[substrate]}{[OmpT]}$$

Equation 2-1 – Specific activity of OmpT cleavage of Abz-ARRAY-NO_2 is calculated from the initial rate of fluorescence change[29, 38], which is related to rate of molar substrate cleavage by a function of endpoint fluorescence and substrate concentration, per mol of OmpT.

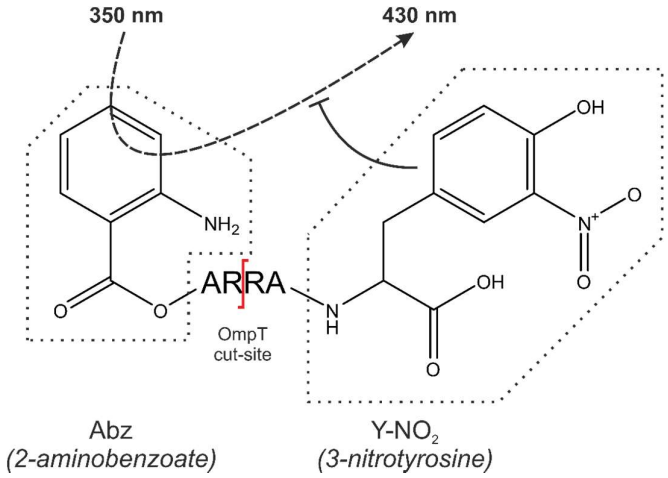

Figure 2-4 – Abz-ARRAY-NO_2 is a self-quenching fluorogenic peptide that is used as a substrate for OmpT activity assays. Excitation of the aminobenzoate (Abz) fluorophore at 350 nm results in emission at 430nm. Prior to cleavage, this is quenched as nitrotyrosine (Y-NO_2) is in close proximity. Cleavage between the consecutive arginine residues (RR) results in separation of Abz and Y-NO_2 and results in an increase in 430 nm emission intensity.

2.4.3.2PagP hydrolysis of its acyl-palmitate substrate

PagP (final concentration 2.5 μM) was added to pre-filtered 25 mM tris·HCl, pH 8.0, 1 mM p-nitrophenol palmitate (p-NPP), 10 % (v/v) 2-propanol, 10 % (v/v) Triton X-100. This was supplemented with 0.02 % (w/v) DDM for assays of PagP activity in DDM micelles. Hydrolysis of p-NPP to p-nitrophenol (p-NP)/palmitate was monitored by monitoring an increase in absorbance at 410 nm (Figure 2-5) [40, 201].

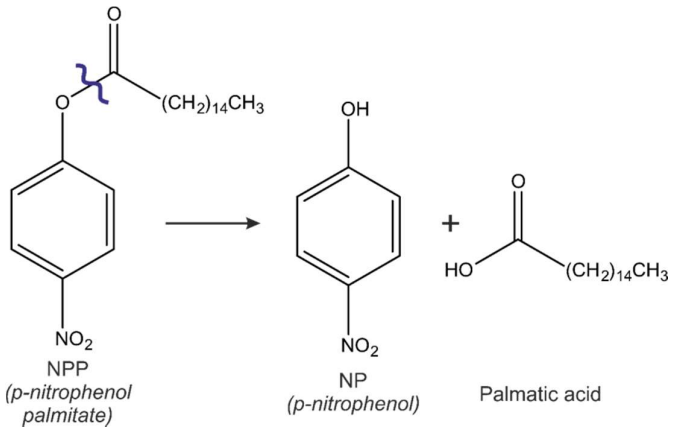

Figure 2-5 – PagP hydrolyses its p-nitrophenol palmitate substrate (NPP) to produce free palmitic acid and p-nitrophenol (NP), which can be detected by an increase in absorbance at 410 nm. NPP has a low solubility in aqueous solution, resulting in a degree of aggregation and precipitation prior to the assay, meaning that true quantification of PagP specific activity is limited.

2.4.4 Size exclusion chromatography of OMP:APol complexes

OMP:APol samples were loaded onto an Superdex 200 10/300 GL analytical SEC column (GE Healthcare, Little Chalfont, Bucks, UK) equilibrated with 250 mM ammonium bicarbonate, pH 7.8. OMPs were eluted at a flow rate of 0.5 $ml.min^{-1}$ and protein-containing fractions (identified by SDS-PAGE and simultaneous absorption at 280 and 220 nm) were pooled and concentrated (using a Vivaspin 2 MWCO 3,000 spin column (GE Healthcare, Little Chalfont, Bucks, UK)) prior to nESI-IMS–MS analysis.

2.5 Native Mass Spectrometry

2.5.1 Sample preparation and ionisation

Immediately prior to native MS analysis, OMPs were buffer exchanged into 100 mM ammonium bicarbonate pH 7.8 (+/- 0.02% (*w/v*) DDM) using two consecutive ZebaSpin desalting columns (Thermo Scientific, Hemel Hempstead, Herts., UK). Samples were loaded into borosilicate capillaries (pulled and coated in-house) for nESI-IMS-MS. The capillary voltage was set to 1.7 kV. All native OMP MS data shown in this thesis were acquired on a Synapt G1 HDMS (Waters, Wilmslow, UK) operating in mobility TOF mode.

2.5.2 Collision induced activation of OMP:detergent and OMP:APol complexes

OMPs were liberated by collision induced activation of their complexes with detergent micelles or APol. Complexes were activated by collision with neutral Ar gas in the Trap region of the Synapt G1 HDMS (Waters, Wilmslow, UK), prior to ion mobility separation in the mobility region of the drift cell. Trap and Transfer voltage parameters (i.e. the acceleration voltages into trap and transfer regions of drift cell, respectively) were tuned for each acquisition, ranging from 30-180 and 50-150 V, respectively. Bias (i.e. the acceleration voltage into the Mobility region of the drift cell) was maintained within an experiment (20-30 V). A bias voltage of about 10 V was essential for release of OMPs but above 30 V resulted in large carry-over in ion mobility and loss of signal.

2.5.3 Determination of collision cross section values of liberated OMPS

2.5.3.1 TWIMS

Liberated OMPs were analysed by IMS-MS. The N_2 flow rate was set to 20 $l.hr^{-1}$ (gas pressure of 6.3 x 10^{-2} mbar) and the travelling wave set with a wave speed of 300 $m.s^{-1}$ and wave height ramping from 5 to 30 V.

2.5.3.2 Calibration against denatured protein calibrants

CCS values were calculated from drift times by calibration against denatured protein ions of known cross section. Trap and Transfer collision voltages were lowered to 6 and 4 V, respectively, but Bias was maintained at value for sample data acquisition (20-30 V). 1 $mg.ml^{-1}$ myoglobin (horse heart, Sigma), cytochrome c (Sigma) and ubiquitin (Sigma) were diluted 10-fold with 50 % (*v/v*) acetonitrile (ACN), 2 % (*v/v*) CH_3COOH and analysed using the same IMS parameters. Denatured reference CCS values were taken from the Clemmer database[202].

2.5.3.3 MOBCAL and PA/PSA values

Theoretical CCS values of OMPs were determined from crystal structures of OmpT (PDB 1I78)[30], PagP (PDB 1THQ)[28] and tOmpA (PDB 1QJP)[20]. Projection approximation values (PA) were calculated using MOBCAL[113-114, 203] (compiled and executed using the Force 3.0 fortran compiler) and PSA values[112] were calculated from the PA values using Equation 2-2.

$$PSA = 1.299\ x\ (PA - 81)$$

Equation 2-2 – Projection superposition approximation (PSA) is a function of projection approximation (PA)

PDB files must be converted into MFJ files (more simple coordinate file) using a script written in-house prior to input into MOBCAL.

2.6 Fast Photochemical Oxidation of Proteins (FPOP)-LC-MS

2.6.1 Photochemical oxidation of model peptides in presence of DDM micelles or A8-35 APol

F1 or W1 peptides (10 µM) (Figure 2-6) in 10 mM sodium phosphate pH 8.0 0.05 % (*v/v*) H_2O_2 were supplemented with 0.02 % (*w/v*) DDM or 5 mg.ml^{-1} A8-35. The samples (100 µl) were infused through a fused silica capillary (i.d. 100 µm, with a window etched using a butane torch) at a flow rate of 20 µL.min^{-1} through the path of a Compex 50 Pro KrF excimer laser operating at 248 nm (Coherent Inc., Ely, UK) with a pulse frequency of 15 Hz and a laser beamwidth of <3 mm at the point of irradiation. Samples were flowed into a collection tube containing 100 mM L-methionine and 1 µM catalase (10 µl per 50 µl of initial sample).

2.6.2 Photochemical oxidation of model peptides in presence of DLPC liposomes or urea

Bradykinin (BK) or AngII (10 µM) (Figure 2-6) in 10 mM sodium phosphate pH 8.0 0.05 % (*v/v*) H_2O_2 were supplemented with DLPC LUVs (4 or 32 mM DLPC) or urea (0.1, 0.4, 1 or 4 M). The samples (100 µl) were infused through a fused silica capillary (i.d. 100 µm, with a window etched using a butane torch) at a flow rate of 20 µL.min^{-1} through the path of a Compex 50 Pro KrF excimer laser operating at 248 nm (Coherent Inc., Ely, UK) with a pulse frequency of 15 Hz and a laser beamwidth of <3 mm at the point of irradiation. Samples were flowed into a collection tube containing 100 mM L-methionine and 1 µM catalase (10 µl per 50 µl of initial sample).

F1	GSGSGKFGSGSGK
W1	GSGSGKWGSGSGK
Bradykinin	RPPGFSPFR
Angiotensin II	DRVYIHPFHL

Figure 2-6 – Sequences of control peptides used in FPOP quenching studies. Radical reactive aromatic F, W and Y residues are highlighted.

2.6.3 Photochemical oxidation of $OmpT_{HT}$

For FPOP analysis, $OmpT_{HT}$ (10 µM in 25 mM tris.HCl +/- 0.02 % (*w/v*) DDM) was buffer-exchanged into 10 mM sodium phosphate, 15 mM L-glutamine at pH 8.0 using Zeba Spin desalting columns (Thermo Fisher, Hemel Hempstead, UK) (supplemented with 0.02 % (w/v) DDM for the detergent-solubilised samples). Immediately before labelling, H_2O_2 was added to a final concentration of 0.05, 0.15, or 0.5 % (*v/v*). The samples (100 µl) were infused through a fused silica capillary (i.d. 100 µm, with a window etched using a butane torch) at a flow rate of 20 $\mu L.min^{-1}$ through the path of a Compex 50 Pro KrF excimer laser operating at 248 nm (Coherent Inc., Ely, UK) with a pulse frequency of 15 Hz and a laser beamwidth of <3 mm at the point of irradiation. Samples were flowed into a collection tube containing 100 mM L-methionine and 1 µM catalase quench solution (10 µl per 50 µl initial sample).

2.6.4 LC-MS of $OmpT_{HT}$ tryptic digests

After labelling, $OmpT_{HT}$ was digested by use of sequencing grade trypsin (Promega UK, Southampton, Hants., UK) (1:20 (w/w) trypsin:OmpT ratio) at 37 °C for 24 h. Digestion was quenched by the addition of formic acid (5 % (*v/v*) final) and the digest was centrifuged at 10,000 x *g* for 10 mins at 4 ^{o}C. The tryptic peptides (1 µl of 100 $fmol.\mu l^{-1}$) were loaded onto a M-Class nanoAcquity UPLC system (Waters, Wilmslow, UK) equipped with a C18 column. Peptides were loaded onto a Vanguard C18 trap column. After a 5 min trapping phase, peptides were separated by a H_2O:ACN gradient at a flow rate of 0.3 $\mu l.min^{-1}$ (Table 2-2) and analysed using a Synapt G2Si (Waters, Wilmslow, UK). Data were acquired in both DDA and MS^e modes.

Time (min)	Flow Rate (µl.min^{-1})	A (%)	B (%)
0	0.3	99	1
0.1	0.3	99	1
30	0.3	60	40
32	0.3	5	95
37	0.3	5	95
39	0.3	99	1
64	0.3	99	1

Table 2-2 – HPLC gradient profile for analysis of tryptic peptides of $OmpT_{HT}$ using a Waters nanoAcquity UPLC system and Waters Synapt G2Si. Flow rate is maintained at 0.3 µl.min^{-1}. Gradient shows a slow ramp from high [H_2O] (A) to moderate [ACN] (B) from 0.1 – 30 min, a fast ramp to high [ACN] (30-32 min), a maintained high [ACN] wash (32 – 37 min) and re-equilibration to high H_2O for subsequent runs (37 – 64 min).

2.6.5 Data Analysis

Qualitative DDA data were imported into PEAKS software (version 7.5, Bioinformatics Solutions, Waterloo, ON, Canada)[204]. Peptides were searched against a UniProt database[205] with addition of the $OmpT_{HT}$ sequence. Precursor and product mass tolerances were set to 20 and 100 ppm, respectively, and false-discovery-rate (FDR) was set to 0.5 %. FPOP oxidation (+15.999 Da) was searched for at Met/Cys/Trp/Tyr/Phe/His residues.

For quantitative MS^e, data were imported into Waters UNIFI software (Waters Corp., Manchester, UK). Peptides were searched against the $OmpT_{HT}$ sequence with precursor and product mass tolerance set to 20 and 100 ppm, respectively. FPOP oxidation (+15.999 Da) was searched for at Met/Cys/Trp/Tyr/Phe/His residues. Measurement of degree of modification was calculated from LC peak area of identified modified and unmodified peptides, as shown in Equation 2-3.

$$\%\, peptide\ modified = \frac{\sum Peak\ area_{modified}}{\sum Peak\ area_{modified} + \sum Peak\ area_{unmodifie}}$$

Equation 2-3 - % peptide modified was determined from the sum of the intensities of LC chromatogram peaks representing modified peptide divided by the sum of the intensities of LC chromatogram peak representing all peptide (modified and unmodified).

2.7 Hydrogen Deuterium Exchange (HDX)-MS

2.7.1 Labelling

$OmpT_{HT}$ (10 µM) solubilised in DDM micelles (0.02 % *w/v*) or NAPol (1:5 $OmpT_{HT}$:NAPol *w/v*) was buffer-exchanged into 10 mM sodium phosphate pH 8.0 +/- 0.02 % DDM (*w/v*). HDX was initiated by 20-fold dilution with deuterated 50 mM sodium phosphate pD 7.0 +/- 0.02 % DDM (*w/v*) on ice. Labelling was quenched by 2-fold dilution with 200 mM sodium phosphate pH 2.2, 4 M guanidine.HCl. All labelling timepoints were repeated in triplicate.

2.7.2 LC-MS of HDX samples

Immediately after quenching, samples were loaded onto a Waters HDX Manager. During the trapping phase, the contents of the sample loop were passed through an on-line Waters Enzymate pepsin column for digestion and peptides were loaded onto a Vanguard C18 trap column. After a 3 min trapping phase, the HDX manager began the analytical phase. Peptides were separated by a H_2O:ACN gradient at a flow rate of 30 µl.min^{-1} (Table 2-3) and analysed using the MS^e method on a Waters Xevo Q-ToF instrument.

Time (min)	Flow Rate (µl.min^{-1})	A (%)	B (%)
0	30	92	8
7	30	65	35
8	30	5	95
10	30	5	95
11	30	92	8
11.5	30	5	95
16	30	5	95
17	30	92	8
18	30	92	8

Table 2-3 – HPLC gradient profile for analysis of on-line pepsin digests of $OmpT_{HT}$ using a Waters HDX Manager system and Waters Xevo G2S. Flow rate was maintained at 30 µl.min^{-1}. Gradient shows a slow ramp from high H_2O (A) to moderate ACN (B) (0 – 7 min), a fast ramp to high ACN (7 - 8 min) and a maintained high ACN wash (8 - 10 min). Gradient briefly returns to low H_2O (10 – 11 min), ramps to high ACN (11 – 11.5 min), maintains a high ACN wash (11.5 – 16 min) and re-equilibrated to high H_2O for subsequent runs (16 – 18 min).

2.7.3 Data Analysis

PLGS software was used to identify peptides in the t=0 data for each condition (DDM and NAPol). Peptide lists were imported into Dynamx 3.0 software. Dynamx was used to filter peptides that were common to all conditions.

3 OmpT Refolding and Native-MS

3.1 Introduction

Work described in this Chapter has been published in Calabrese et al., *Anal Chem*, 2014[206] and Watkinson et al., *Int. J. Mass Spectrom.*, 2015[207].

In order to maintain the native structure of membrane proteins *in vitro*, they must be solubilised with an appropriate surfactant. This often means extensive screening of detergents and lipids. Development of alternative surfactants, such as APols, aims to improve the solution phase properties of membrane proteins and provide a generic approach to solubilising membrane proteins. Addition of an excess of A8-35 (commonly in a 1:5 MP:A8-35 ratio (*w/w*)) has been used both to refold denatured membrane proteins and to trap detergent-solubilised native membrane proteins[58, 60, 62, 208]. A8-35 has been shown to improve the thermal, chemical and kinetic stability of MPs relative to those solubilised in detergent micelles[58, 60, 209].

MS had been used previously to study native membrane proteins and membrane proteins complexes, predominantly with detergent micelles as the solubilising media. nESI-IMS-MS with gas-phase collisional activation has shown MPs delivered to the gas phase in a native-like conformation and has uncovered details of the structure, stoichiometry and topology of MPs and their complexes from detergent micelles[17, 140-142, 146, 149-151, 210]. A8-35 has also been used to deliver native MPs into the gas phase for CCS analysis using IMS[75]. Previous observations of OMPs in the gas phase using A8-35 showed the presence of native-like OmpT and PagP but required high collision energies in order to be liberated from A8-35[75, 141]. Although CCS values confirmed native-like conformations of OmpT and PagP, optimisation of solution and gas phase conditions should improve observation of native-like MPs by IMS-MS.

Data shown in this chapter covers the optimisation of such conditions, investigating the effect of MP:APol ratios and SEC, how APols compare to detergent micelles in delivering native-like MPs to the gas phase and properties of APols that may benefit or hinder observation of native-like MPs in the gas phase.

3.2 Results

3.2.1 Preliminary nESI-IMS-MS of OmpT:A8-35

OmpT was folded directly from a 8 M urea denatured state into A8-35 (1:5 *w/w* OmpT:A8-35) by dialysis against 100 mM ammonium bicarbonate pH 7.8. Densitometry of cold-SDS-PAGE analysis measures the relative abundance of folded, SDS-stable OmpT that has migrated at an apparent lower M_w and denatured OmpT migrating at its true M_w (shown as $OmpT_F$ and $OmpT_U$ in, respectively, Figure 3-1a). This method showed OmpT to have a folding yield often in excess of 95%. The native state was confirmed by CD spectra and a peptidase activity assay monitoring the cleavage of a self-quenching fluorogenic peptide (Section 2.4.3.1). CD was used to probe the presence of secondary structure elements of proteins and a minimum at 218 nm is typical of β-sheet (β-barrel) structure (Figure 3-1b). The OmpT activity assay monitors emission at 430 nm following excitation at 325 nm, with a fluorescence increase over time as a result of cleavage of a self-quenching fluorogenic peptide (Abz-ARRAY-NO_3). OmpT targets its peptide substrate between consecutive basic residues and results in separation of the fluorophore (3-nitro-tyrosine, Y-NO_3) and quenching group (aminobenzoate, Abz). Refolded OmpT:A8-35 is shown to be native-like as a time-dependent increase in fluorescence was observed, that is dependent on concentration of OmpT. Additionally, the presence of LPS enhances OmpT function(Figure 3-1c).

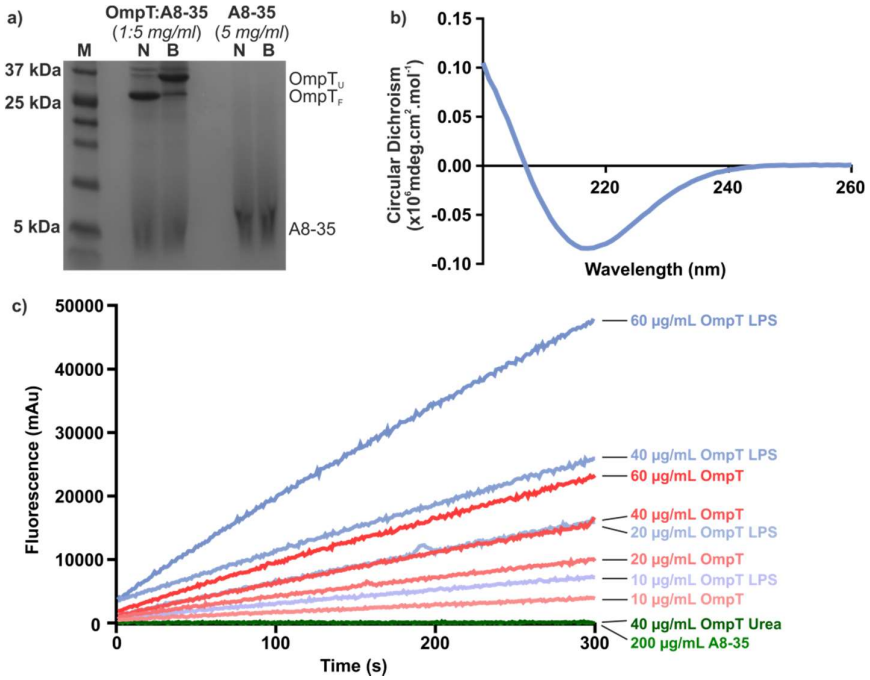

Figure 3-1 – Confirmation of the folded state of OmpT following direct refolding into A8-35 APol by dialysis against urea-free 100 mM ammonium bicarbonate. a) Cold-SDS-PAGE shows the differential electrophoretic mobilities of folded (OmpT$_F$) and unfolded (OmpT$_U$) OmpT when loaded native (N) and after boiling (B). b) CD spectrum shows a minimum at 218 nm, indicative of β-sheet secondary structure. c) Concentration- and LPS-dependent activity of OmpT is shown by following the increase in fluorescence following cleavage of self-quenching fluorogenic peptide, Abz-ARRAY-NO$_3$. Traces of OmpT in the presence and absence of LPS are shown in blue and red, respectively, and unfolded OmpT and A8-35-alone controls are in green.

Folded OmpT:A8-35 was analysed further by nESI-IMS-MS to observe the folded state of OmpT in the gas phase. This was performed under the same conditions as previously published[75] and showed highly comparable results. Figure 3-2 highlights the power of nESI-IMS-MS to resolve native MPs from the large excess of heterogenous A8-35 ions. However, due to the heterogenous nature of A8-35, MP ions must first be liberated from complexes with A8-35 by collisional activation with neutral Argon buffer gas in the trap region of the drift cell of the Synapt G1 HDMS. Greatly elevated collision energies in the entrance to the trap (Trap), ion mobility (Bias) and transfer (Transfer) regions of the drift cell allow observation of 6-9$^+$ ions of OmpT (Figure 3-2). These elevated collision energies risk unfolding protein ions but IMS-MS is used to validate the native state of proteins.

Activation of MP:A8-35 complexes in the trap region of the instrument allows subsequent analysis of liberated OmpT ions by use of IMS-MS, relating drift time through a buffer gas filled region to the CCS of free ions. Two distinct conformers of OmpT were observed; 6-8^{+} ions of OmpT populate a more compact conformer (CCS values of **2647.1-2694.7** Å^2), whereas 9^{+} ions of OmpT populate a more extended conformer (**3499.8** Å^2) (Figure 3-2 and Table 3-1). Relative to the theoretical CCS value of **2957** Å^2 predicted using the PSA value[112] from the crystal structure, the two conformers would appear to be a denatured and a collapsed form of the native state (either process is most likely to have occurred in the extended barrel or loop regions of OmpT).

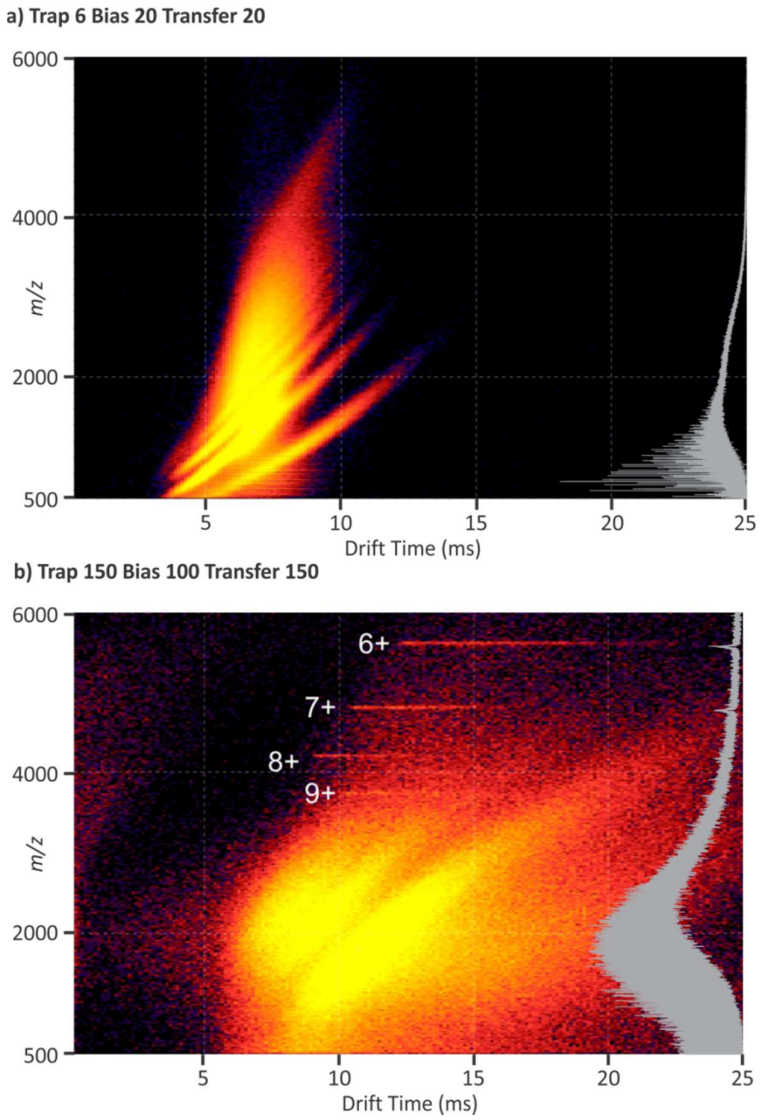

Figure 3-2 – ESI-IMS-MS analysis of OmpT:A8-35 (1:5 w/w) using a Waters Synapt G1 HDMS in a) low and b) high energy collision conditions, as indicated. Elevated Trap, Bias and Transfer voltages (as in b)) resulted in the observation of free OmpT ions (6-9^{+}) that were otherwise not visible when in complex with highly heterogenous A8-35 (as in a)). Ion intensity is displayed in a colour spectrum of black through blue and orange to yellow as the most intense.

z	CCS (Å^2)
6	2650.7
7	2647.1
8	2694.7
9	3499.8

Table 3-1 – Collision cross section values of OmpT released from A8-35. OmpT is observed in two conformations, a more compact (6-8$^+$) and a more expanded conformation (9$^+$).

It was mentioned previously that significant collisional activation was needed to activate MP:A8-35 complexes and this can result potentially in loss of ion transmission, native structure or ligand/protein binding events. With some optimisation, observation of native-like OmpT from A8-35 is greatly improved using nESI-IMS-MS. Preliminary analyses shown here (Figure 3-2 and Figure 3-3a) and previously published[75] were performed on OmpT:A8-35 (1:5 *w/w*) at 1 mg.ml^{-1} (or ~**30** µM) protein. Simple sample modifications, such as a 10-fold reduction in protein (and A8-35) concentration, allowed observation of OmpT ions using considerably lower collision energies (Trap **150** → **30** V, Bias **100** → **20** V, Transfer **100** → **75** V). OmpT analysed at the lower concentration generates ions populating a broader distribution of charge states (**7-13$^+$**) relative to preliminary analyses of OmpT:A8-35 (**6-9$^+$**) (Figure 3-3). Despite the higher charge states (which would normally indicate more unfolded conformation), these OmpT ions have CCS values ranging from (**2595.3 – 3221.7 Å^2**) (Table 3-2) that are comparable to the more compact conformer observed previously (Table 3-1).

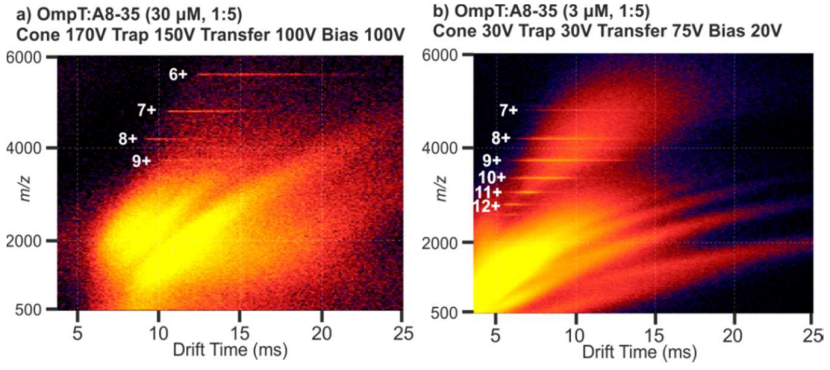

Figure 3-3 – nESI-IMS-MS of 1:5 OmpT:A8-35 (w/w) at a) 30 µM and b) 3 µM. The respective voltages required to observe OmpT ions at these concentrations are shown above each plot.

z	CCS (Å²)	
	30 µM	3 µM
6	2650.7	-
7	2647.1	2595.3
8	2694.7	2765.2
9	3499.8	2888.7
10	-	2967.5
11	-	3003.2
12	-	3221.7

Table 3-2 - CCS-z values of OmpT from A8-35 analysed at 30 or 3 µM OmpT.

The influence of reducing the concentration of A8-35 suggests that the presence of excess free A8-35 may in fact be perturbing the ionisation of MPs and/or their gas-phase release (possibly through non-specific interactions), hence preventing their observation in the gas phase. Refolding OmpT in a 1:2 OmpT:A8-35 (*w/w*) ratio improved the "signal-to-noise" of observed OmpT (by both MS and IMS-MS) relative to that refolded in a 1:5 ratio (Figure 3-4). Charge state distribution (**$8\text{-}13^{+}$**) and arrival times of OmpT ions remain consistent with different OmpT:A8-35 ratios, suggesting that the complex remains the same and it is the relative abundance of free A8-35 that allows greater observation of native-like OmpT.

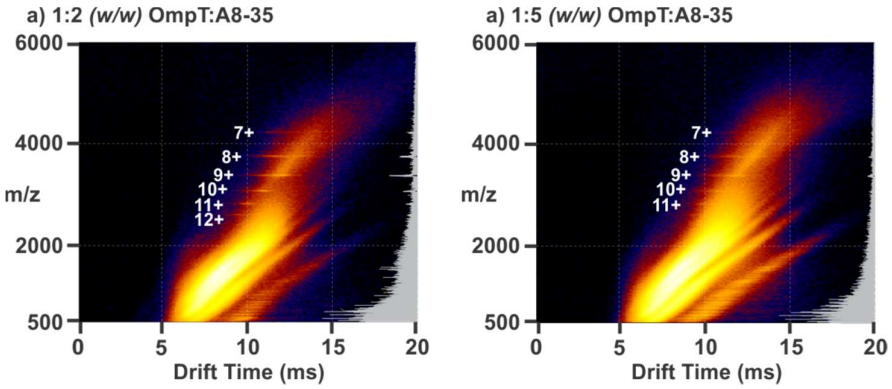

Figure 3-4 – nESI-IMS-MS analysis of OmpT:A8-35 refolded in a a) 1:2 or b) 1:5 ratio (w/w). Inset, respective m/z spectra. Under identical instrument conditions (Figure 3-3b)

3.2.2 OmpT Refolding Optimisation

The literature states that an excess of A8-35 is required to maintain the folded state of MPs, either through the selection of A8-35 molecules from a heterogenous mixture or exchange of A8-35 molecules associated with the MP and those free in solution. As discussed previously, the presence of an excess of highly heterogenous APol is detrimental to the observation of gas phase MP ions. This could be a result of reduced ionisation efficiency of MP:A8-35 complexes when in the presence of a large concentration of the highly negatively charged A8-35 or by obscuring peaks representing free MPs in mass spectra with high intensities of heterogenous A8-35 ions. OmpT:A8-35 ratios were therefore screened to observe the maximal folding yield with the minimum amount of A8-35 present. OmpT (1 $mg.ml^{-1}$) in a 8 M urea denatured state was refolded into A8-35 as before, but in a 1:1, 1:1.5, 1:2 and 1:5 OmpT:A8-35 ratio (*w/w*). Densitometry of cold-SDS-PAGE showed the folding yield to be dependent on the ratio of OmpT:A8-35, with near maximal folding achieved at a 1:2 OmpT:A8-35 (*w*/*w*) ratio (Figure 3-5 and Table 3-3).

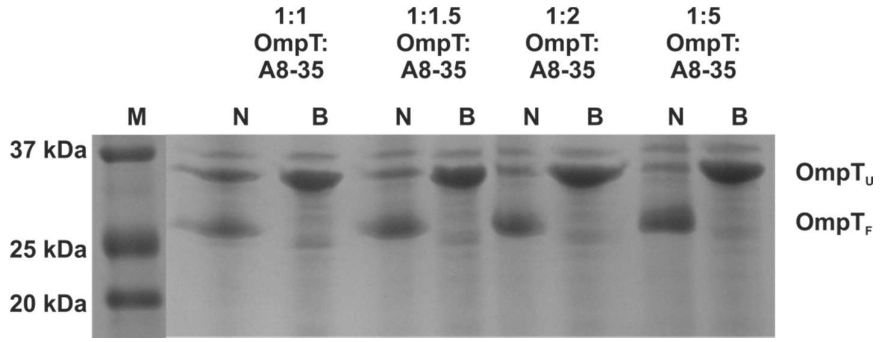

Figure 3-5 – Cold SDS-PAGE shows OmpT to fold (although with lower yield) in OmpT:A8-35 ratios as low as 1:1 (w/w). Folded and unfolded OmpT are indicated by $OmpT_F$ and $OmpT_U$, respectively.

These folding yields are comparable to results obtained by the use of SEC (Table 3-3 and Figure 3-8). Where protein absorbs at 280 and 200 nm, A8-35 absorbs only at 220 nm. When simultaneously measuring absorbance at 280 and 220 nm, free A8-35 (~**11** ml) can be distinguished from protein-containing fractions by a response exclusively on the A220 trace, where protein will absorb at both wavelengths. By the use of SEC, a more unfolded (eluting at ~**8.5** ml) and a more compact (~**9.5** ml) species of OmpT:A8-35 can be observed (Figure 3-6).

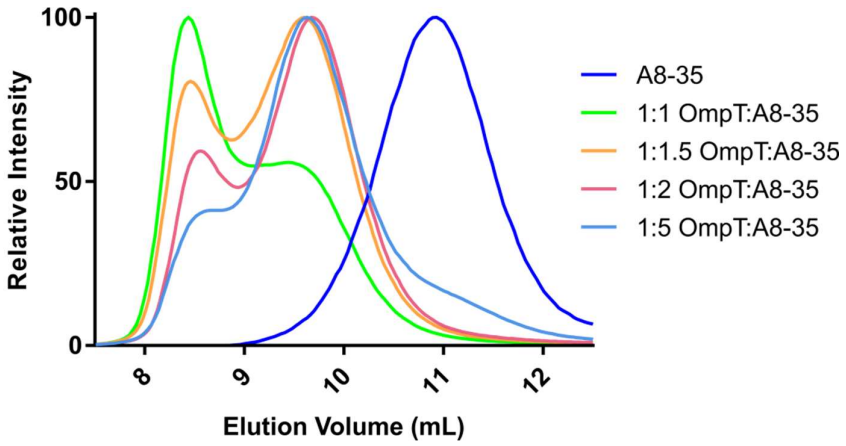

Figure 3-6 – SEC profiles of free A8-35 and OmpT folded in a range of OmpT:A8-35 ratios (w/w), observed by absorption at 220 nm. Folding in the presence of a higher ratio of A8-35:OmpT results in an increase in the abundance of a more compact conformation (~9.5 ml) relative to a more expanded conformation (~8.5 ml). Free A8-35 (~11 ml) is only observed for OmpT refolded in a 1:5 OmpT:A8-35 ratio (w/w).

By fitting Gaussians to the elution profile and measuring areas under the curves, the folding yield can be calculated in each refolding ratio (Figure 3-7). The maximal folding yield is observed where OmpT is refolded in a 1:2 OmpT:A8-35 ratio (*w/w*) (Figure 3-8 and Table 3-3) at an OmpT concentration of 1mg.ml^{-1}. Despite this, free A8-35 can only be observed in the elution profile of 1:5 OmpT:A8-35 (where maximal folding yield, **83 %**, has been achieved) but not in the other folding ratios (Figure 3-7). This suggests that in the case of OmpT, an excess of A8-35 is not necessarily required and the amount of free A8-35 can be minimised for subsequent analyses of MPs.

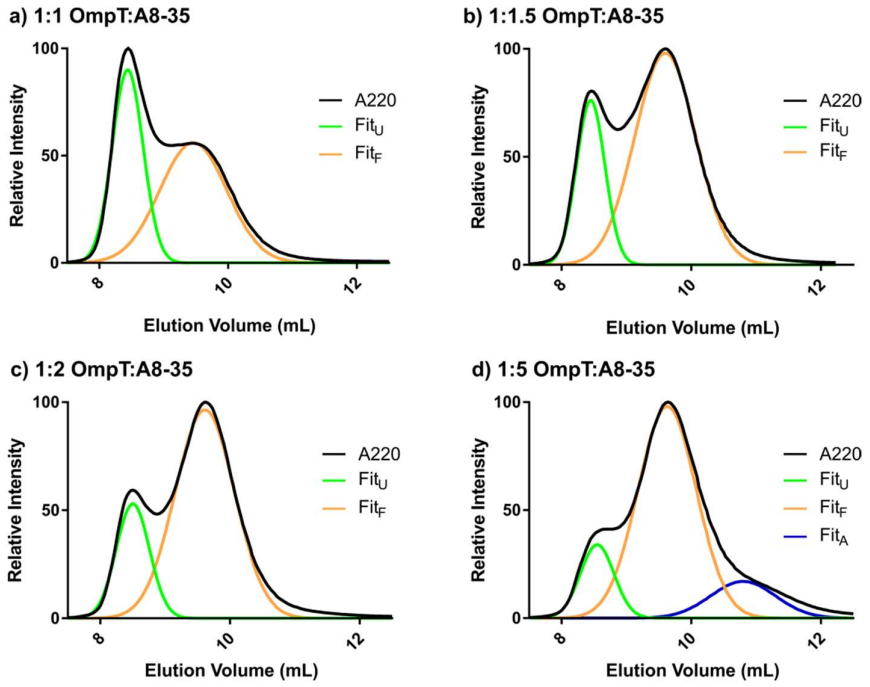

Figure 3-7 – Gaussian fitting to SEC profiles shows the relative abundance of folded (orange, Fit$_F$) and unfolded (green, Fit$_U$) conformers of OmpT and free A8-35 (blue, Fit$_A$) when refolded in a a) 1:1, b) 1:1.5, c) 1:2 or d) 1:5 OmpT:A8-35 ratio (w/w). A greater abundance of folded conformer of OmpT is observed with increasing A8-35 and free A8-35 only when OmpT is folded with greater than a 1:5 OmpT:A8-35 ratio (w/w).

A similar trend is observed for the folding yield of OmpT in the presence of different ratios of OmpT:A8-35, whether measured by densitometry of cold-SDS-PAGE or SEC. Maximal folding yield is achieved between a 1:2 and 1:5 (*w/w*) OmpT:A8-35 ratio, the fits shown in Figure 3-8 suggest an approximate 1:3 (*w/w*) OmpT:A8-35 ratio is ideal. This is an interesting phenomenon but the specific optimum folding ratio may be highly dependent on the size and structure of the MP of interest and hence need to be screened on a protein by protein basis.

A8-35:OmpT (*w/w*)	Folding Yield (%)	
	PAGE	SEC
1	60	57
1.5	75	73
2	83	76
5	87	83

Table 3-3 – Folding yield of OmpT in the presence of increasing A8-35 calculated using cold-SDS PAGE densitometry or SEC are comparable and show maximal folding yield between 1:2 and 1:5 OmpT:A8-35 ratio (w/w).

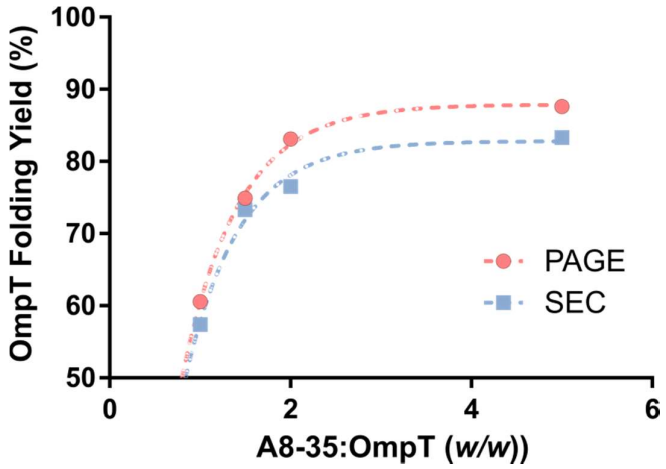

Figure 3-8 – Folding yields for OmpT:A8-35 at a 1:1, 1:1.5, 1:2 and 1:5 (w/w) ratio as calculated using either densitometry from cold-SDS-PAGE or Gaussian fitting to SEC elution profiles. Data points are fitted with an exponential decay for graphical representation of maximal folding yield between the 1:2 and 1:5 refolding ratios.

3.2.3 SEC-MS of OmpT:A8-35

To further our understanding of the influence of free A8-35 on MS analyses of MPs, fractions corresponding to the more compact species of OmpT:A8-35 were collected and isolated from unfolded conformers and excess free A8-35. Subsequent nESI-IMS-MS analysis of collected fractions of OmpT:A8-35 refolded at different ratios results in highly comparable charge-state distributions (**8-14**$^{+}$) (Figure 3-9) and CCS-z relationships (Figure 3-10 and Table 3-4), with an improved "signal-to-noise" ratio of free OmpT ions.

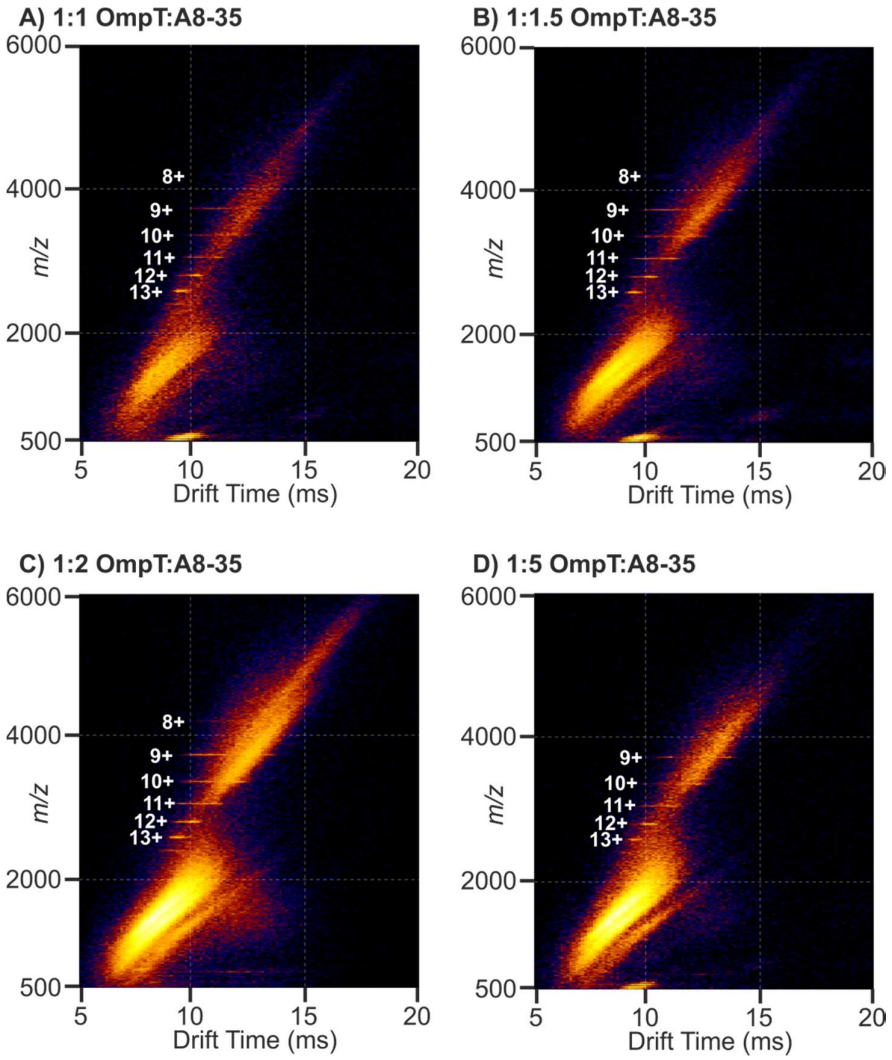

Figure 3-9 – nESI-IMS-MS Driftplots of OmpT:A8-35 isolated from excess A8-35 by SEC after refolding at a a) 1:1, b) 1:1.5, c) 1:2 and d) 1:5 OmpT:A8-35 ratios (w/w). OmpT is refolded and purified by SEC at 1mg.ml^{-1} and concentrated to 3 µM following fractionation for nESI-IMS-MS analysis.

CCS values calculated using nESI-IMS-MS drift time data show the presence of a native-like (**2681.4 – 3097.1 Å²**) and a more collapsed (**2384.2 – 2783.3 Å²**) conformation of OmpT (Figure 3-10 and Table 3-4). The presence of these two conformations that do not appear to be that of fully denatured OmpT, suggest some degree of flexibility of OmpT when maintained in the presence of minimal levels of A8-35. It has been posited previously[64, 78], and since these observations[206-207, 211], that the presence of an excess of A8-35 could have large protective effects on the native-like state of OmpT.

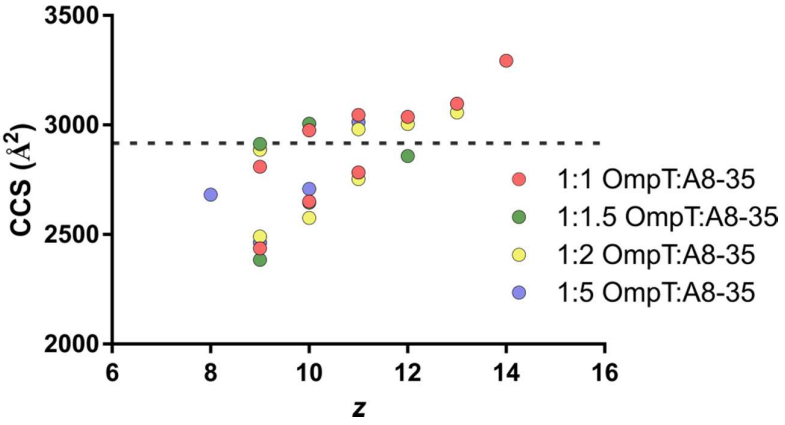

Figure 3-10 – CCS-z relationship of SEC-isolated folded OmpT:A8-35 after refolding at 1:1 (red), 1:1.5 (green), 1:2 (yellow) and 1:5 (blue) OmpT:A8-35 ratios (w/w). Dashed line represents the theoretical CCS value of OmpT (2917 Å², 1I78).

z	1:1 (*w/w*) OmpT:A8-35	1:1.5 (*w/w*) OmpT:A8-35	1:2 (*w/w*) OmpT:A8-35	1:5 (*w/w*) OmpT:A8-35
8	-	-	-	2681.4
9	2436.3	2384.2	2490.5	2463.4
9	2808.8	2913.5	2886.9	2886.9
10	2650.2	2645.6	2575.9	2708.2
10	2975.5	3005.4	2975.5	3005.4
11	2783.3	2783.3	2752.6	2783.3
11	3046.2	-	2980.1	3013.2
12	3037.4	2857.9	3003.8	3037.4
13	3097.1	-	3057.4	3097.1
14	3293.6	-	-	-

Table 3-4 – CCS values (Å²) for each of the charge state ions of OmpT observed following nESI-IMS-MS analysis of SEC-isolated OmpT:A8-35 at each refolding ratio. CCS values of a native-like, a collapsed or a more expanded conformer of OmpT are highlighted in green, orange and red, respectively.

The results presented above show that SEC is a highly useful tool for improving observation of native-like MPs solubilised using A8-35, through removal of excess A8-35. This removal of excess A8-35 has a significant impact on the charge state distribution of OmpT:A8-35, resulting in more highly charged ions of OmpT. OmpT charge distributions are centred on the 10^+ ions when analysed directly from A8-35 in a 1:5 OmpT:A8-35 ratio (*w/w*) (Figure 3-11a), whereas following SEC, the OmpT charge state distribution is centred on the $11/12^+$ ions (Figure 3-11b). Following addition of 1 $mg.ml^{-1}$ A8-35 or 10 mM imidazole (a charge reducing agent), the distribution is similar to the pre-SEC state but not to the fullest extent

(Figure 3-11c and d). Addition of supercharging agent, *m*-nitrobenzylalcohol (*m*NBA, 1 %, *w/v*) can shift the OmpT charge state distribution still further towards more highly charged ions (Figure 3-11e).

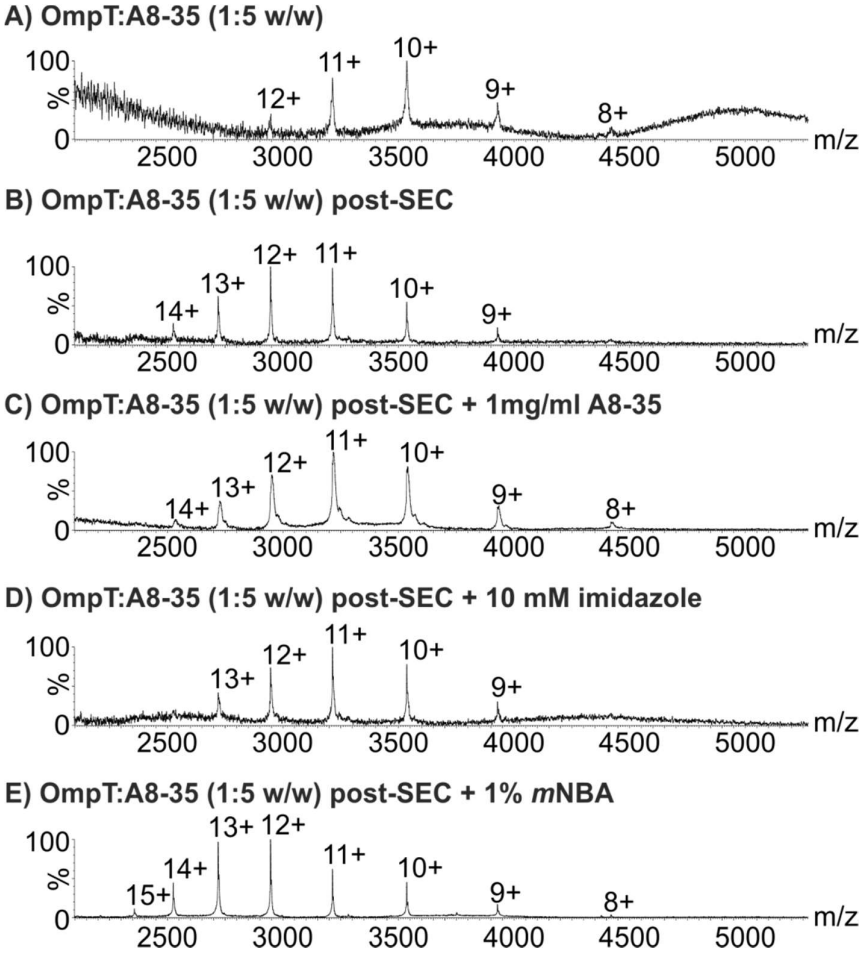

Figure 3-11 – nESI-MS analysis of OmpT:A8-35 a) prior to and b) following SEC isolation of folded conformers results in a shift towards higher charge states (although native-like CCS values are still observed). Addition of c) 1 mg.ml^{-1} A8-35 or d) 10 mM imidazole (as a charge reducing agent) do not return the charge state distribution to that of a) non-SEC isolated OmpT:A8-35. e) addition of 1% (w/v) mNBA (a supercharging agent) does further increase the charge states of OmpT observed.

3.2.4 $OmpT_{HT}$:DDM vs $OmpT_{HT}$:A8-35

DDM is a commonly used detergent for both solubilisation of MPs from membranes and delivery of native MPs to the gas phase for nESI-IMS-MS analysis. The following experiments tested how DDM micelles compare to A8-35 in delivering native MPs to the gas phase. $OmpT_{HT}$ was folded into LDAO micelles (0.5 % *w/w*) and subsequently exchanged into DDM micelles (0.02 % *w/w*) whilst immobilised on a HisTrap column (Section 2.3.2) and can be subsequently exchanged into APol by addition of A8-35 in a 1:5 MP:A8-35 ratio (*w/w*) and removal of detergent using BioBeads (Section 2.3.4). LDAO micelles allow for a greater folding yield of $OmpT_{HT}$ and PagP and subsequent exchange in DDM micelles provides a more native-like environment for OMPs as a result of being a softer non-ionic detergent.

$OmpT_{HT}$ was shown to be equally folded in DDM micelles and A8-35 APol. Cold-SDS-PAGE shows that $OmpT_{HT}$ has a folding yield greater that 90 % in DDM micelles and this is maintained following exchange into A8-35 (Figure 3-12a). Minima at 218 nm in CD spectra confirm β-sheet (β-barrel) structure (Figure 3-12b). Following incubation with LPS, $OmpT_{HT}$ is active (monitored by cleavage of a self-quenching fluorogenic peptide) in DDM micelles and A8-35 APol. However, activity in A8-35 (0.035 $mol_{peptide}.mol_{OmpT}.s^{-1}$) is reduced to approximately one fifth of that in DDM micelles (0.177 $mol_{peptide}.mol_{OmpT}.s^{-1}$) (Figure 3-12c).

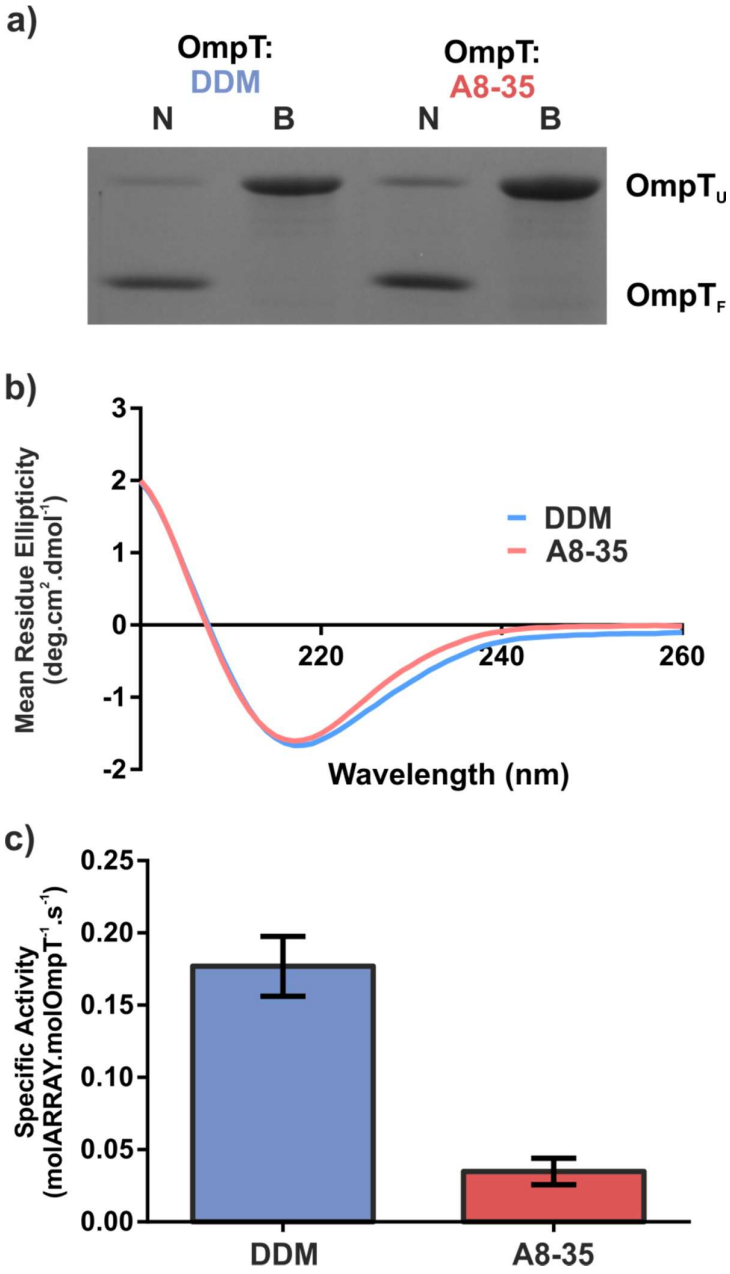

Figure 3-12 – OmpT$_{HT}$ was refolded into DDM micelles and subsequently exchanged into A8-35. Bandshift by a) cold-SDS-PAGE shows an SDS-resistant structure of OmpT$_{HT}$, and minima at 218 nm of b) circular dichroism spectra shows presence of β-sheet (β-barrel) structure. c) activity assays show OmpT$_{HT}$ to be active in both DDM micelles and A8-35 detergent but with ~5-fold decrease in activity after exchange into A8-35 (n=12, errors calculated using 4 concentrations in 3 repeats).

nESI-IMS-MS analysis of OmpT$_{HT}$ solubilised in either DDM micelles or A8-35 shows stark differences in the charge state distribution (Figure 3-13) and the conformations that OmpT$_{HT}$ populates in the gas phase as shown by CCS values of free OmpT$_{HT}$ (Figure 3-14 and Table 3-5).

OmpT$_{HT}$ released from DDM micelles populates a broad range of charge states (**5-14^{+}**, Figure 3-13a) relative to OmpT$_{HT}$ released from A8-35 (**5-8^{+}**, Figure 3-13b), suggesting a greater extent of conformational of flexibility of OmpT$_{HT}$ in DDM compared to A8-35. OmpT is observed in the most native charge states (**5-8^{+}**) when released from either medium but the most highly charged states of OmpT$_{HT}$ are only observed following release from DDM micelles, suggesting detergent promotes greater potential for unfolding of OmpT$_{HT}$ during, or prior to, the ionization process.

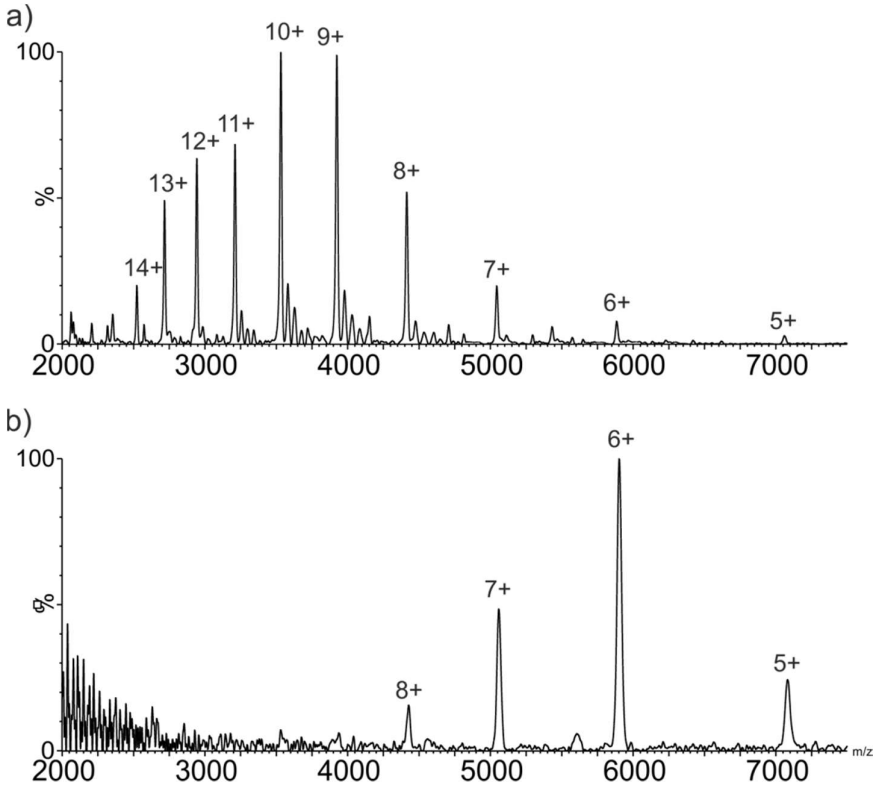

Figure 3-13 – nESI-MS spectra of OmpT$_{HT}$ released from a) DDM micelles or b) A8-35 (OmpT:A8-35 1:5 (w/w)). a) OmpT$_{HT}$ released from DDM micelles is observed with a broad distribution of charge states (5-16^{+}, 5-14^{+} are labelled) and up to 4 DDM molecules bound. b) OmpT$_{HT}$ released from A8-35 populates a narrower distribution (5-8^{+}).

CCS values from IMS-MS data show that OmpT$_{HT}$ analysed from DDM populates a native-like conformation (**2767.6 – 2932.9** Å^2), consistent with the compact conformer that OmpT$_{HT}$ exists in exclusively when released from A8-35 (Figure 3-13a,b and Figure 3-14a,b,e). The CCS values of these native-like ions of OmpT$_{HT}$ correlate well with the theoretical PSA value predicted from the crystal structure

of OmpT (2957 Å^2, PDB 1I78[30]) . However, DDM also promotes unfolding of $OmpT_{HT}$ and the presence of two further expanded conformers (**3167.3 – 3895.8** and **4388.1 – 4657.6** Å^2) (Figure 3-14b,e and Table 3-5). Arrival time distributions (ATDs) of charge states common to ions released from DDM micelles and A8-35 are comparable in terms of approximate peak centre and width, and show $OmpT_{HT}$ (in the most native-like charge states) to populate a single conformation that is no more or less prone to gas phase unfolding from one solubilising media or another (Figure 3-14c and d).

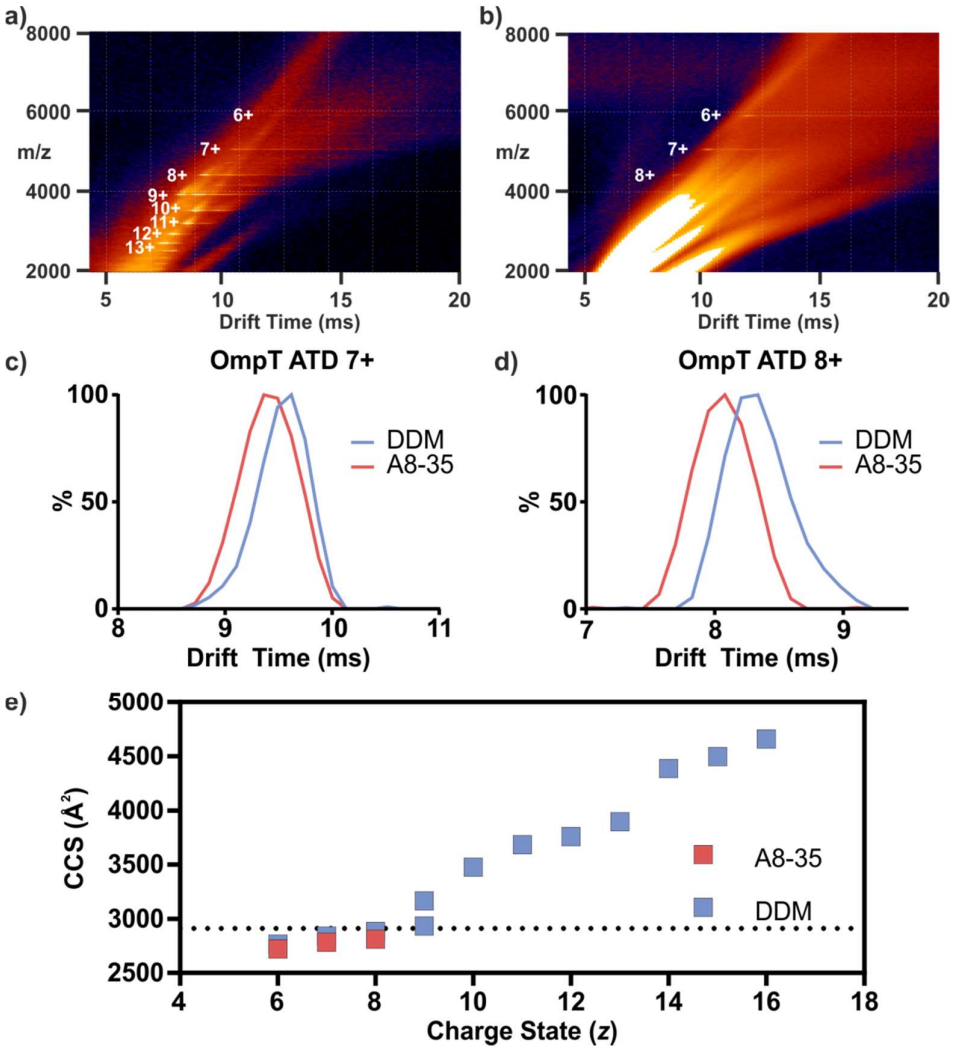

Figure 3-14 – nESI-IMS-MS driftplots of $OmpT_{HT}$ released from a) DDM micelles or b) A8-35 ($OmpT_{HT}$:A8-35 1:5 (w/w)); arrival time distributions of c) 7⁺ and d) 8⁺ $OmpT_{HT}$ and e) CCS-z relationship for $OmpT_{HT}$ released from DDM micelles or A8-35.

z	CCS (Å²)	
	DDM	A8-35
6	2767.6	2721.8
7	2841.2	2783.1
8	2883.0	2813.8
9	2932.9	-
9	3167.3	-
10	3477.5	-
11	3685.8	-
12	3758.6	-
13	3895.8	-
14	4388.1	-
15	4498.2	-
16	4657.6	-

Table 3-5 – CCS values for charge states of $OmpT_{HT}$ released from DDM micelles or A8-3.

3.2.5 nESI-IMS-MS analysis of PagP, Mhp1 and GalP from DDM micelles or A8-35 APol

All data under subheading 3.2.5 (relating to nESI-IMS-MS analysis of PagP, Mhp1 and GalP in DDM micelles or A8-35) were acquired by Dr. Antonio Calabrese and published together with work under heading 3.1.4 in Calabrese et. al, 2015[206]. This work shows the same approach applied to other MPs and provides some context for discussion of the $OmpT_{HT}$ nESI-IMS-MS data.

The effects of solubilisation in DDM micelles or A8-35 are highly dependent on the MP being studied. PagP (a β-barrel bacterial outer membrane protein) liberated from DDM micelles and A8-35 populates a similar charge state distribution (**5-9**$^{+}$ from DDM and **5-11**$^{+}$ from A8-35) and observed ions have a highly comparable CCS-z relationships (Figure 3-15a). PagP from DDM micelles or A8-35 is found to populate a native-like (**1857 - 1984** Å²) and a more expanded (**2324 – 2584** Å²) conformation equally, whether liberated from DDM micelles or A8-35 (Figure 3-15a).

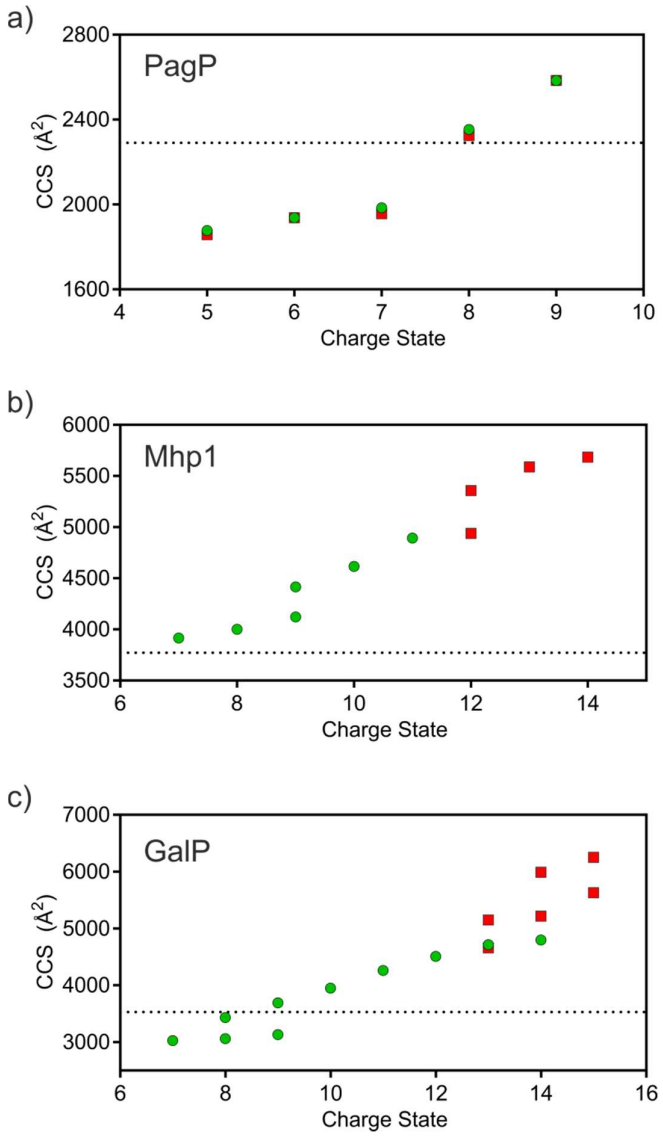

Figure 3-15 – CCS-z relationships of a) PagP, b) Mhp1 and c) GalP released from DDM micelles (red) or A8-35 (green). a) Observed charge states of PagP (5-9⁺) and their respective CCS values (1857-2584 Å²) are comparable from DDM micelles and A8-35. b) The most lowly charged states of Mhp1 (7-11⁺) and more native-like CCS values (3916-4892 Å²) are observed only from A8-35 and the more highly charged (12-14⁺) and expanded ions (4939-5684 Å²) Mhp1 ions are only observed from DDM micelles. c) GalP from A8-35 populates more lowly charged (7-14⁺) and compact states (3028-4717 Å²) but the more highly charged (13-15⁺) and expanded states (4657-5361 Å²) when released from DDM micelles. Dashed line represents the theoretical CCS (PSA) value predicted from the solved structures.

In addition to observing how nESI-IMS-MS analysis of β-barrel OMPs differs when they are solubilised in detergent micelles or APols, α-helical 12-TM MPs Mhp1 and

GalP were solubilised from *E. coli* membranes into DDM micelles, exchanged into A8-35 and subsequently analysed by nESI-IMS-MS.

Mhp1, a bacterial inner membrane hydantoin transporter protein[7], analysed when solubilised in DDM micelles populates only the most highly charged states (**12-14$^+$**), representing the most expanded conformations of Mhp1, as shown by CCS values (**4939 – 5684** Å^2) (Figure 3-15b). In contrast, when released from A8-35, ions of Mhp1 exist in two more compact conformations. One conformation is a native-like state (**7-9$^+$**) with CCS values (**3916 – 4121** Å^2) that compare well with the theoretical values from crystal structures (**3753** and **3771** Å^2) and an intermediate state (**9-11$^+$**, CCS values of **4415 – 4892** Å^2) between the previously mentioned native-like state from A8-35 and the fully denatured state observed from DDM (Figure 3-15b).

nESI-IMS-MS analysis of GalP[212-214] was similar to that of Mhp1. From DDM, GalP exists in a narrow distribution of more highly charged states (**13-15$^+$**) with corresponding larger CCS values (**4657-5631** Å^2) (Figure 3-15c). From A8-35, GalP is found in a wider distribution of charge states (**7-13$^+$**) populating a more native-like conformation (**7-9$^+$**, CCS values of **3028 – 3130** Å^2) and an intermediate state (**10-13$^+$**, CCS values of **3950 – 4714** Å^2) (Figure 3-15c). The CCS values of the most native-like GalP ions appear to underestimate the theoretical CCS value of **3530** Å^2. This may indicate some degree of collapse, although the theoretical value is calculated from a model structured generated from homologous protein, XylE[215].

3.2.6 Alternative APols for native MS of OMPs

Previous work in this chapter has established that A8-35 APol is proven to be an effective solubilising media for delivering OmpT into the gas phase for nESI-IMS-MS analysis. To explore how the properties of APols can further benefit the observation of gas phase MPs, three outer membrane proteins (OMPs) $OmpT_{HT}$, tOmpA and PagP were refolded into detergent micelles ($OmpT_{HT}$ and PagP into DDM via LDAO (Section 2.3.2) and tOmpA into β-OG (the detergent that provides the best folding yield of tOmpA) (Section 2.3.3)) and exchanged into a range of APols. These APols vary in their precursor mass, degree of grafting (and hence charge) and incorporation of different functional groups (Figure 3-16).

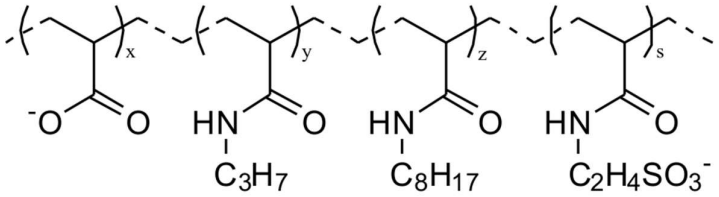

	A8-35	A8-75	SAPol	A34-35	A34-75
X	~35%	~75%	~35%	~35%	~75%
Y	~40%	-	-	~40%	-
Z	~25%	~25%	~25%	~25%	~25%
S	-	-	~40%	-	-
Mw (kDa)	4.3	4.1	5.6	17	16

Figure 3-16 – A8-35-like APols vary in size and charge and carry different functional groups as a result of grafting. A8-35 has isopropyl (Y, ~40%) and octyl (Z, ~25%) grafts to provide hydrophobicity for MP solubilisation and the remaining free acids (X, ~35%) mediate the solubility of APols and their complexes with MPs. A8-75 has a similar degree of octyl grafting (Z, ~25%) to A8-35 but lacks the isopropyl grafting and has a larger number of remaining free acids (X, ~75%) and hence higher charge density. A34-35 and A34-75 are grafted in a similar fashion to A8-35 and A8-75, respectively, but onto a larger precursor polyacrylate molecule. SAPol is similar to A8-35, with taurine grafting (S, ~40%) in place of isopropyl, providing a higher pH independent charge density.

Firstly, $OmpT_{HT}$ was refolded into DDM micelles and exchanged into each of the APols. Densitometry following cold-SDS-PAGE showed the folding yield to be greater than 90 % in DDM micelles and that the folding yield was maintained following exchange into different APols (Figure 3-17a). CD spectra were highly comparable in detergent and in all of the APols, with minima at 218 nm confirming

β-sheet (β-barrel) structure (Figure 3-17b). Despite $OmpT_{HT}$ being enzymatically active in all media used, the specific activity was found to be dependent on the APol used. Relative to DDM solubilised $OmpT_{HT}$, the specific activity was reduced in all but A34-35 (~4-fold increase in activity), with the effect being exaggerated for the more highly negatively charged APols A8-75, SAPol and A34-75 (Figure 3-17c).

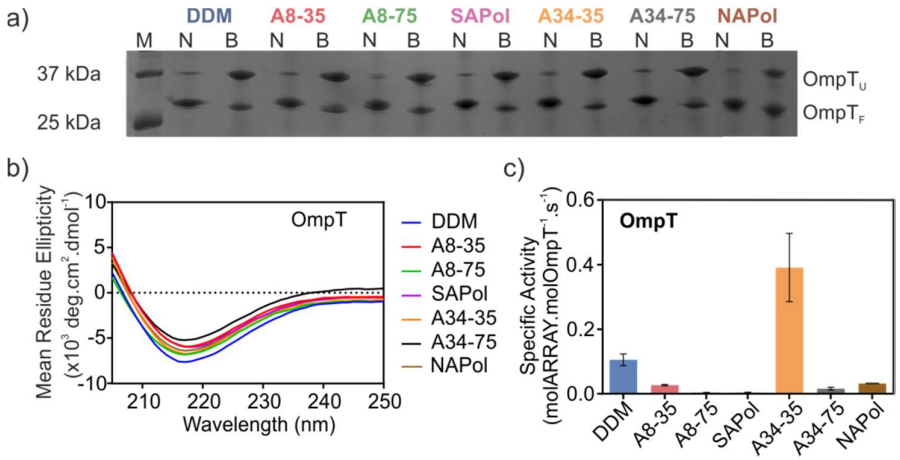

Figure 3-17 – $OmpT_{HT}$ refolded into DDM micelles and subsequently exchanged into a range of APols (OMP:APol 1:5 (w/w)) is shown to be folded by a) relative abundance of folded ($OmpT_F$) and unfolded ($OmpT_U$) OmpT by cold-SDS-PAGE, b) circular dichroism and c) peptide cleavage assay. a) Folding yield is maintained following exchange into APols and b) minima at 218 nm in CD spectra indicate native-like β-sheet structure (and presumably β-barrel topology). c) Activity shows $OmpT_{HT}$ to have variable activity depending on solubilising media. Relative to detergent micelles, $OmpT_{HT}$ activity is reduced in all but A34-35 with this exaggerated in the more negatively charged A8-75, SAPol and A34-75.

As with $OmpT_{HT}$, PagP was refolded into DDM micelles (>90 % folding yield by cold-SDS-PAGE), exchanged into APols (Figure 3-18a) and β-sheet (β-barrel) structure was identified by minima at 218 nm by circular dichroism (Figure 3-18b). CD spectra of PagP show additional maxima at 232 nm, a phenomenon resulting from the specific interaction of Tyr26 and $Trp66^{216}$, further evidence for the maintainance of the native state of PagP following exchange. PagP activity was assayed by monitoring the increase in absorption at 410 nm following hydrolysis of a palmitate substrate, *p-NPP*. Like $OmpT_{HT}$, although to a lesser extent, PagP exhibited APol-dependent activity. Relative to DDM, PagP showed greater activity in the most negatively charged APols (A8-75, SAPol and A34-75) and activity

remained similar to that of DDM micelles in the less negatively charged A8-35 and A34-35 and the neutral NAPol (Figure 3-18c).

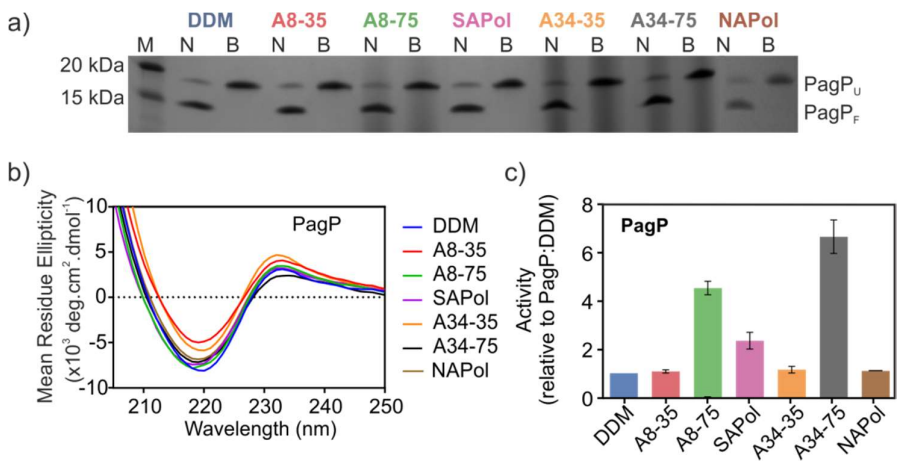

Figure 3-18 - PagP refolded into DDM micelles and subsequently exchanged into a range of APols (OMP:APol 1:5 (w/w)) is shown to be folded by a) cold-SDS-PAGE, b) circular dichroism and c) palmitate substrate hydrolysis assay. a) Folding yield is maintained following exchange into APols and b) minimum at 218 nm in circular dichroism spectra indicate native-like β-sheet structure (and presumably β-barrel topology) and presence of maximum at 232 nm is further evidence of the native-like structure. c) Activity shows PagP to have variable activity depending on solubilising media. Relative to detergent micelles and the less negatively charged A8-35, A34-35 and NAPol, activity is potentiated in the more negatively charged A8-75, SAPol and A34-75.

These deviations in the activity of OMPs in different APols (despite consistent cold-SDS-PAGE and CD spectra) suggest some charge dependent perturbations in local structure with global structure of OMPs being mostly unchanged.

Without an activity assay for tOmpA, it is only possible to comment on the presence of a compact SDS-stable β-barrel structure in different solubilising media. Unlike OmpT$_{HT}$ and PagP, tOmpA does not readily refold into LDAO or DDM micelles. tOmpA is refolded into β-OG micelles using a heat-shock refolding protocol (>90 % folding yield by cold-SDS-PAGE) and exchanged into APols (Figure 3-19a) and comparable CD spectra show minima at 218 nm, confirming β-sheet (β-barrel) structure (Figure 3-19b).

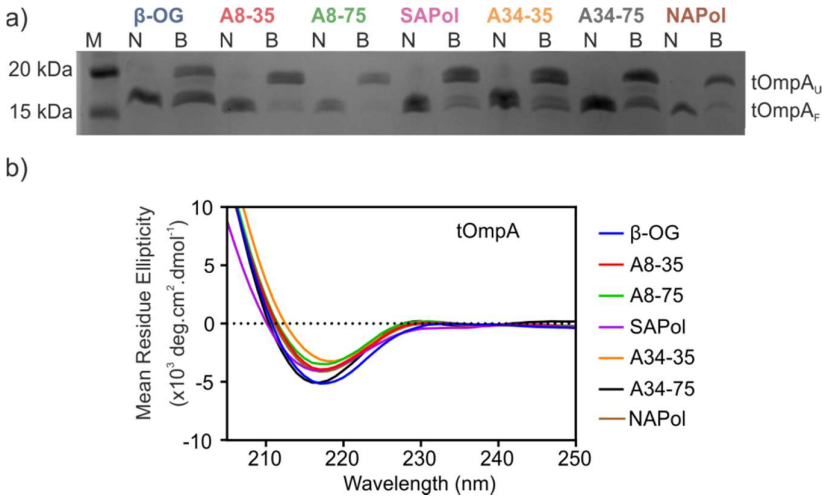

Figure 3-19 - tOmpA refolded into β-OG detergent micelles and subsequently exchanged into a range of APols (OMP:APol 1:5 (w/w)) is shown to be folded by a) cold-SDS-PAGE and b) circular dichroism. a) Folding yield is maintained following exchange into APols and b) minimum at 218 nm in circular dichroism spectra indicate native-like β-sheet structure (and presumably β-barrel topology).

All OMPs were shown to be folded in detergent micelles and in all of the APols used. Following buffer exchange into 100 mM ammonium bicarbonate (+/- 0.02 % (*w/v*) DDM), OMPs solubilised in all media were analysed by use of nESI-IMS-MS. OMP complexes had to be collisionally activated in the Trap region of the drift cell prior to IMS analysis. Observation of free OMPs was shown to be highly dependent on the media used. All OMPs were readily observed from DDM micelles and A8-35, but show far more selectivity for the other APols.

Similarly to earlier data (Section 3.2.4), OmpT$_{HT}$ populates more lowly charged, native-like conformations when released from A8-35 relative to DDM. The only other APol that OmpT$_{HT}$ was released from was A34-35 and this produced a charge state distribution comparable to that of OmpT$_{HT}$ from A8-35, suggesting that A34-35 had the same protective effect as that of A8-35 on the native-state on MPs (Figure 3-20a).

tOmpA was released from DDM micelles and all APols with the exception of A34-75. However, tOmpA could only be released from A34-35 following SEC isolation of the tOmpA:A34-35 complex. tOmpA charge state distributions were comparable when released from DDM micelles and the smaller APols, A8-35, A8-75 and SAPol (**5-7**$^+$) but differ from other media. From A34-35, tOmpA ions populate a broader,

more highly charged distribution (**5-10**$^{+}$). However, this is likely as a result of SEC clearing excess A34-35, which was shown earlier to promote higher charging of observed OMPs (Figure 3-11). More interestingly, tOmpA from NAPol populates a narrower distribution of these higher charge states (**7-10**$^{+}$) without prior SEC isolation of the tOmpA:NAPol complex, suggesting that tOmpA from NAPol populates a less native-like conformation (Figure 3-20b).

Whereas $OmpT_{HT}$ and tOmpA showed release from solubilising media, PagP was only released from DDM micelles and A8-35. Charge state distributions (**6-11**$^{+}$) are highly comparable to those observed previously (Figure 3-20c).

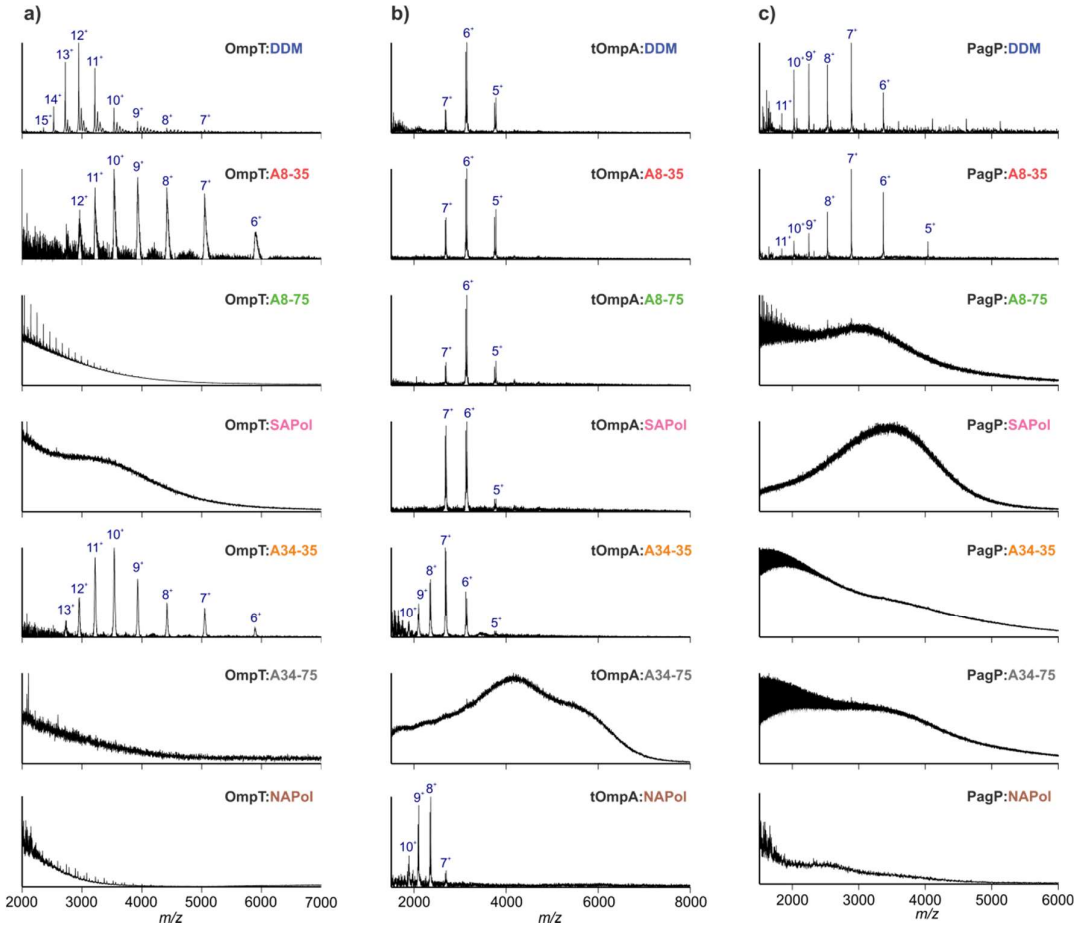

Figure 3-20 - nESI-MS spectra show variable gas-phase release of a) $OmpT_{HT}$, b) tOmpA and c) PagP from DDM micelles or a range of APols (A8-35, A8-75, SAPol, A34-35, A34-75, NAPol (OMP:APol 1:5 (w/w))). Where OMPs could not be observed, IMS-MS analyses were repeated after SEC purification of the compact OMP:APol species. This was ineffective for all but tOmpA:A34-35, for which the corresponding spectrum is shown.

Following release of OMPs from their complexes with APol, ion mobility data allowed the calculation of gas phase CCS values. CCS-z relationships showed that native-like OMPs are delivered to the gas phase irrespective of solubilising media. $OmpT_{HT}$ populates a compact (**6-9$^+$**, **2540.9 – 2887.9** Å^2) (Figure 3-21a, Figure 3-22, Table 3-6) and a more expanded conformer (**8-16$^+$**, **3103.4 – 4221.4** Å^2) when released from DDM micelles and A8-35 or A34-35, albeit with different relative abundancies as shown by the *m/z* spectra (Figure 3-20a, Figure 3-21a, Table 3-6). The same was observed for PagP, both the native-like (**5-7$^+$**, **1901.1 - 2004.1** Å^2) and the more expanded conformers (**8-11$^+$**, **2321.4 – 3080.9** Å^2) were observed following release from both DDM micelles and A8-35 (Figure 3-21c, Figure 3-22, Table 3-6). The CCS-z relationship of tOmpA is more dependent on the solubilising media. From DDM, A8-35, A8-75 and SAPol, tOmpA exists in a native-like state (**5** and **6$^+$**, **1675.6 – 1778.4** Å^2) that compares well with the theoretical value calculated from the crystal structure (1717 Å^2, 1QJP) and a more expanded conformer (**7$^+$**, **1956.7 – 2067.4** Å^2) (Figure 3-21b, Figure 3-22, Table 3-6). tOmpA from A34-35 (following SEC) populates the same conformations but over a broad range of charge states, with both conformers observed for 8$^+$ and 9$^+$ ions. From NAPol, tOmpA is more highly charged (**7-10$^+$**) but still populates the more native-like conformation observed from DDM, A8-35, A8-75 or SAPol (**7$^+$**, **1704.3** Å^2) and the 9$^+$ ion of tOmpA has a similar CCS value (**1976.7** Å^2) to that of the 7$^+$ tOmpA from DDM, A8-35, A8-75, SAPol or A34-35 (Figure 3-21b, Table 3-6). Thus, while the charge state distribution alone suggests that NAPol is less readily stabilising a native-like conformation of tOmpA, IMS-MS data show that tOmpA maintains a native-like state despite increasing unfolding pressure from Coloumbic repulsion.

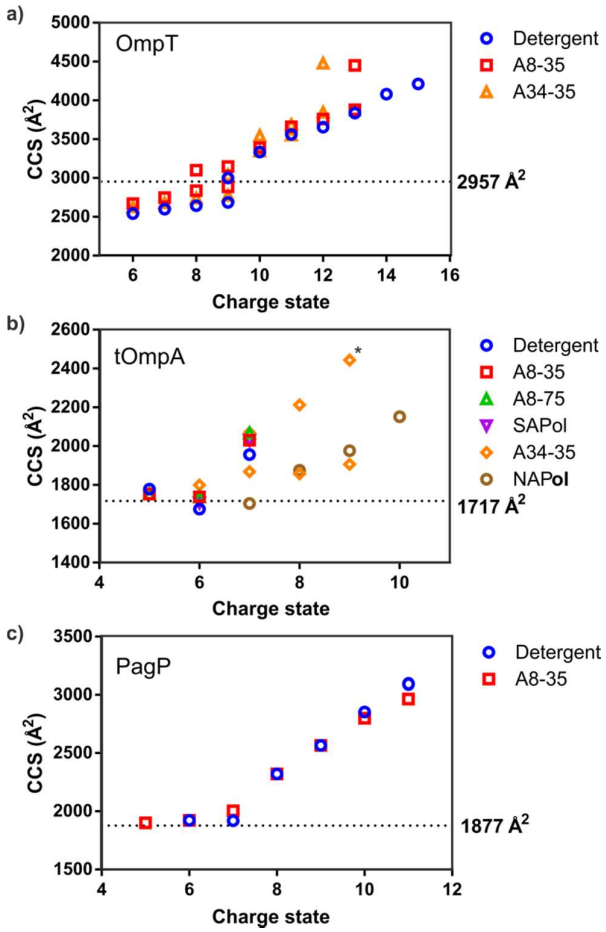

Figure 3-21 – CCS-z relationships show that a) OmpT$_{HT}$, b) tOmpA and c) PagP ions populate similar conformations, independent of solubilising media used. b) The most compact conformation of tOmpA is observed from all solubilising media. In addition, the most native-like tOmpA ions can be seen to persist at higher charge states when released from NAPol.

To simplify, if we consider only the most native-like OMP ions (those of the lowest charge), IMS-MS data show that OMP conformation is independent of solubilising media. Measured CCS values of OmpT$_{HT}$ (~**2600** Å^2) are consistently lower than the theoretical value (**2957** Å^2) calculated from the solved structure (PDB 1I78)[30], suggesting a degree of collapse, most likely in the extended barrel and loop regions. tOmpA (~**1700** Å^2) and PagP (~**1900** Å^2) compare favourably to their theoretical values (**1717** (1QJP)[20] and **1877** (1THQ)[28] Å^2, respectively) (Figure 3-22).

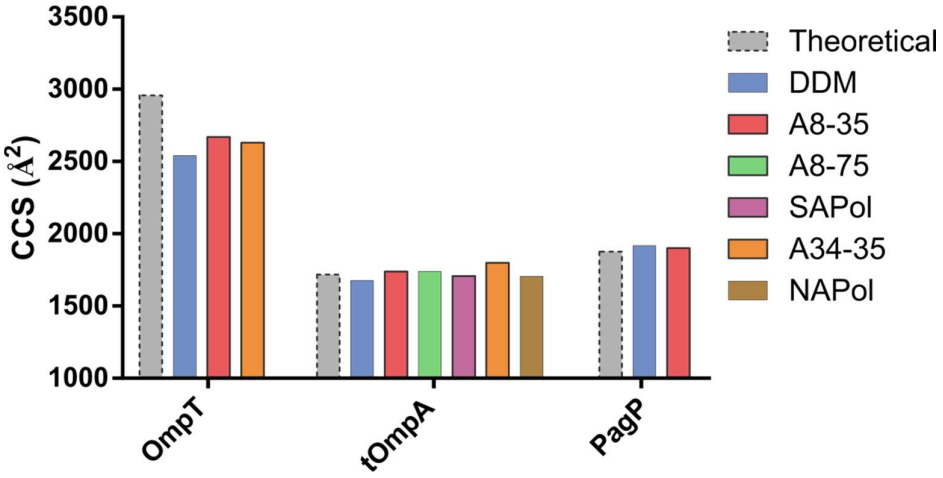

Figure 3-22 –CCS values of lowest charge state ions of $OmpT_{HT}$, tOmpA and PagP observed from each solubilising media. CCS values of $OmpT_{HT}$ appear to be collapsed relative to theoretical value calculated from the solved structure (PDB 1I78)[30]. tOmpA and PagP compare well with theoretical values calculated from their respective solved structures (PDB 1QJP[20] and 1THQ[28], respectively).

	z	CCS (Å²)					
		DDM	A8-35	A8-75	SAPol	A34-35	NAPol
$OmpT_{HT}$ 2957 Å² PDB: 1I78	5						
	6	2540.9	2670.6			2629.4	
	7	2599.4	2747.7			2681.3	
	8	2643.3	2839.0			2741.3	
	8		3103.4				
	9	2685.1	2887.9			2776.6	
	9	3004.1	3151.1			3042.4	
	10	3339.2	3396.6			3351.1	
	10					3550.8	
	11	3567.3	3666.2			3559.1	
	11					3693.4	
	12	3660.3	3765.7			3853.6	
	12					4490.0	
	13	3843.0	3885.5				
	13		4460.2				
	14	4088.7					
	15	4221.4					
tOmpA 1717 Å² PDB: 1QJP	5	1778.4	1753.1	1753.1			
	6	1675.6	1739.0	1739.0	1707.3		
	7	1956.7	2030.6	2067.4	2030.6	1799.0	1704.3
	8					1868.6	
	8					2069.8	1875.9
	9					1857.8	
	9					2212.6	1976.7
	10					1906.6	
	10					2443.3	2151.9
PagP 1877 Å² PDB: 1THQ	5		1901.1				
	6	1923.2	1923.2				
	7	1918.5	2004.1				
	8	2321.4	2321.4				
	9	2565.8	2565.8				
	10	2852.4	2799.5				
	11	3080.9	2963.8				

Table 3-6 – CCS values for $OmpT_{HT}$, tOmpA and PagP released from DDM micelles and a range of APols (OMP:APol 1:5 (w/w)).

3.3 Discussion

There is an increasing amount of literature referring to the use of native mass spectrometry for the observation of MPs and MP complexes, and the study of their structures and mechanisms of release in the gas phase[118, 158, 217].

2D mass spectra alone tell us much about the native state of a MP or MP complex. The molecular mass of a protein can be related to the theoretical surface area, which further relates to the predicted average charge states feasible. Furthermore, following the release of a native MP complex from detergent micelles, additional collisional activation results in the ejection of subunits from the complex. Formation of such subcomplexes informs on the topology of a complex, as shown with the V-ATPase from *Thermus thermophilus*[16] and the ATP-binding cassette transporter $BtuC_2D_2$[140]. 2D mass spectra can also be used to identify binding events and determine how they affect the gas-phase stability of MP complexes[17, 145, 152, 155].

IMS-MS provides a further level of characterisation of the native state of MPs and their complexes. Analyses from detergent micelles have shown numerous complexes to be in a native-like state judged by their CCS values comparing favourably to theoretical values from solved crystal structures. Prime examples are the KirBac3.1 potassium channel[150], $BtuC_2D_2$[150] and the A-ATPase from *Thermus thermophilus*[17]. In combination with targeted labelling, IMS can even inform on the functional workings of a MP complex, such as MscL, a pore protein that shows a graded opening upon treatment with a bulky thiol labelling group targeted to the pore forming region of the protein[151].

These findings show the scope of MP study using mass spectrometry but are largely limited to MPs solubilised in detergent micelles. The spherical shape of detergent micelles is not truly representative of a native lipid bilayer, and can perturb protein structure. This, in conjunction with the dynamic nature of micelles, results in MPs *in vitro* being prone to misfolding and aggregation. For this reason, novel surfactants have been applied for MS analyses of MPs, namely the use of APols and lipid bilayer mimetics such as nanodiscs and bicelles[50, 53, 157, 159]. This is being carried out with the aim of assuring the most native-like state of MPs in the

gas phase. 2D MS analysis showed DAGK to be stabilised from solubilising media other than detergent micelles[159]. From APol, DAGK trimer is observed to a lesser extent than when released from bicelles or nanodiscs, although considerable collisional activation is required, most likely due to large amount of non-protein material that must be removed from the complex.

With the use of a number of techniques, APols have been shown to improve on the solution phase properties of MPs and suggest potential for delivery of MPs into the gas phase. Except for the data shown here, MS analysis of MP:APol complexes is limited. NAPol solubilised BR was delivered to the gas phase following MALDI ionisation[63]. In the absence of ion mobility and charge state distribution information, this only serves to tell us that BR is liberated in the gas phase. Leney *et al*. described the first use of IMS-MS to validate the native state of MPs in the gas phase from a APol bound state and acts as the platform for work shown here[75]. Low charge states of OmpT and PagP are indicative of a compact native-like state, confirmed by calculation of CCS values that compare favourably to theoretical values from solved crystal structures. In this work, high activation energies were required to release the MP in the gas phase, which can potentially be perturbing to the native state of MPs and could be detrimental to any future experiments that would involve observation of protein:protein or protein:ligand interactions.

Early work presented in this chapter shows how simple modifications to sample conditions, notably analyte concentration (Figure 3-3) and optimised MP:APol refolding ratios (Figure 3-4), can give greater confidence in the native state of MPs in the gas phase by allowing observation of MPs at lower activation energies and with greater "signal-to-noise" ratios. With techniques such as SEC (Figure 3-6 and Figure 3-9), observation of native-like MPs is improved further and allows analysis of individual conformers of a MP (Figure 3-7) in the absence of factors, such as excess free APol, that may perturb analyses.

OMPs have been observed from APols using MS in multiple instances, but there has not yet been a detailed comparison of detergent micelles or APols as a means of studying the native state of MPs by MS. DDM is a commonly used detergent, ideal for native mass spectrometry because it is non-ionic, non-denaturing and has a

very low critical micelle concentration (CMC) (0.008 % (*w/v*))[140, 147]. MPs (α-helical and β-barrel) are readily folded in the solution phase in either DDM micelles or A8-35 APol. In solution, A8-35 shows a great ability to improve the stability of MPs (Figure 3-17, Figure 3-18 and Figure 3-19). MPs solubilised in detergent micelles are often rapidly denatured and aggregated[62, 65, 209], due to the highly dynamic and spherical nature of the micelle. In the same instance, MPs solubilised in A8-35 are still folded, functional and soluble after months[62, 65, 209]. The best understanding of this phenomenon is a result of kinetic stability of the complex. Pocanschi et al. 2013 show that OmpA refolded in A8-35 is actually thermodynamically less stable than when refolded into LDAO micelles[60]. However, the nature of the APol molecule results in a very large number of small hydrophobic interactions, meaning the interaction of APol with MPs is near irreversible due to the statistical probability of all interactions being lost at once.

Direct comparison of nESI-IMS-MS (3D) analyses of MPs released from DDM micelles and A8-35 APol show that this improved stability is translated into the gas phase. Three of four studied proteins ($OmpT_{HT}$, Mhp1 and GalP) existed in the lowest charge states when released from A8-35 (Figure 3-13 and Figure 3-15b,c). These charge states represent the most native-like conformations, as shown by CCS values that compare most favourably to theoretical values from crystal structures. This is indicative of the proteins being in a more compact state as they are ionised. This effect is far greater for the α-helical Mhp1 and GalP with charge states shifting from 12-14$^+$ and 13-15$^+$ to 7-13$^+$ and 7-14$^+$, respectively (Figure 3-15b,c) than for the β-barrels, $OmpT_{HT}$ and PagP (Figure 3-12 and Figure 3-15a). PagP charge state distributions and CCS-z relationships are near identical when released from DDM micelles or A8-35 APol (Figure 3-15a) and although $OmpT_{HT}$ from DDM micelles does populate the most native like states, it does so to a far greater extent when released from A8-35. This difference between α-helical and β-barrel proteins can be easily explained by the β-barrel proteins being proven to be more stable than other MPs.

$OmpT_{HT}$ differs from PagP in that it has ~50 % of its barrel surface protruding from the membrane (Figure 1-2). This explains how $OmpT_{HT}$ is prone to such unfolding, despite the innate stability of β-barrels, and suggests one mechanism by

which A8-35 may be protecting the MPs. It has been posited that extra contacts can be formed between APols and MPs, shown by NMR of BR in NAPol or DDM micelles[78] and MD simulations of OmpX solubilised in A8-35[64]. Extra contacts could both directly stabilise the native state of MPs and protection from excess charging would limit the potential of gas phase unfolding of MPs due to coloumbic repulsion.

In addition to any protective effects of extra contacts of APols with MPs, further protection is afforded to the MP gas phase ions by the manner of APol dissociation. It has been shown that a process of evaporative cooling is greatly beneficial to stabilising the native state of MPs[118]. Dissociation of detergent molecules such as DDM allows MP ions to remain more compact. The large number of contacts formed between A8-35 molecules and the surface of MPs, compared to DDM molecules, causes A8-35 to dissociate more slowly. This will result in a MP being exposed to fewer gas phase collisions following liberation and reduced gas phase unfolding.

Having established the potential of APols to exert a greater stabilisation of gas phase MP ions relative to detergent micelles, the properties beneficial for delivery of MPs to the gas phase were then explored. A range of APols have been previously developed to expand their repertoire of uses. NAPol and SAPol have been developed to be soluble in acidic conditions and in the presence of divalent cations in which A8-35 would be insoluble[33, 58]. Other APols, that are more chemically similar to A8-35, use larger precursors and vary in their degree of grafting (which in turn changes the charge density). The solution phase properties of many of these APols (free in solution) has been have been characterised and a small number applied to a range of techniques for structural biology [62, 69-76]. Prior to this work only A8-35 and NAPol had been applied to the delivery of native MPs to the gas phase for MS analysis[63, 75] and the work here is one of the most comprehensive direct comparisons of multiple APols for use by a single technique.

Cold-SDS-PAGE and circular dichroism showed that OMPs adopt an equivalent global structure regardless of the solubilising media used, much like our comparison of DDM micelles and A8-35 shown above. This is correlated with IMS

data that show all OMPs (where observed) populate the most native-like states independent of the APol (Figure 3-21 and Figure 3-22). There are, however, APol dependent differences in the local structure of OMPs and in the observation of OMPs in the gas phase (Figure 3-20). These differences in local structure are evidenced by a difference in the enzymatic activity of OmpT and PagP and seem to be mostly related to the charge density of the solubilising media (Figure 3-17c and Figure 3-18c). OmpT activity is greatly reduced in the APols with the greatest charge density and PagP has a potentiated activity in the most charged APols. Even the less negatively charged A8-35 and A34-35 have fairly high charge density and it is understandable that these and, more so, the more highly charged APols can create an electrostatic effect that may slightly perturb structure.

2D mass spectra show that observation of OMPs in the gas phase is highly dependent on the APol used (Figure 3-20). With the exception of tOmpA from A8-75 and SAPol, OMPs are not observed when solubilised in the most negatively charged APols. Considering the high negative charge density of APols (and their respective complexes with OMPs), this likely results from poor ionisation of the complex using positive mode nESI. Although, ionisation in negative mode did not allow for observation of OMPs or APols. Also, worth noting is that OMPs are not readily released from the larger APols, OmpT is seen from A34-35, tOmpA is only seen from A34-35 following SEC isolation of protein material and no OMPs are observed at all from A34-75. These larger molecules would have potential for forming more contacts with OMPs than the smaller A8-35, which would result in even greater kinetic stability of the MP:APol complexes. This increased stability could underpin the means by which the complexes remain intact in the gas phase and prevent the observation of OMPs. Combined, this work provides good insight (from a technical standpoint) into the mechanisms of APol mediated delivery of MPs to the gas phase and highlights how charge and molecule size are important in delivery, and maintain the native-state of MPs in the gas phase.

4 Using Fast Photochemical Oxidation of Proteins (FPOP)-LC-MS to investigate the manner of interactions of MPs with detergent micelles and APols

4.1 Introduction

The work described in this Chapter has been published in Watkinson et al. 2016, J. Am. Soc. Mass Spectrom.[211].

FPOP covalently labels the solvent accessible side chains of a protein[163-166]. The process involves UV-photolysis of H_2O_2 to generate ·OH radicals, which (in the presence of a scavenger e.g. 15 mM glutamine) have a lifetime of ~1 μs[166]. Radical species react rapidly with the most reactive side chains (Met, Cys, Trp, Tyr, Phe and His). Oxidation of amino acid side chains results in a number of possible modification but most commonly a +16 Da mass addition[165]; such modifications are readily identified using MS and can be identified at the peptide and residue level using LC-MS/MS for oxidation mapping of protein digests[166, 169, 174].

FPOP-LC-MS has been used previously to probe protein structure[174, 177, 179-180, 218], folding and dynamics[163, 169, 173], as well as mapping binding epitopes in protein-protein and protein-ligand interactions[167, 175, 180]. This has been achieved using both quantitative and qualitative LC-MS approaches. FPOP-LC-MS has been used to identify solvent exposed residues of BR in semi-denaturing conditions[177], observe regions of Im7 (a well-studied standard in protein folding) that are solvent exposed when trapped in a number of intermediate folding states[169] and tracks protection of residues in EGFR (epithelial growth factor receptor) upon binding to adnectin in order to map the binding site[175]. FPOP-LC-MS is a powerful technique that relates identification of a simple mass addition to the solvent exposure state of a particular residue and, hence, to the structure of a protein (or protein complex) at a residue level.

The more conventional DDA[161] MS/MS analysis involves using the quadrupole to mass select the most intense species eluted from an analytical LC column, fragmenting the selected peptide ion and acquiring peptide fragment ions of the selected precursor (Section 1.6.9). Waters MS^e does not use mass selection prior to

fragmentation (Section 1.6.9)[219]. Instead, the instrument constantly switches between high and low collision energy settings and acquires fragment and precursor ions simultaneously for all co-eluting species. This continuous acquisition method results in more accurate peak shape in LC chromatograms, making it a better method for more reliable quantitation, but can result in the need for more complicated data analysis using proprietary software. Both the DDA and MS^e methods have been used to here as a means for qualitative and quantitative analysis, respectively.

Work presented in the previous chapter has shown how MPs have different gas-phase and solution-phase properties when solubilised in detergent micelles or APol. FPOP-LC-MS could provide structural data at the peptide and residue level to better understand the means of surfactant interactions with MPs and how this translates into structural differences. $OmpT_{HT}$, in particular, was shown to have different enzymatic activities in detergent or APol (Sections 3.2.4 and 3.2.6) and an intriguing shift in charge state distributions observed with nESI-IMS-MS analyses that is not observed in smaller OMPs (PagP and tOmpA, which do not have the extended β-barrel domain that $OmpT_{HT}$ possesses[20, 28, 30, 37]) (Figure 1-2, Section 3.2.6). The previously described shift in charge state distribution had been attributed to extra contacts formed between A8-35 and the extramembrane region of $OmpT_{HT}$. Extra contacts may result in better constraining of flexible loop regions (that would accommodate more charge with greater flexibility) relative to $OmpT_{HT}$ solubilised in DDM micelles and/or direct protection from surplus charging by excluding these parts of the protein surface from solvent.

Work shown in this chapter aims to explore the use of both qualitative and quantitative FPOP-LC-MS to explore the properties of the membrane protein $OmpT_{HT}$ solubilised in either DDM micelles or A8-35.

4.2 Results

4.2.1 Oxidation of model peptides to study the quenching effect of MP buffer components

FPOP is highly sensitive to the chemical environment. Radical reactive species in the sample buffer can potentially quench labelling by reducing the effective dose of hydroxyl radicals[170]. MP structure and stability in solution is often highly dependent on complex sample buffers, with the presence of detergents, lipids and other stabilising factors such as salt and substrates often being necessary.

DDM micelles and A8-35 are used in work presented here and as such it was important to be aware of whether these MP solubilising agents affect the oxidative labelling process.

Model peptides (Figure 4-1) were chosen to determine the efficiency of photo-oxidative modification of radical reactive aromatic residues (Trp (W), Tyr (Y) and Phe (F)) in the presence of MP solubilising buffer components. Below it is shown how modification of these model peptides was affected by DDM micelles, A8-35, urea and DLPC liposomes.

F1	GSGSGKFGSGSGK
W1	GSGSGKWGSGSGK
Bradykinin	RPPGFSPFR
Angiotensin II	DRVYIHPFHL

Figure 4-1 – Sequences of control peptides used in FPOP quenching studies. Radical reactive aromatic F, W and Y residues are highlighted.

Model peptides, W1 and F1 (Figure 4-1)(10 μM), were incubated with 0.05 % (v/v) H_2O_2 in the presence of 0.02% DDM (w/v), 5 $mg.ml^{-1}$ A8-35 APol or in the absence of either. Peptides were modified by irradiation with a UV laser as the sample was passed through a capillary and into a quench solution (Section 2.6.1). Peptides were loaded onto a Waters nanoAcquity UPLC system for analysis by LC-MS/MS (Section 2.6.3). F1 (10 μM) incubated with 0.05 % (v/v) H_2O_2 was unmodified (m/z **556.26**) prior to UV irradiation (Figure 4-2a). Following UV irradiation, F1 was

both singly (+16 Da, *m/z* **564.26**) and doubly (+32 Da, *m/z* **572.26**) modified (Figure 4-2b). Addition of 0.02 % (*w/v*) DDM did not change the relative abundance of unmodified or singly or doubly modified peptide, whereas addition of 5 mg.ml^{-1} resulted in a reduced abundance of the modified F1 peptide (Figure 4-2c,d).

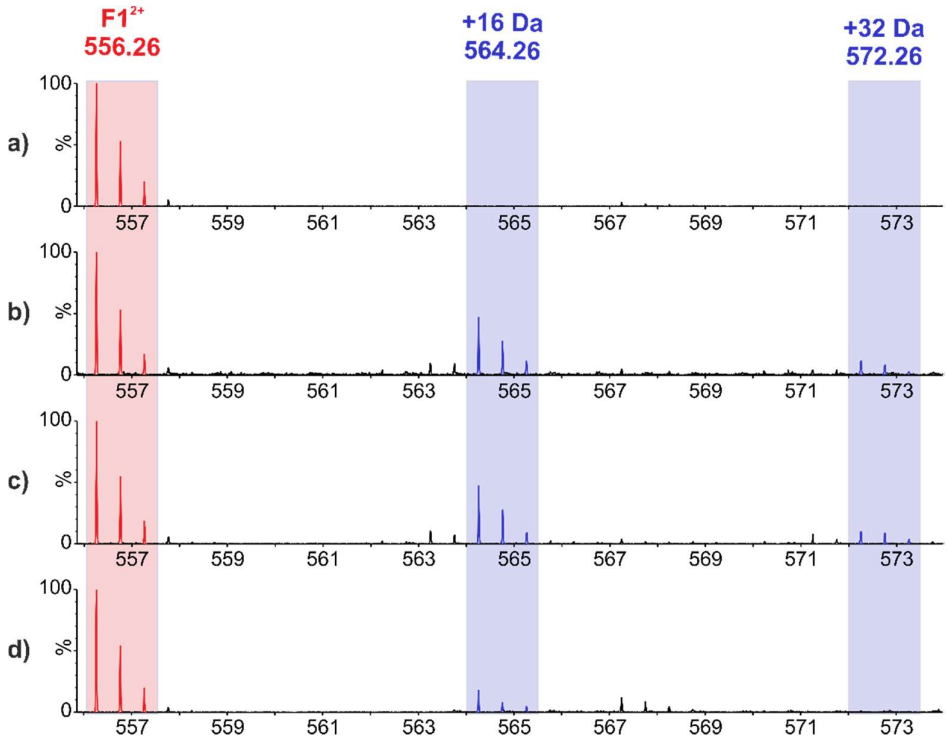

Figure 4-2 – Model peptide F1 (10 µM) analysed using FPOP-LC-MS in the presence of DDM micelles or A8-35 (Figure 4-1) in 10 mM sodium phosphate pH 8.0 0.05 % (v/v) H_2O_2 was analysed using LC-MS (a) without UV irradiation, (b) following UV irradiation and following UV irradiation in the presence of (c) 0.02 % (w/v) DDM or (d) 5 mg.ml^{-1} A8-35. Unmodified F1 (m/z 556.26) is shown in red and singly (+16 Da, m/z 564.26) and doubly charged (+32 Da, m/z 572.26) F1 are shown in blue. (a) F1 shows no oxidation (blue) without UV irradiation and (b) F1 is modified following UV irradiation. Modification of F1 is maintained with the addition of (c) DDM and reduced with the addition of (d) A8-35.

Like F1, W1 (10 µM) incubated with 0.05 % (*v/v*) H_2O_2 was unmodified (*m/z* **575.77**) prior to UV irradiation (Figure 4-3a). Following UV irradiation, W1 was both singly (+16 Da, *m/z* **583.76**) and doubly (+32 Da, *m/z* **591.76**) modified (Figure 4-3b). Addition of 0.02 % (*w/v*) DDM did not change the relative abundance of unmodified or singly or doubly modified peptide, whereas addition

of 5 mg.ml^{-1} A8-35 results in a reduced abundance of the modified W1 peptide (Figure 4-3c,d).

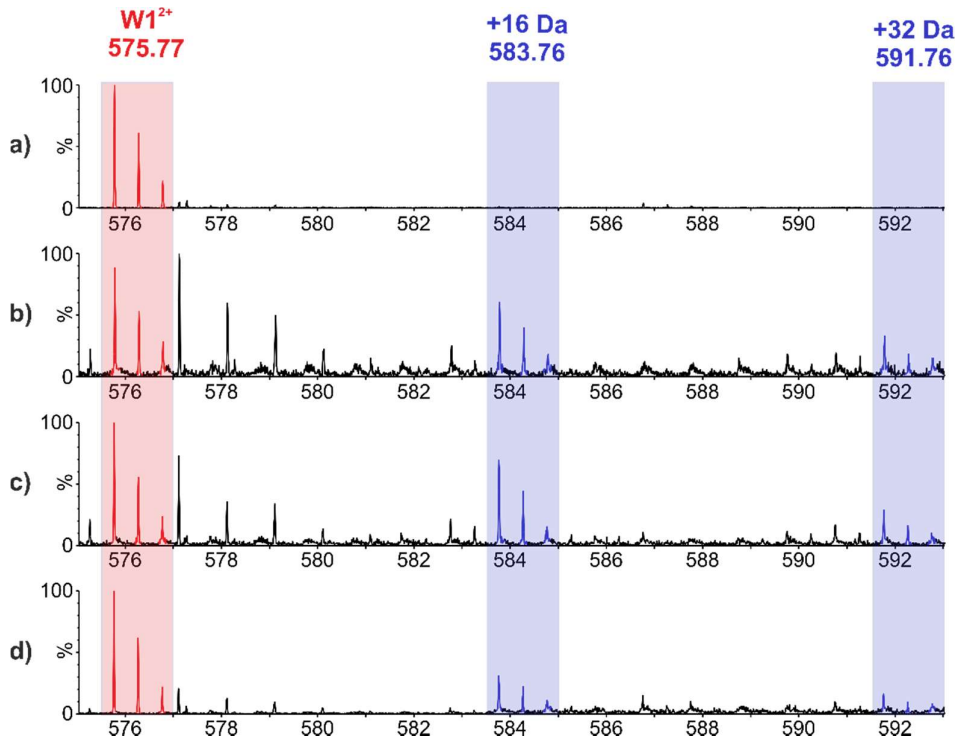

Figure 4-3 - Model peptide W1 (10 µM) analysed using FPOP-LC-MS in the presence of DDM micelles or A8-35 APol (Figure 4-1) in 10 mM sodium phosphate pH 8.0 0.05 % (v/v) H_2O_2 was analysed using LC-MS (a) without UV irradiation, (b) following UV irradiation and following UV irradiation in the presence of (c) 0.02 % (w/v) DDM or (d) 5 mg.ml^{-1} A8-35. Unmodified W1 (m/z 575.77) is shown in red and singly (+16 Da, m/z 583.76) and doubly charged (+32 Da, m/z 591.76) W1 are shown in blue. (a) W1 shows no oxidation (blue) without UV irradiation and (b) W1 is modified following UV irradiation. Modification of W1 is maintained with the addition of (c) DDM and reduced with the addition of (d) A8-35.

F1 and W1 were modified to a lesser degree following the addition of 5 mg.ml^{-1} A8-35 (F1 = **30.2** % -> **4.5** %, W1 = **27.8** % -> **8.4** %) but the degree of modification remained unchanged in the presence of 0.02 % (*w/v*) DDM (Figure 4-4). This suggests that A8-35 is protecting small peptides from oxidative labelling in solution, either because of a reduction in the radical dose through quenching or an interaction of the peptides with A8-35 APol in solution.

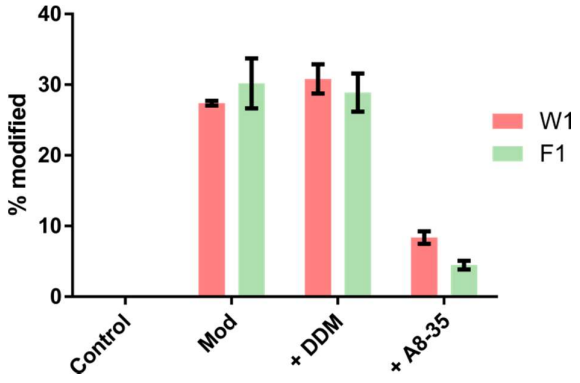

Figure 4-4 – W1 and F1 peptides are oxidatively labelled by FPOP in the presence of DDM micelles or A8-35 and 0.05 % H_2O_2. Degree of modification of W1 and F1 peptides are measured alone (Mod) or in the presence of DDM micelles (0.02 % w/v) or A8-35 (5 mg.ml^{-1}). Control is treatment with H_2O_2 but without UV irradiation. Error bars show SEM (n=3).

In studies investigating the mechanisms of OMP folding, OMPs are often refolded into synthetic liposomes from a chemically denatured state, such as using up to 8 M urea. Folding yields and rates can be controlled by the final concentration of urea, with fully folded OMPs being formed in the presence of up to and greater than 1 M urea. For this reason, data here is presented to show the effect of DLPC liposomes (up to 32 mM) and urea (up to 4 M) on the photochemical oxidation of peptides and how they would impact on any future OMP refolding experiments using FPOP-LC-MS.

BK (10 µM) incubated with 0.05 % (*v/v*) H_2O_2 was not modified (*m/z* **531.34**) prior to UV irradiation (Figure 4-5a) but is singly (+16 Da, *m/z* **539.34**) and doubly (+32 Da, *m/z* **547.34**) modified following irradiation (Figure 4-5b). The relative abundance of modified and unmodified BK were maintained with the addition of 4 mM DLPC (as 100 nm LUVs) (Figure 4-5c,d, Figure 4-9).

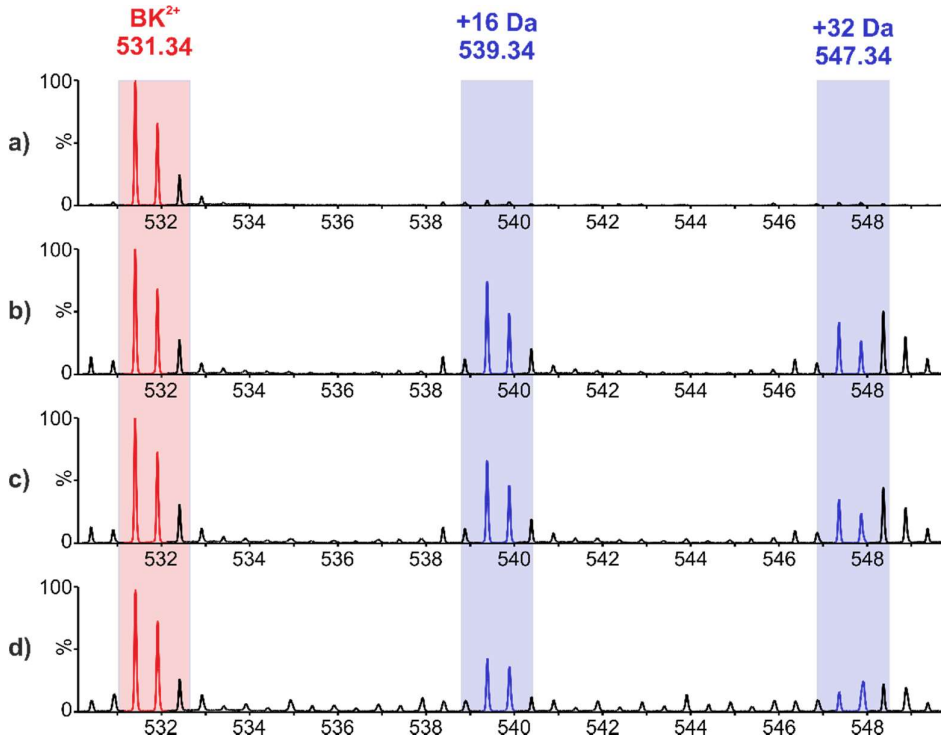

Figure 4-5 – BK (10 µM) was analysed by FPOP-LC-MS in the presence of DLPC liposomes (Figure 4-1) in 10 mM sodium phosphate pH 8.0 0.05 % (v/v) H_2O_2 was analysed using LC-MS (a) without UV irradiation, (b) following UV irradiation and following UV irradiation in the presence of (c) 4 mM or (d) 32 mM DLPC. Unmodified BK (m/z 531.34) is shown in red and singly (+16 Da, m/z 539.34) and doubly charged (+32 Da, m/z 547.34) BK are shown in blue.

AngII (10 µM) incubated with 0.05 % (*v/v*) H_2O_2 was not modified (*m/z* **524.23**) prior to UV irradiation (Figure 4-6a) but was singly (+16 Da, *m/z* **532.23**) and doubly (+32 Da, *m/z* **540.23**) modified following irradiation (Figure 4-6b). The relative abundance of modified and unmodified BK were maintained with the addition of 4 mM DLPC (as 100 nm LUVs) (Figure 4-6c,d, Figure 4-9).

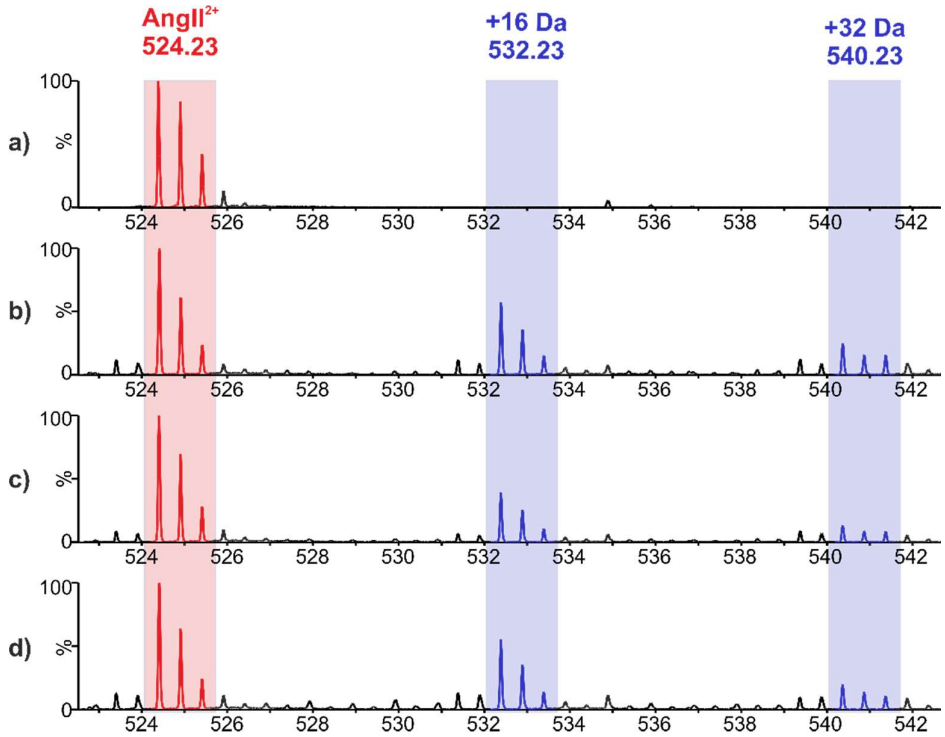

Figure 4-6 - AngII (10 µM) was analysed by FPOP-LC-MS in the presence of DLPC liposomes (Figure 4-1) in 10 mM sodium phosphate pH 8.0 0.05 % (v/v) H_2O_2 was analysed using LC-MS (a) without UV irradiation, (b) following UV irradiation and following UV irradiation in the presence of (c) 4 mM or (d) 32 mM DLPC. Unmodified AngII (m/z 524.23) is shown in red and singly (+16 Da, m/z 532.23) and doubly charged (+32 Da, m/z 540.23) AngII are shown in blue.

BK (10 µM) incubated with 0.05 % (*v/v*) H_2O_2 was not modified (*m/z* **531.34**) prior to UV irradiation (Figure 4-7a) but was singly (+16 Da, *m/z* **539.34**) and doubly (+32 Da, *m/z* **547.34**) modified following irradiation (Figure 4-7b). The relative abundance of modified and unmodified BK decreased with increasing concentrations of urea (Figure 4-9b), although it was a modest decrease that was difficult to observe on representative 1D mass spectra of a single experimental repeat (Figure 4-7c-f).

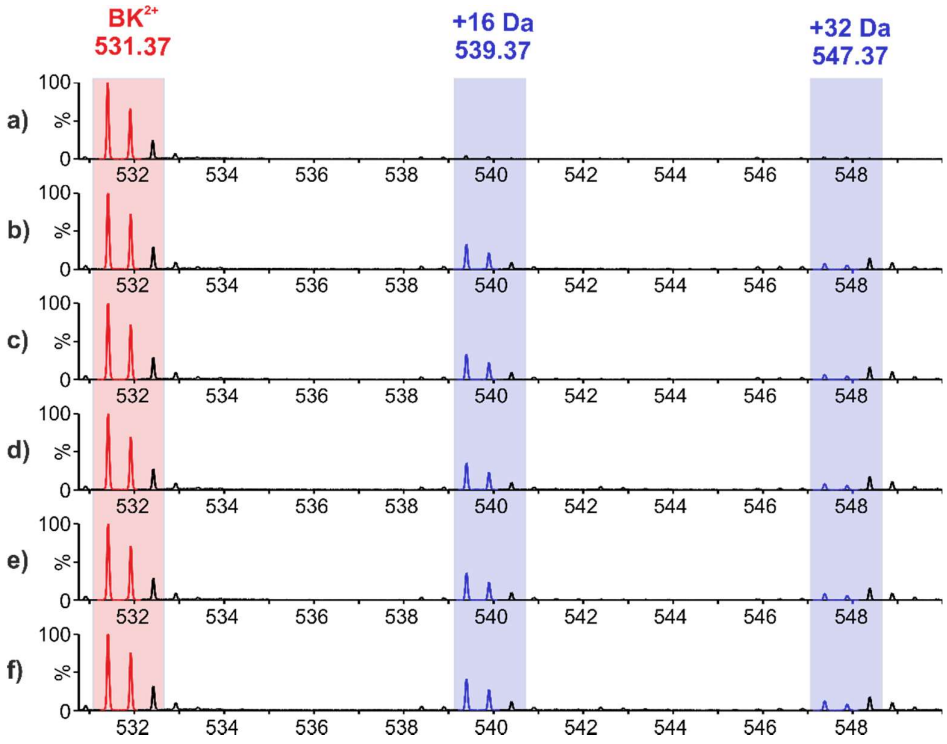

Figure 4-7 - BK (10 µM) was analysed by FPOP-LC-MS in the presence of urea (Figure 4-1) in 10 mM sodium phosphate pH 8.0 0.05 % (v/v) H_2O_2 was analysed using LC-MS (a) without UV irradiation, (b) following UV irradiation and following UV irradiation in the presence of (c) 0.1 M, (d) 0.4 M, (e) 1 M or (f) 4 M urea. Unmodified BK (m/z 531.37) is shown in red and singly (+16 Da, m/z 539.37) and doubly charged (+32 Da, m/z 547.37) BK are shown in blue.

AngII (10 µM) incubated with 0.05 % (*v/v*) H_2O_2 is not modified (*m/z* **524.23**) prior to UV irradiation (Figure 4-8a) but is singly (+16 Da, *m/z* **532.23**) and doubly (+32 Da, *m/z* **540.23**) modified following irradiation (Figure 4-8b). Relative abundance of modified and unmodified AngII decreases with increasing concentrations of urea (Figure 4-9b), although it is a modest decrease that is difficult to observe on representative 1D mass spectra of a single experimental repeat (Figure 4-8c-f).

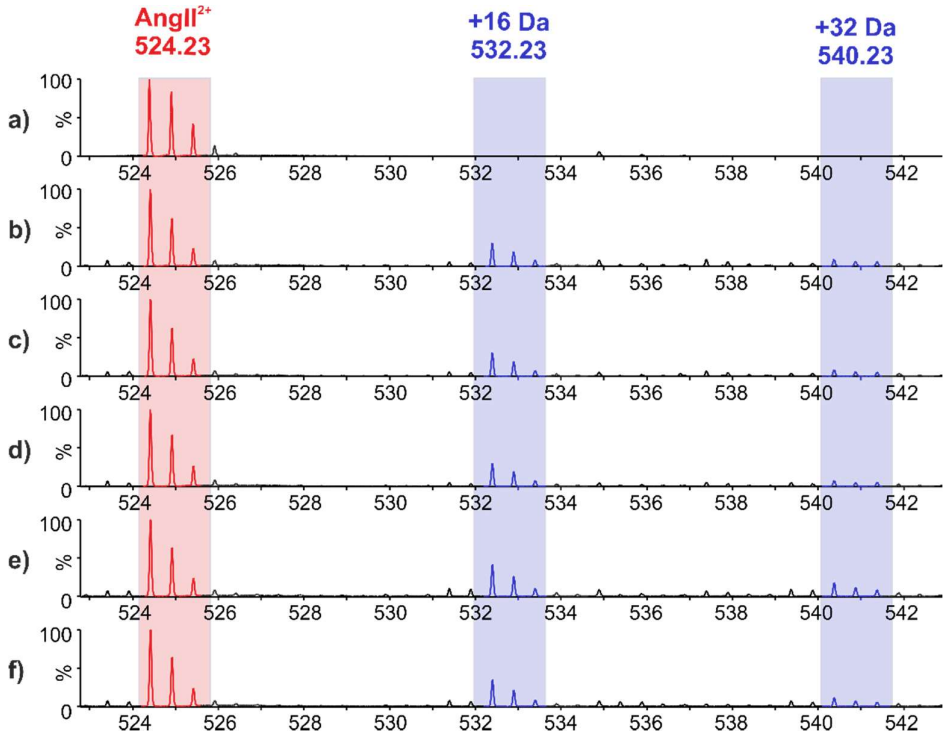

Figure 4-8 - AngII (10 µM) was analysed by FPOP-LC-MS in the presence of urea (Figure 4-1) in 10 mM sodium phosphate pH 8.0 0.05 % (v/v) H_2O_2 was analysed using LC-MS (a) without UV irradiation, (b) following UV irradiation and following UV irradiation in the presence of (c) 0.1 M, (d) 0.4 M, (e) 1 M or (f) 4 M urea. Unmodified AngII (m/z 524.23) is shown in red and singly (+16 Da, m/z 532.23) and doubly charged (+32 Da, m/z 540.23) AngII are shown in blue.

BK and AngII (Figure 4-1) were labelled by FPOP in the presence of DLPC lipid extruded into 100 nm LUVs or in up to 4 M urea. The results show that oxidation of peptides is unaffected by addition of DLPC liposomes up to 32 mM (Figure 4-9); which is equivalent to a LPR (lipid:protein molar ratio) of 3200, comparable to that commonly used in OMP refolding assays[27, 40, 201, 220]. Urea added above 0.4 M results in a mild reduction in degree of modification of BK and AngII, with oxidation reduced by ~ one third in the presence of 4M urea (BK = **50.9** % -> **33.9** %, AngII = **55.2**% -> **39.8** %) (Figure 4-9).

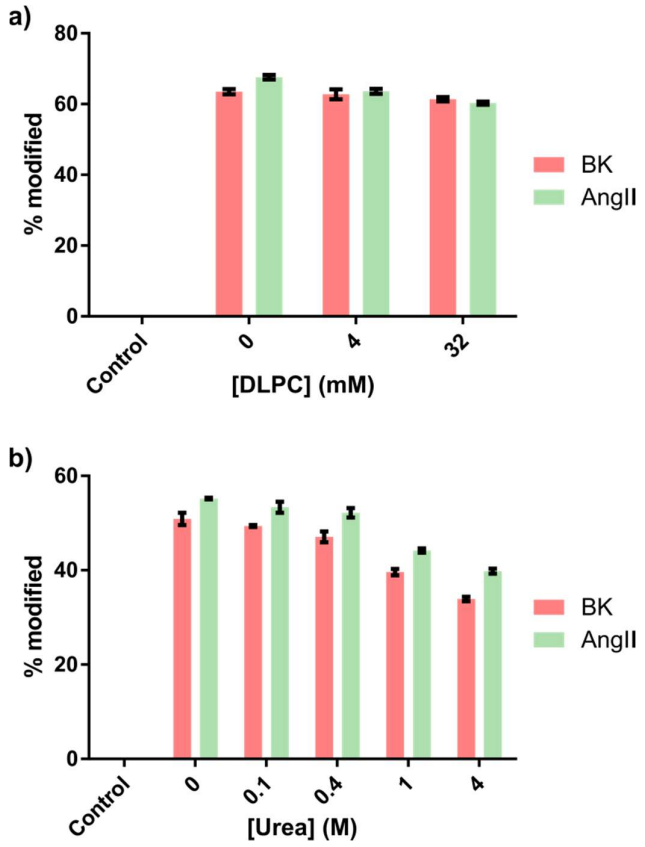

Figure 4-9 – Bradykinin (BK, red) and Angiotensin II (AngII, green) are oxidatively labelled by FPOP in various concentrations of a) DLPC synthetic liposomes or b) urea. Control is treatment with H_2O_2 but without UV irradiation. Error bars show SEM (n=3).

In these simple systems tested here, some common components of FPOP sample buffers are shown to result in a reduced degree of modification by FPOP. In cases such as urea, this effect is modest and can be quantified and corrected for during analysis. In the case of A8-35, there may be other more complex contributions to the reduced labelling that may become more or less important in more complex samples, as will be discussed later with work on FPOP analysis of native $OmpT_{HT}$.

4.2.2 Identification of Oxidation sites of $OmpT_{HT}$ in DDM micelles or A8-35 APol using data directed analysis (DDA) LC-MS

DDA LC-MS analysis of FPOP treated $OmpT_{HT}$ gives valuable qualitative data on the sequence coverage of $OmpT_{HT}$ and the location of oxidation sites. $OmpT_{HT}$ solubilised in either DDM micelles or A8-35 was labelled by FPOP in the presence of 0.15 % (*v/v*) H_2O_2 and 15 mM glutamine, which acts as a scavenger (Section 2.6.2). The modified $OmpT_{HT}$ was then digested by trypsin, which was added in a 20:1 $OmpT_{HT}$:trypsin ratio (*w/w*) for 24 hours at 37 ^{o}C. Peptides were separated by LC using a Waters nanoAcquity UPLC system and analysed using a Waters Synapt G2Si mass spectrometer using a DDA acquisition method (Section 2.6.3).

PEAKS analysis software was used to search the DDA LC-MS data and peptide sequencing data were manually validated (Section 2.6.4). The sequence coverage searches included tryptic peptides (denoted as TX, representing the peptide preceding the Xth K/R residue) and peptides with one non-tryptic end (such as those used to cover the long 38-residue N-terminal region of $OmpT_{HT}$ that precedes the first K/R residues) (Figure 4-10 and Figure 4-11). Sequence coverage of OmpT in DDM micelles (Figure 4-10) and A8-35 (Figure 4-11) were 92 % and 93 %, respectively. Two short regions of $OmpT_{HT}$ with a high density of K/R residues were missing from sequence coverage (182-190 and 232-237, Figure 4-10 and Figure 4-11), most likely as a result of the small peptides lacking the hydrophobicity required to bind the analytical columns used in the LC-MS analysis.

PEAKS software was also used for identification of +16 Da modification of M, W, Y, F or H residues (the $OmpT_{HT}$ sequence contains no C residues and were therefore not included in the search). Of the 32 possible tryptic peptides, 13 (T4, 6, 8, 9, 10, 11, 12, 14, 15, 19, 27, 30, 31) were identified with +16 Da modifications. Within these 13 peptides, 20 oxidation sites were identified and all are common to $OmpT_{HT}$ solubilised in either DDM micelles or A8-35 APol (Figure 4-10 and Figure 4-11). This suggests that solubilisation in either media does not result in gross changes in structure that would lead to exposure of other radical reactive residue side chains.

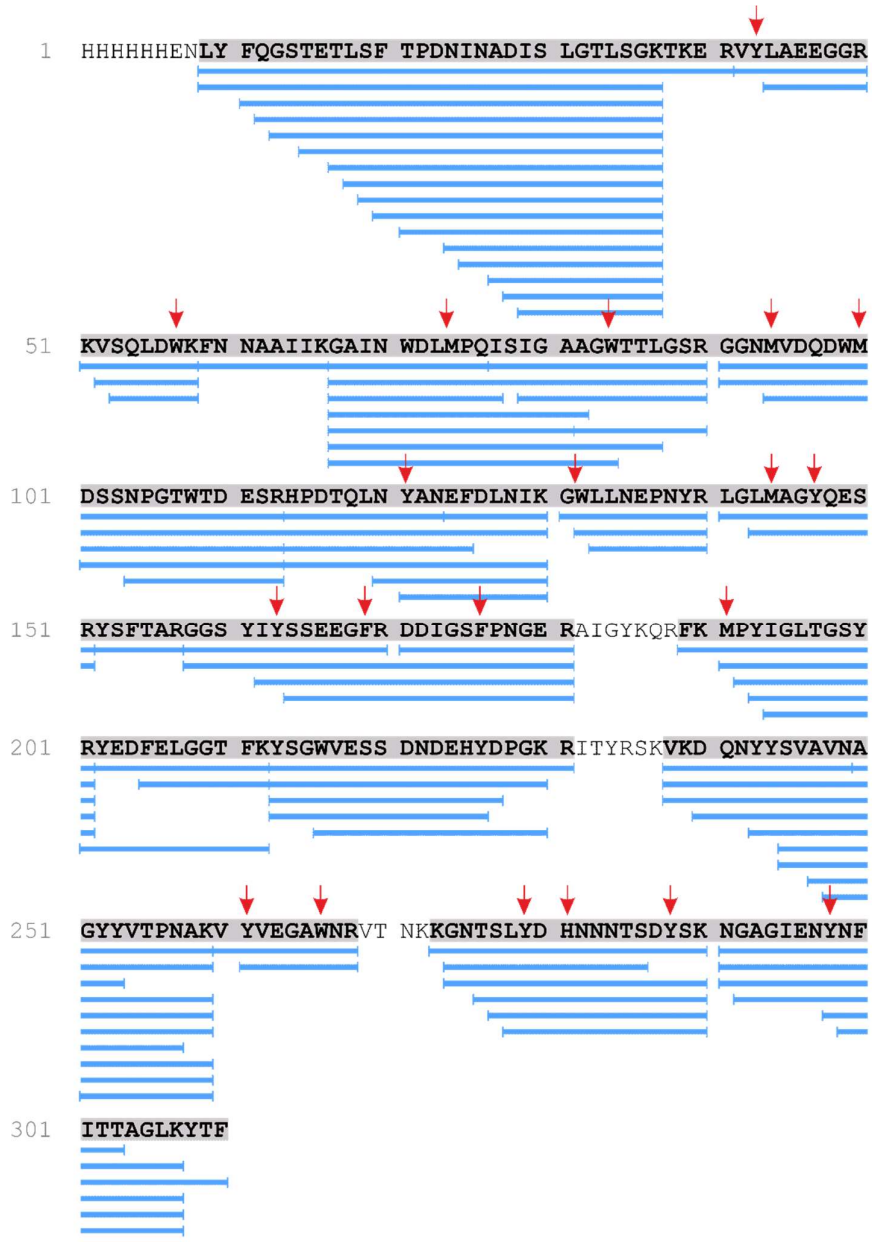

Figure 4-10 – OmpT$_{HT}$ peptide map from the tryptic digest of FPOP modified OmpT$_{HT}$ in DDM micelles. Identified tryptic peptides of OmpT$_{HT}$ (blue) result in a 92% sequence coverage. PEAKS software identified FPOP oxidation sites by a 15.99 Da mass addition at Met, Trp, Tyr, Phe and His residues. These sites of oxidation were manually validated by inspecting MS/MS spectra for modified peptides and are highlighted by downward facing red arrows.

Figure 4-11 – OmpT$_{HT}$ peptide map from the tryptic digest of FPOP modified OmpT$_{HT}$ in A8-35. Identified tryptic peptides of OmpT$_{HT}$ (blue) result in a 93% sequence coverage. PEAKS software identified FPOP oxidation sites by a 15.99 Da mass addition at Met, Trp, Tyr, Phe and His residues. These sites of oxidation were manually validated by inspecting MS/MS spectra for modified peptides and are highlighted by downward facing red arrows.

The identified oxidation sites and remaining unmodified reactive residues were mapped onto the structure of OmpT (highlighted in red and blue, respectively, PDB 1I78[30]) in Figure 4-12 and Figure 4-13. The majority of the unmodified reactive residues were located in the boundaries of the TM domain of $OmpT_{HT}$ or are buried in the lumen of the barrel and the majority of modified residues observed were in the extramembrane domain. The identification of modified residues in the regions of the OmpT structure that would be most solvent accessible acts a degree of positive validation of the FPOP data.

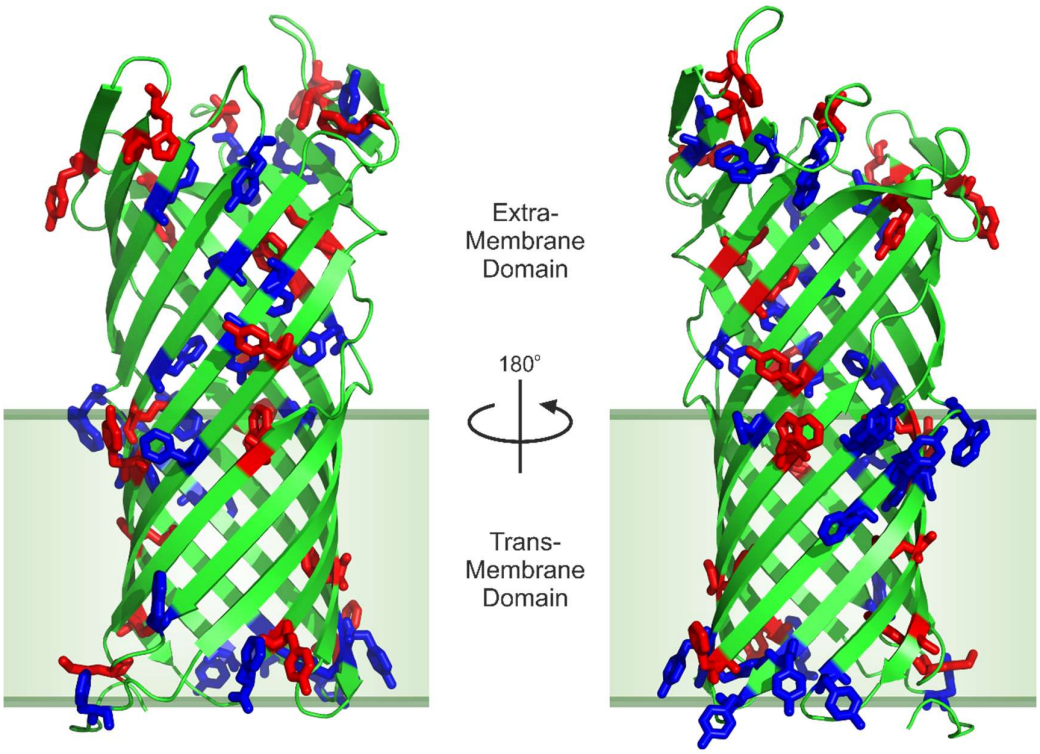

Figure 4-12 – Identified oxidation sites (red) of $OmpT_{HT}$ in A8-35 and DDM micelles are predominantly localized to the extramembrane region of $OmpT_{HT}$ and shallow inward facing residues. Non-oxidised Met, Trp, Tyr, Phe and His residues (blue) are predominantly located around the TM region of $OmpT_{HT}$ (green box) and more deeply buried on the inner face of the barrel. PDB 1I78[30].

The top and bottom views of $OmpT_{HT}$ greater show this degree of protection afforded to the lower boundary of the TM domain and the barrel lumen, as evidenced by a large density of blue-highlighted residues (Figure 4-13).

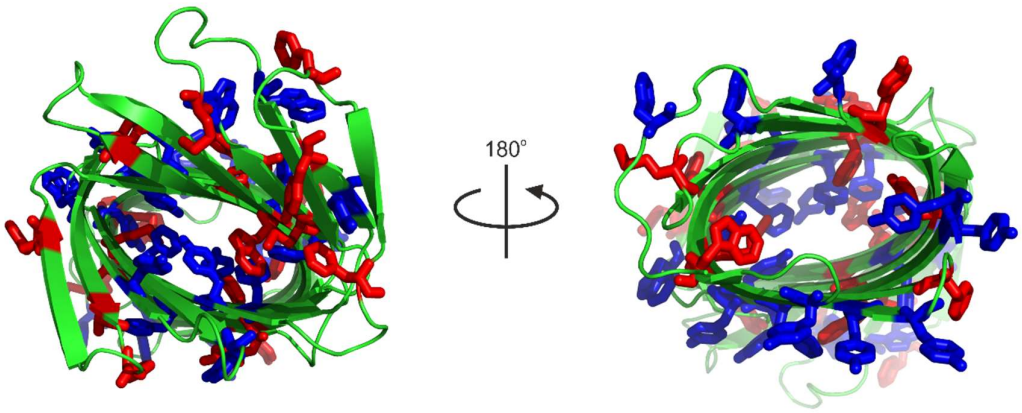

Figure 4-13 – (left) Top view of $OmpT_{HT}$ shows unmodified residues (blue) more deeply buried in the barrel lumen than modified residues (red). (right) Bottom view of $OmpT_{HT}$ shows a large number of unmodified residues (blue) at the lower parts of the TM region, suggesting significant protection of this region by solubilising media.

Oxidation sites have been identified for $OmpT_{HT}$ solubilised in DDM micelles or A8-35. These sites are unchanged with solubilisation in different media, suggesting that the solution structure of $OmpT_{HT}$ is mostly unchanged. A quantitative analysis of $OmpT_{HT}$ FPOP labelling was therefore employed, to help show more subtle differences in the structure of $OmpT_{HT}$ in different solubilising media, and/or inform on the way in $OmpT_{HT}$ interacts differently with DDM micelles and A8-35 APol.

4.2.3 Quantitative analysis of oxidative labelling of $OmpT_{HT}$ in DDM micelles or A8-35 using MS^e LC-MS shows surfactant dependent degree of modification

LC-MS data acquired using the Waters MS^e method allows quantitative analysis of the oxidation sites of FPOP-modified proteins. Due to the nature of the MS^e method (which fragments and analyses co-eluting peptides simultaneously without quadrupole-mass selecting precursor peptide), LC elution profiles from MS^e analyses have a faster, constant sample rate, generating more accurate peaks and allowing for more reliable quantitative analysis.

$OmpT_{HT}$ (10 μM) solubilised in either DDM micelles (0.02% *w/v*) or A8-35 (1:5 $OmpT_{HT}$:APol *w/w*) was FPOP-labelled in the presence of 15 mM glutamine and 0, 0.05, 0.15 or 0.5 % (*v/v*) H_2O_2 (Section 2.6.2), trypsin was added in a 20:1

$OmpT_{HT}$:trypsin ratio (*w/w*) for 24 hours at 37 °C and the digest was analysed using LC-MS^e. The modification sites were identified and quantified using LC-MS data analysed and processed with Waters UNIFI software (Section 2.6.3 and 2.6.4). Although modification sites were identified to a residue-level, the results here are quantified to a peptide level in order to simplify interpretation of multiply modified peptides.

Peptides with Met residues (T8, T9, T12 and T19) were modified to a greater extent than those modified at only Trp, Tyr, Phe or His residues (T4, T6, T10, T11, T14, T15, T27, T30, and T31) (Table 4-1), with up to **35.3**, **87.6**, **30.2** and **35.1** % of T8, T9, T12 and T19 being modified, respectively. This correlates well with what is known about the relative reactivity of amino acid side chains and the previous observation of FPOP oxidation of MPs almost exclusively at Met residues[178, 221].

Tryptic Peptide	Degree of modification (% total peptide with identified oxidation site) +/- SEM		Location(s)
	DDM	A8-35	
T4	2.72 ± 0.10	2.36 ± 0.2	Y44
T6	3.28 ± 0.54	0.94 ± 0.50	W58
T8	7.48 ± 3.74	29.03 ± 8.00	M75,W85
T9	80.39 ± 10.4	54.67 ± 7.58	M95,M101
T10	2.60 ± 0.79	2.54 ± 0.80	Y122
T11	5.05 ± 0.90	4.15 ± 0.48	W133
T12	18.71 ± 0.73	19.85 ± 2.91	M145,Y148
T14	6.47 ± 0.95	6.28 ± 1.13	Y164,F170
T15	4.01 ± 1.37	2.24 ± 0.26	F177
T19	19.36 ± 0.46	24.86 ± 0.11	M192
T27	5.88 ± 1.74	1.71 ± 0.24	Y262,W267
T30	7.03 ± 1.00	6.77 ± 1.25	Y280,H282,Y289
T31	0.00	1.62 ± 0.81	Y299

Table 4-1 – Degree of modification (%) of $OmpT_{HT}$ tryptic peptides with one or more identified oxidation sites in DDM micelles (blue) or A8-35 (red). Data are shown at the peptide-level for $OmpT_{HT}$ labelled using FPOP in the presence of 0.15 % (v/v) H_2O_2 and identified oxidation sites in each peptide are shown. Error is SEM (n=3).

Of the 13 tryptic peptides of $OmpT_{HT}$ with modification sites identified (Table 4-1), eight show no significant difference in the degree of modification (Figure 4-14) between DDM micelle- or A8-35-solubilised $OmpT_{HT}$. Identified sites within the sequence of these peptides are located in various positions across the structure of

OmpT$_{HT}$, although they are predominantly in the extramembrane region of the protein and the inner surface of the barrel.

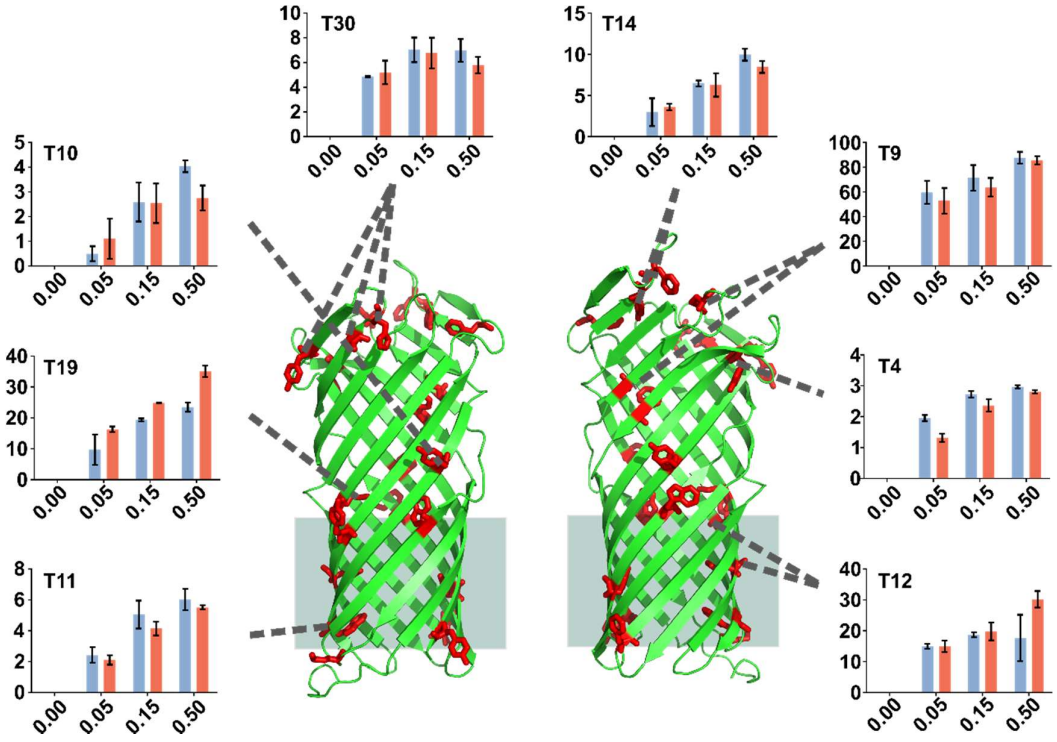

Figure 4-14 – Degree of oxidation (%) of eight of the 13 tryptic peptides of FPOP-modified OmpT$_{HT}$ remains unchanged when solubilised in either DDM micelles or A8-35. The inset graphs show the degree of modification (% modified) of the indicated peptide as a function of [H_2O_2] (%, v/v) in DDM micelles (blue) or A8-35 (red). Identified residues within the respective peptide are indicated by dashed lines. Error bars show SEM (n=3).

Despite most peptides remaining mostly unchanged, five of the tryptic peptides were modified differently in DDM micelles and A8-35 solubilised OmpT$_{HT}$. T8 and T31 peptides were modified to a greater extent in A8-35 solubilised OmpT$_{HT}$. When labelled with 0.15 % H_2O_2, **7.5** and **29.0** % of T8 and **0.0** and **1.6** % of T31 was modified in DDM and A8-35, respectively (Figure 4-15b and Table 4-1). Both of these peptides have identified modification sites at the bottom boundary of the TM domain (M75 in T8 and Y299 in T31) (Figure 4-15a). This shows that DDM micelles are having a protective effect on the labelling of this region of the protein relative to A8-35.

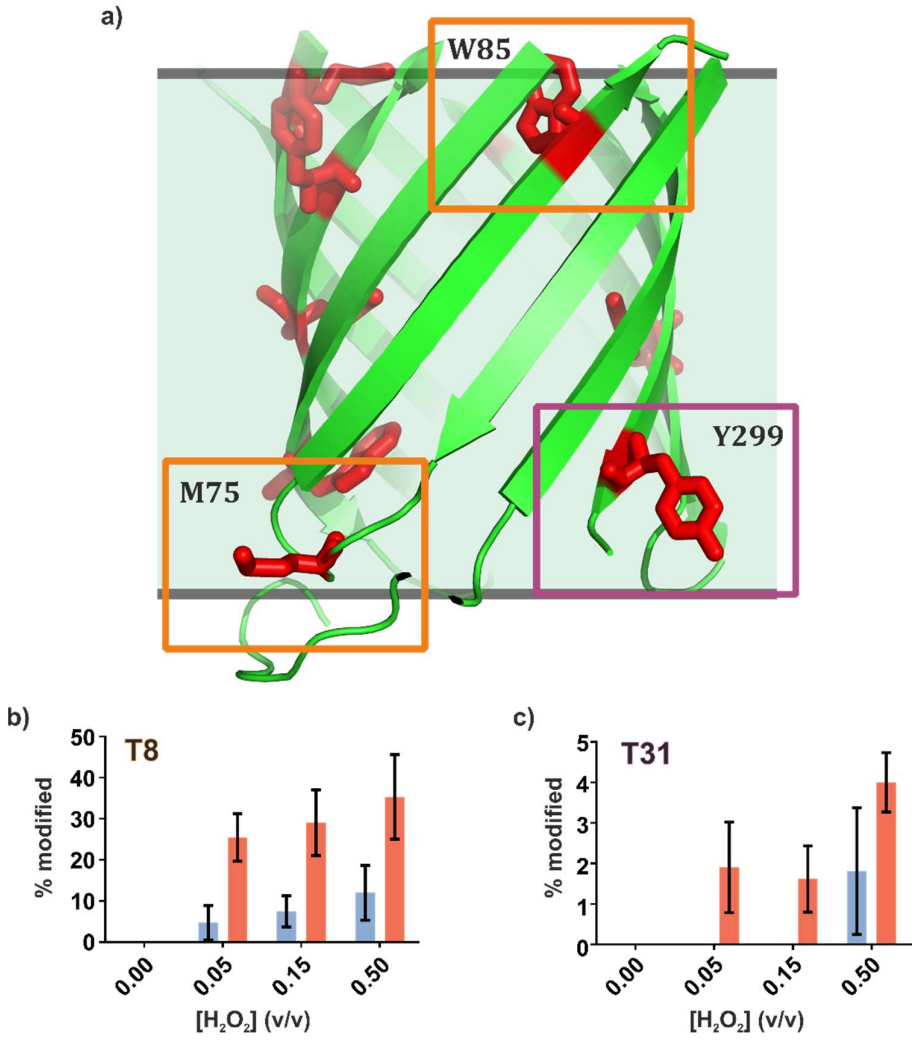

Figure 4-15 – Zoom of the TM region of OmpT$_{HT}$ containing residues oxidized to a greater extent in A8-35 than in DDM micelles. a) Outward-facing M75 and inward-facing W85 of tryptic peptide T8 are highlighted by orange boxes and outward-facing Y299 of tryptic peptide T31 is highlighted by a purple box. Graphs displaying the degree of peptide modification as a function of H_2O_2 concentration show that b) T8 and c) T31 are modified to a lesser extent in DDM micelles (blue) than in A8-35 (red), suggesting that detergent micelles afford OmpT$_{HT}$ protection from oxidation in the lower boundary of the TM domain.

Conversely to the observed protection of T8 and T31 by DDM micelles. Peptides T27, T6 and T15 are modified to a lesser extent in A8-35 than in DDM micelles. T27 (like T8 and T31) has identified modification sites in the TM domain of $OmpT_{HT}$, although identified residues are at the upper boundary of the TM domain (W267) and on the inner face of the barrel (Y262) (Figure 4-16a). **5.9** and **1.7** % of T27 was labelled in DDM micelles and A8-35, respectively (Figure 4-16 and Table 4-1).

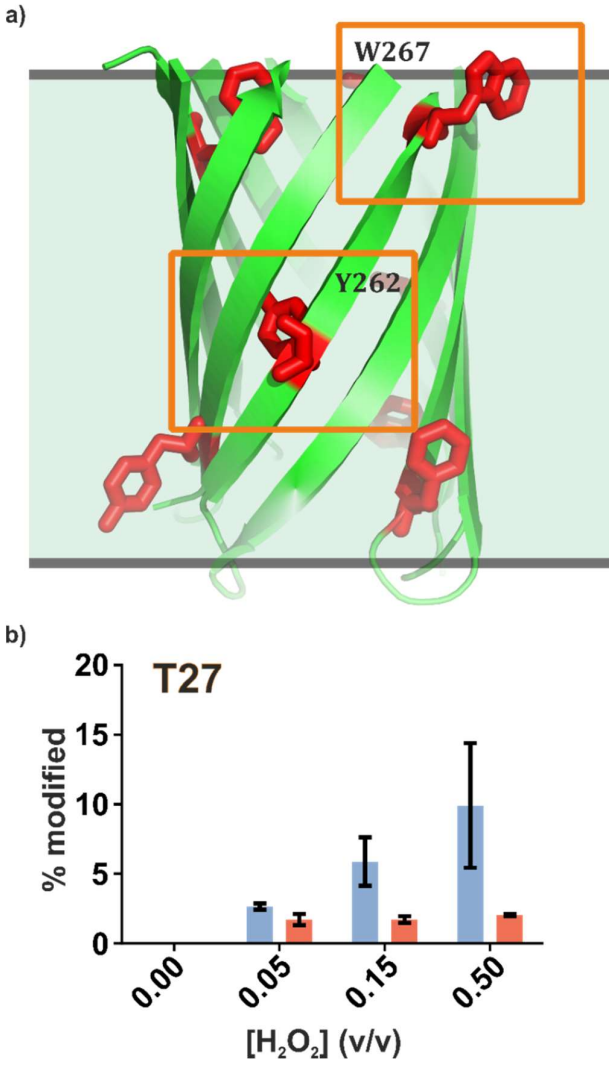

Figure 4-16 – Zoom of the TM region of $OmpT_{HT}$ containing residues oxidized to a lesser extent in A8-35 than in DDM micelles. a) Outward-facing W267 and inward-facing Y262 of tryptic peptide T27 are highlighted by orange boxes. b) Graph displaying the degree of peptide modification as a function of H_2O_2 concentration show that T27 is modified to a greater extent in DDM micelles (blue) than in A8-35 (red), suggesting that APol affords $OmpT_{HT}$ protection from oxidation in the upper boundary of the TM domain, relative to detergent micelles.

Like T27, T6 and T15 are also modified to a lesser extent in A8-35 APol than in DDM micelles but these modification sites are located in the extramembrane domain of OmpT$_{HT}$. W58 of T6 is located on the inner face of the extramembrane domain of the barrel and F177 of T15 is found on one of the extracellular loops (Figure 4-17a). **3.3** and **0.9** % of T6 and **4.0** and **2.2** % of T15 were modified in DDM micelles and A8-35 APol, respectively (Figure 4-17b and Table 4-1). This shows that A8-35 is having a protective effect against the oxidative labelling of the extramembrane region of OmpT$_{HT}$.

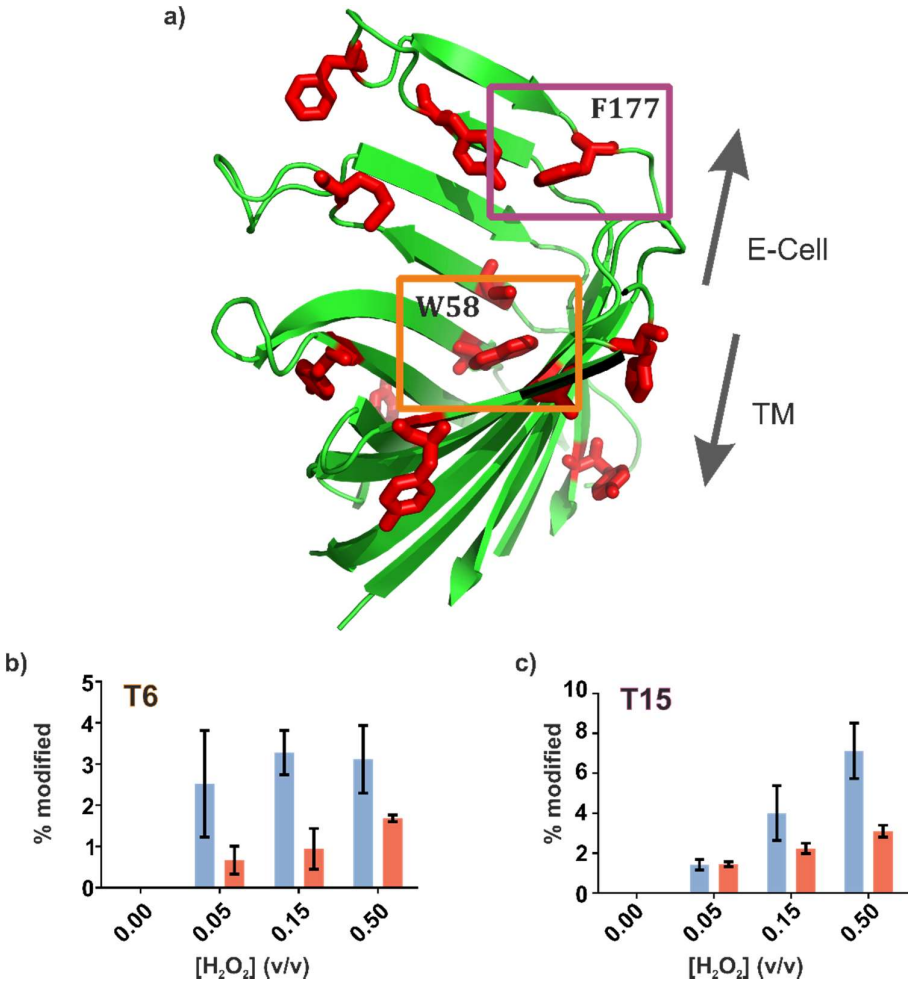

Figure 4-17 – Zoom of the extramembrane (extracellular) region of OmpT$_{HT}$ containing residues oxidized to a lesser extent in A8-35 than in DDM micelles. a) W58 of tryptic peptide T6 and F177 of tryptic peptide T15 are highlighted by an orange or purple box, respectively. Graphs displaying the degree of peptide modification as a function of H_2O_2 concentration show b) T6 and c) T15 are modified to a greater extent in DDM micelles (blue) than in A8-35 (red), suggesting that APol affords OmpT protection from oxidation in regions of OmpT$_{HT}$ spatially separate from the TM domain, relative to detergent micelles.

4.3 Discussion

Early experiments shown in this chapter describe how different surfactants and buffer components affect the photooxidation of proteins by labelling small peptides in the presence of DDM micelles, A8-35, DLPC liposomes or urea. These data show that A8-35 and urea (above 1 M) reduce the degree of labelling of these peptides (Figure 4-4 and Figure 4-9).

In the case of urea, the effect is subtle (a decrease of approximately one third at 4 M) and allows for observation of labelling of peptides (Figure 4-9). These concentrations are potentially relevant, as OMP refolding is regularly performed in >1 M urea, as it can be used to control the rate of refolding and optimum folding yield[27, 40-41, 201, 222]. The results obtained using the model peptides should allow the degree of modification to be corrected for the effect of urea on efficiency of photooxidation, at least for urea concentrations explored here.

In comparison, A8-35 at 5 $mg.ml^{-1}$ shows a more substantial effect on the oxidation of small peptides by FPOP (Figure 4-4). This does not correlate with observations in the quantitative analysis of the degree of modification of $OmpT_{HT}$ solubilised in DDM micelles or A8-35 APol. There appears to be no global trend in degree of modification of $OmpT_{HT}$ peptides towards greater labelling in DDM micelles relative to A8-35 (Figure 4-14, Figure 4-15, Figure 4-16 and Figure 4-17). This suggests that the effect of A8-35 on labelling of small peptides (where labelling remains unchanged in the presence of DDM micelles) is not simply the effect of reduced radical dose in the presence of APol[170]. It is possible that small peptides are interacting with A8-35 and hence the solvent accessibility of reactive residues is lessened as they are not exposed to H_2O_2 and subsequent UV-generated $\cdot OH$ radicals.

Qualitative DDA LC-MS analysis of FPOP treated $OmpT_{HT}$ shows the locations of protected residues when solubilised in DDM micelles or A8-35. These sites are located in regions of $OmpT_{HT}$ (within the TM region and inside the barrel lumen) that are expected to be solvent inaccessible, which is normally the determining factor in whether a residue is labelled. The location of modification sites agrees with what is known about FPOP of MPs, where even highly reactive Cys and Met

residues are labelled to a much lesser extent (or not at all) in the more buried regions of BR[177, 179, 221] or GF[178], respectively. The identification of oxidation sites at Trp/Tyr/Phe/His residues is a significant development for FPOP analyses of MPs, with the more reactive aromatic groups being closer to the surface suggesting that FPOP may be aptly suited to studies of MPs, a major family of proteins.

The qualitative DDA LC-MS analysis of $OmpT_{HT}$ in DDM micelles or A8-35, showed identical oxidation sites of $OmpT_{HT}$ in DDM micelles and A8-35 (Figure 4-10 and Figure 4-11). This suggests that there are no major changes in the structure of $OmpT_{HT}$ in either solubilising media that would expose any of the unmodified Trp, Tyr, Phe or His residues in the TM domain or the inner face of the barrel, or protect any of the otherwise identified residues. Proteins may have to undergo significant structural changes in order to expose previously protected residues to oxidative labelling by FPOP. BR in semi-denaturing conditions (solubilisation in SDS-detergent or heat denaturation) show the more-buried identified modification sites to be labelled to greater extent but no new oxidation sites are revealed[177]. If the structure of $OmpT_{HT}$ is not grossly changed in the different solubilising media, then observed differences in protein activity, kinetic stability, ionisation by electrospray and gas phase unfolding must be elicited through a more subtle, secondary means.

Quantitative MS^e LC-MS data may go some way to explain some of these differences. $OmpT_{HT}$ shows region-specific differences in the degree of oxidation when solubilised by DDM micelles or A8-35, with the extremes of the TM domain and the extramembrane domain of $OmpT_{HT}$ being the most different in the two surfactants. The lower boundary of the TM domain is labelled to a lesser extent in DDM micelles, as shown by peptides T8 and T31 (Figure 4-15), but the upper boundary of the TM and the extramembrane domain are more protected in A8-35, as shown by peptides T6, T15 and T27 (Figure 4-16 and Figure 4-17). The manner and location of interactions of these two different surfactants with MPs likely underpins the mechanism of protection from oxidation.

Previous literature[60, 206] and work in the previous chapter of this thesis has demonstrated that extra contacts made between MPs and APols[64, 78, 223] can

promote the observed protective effect of APols on MPs in both the gas and solution phase. The uniform, spherical nature of detergent micelles would provide a clear boundary for regions of the protein that are solvent exposed, which the data shown here suggest is from the very bottom of $OmpT_{HT}$ to the aromatic girdle at the upper boundary of the TM region (Figure 1-3). Previous EM studies of APol solubilised MP complexes[224] have shown APols to be considerably more diffuse, forming a non-uniform boundary about the TM domain of MPs. MD[64] and NMR[78, 223] data of MPs solubilised in APols or detergent micelles and MS data described in the previous chapter have shown how APols can form extra contacts with non-TM regions of MPs. The results shown here further corroborate this phenomenon, A8-35 not forming a strict border at the lower boundary of TM results in an increase in oxidation (T8 and T31 peptides) relative to the defined border provided by DDM micelles. Interactions of A8-35 with the upper boundary of TM domain and the extramembrane domain result in the protection afforded to residues of peptides T6, T15 and T27, whereas uniform DDM micelles do not interact beyond the TM domain. These A8-35 interactions with $OmpT_{HT}$ are likely transient and/or non-specific and may explain why oxidation at these residues is not completely inhibited. Although DDM micelles are more uniform than A8-35, they are still highly dynamic and may also allow for oxidation of small populations of residues in the lower TM domain boundary of $OmpT_{HT}$, much like with A8-35.

As mentioned previously, these interactions could well explain the structural benefits afforded to MPs by APols. The kinetic stability of MP:APol complexes has been attributed to the quasi-irreversible association of APol with MPs, the large number of contacts are difficult to remove simultaneously[60]. Gas phase stability of MPs released from APols could be afforded to a number of processes resulting from these extra interactions; such as direct charge reduction by shielding of the protein surface which in turn prevents charge-dependent unfolding or better constraining of the protein structure which will prevent excess charging and unfolding. Extra contacts with non-TM regions of $OmpT_{HT}$ may also explain how the above described protection from charging and unfolding are not observed in smaller OMPs (PagP and tOmpA) which do not have extramembrane regions.

5 Using Hydrogen Deuterium Exchange (HDX)-MS to investigate the manner of interactions of MPs with detergent micelles and APols

5.1 Introduction

HDX-MS has been shown to be a powerful technique for determining the dynamic properties of proteins, identifying perturbations in protein structure and dynamics under different conditions and following the interaction of ligands and proteins at positions adjacent to and spatially distinct from the site of interaction[181-183]. This also applies to MPs, with HDX-MS having identified helices that are more mobile in the ion selectivity filter of GF[178] and an increase in the flexibility of BR in the active, light-treated, form[193].

FPOP-LC-MS data of $OmpT_{HT}$ in DDM micelles and A8-35 (Chapter 4) did not show any gross differences in global or local structure dependent on the solubilising media used. Differences in the degree of modification by FPOP in the extramembrane region in the presence of APols and DDM micelles were attributed to non-specific and transient interactions of the MP with the solubilising media used. This is corroborated by native MS analyses of MPs that shows protection from excess charging and/or unfolding of OMPs with extramembrane domains, a phenomenon not observed in small OMPs without these extramembrane domains (Section 3.2.6). These additional interactions may explain differences in the gas phase stability of MP ions and the kinetic stability of MP:APol complexes relative to MP:DDM complexes[60].

HDX-MS can be used to observe the dynamics of MPs over longer timescales (μsec to hours) than FPOP (which labels for ~1 μs). HDX-MS was employed here to probe how $OmpT_{HT}$ dynamics are changed when solubilised in APol or detergent micelles and to investigate further the nature of the interactions of APols with $OmpT_{HT}$.

5.2 Results

5.2.1 Pepsin digest of $OmpT_{HT}$ yields high sequence coverage

$OmpT_{HT}$ solubilised in DDM micelles (0.02 % (*w/v*)) or NAPol (1:5 $OmpT_{HT}$:NAPol (*w/w*)) was buffer exchanged into 50 mM sodium phosphate buffer pH 7.0 +/- 0.02 % DDM (*w/v*). Labelling was initiated by dilution 20-fold with 50 mM sodium phosphate (D_2O) pD 7.0 +/- 0.02 % DDM (*w/v*) and quenched after different times (0.5, 2, 10, 30 and 60 mins) by dilution 2-fold with 200 mM phosphate buffer pH 2.2 +/- 0.02 % DDM (*w/v*) (Section 2.7.1). NAPol was used in place of A8-35 because of its solubility at pH[33, 58]. By contrast, A8-35 and MPs in complex with A8-35 become insoluble below pH 7.0[33, 58], which makes A8-35 incompatible with the HDX-MS work flow, which requires an acidic quench step prior to analysis.

Quenched samples were analysed by $LC\text{-}MS^e$ using a Waters HDX Manager with online pepsin digest coupled to a Waters Xevo Q-ToF (Section 2.7.2). t=0 time point $LC\text{-}MS^e$ data were analysed using PLGS software for peptide sequencing and identification and the resultant peptide list was imported in Dynamx 3.0 software. Peptides that were not common to $OmpT_{HT}$ solubilised in DDM micelles and NAPol (Section 2.7.3) were removed on importing into Dynamx.

Common peptides provide an $OmpT_{HT}$ sequence coverage of 100 % as shown in the $OmpT_{HT}$ peptide map (Figure 5-1). Peptide coverage has redundancy in all regions of the sequence, except for ten N-terminal residues, which is important for pseudo-residue-level analysis of deuterium uptake. Overlapping peptides can allow for calculation of a sequence position's contribution to deuterium uptake despite uptake being calculated to a peptide-level in the raw data. Representative peptides are described throughout the chapter, covering a range of regions of $OmpT_{HT}$, differing in their spatial location on the structure of $OmpT_{HT}$. Figure 5-2 shows sequencing data for $OmpT_{HT}$ peptic peptides 30-45 (ISLGTLSGKTKERVYL), 156-162 (TARGGSY), 213-217 (KYSGW), 256-261 (TPNAKV) and 289-301 (YSKNGAGIENYNF). Data is acquired using $LC\text{-}MS^e$ which analyses fragmentation data of co-eluting species simultaneously. This results in a large number of fragment ion peaks representing multiple precursors, which are left unassigned in the following spectra.

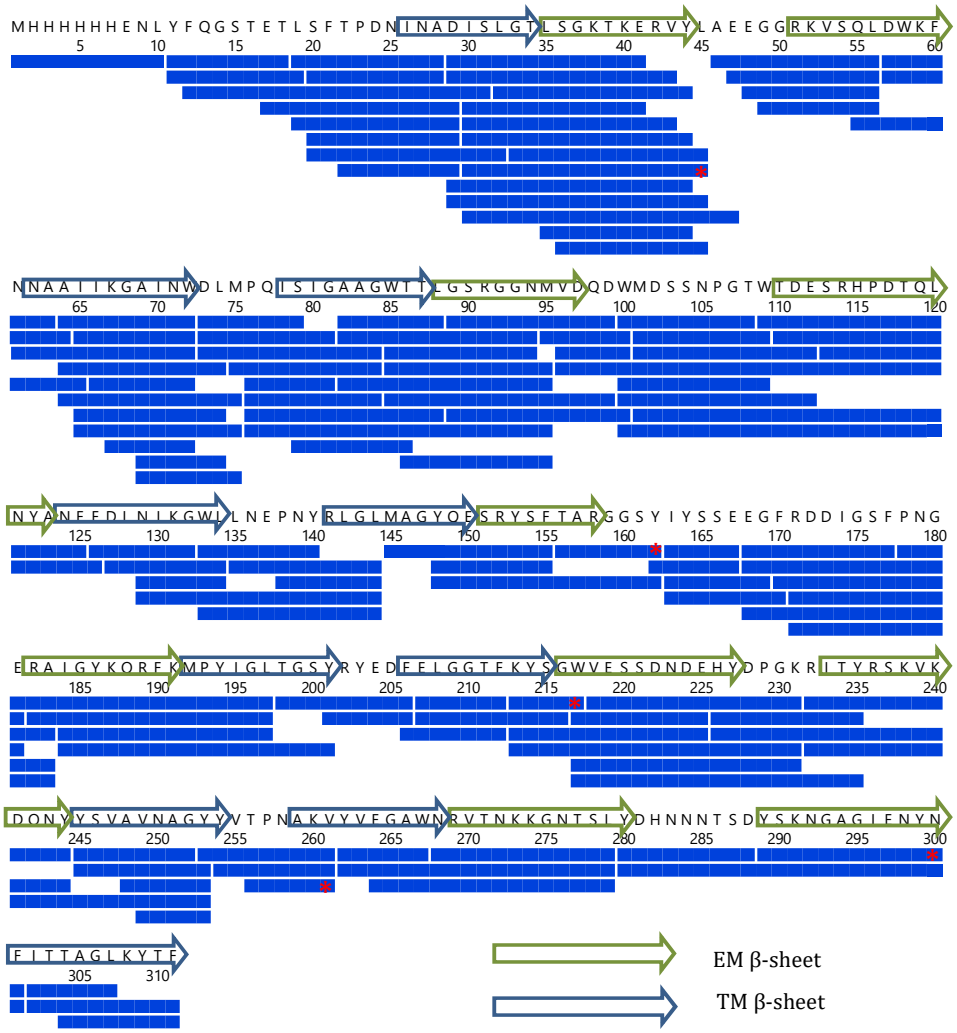

*Figure 5-1 – $OmpT_{HT}$ peptide map following on-line pepsin digest and LC-MS^e. Peptides shown are identified using PLGS software and imported into Dynamx 3.0 software. All peptides shown are common to t=0 analyses of $OmpT_{HT}$:DDM and $OmpT_{HT}$:NAPol. This peptide map provides 100 % sequence coverage of $OmpT_{HT}$ with a redundancy of 4.79 (score generated by Dynamx 3.0), which allows for pseudo-residue level analysis in certain regions of $OmpT_{HT}$. Representative peptic peptides that are described throughout the following chapter are indicated by **.*

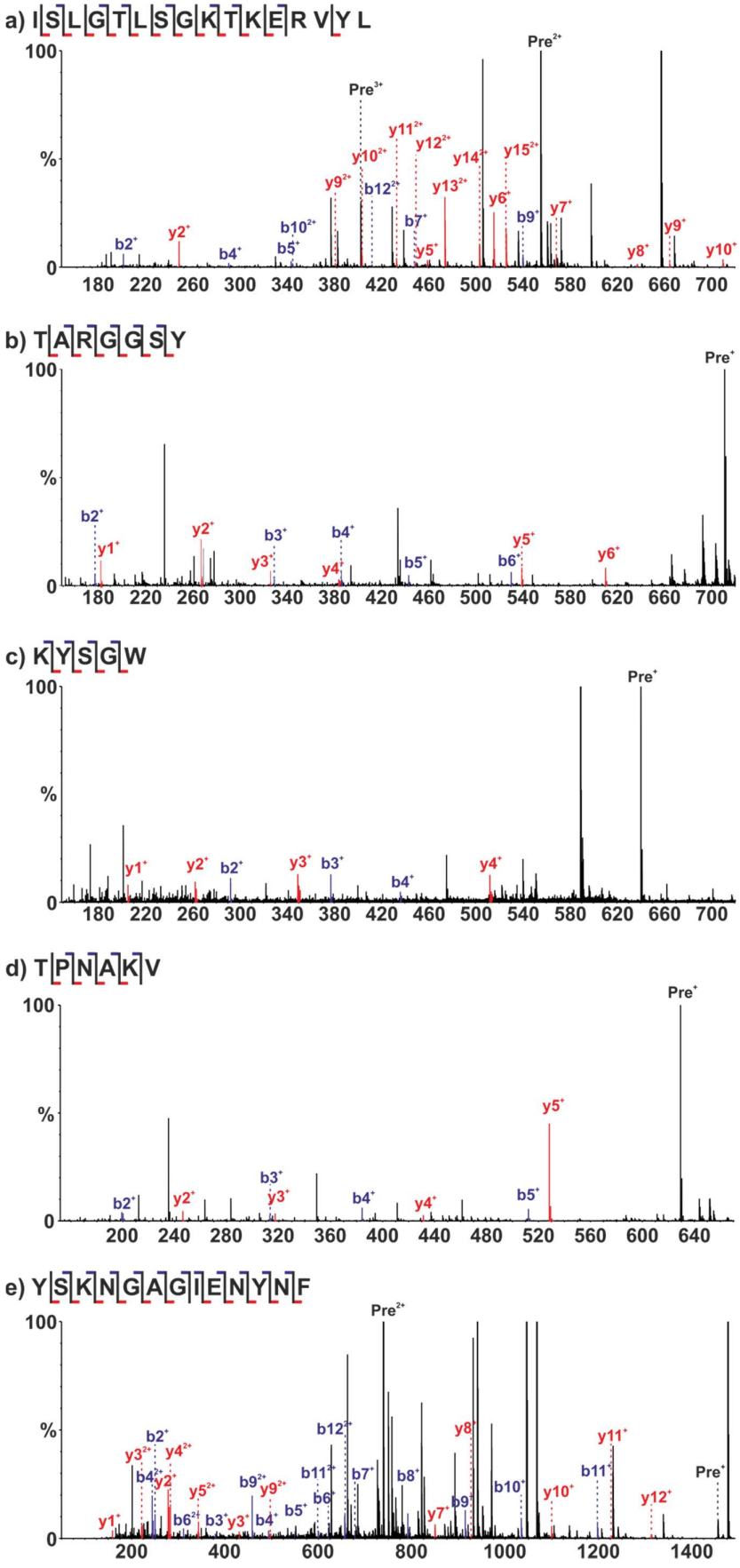
a) I S L G T L S G K T K E R V Y L
b) T A R G G S Y
c) K Y S G W
d) T P N A K V
e) Y S K N G A G I E N Y N F
Pre
%
0
100

Figure 5-2 – Representative MS/MS fragment spectra of $OmpT_{HT}$ peptic peptides analysed by LC-MS^e. a) 30-45 ISLGTLSGKTKERVYL, b) 156-162 TARGGSY, c) 213-217 KYSGW, d) 256-261 TPNAKV and e) 289-301 YSKNGAGIENYNF peptides are indicated in Figure 5-1 and cover different regions of $OmpT_{HT}$ in both sequence and structure. Peptides are co-eluted with other precursor ions (unassigned, black) and fragmented by CID. Peaks representing b and y'' fragment ions are coloured in blue and red, respectively (1+ and 2+ charges indicated on peak labels). Fragments are numbered and fragmentation sites are indicated on the peptide sequence (above each respective spectrum). All peptide sequences are well covered by identified fragment peaks.

5.2.2 DDM micelles and NAPol protect TM domain of $OmpT_{HT}$ from HDX

The heat map shown in Figure 5-3 displays the amount of deuterium uptake at each position of the $OmpT_{HT}$ sequence in each state (i.e. $OmpT_{HT}$ solubilised in DDM micelles or NAPol) and at each time point. Regions of the $OmpT_{HT}$ sequence that undergo deuterium exchange are comparable when solubilised in DDM micelles or NAPol, although uptake appears to greater in these regions when $OmpT_{HT}$ is labelled in NAPol.

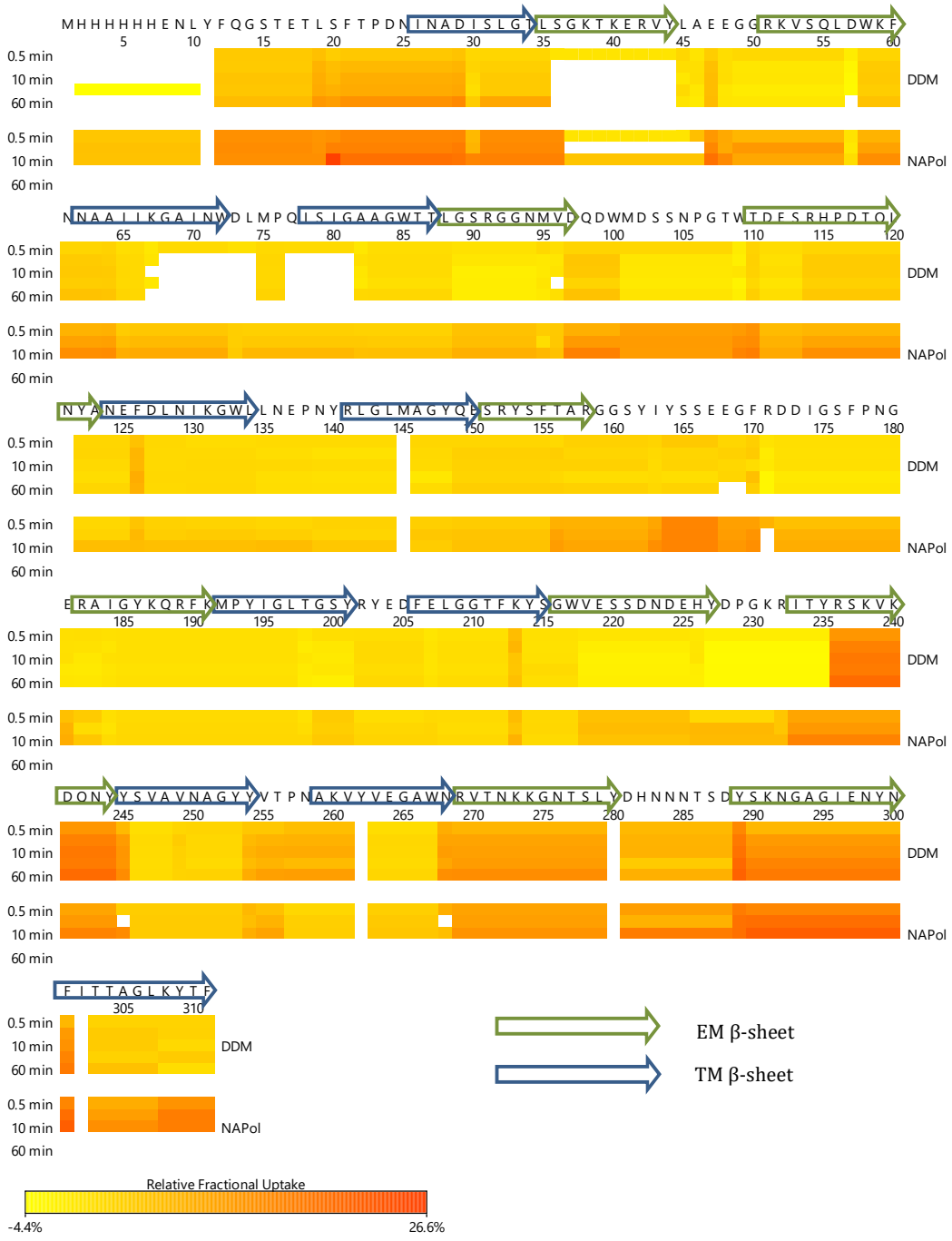

Figure 5-3 – Similar regions of OmpT_{HT} undergo deuterium exchange whether it is solubilised in DDM micelles or NAPol. The heat map shows the relative deuterium uptake at each sequence position, at each time point and in each condition (i.e. DDM or NAPol).

The observation of comparable regions of increased uptake is shown in the following butterfly plot (Figure 5-4). This plot compares deuterium uptake in identified peptides (where each point on respective line shows a peptide with

increasing N-terminal residue from left to right) for each measured timepoint (each represented by a different colour line). When represented like this, the data show an increased level of uptake in distinct regions of the $OmpT_{HT}$ sequence (highlighted in blue boxes). These peptides resemble regions of the $OmpT_{HT}$ sequence from residues 1-74, 82-120, 133-183 and 226-311, which cover almost the entire sequence of $OmpT_{HT}$, showing the power of redundant peptides to localise regions of increased deuterium uptake when long peptides would obscure this.

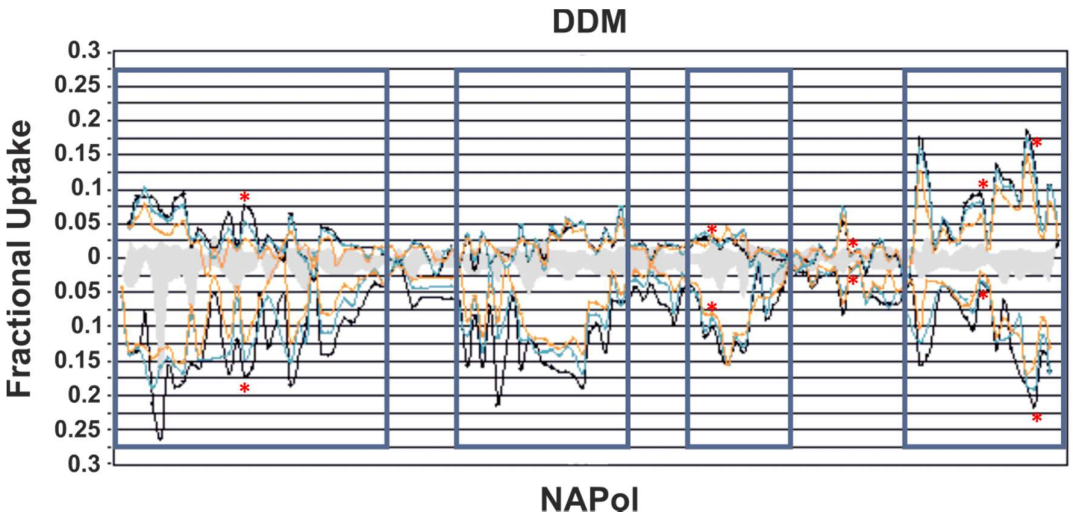

*Figure 5-4 – Butterfly plot shows the fractional uptake (deuterium incorporated per residue) of each identified peptide of $OmpT_{HT}$ solubilised in DDM micelles (top) or NAPol (bottom). Each point represents a peptide, with increasing starting sequence position from left to right (resulting in a non-linear axis). Data shows uptake at 30 s (orange), 2 min (blue) and 10 mins (black). Greater deflection from the central axis represents more uptake in that peptide at that time point (positive deflection for DDM and negative deflection for NAPol). This plot highlights regions of a protein sequence that uptake deuterium to greater extent or at a greater rate. Regions of $OmpT_{HT}$ with a greater degree of deuterium uptake identified in DDM micelles or NAPol are indicated by blue boxes and representative peptides described in Figure 5-1, Figure 5-7, Figure 5-8, Figure 5-9, Figure 5-10 and Figure 5-11 are indicated by **.*

These deuterium uptake data are mapped onto the structure of OmpT (PDB 1I78)[30] (Figure 5-5), with the results indicating that the regions of greatest deuterium uptake after 10 min timepoint are found in the extramembrane domain of $OmpT_{HT}$. This suggests protection of the TM domain of $OmpT_{HT}$ by both DDM

micelles and NAPol, either through exclusion from the solvent environment or through stabilisation of a tight hydrogen bonding network.

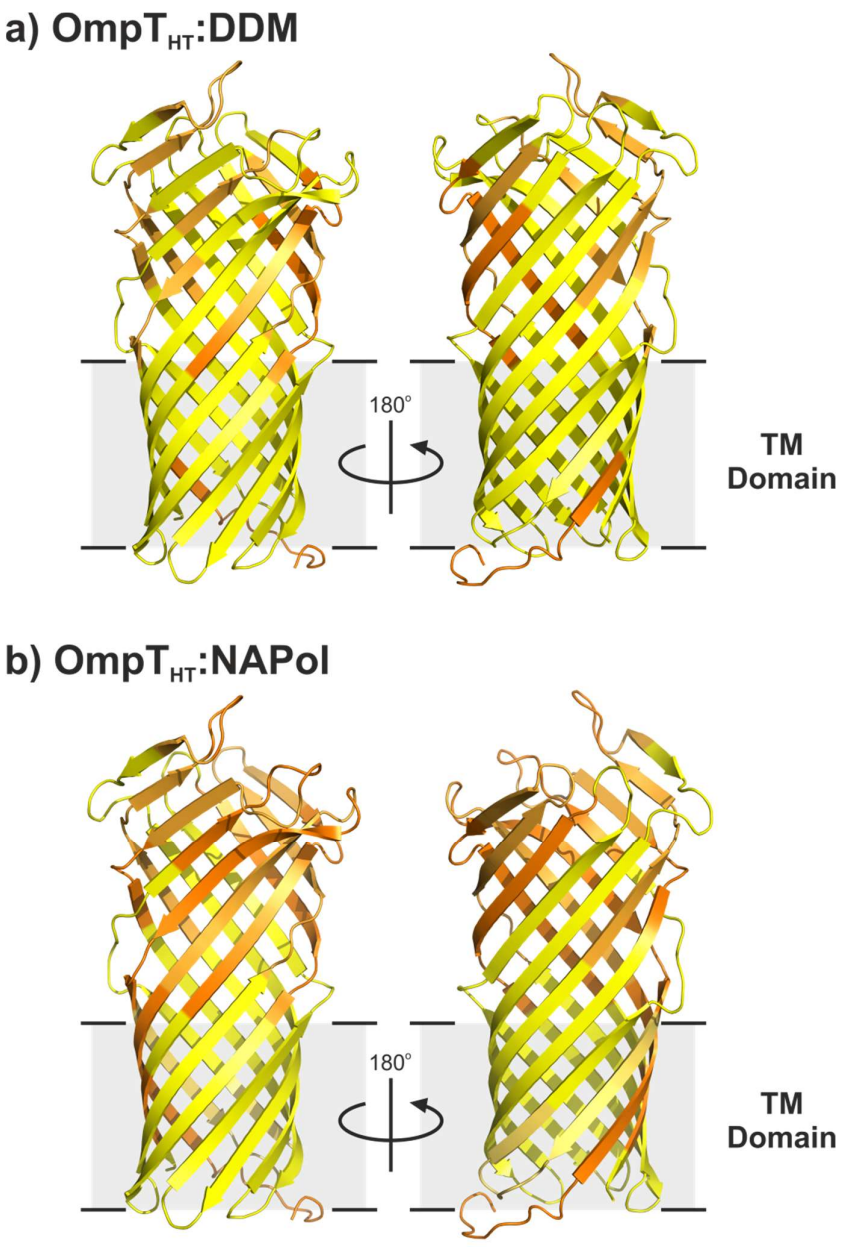

Figure 5-5 – Relative uptake shown on the heat map in Figure 5-3 are mapped on the structure of OmpT (PDB 1I78)[30]. Regions of low deuterium uptake are coloured in yellow and regions with more uptake are coloured in increasingly dark orange. OmpT$_{HT}$ solubilised in either a) DDM micelles or b) NAPol show an increased degree of uptake in the extramembrane region, although with a greater degree of uptake in NAPol than DDM micelles.

5.2.3 Uptake rates in the extramembrane domain of $OmpT_{HT}$ are dependent on solubilising media

As mentioned previously, the extent of HDX is greater in many peptides of the extramembrane domain of $OmpT_{HT}$ when solubilised in NAPol compared with DDM micelles, as highlighted in the difference heat map (Figure 5-6).

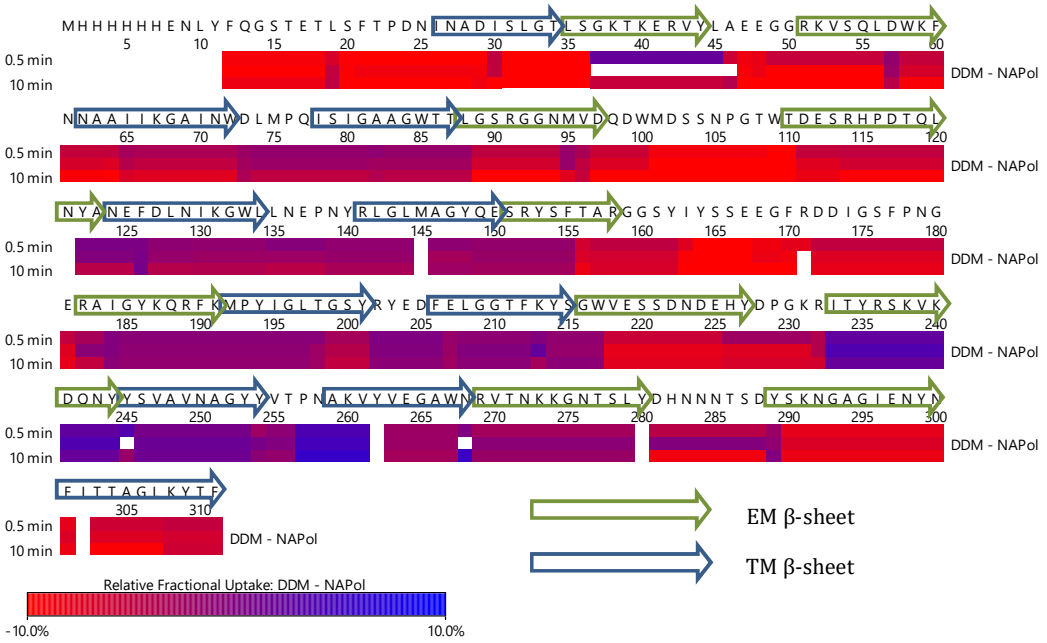

Figure 5-6 – Heat map of relative deuterium uptake between $OmpT_{HT}$ solubilised in either DDM micelles or NAPol at 30 sec, 2 min or 10 min. The plots show regions of the $OmpT_{HT}$ sequence that undergo similar (purple) levels of exchange or greater exchange in DDM micelles (blue) or NAPol (red). β-sheets of the extramembrane and TM regions of $OmpT_{HT}$ are shown by green and blue arrows over the structure, respectively.

Representative $OmpT_{HT}$ peptides, described previously, highlight region-specific differences in the relative uptake of deuterium. 30-45 (Figure 5-7) and 289-301 (Figure 5-11) are larger peptides covering extramembrane regions of the extended β-barrel of $OmpT_{HT}$ and show increased uptake when solubilised in NAPol. It can be seen that there was a second, more unprotected state (that undergoes greater exchange) when solubilised after 2 mins that is not observed in DDM micelles (Figure 5-7b and Figure 5-11b).

156-162 (Figure 5-8), which covers the end of the extramembrane region of β-sheet 5 and the subsequent extracellular loop, also undergoes increased uptake in

NAPol than in DDM micelles after 2 and 10 mins but does not possess the second unprotected state present in the larger peptides.

213-217 (Figure 5-9) is a short peptide spanning the boundary of the TM and extramembrane domain in β-sheet 7. 213-217 undergoes minimal exchange up to 10 mins whether $OmpT_{HT}$ is solubilised in NAPol or DDM micelles, indicating that this region of the $OmpT_{HT}$ structure is highly stable/protected in either solubilising media.

256-261 (Figure 5-10) is a short peptide that covers the short periplasmic loop between β-sheets 8 and 9 and the start of the TM region of β-sheet 9. Deuterium uptake at this position is low whether $OmpT_{HT}$ is solubilised in NAPol or DDM micelles. The degree of uptake is greater when solubilised in DDM micelles.

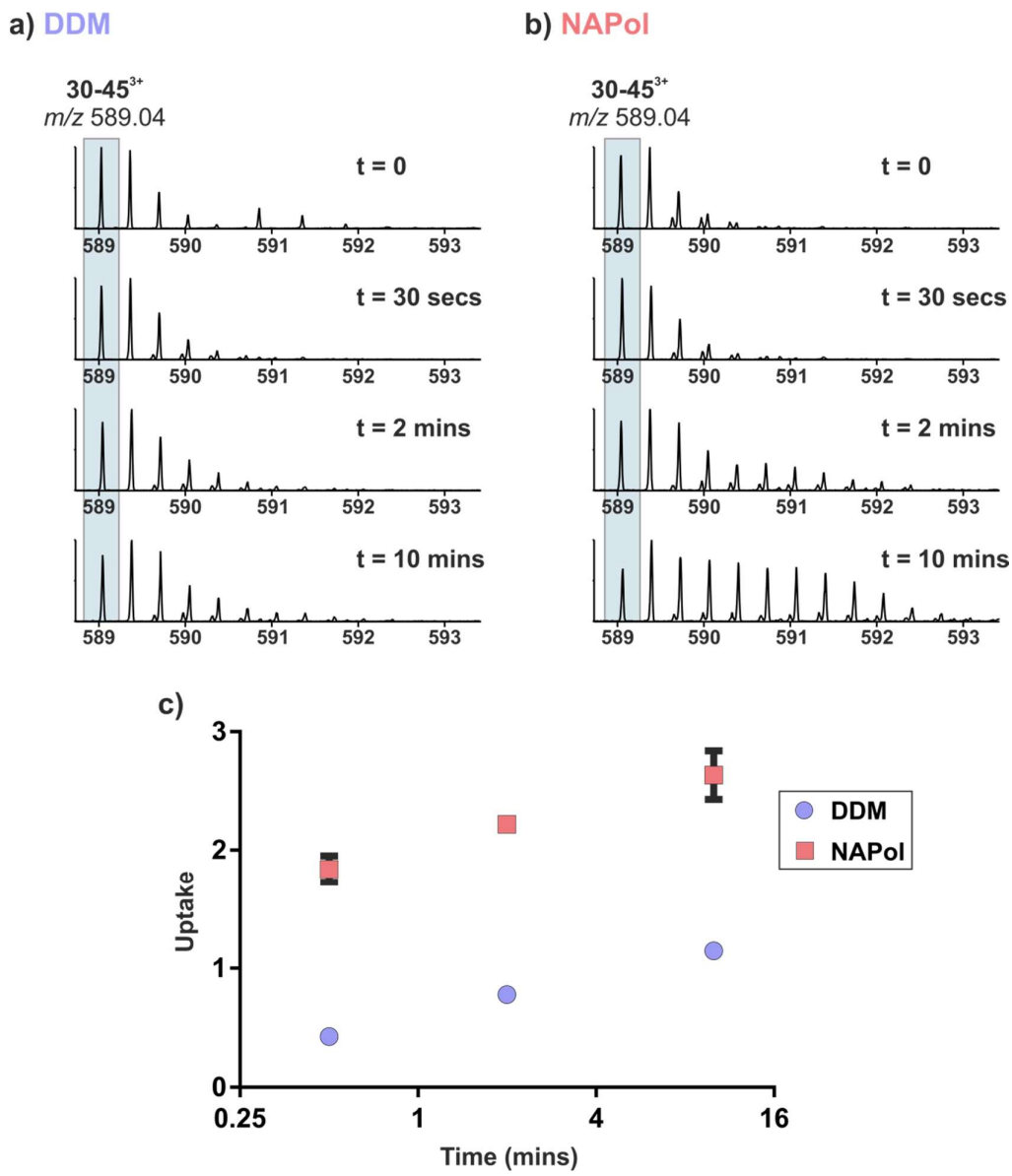

Figure 5-7 – OmpT$_{HT}$ peptic peptide 30-45 undergoes greater deuterium exchange when solubilised in NAPol than in DDM micelles. Mass spectra of peptide 30-45 show deuterium incorporation at 0 secs, 30 secs, 2 mins and 10 mins when OmpT$_{HT}$ is solubilised in a) DDM micelles or b) NAPol and indicate a second less-protected state in the presence of NAPol that is not present in the presence of DDM micelles. c) Mean deuterium uptake shows a steady increase in uptake over time in peptide 30-45 and a greater degree of deuterium uptake in OmpT$_{HT}$ solubilised in NAPol (red) than in DDM (blue) micelles. Error bars represent SEM (n=3). Where not shown error bars were smaller than the data point radius.

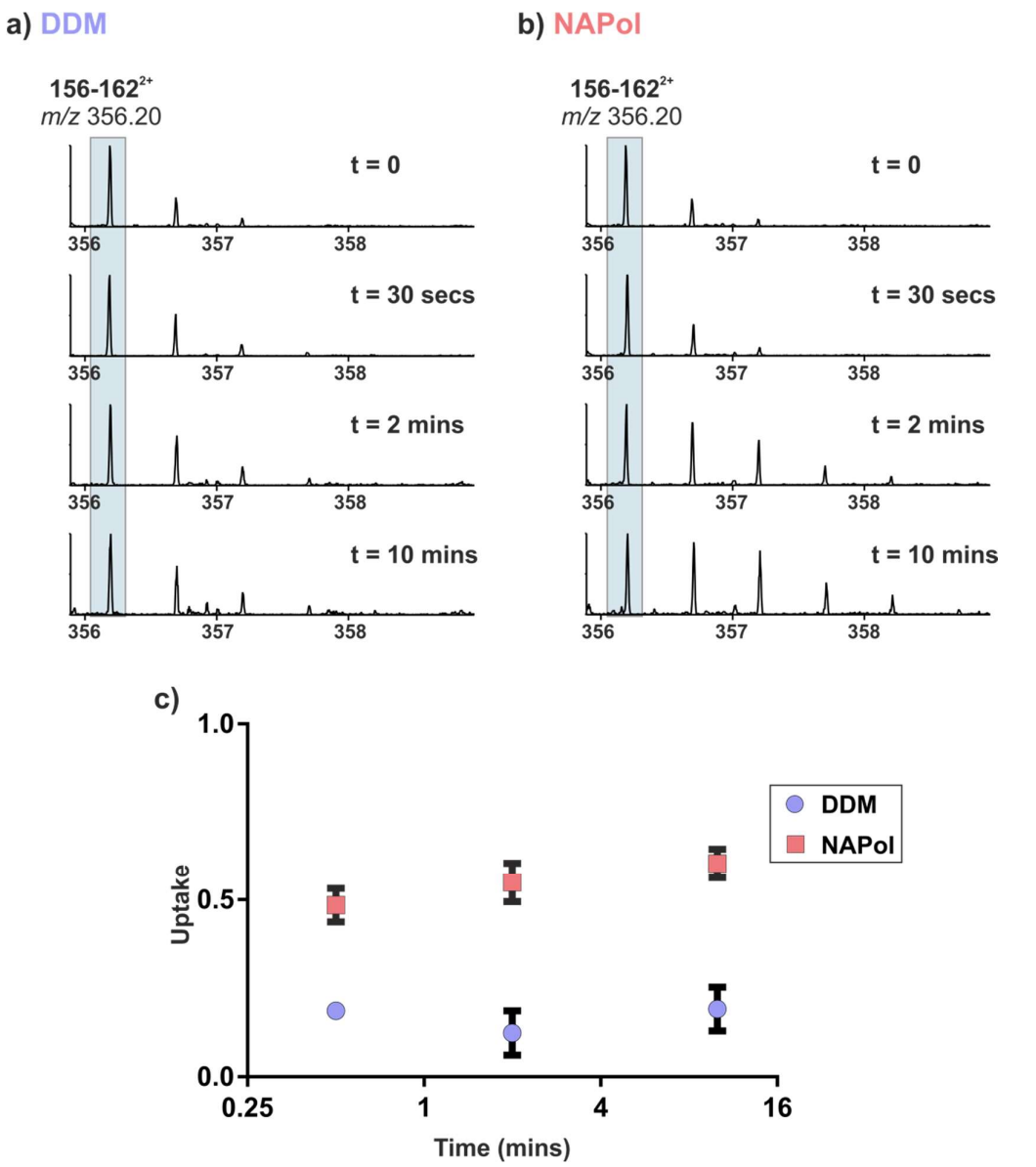

Figure 5-8 - OmpT$_{HT}$ peptic peptide 156-162 undergoes greater deuterium exchange when solubilised in NAPol than in DDM micelles. Mass spectra of peptide 156-162 show deuterium incorporation at 0 secs, 30 secs, 2 mins and 10 mins when OmpT$_{HT}$ is solubilised in a) DDM micelles or b) NAPol and show greater exchange at the 2 and 10 min timepoints in the presence of NAPol compared to DDM micelles. c) Mean deuterium uptake shows a steady increase in uptake over time in peptide 156-162 from OmpT$_{HT}$ solubilised in NAPol (red) but little exchange when solubilised in DDM micelles (blue). Error bars represent SEM (n=3). Where not shown error bars were smaller than the data point radius.

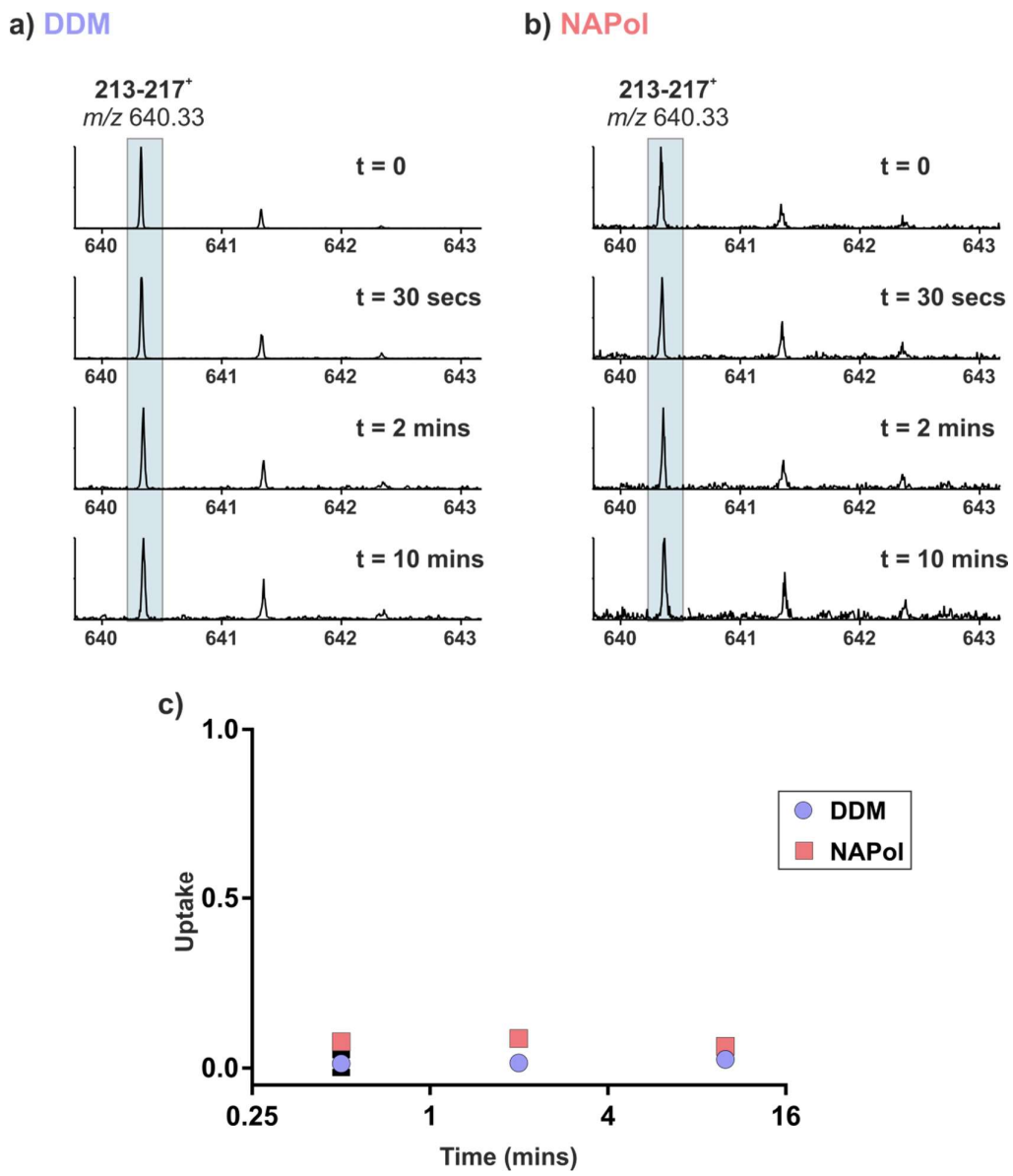

Figure 5-9 - OmpT$_{HT}$ peptic peptide 213-217 undergoes minimal deuterium exchange when solubilised in NAPol or DDM micelles. Mass spectra of peptide 213-217 show deuterium incorporation at 0 secs, 30 secs, 2 mins and 10 mins when OmpT$_{HT}$ is solubilised in a) DDM micelles or b) NAPol and show little exchange in the presence of NAPol or DDM micelles. c) Mean deuterium uptake shows a minimal increase in uptake over time in peptide 213-217 from OmpT$_{HT}$ solubilised in NAPol (red) or DDM micelles (blue). Error bars represent SEM (n=3). Where not shown error bars were smaller than the data point radius.

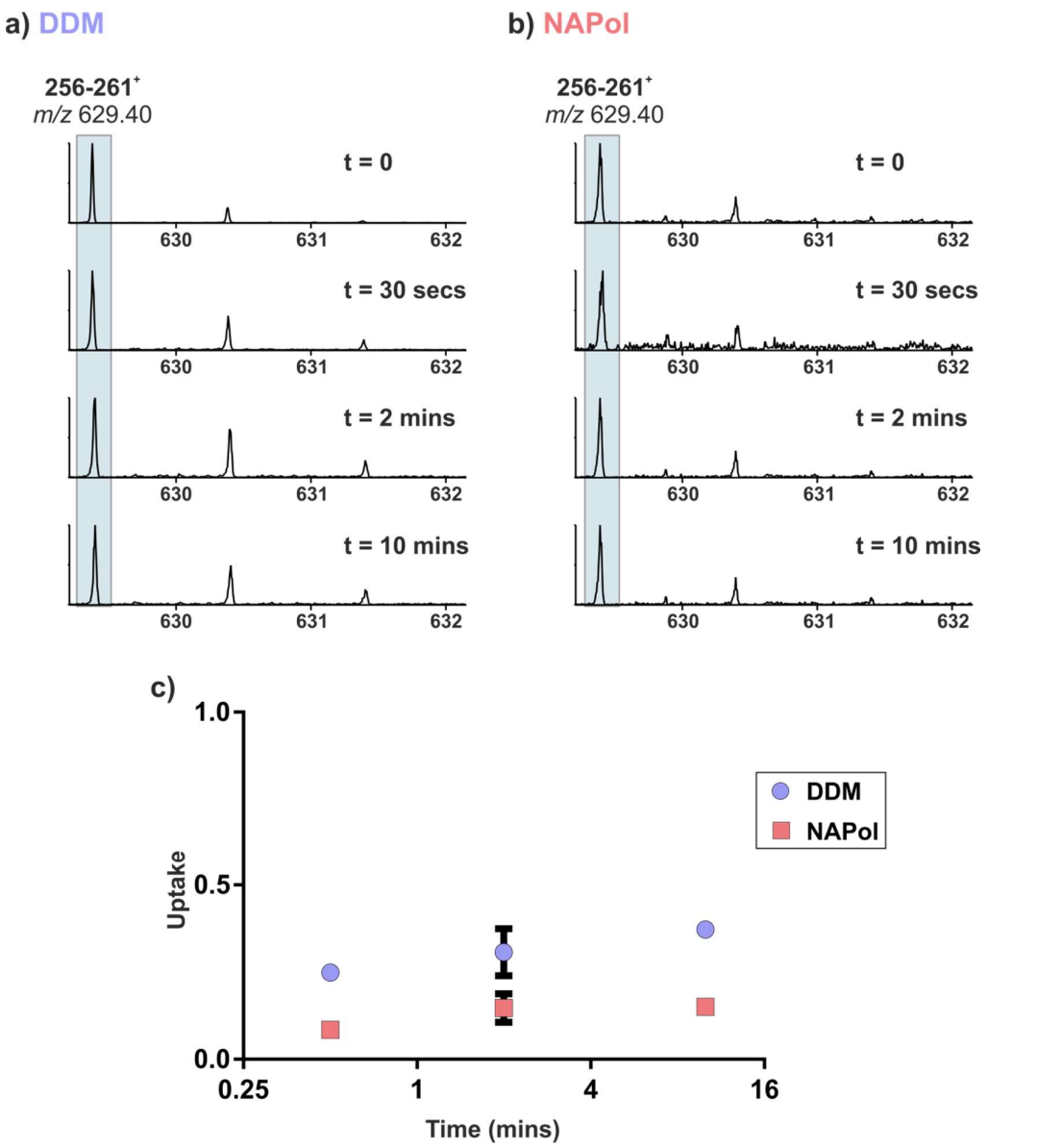

Figure 5-10 - OmpT$_{HT}$ peptic peptide 256-261 undergoes greater deuterium exchange when solubilised in DDM micelles compared to NAPol. Mass spectra of peptide 256-261 show deuterium incorporation at 0 secs, 30 secs, 2 mins and 10 mins when OmpT$_{HT}$ is solubilised in a) DDM micelles or b) NAPol and show greater exchange at the 30 sec, 2 min and 10 min timepoints in the presence of DDM micelles compared to NAPol. c) Mean deuterium uptake shows a steady increase in uptake over time in peptide 256-261 from OmpT$_{HT}$ solubilised in DDM micelles (blue) but little exchange when solubilised in NAPol (red). Error bars represent SEM (n=3). Where not shown error bars were smaller than the data point radius.

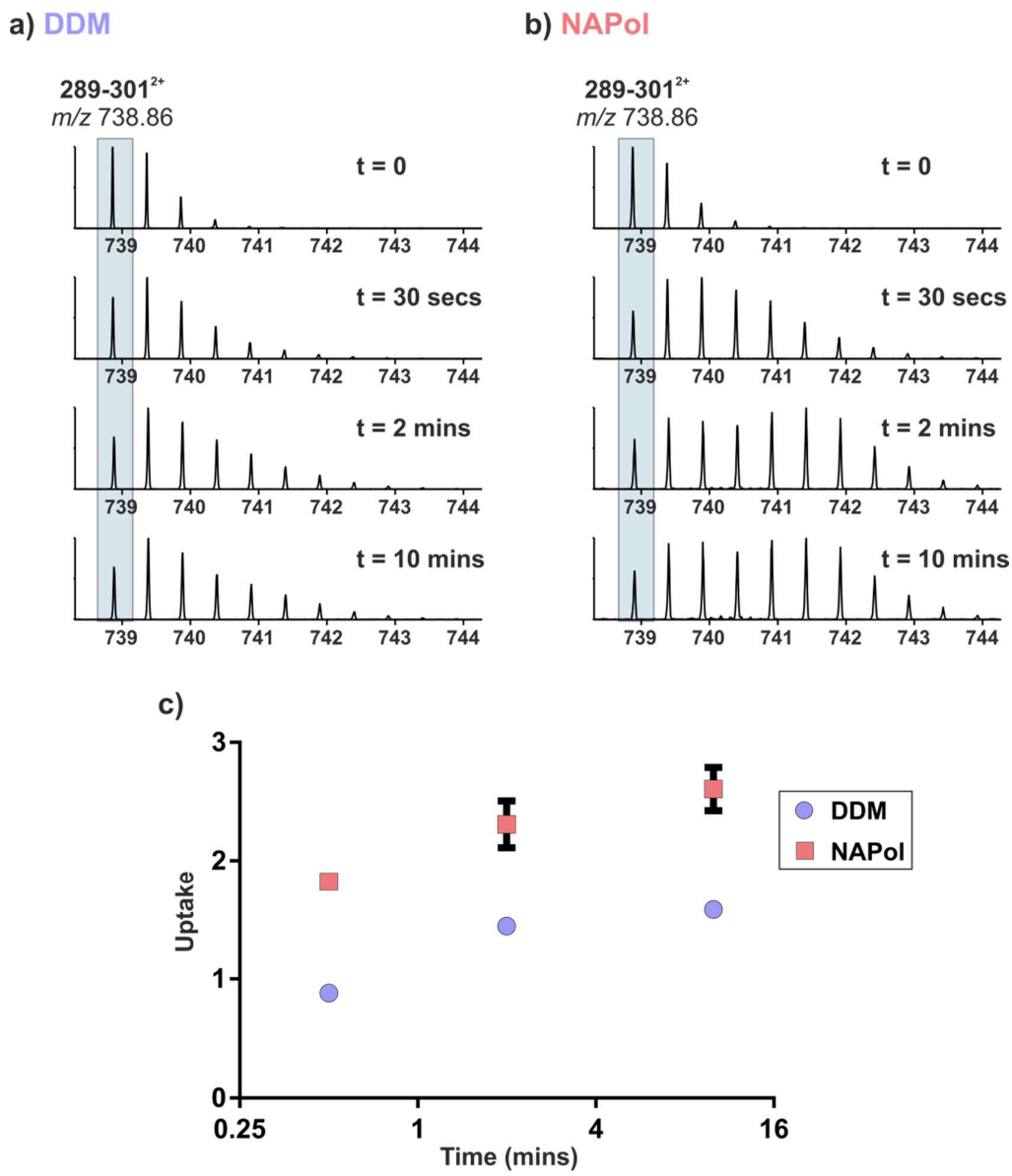

Figure 5-11 - OmpT$_{HT}$ peptic peptide 289-301 undergoes greater deuterium exchange when solubilised in NAPol than in DDM micelles. Mass spectra of peptide 289-301 show deuterium incorporation at 0 secs, 30 secs, 2 mins and 10 mins when OmpT$_{HT}$ is solubilised in a) DDM micelles or b) NAPol and indicate a second less-protected state in the presence of NAPol that is not observed in the presence of DDM micelles. c) Mean deuterium uptake shows a steady increase in uptake over time in peptide 289-301 and a greater degree of deuterium uptake in OmpT$_{HT}$ solubilised in NAPol (red) than in DDM (blue) micelles. Error bars represent SEM (n=3). Where not shown error bars were smaller than the data point radius.

Regions of greater deuterium uptake shown in the heat map in Figure 5-6 are mapped onto the structure of OmpT (PDB 1I78)[30]. The results show a number of regions in the extramembrane domain of $OmpT_{HT}$ that undergo a greater degree of deuterium uptake when solubilised in NAPol (red, Figure 5-12) and a few shorter regions of the $OmpT_{HT}$ sequence (in the extramembrane and the TM domains) when solubilised in DDM micelles (blue, Figure 5-12). Residues within the TM domain of $OmpT_{HT}$ undergo a comparable degree of deuterium uptake, whether solubilised in DDM micelles or NAPol.

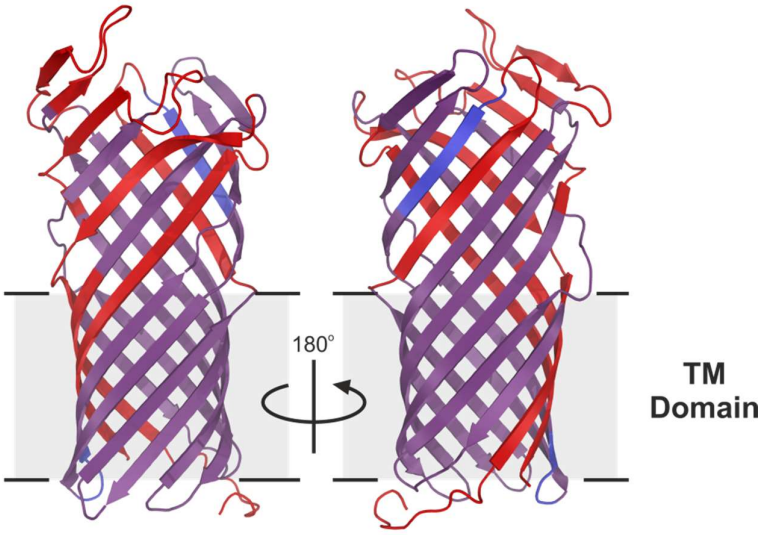

Figure 5-12 - Relative deuterium uptake in $OmpT_{HT}$ solubilised in DDM micelles or NAPol after 10 min (displayed in Figure 5-6) mapped onto the structure of OmpT (PDB 1I78)[30]. Regions with greater uptake in DDM micelles (blue) or NAPol (red) are found within the extramembrane domain of $OmpT_{HT}$, while uptake in the TM domain of $OmpT_{HT}$ is comparable whether solubilised in DDM micelles or NAPol.

This increase in uptake (presumably flexibility) is not in keeping with previous findings pertaining to solubilisation of MPs by APols (discussed further later). The following data is shown to determine if this is an effect of a change in native exchange properties of proteins in the presence of DDM micelles or NAPol. BK and AngII in the presence of 0.02 % (*w/v*) DDM or 2 $mg.ml^{-1}$ NAPol were deuterium labelled and analysed in the same manner as previously for $OmpT_{HT}$. For both BK and AngII, uptake rate and total deuterium uptake is comparable whether supplemented with DDM micelles or NAPol (Figure 5-13). Suggesting that

differences in $OmpT_{HT}$ uptake are as a result of the effect of solubilising media on the protein.

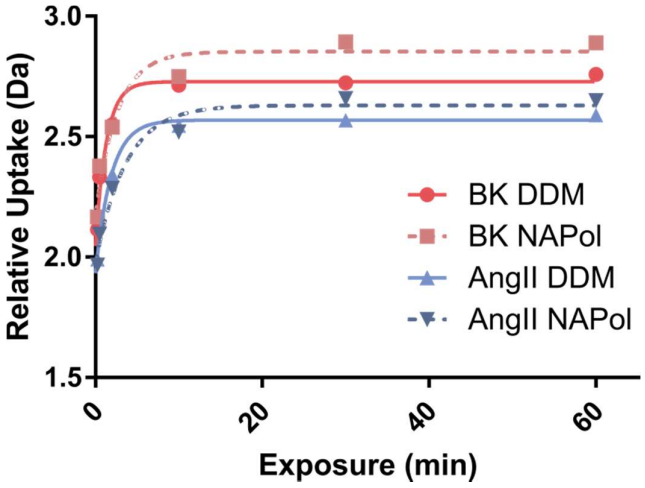

Figure 5-13 – BK (red) and AngII (blue) are deuterium labelled in the presence of 0.02 % (w/v) DDM (solid lines) or 2 mg.ml^{-1} NAPol (dashed lines) in order to identify any potential impact they may have on uptake. Maximal uptake of BK and AngII is reached after 10 minutes, in the presence of either DDM or NAPol. Maximal uptake is comparable when in the presence of DDM or NAPol, for each peptide.

5.3 Discussion

Deuterium incorporation into the TM domain of $OmpT_{HT}$ was low relative to the extramembrane domain, whether $OmpT_{HT}$ was solubilised in DDM micelles or NAPol (Figure 5-3, Figure 5-4 and Figure 5-5). This is common among MPs[194, 196, 198, 225], as the surfactant associated to the TM domain excludes solvent and stabilises the hydrogen bond network. Figure 5-6 and Figure 5-12 show that the degree of deuterium uptake is the same for the TM domain of $OmpT_{HT}$ in DDM micelles and NAPol. This correlates with previously shown FPOP data on $OmpT_{HT}$ (Chapter 4), which shows that the degree of oxidation is also similar in the TM domain when solubilised in DDM micelles or A8-35 APol. Together, the results suggest that $OmpT_{HT}$ remains structurally similar and solvent exclusion by each surfactant is similar.

HDX-MS studies on other MPs have found that environment-dependent differences in deuterium uptake are confined mainly to non-TM domains. This is shown in the change of the solvent exposure in the cavity of BmrA formed by the intracellular

domain despite a significant global rearrangement of the structure[194], and the extra- and intracellular faces of rhodopsin are labelled differently in the opsin and rhodopsin state[196]. There is evidence for changes in the deuterium uptake in TM domains of MPs, such as the deep cavity in the ATP/ADP carrier in the presence of different inhibitors[197-198]. However, this is a region of the ATP/ADP carrier that is functionally dependent on the cavity being solvent exposed in response to stimuli, where $OmpT_{HT}$ may not be required to undergo such solvent dependent changes in structure. Native MS of MPs in APols also shows that the smaller β-barrel MPs without extramembrane domains, such as PagP and tOmpA, are little affected by solubilisation in detergent micelles or APols (Section 3.2.5-6), further suggesting little distinction between the dynamic or structural properties of their TM domains in these solubilisation media and that APols influence on structure and stability are exerted on extramembrane regions.

Despite similarities in the HDX observed in the TM domain of $OmpT_{HT}$ solubilised in DDM micelles and NAPol, there is a marked difference in the degree of deuterium uptake in the extramembrane domain (Figure 5-6 and Figure 5-12). When solubilised in NAPol, the extramembrane domain of $OmpT_{HT}$ uptakes deuterium to a greater extent than when solubilised in DDM micelles. Assuming NAPol interacts with MPs in a similar fashion to A8-35-like APols, this is unexpected. APols have been posited to form extra interactions with non-TM domains, which can underpin the improved kinetic stability of their complexes with MPs[64, 223]. This would presumably result in an increased stability of the extramembrane domains of MPs. NAPol has been stated to be the most native-like APol for solubilisation of MPs[58-59], more so than detergent micelles, which would translate into reduced deuterium uptake. This can be explained by one of two phenomena. Either OMPs are uncharacteristically perturbed by NAPol, this could justify the increased charging of tOmpA solubilised in NAPol when observed by nESI-IMS-MS (although native-like CCS values of tOmpA are observed) and the broader charge state distribution (Figure 3-19b), suggesting an increased degree of flexibility; or the inherent properties of NAPol and detergent micelles influencing the solution environment during the labelling process and result in different rates and degrees of deuterium uptake. A simple experiment using

peptides in the presence of DDM micelles or NAPol shows extent and rate of labelling is not affected by these buffer components, suggesting that the former is true. In addition, although thought to be less native-like than NAPol, SAPol behaves more closely to the A8-35-like APols by native MS. Analysis of $OmpT_{HT}$ using other acid-soluble APols such as SAPol could result in different labelling that better agrees with native MS and FPOP-LC-MS data.

6 Concluding Remarks

The overall aim of the work presented here was to aid the development of methods for the study of MPs using MS-based techniques. This was carried out primarily by investigating the potential of applying APols as solubilising media for MPs compared with the use of detergent micelles, the current standard for MS-based experiments[118, 140, 158]. Additionally, different MS-related techniques were used to identify the nature of APol interactions with MPs and how this may relate to the benefits of solubilising MPs in APols over detergent micelles.

Native MS alone and in conjunction with gas phase techniques such as IMS and CIU is becoming a more commonly used technique for studying native proteins, particularly MPs[140, 147, 154]. Furthermore, with a greater understanding of the processes involved in solubilising MPs and delivering them to the gas phase, native MS is a more powerful and reliable technique for studying MPs[118, 147, 154, 156, 217].

Work in this thesis shows how sample conditions can be maximised for greater observation of native MPs by MS (Sections 3.2.1, 3.2.2 and 3.2.3). Screening refolding ratios of OmpT:A8-35, minimising concentrations of free A8-35 and purification of folded conformations of OmpT:A8-35 using SEC greatly improves the quality of native MS data acquired for MPs. These data show how an excess of A8-35 is not necessary to maintain the maximal folding yield of OmpT, which was previously thought to be the case.

The thesis describes the first direct comparison of detergent micelles and APols as solubilising media for MPs analysed using nESI-IMS-MS (Section 3.2.4). The data show that A8-35 is capable of delivering the most native-like state of both α-helical and β-barrel MPs to the gas phase, where detergent micelles were more likely to result in unfolding of MPs. This was shown by the differential charge state distributions and CCS-*z* relationships of OmpT, Mhp1 and GalP solubilised in DDM micelles or A8-35. This improved ability to deliver the most native-like state of MPs to the gas phase and the greater kinetic stability of MP:APol complexes was posited to be a result of the means by which APols associate with MPs. By forming many weak contacts, there is a reduced possibility of all contacts between APol and MP dissociating simultaneously. PagP was shown to be folded equally well in both

DDM micelles and A8-35. This was the first evidence that APol mediates its stabilising effects by interacting with non-TM regions of MPs, which are more substantial in OmpT than PagP. The presence of extra contacts had been proposed previously in MD and NMR studies of MPs solubilised in detergent micelles or APol[64, 76, 78].

Having shown the power of APols for delivering native-like MPs into the gas phase, a range of APols varying in size, charge and inclusion of different functional groups were used to determine if certain properties of APols can be optimised for native MS studies of MPs (Section 3.2.6). It was determined that the smallest and least negatively charged APol, A8-35, was the most reliable for the delivery of OMPs into the gas phase. The reduced observation of OMPs from the larger APols further corroborates the mechanism of MP:APol stability described earlier, with a larger APol making more contacts with the protein, thus further reducing the probability of complete dissociation of an APol molecule in solution and in the gas phase. nESI-IMS-MS data shown here were acquired in positive ionisation mode, this obscures whether the reduced observation of OMPs from the more negatively charged APols is a result of a lower ionisation efficiency or whether the OMPs are less readily released. NAPol only allowed observation of one of the studied OMPs and resulted in more highly charged states than the other APols despite populating the most native-like conformations as shown by CCS values calculated using IMS. This was initially attributed to the lack of negative native charge promoting greater ionisation with the most native-like state being sustained due to the more native-like environment provided by NAPol; however, understanding of this was obscured by subsequent HDX-MS data.

In addition to altering the observation of OMPs by nESI-IMS-MS, different properties of APols were found to modulate the enzymatic functions of $OmpT_{HT}$ and PagP. $OmpT_{HT}$ activity was lessened in the most highly charged APol and PagP activity was potentiated in these APols, suggesting a charge-dependent perturbation in local structure not observed by other solution techniques such as CD and SDS-PAGE that assess global folding. This inspired the use of chemical labelling techniques that use the high analytical power of LC-MS to resolve MP structure to peptide and residue levels.

FPOP-LC-MS is a solution phase oxidative labelling technique that uses UV irradiation to generate hydroxyl radicals, which label reactive amino acid side chains[165-166]. These oxidation sites can be identified to a residue-level following proteolysis using LC-MS/MS on tryptic peptides. Where IMS informs on global structure of MPs, FPOP-LC-MS can inform on local structure and potentially explain differences in activity of OmpT in different solubilising media.

FPOP-LC-MS data of $OmpT_{HT}$ solubilised in DDM micelles or A8-35 yielded a number of novel findings (Chapter 0). Differences in the means of interaction of the surfactants with $OmpT_{HT}$ were observed. Residues at the periplasmic side of the TM domain were found to be more protected from solvent in DDM micelles and residues in the extramembrane domain are more protected from solvent in APol. This suggests a defined interaction surface of DDM micelles with $OmpT_{HT}$ that is distinct from that in APol and the presence of extra contacts formed between APol and non-TM regions of OmpT, which could afford the kinetic stability of MP:APol complexes and explain how $OmpT_{HT}$ is stabilised during nESI-IMS-MS. These observations were achieved by observing oxidation sites (quantitatively) at Trp/Tyr/Phe/His residues in addition to the Met residues. Previous studies on MPs using FPOP-LC-MS had only reported on oxidation at Met/Cys residues[177, 179]. This is a significant development in FPOP-LC-MS for MP study, with a larger proportion of surface facing aromatic residues than their water soluble counterparts.

HDX-MS is another powerful technique commonly used to investigate the structural and dynamic properties of proteins. All regions of a protein can be probed over a timecourse, in multiple states (e.g. ligand-bound or in differing solubilising media) and at a peptide or pseudo-residue level[181, 183, 186]. HDX-MS is also a useful complementary technique to FPOP-LC-MS, in that it probes the protein backbone and observes differences over different timescales, looking at μsec to mins where FPOP labels proteins in a ~1 μs snapshot. This means HDX-MS can further inform on the nature of these extra contacts formed between $OmpT_{HT}$ and APols and how they affect dynamic properties of $OmpT_{HT}$.

HDX-MS experiments were performed to compare $OmpT_{HT}$ solubilised in DDM micelles or NAPol (used in place of A8-35, due to the insolubility of A8-35 and its complexes with MPs in the low pH quench step required to prevent HDX back-exchange) (Chapter 5). The data showed deuterium uptake to be greater in the extramembrane region of $OmpT_{HT}$ when solubilised in NAPol compared to DDM micelles, which could appear contradictory to previous observations of $OmpT_{HT}$ by native MS and FPOP-LC-MS. However, tOmpA from NAPol was more highly charged than from DDM micelles when analysed by nESI-IMS-MS, suggesting a unique effect of NAPol on OMPs that actually promotes a more dynamic structure when combined with presently shown HDX-MS data.

The results presented in this thesis have shown here that firstly, APols, particularly A8-35, can be used universally to provide a reliable method for stabilisation of a native-like state of MPs and deliver it into the gas-phase for study by nESI-IMS-MS. Secondly, these stabilisation effects are likely mediated through extra contacts of APols with MPs in non-TM regions. Thirdly, MS-based techniques including native MS, FPOP-LC-MS and HDX-MS can be used concurrently to provide a high-degree of understanding of MP structure and how it may be impacted by its environment.

Work shown here also sets the groundwork for a number of further developments in studying MP structure and MP:APol complexes using MS. Native-MS has been used to study the conformation of fully integral MP complexes and MP complexes with peripheral accessory subunits[16-17]. APols may provide useful stabilisation for observation of these in the gas phase. MS is a powerful technique for observing ligand/protein binding and its effect on structure and stability, something which has not been examined directly using APols. APols may also prove to be a valuable tool in this sense, as reported reduced flexibility of MPs in APols, may suggest APol can be used for trapping select conformations.

FPOP-LC-MS can be employed further to observe the impact of such binding events at the residue-level and could be especially powerful by combining the approach with constructs containing radical-reactive residues rationally inserted in regions of interest, allowing enhanced sensitivity in regions of interest and simplicity in data analysis and interpretation. FPOP-LC-MS has been used for epitope mapping

of binding sites in soluble proteins[167], which has yet to have been tested in MPs and can be investigated using methodologies similar to those described here.

In addition to the effects on native MPs, the data shown here have shown that buffer components present in OMP refolding experiments (e.g. urea and lipids) are not inhibitory to oxidative labelling by FPOP, opening up the possibility of using FPOP-LC-MS for the study of folding mechanisms of MPs. Introduction of controlled mixing would also allow for an expanded timecourse range for such experiments.

HDX-MS data using NAPol as the APol of interest has also further enhanced our understanding of MP:APol complexes, suggesting an interesting increase in dynamics which were not observed using FPOP. Whether this is specific to NAPol remains unsolved. This can be remedied by repeats of such experiments comparing OmpT solubilised in more A8-35-like APols that are insensitive to low pH, such as SAPol or PC-APol. In addition, like FPOP-LC-MS, HDX-MS has been used commonly with water soluble proteins to map binding sites and determine the effects of such binding events. This is an important aspect of HDX-MS that could well be pursued in MP study.

In conclusion, the work presented here has furthered our understanding of methodologies and technical approaches that can be used by many to better approach problems relating to MP structure and function, an immensely important and exciting aspect of biological science.

7 References

1. BOWIE, J. U., Solving the membrane protein folding problem. *Nature* **2005,** *438* (7068), 581-589.

2. BOOTH, P. J.; CURNOW, P., Folding scene investigation: membrane proteins. *Current Opinion in Structural Biology* **2009,** *19* (1), 8-13.

3. ROSENBAUM, D. M.; RASMUSSEN, S. G.; KOBILKA, B. K., The structure and function of G-protein-coupled receptors. *Nature* **2009,** *459* (7245), 356-363.

4. CATTERALL, W. A., Structure and function of voltage-gated ion channels. *Annual Review of Biochemistry* **1995,** *64*, 493-531.

5. KAUPP, U. B.; SEIFERT, R., Cyclic nucleotide-gated ion channels. *Physiological Reviews* **2002,** *82* (3), 769-824.

6. DEAN, M.; RZHETSKY, A.; ALLIKMETS, R., The human ATP-binding cassette (ABC) transporter superfamily. *Genome Research* **2001,** *11* (7), 1156-1166.

7. SHIMAMURA, T.; WEYAND, S.; BECKSTEIN, O.; RUTHERFORD, N. G.; HADDEN, J. M.; SHARPLES, D.; SANSOM, M. S.; IWATA, S.; HENDERSON, P. J.; CAMERON, A. D., Molecular basis of alternating access membrane transport by the sodium-hydantoin transporter Mhp1. *Science* **2010,** *328* (5977), 470-473.

8. SMITH, S. G. J.; MAHON, V.; LAMBERT, M. A.; FAGAN, R. P., A molecular Swiss army knife: OmpA structure, function and expression. *FEMS Microbiology Letters* **2007,** *273* (1), 1-11.

9. CATTERALL, W. A., Ion Channel Voltage Sensors: Structure, Function, and Pathophysiology. *Neuron* **2010,** *67* (6), 915-928.

10. VON HEIJNE, G., Membrane-protein topology. *Nature Reviews Molecular Cell Biology* **2006,** *7* (12), 909-918.

11. SCHULZ, G. E., The structure of bacterial outer membrane proteins. *Biochimica et Biophysica Acta (BBA)* **2002,** *1565* (2), 308-317.

12. SCHLEIFF, E.; MAIER, U. G.; BECKER, T., Omp85 in eukaryotic systems: one protein family with distinct functions. *Biological Chemistry* **2011,** *392* (1-2), 21-27.

13. SOMMER, M. S.; DAUM, B.; GROSS, L. E.; WEIS, B. L.; MIRUS, O.; ABRAM, L.; MAIER, U. G.; KUHLBRANDT, W.; SCHLEIFF, E., Chloroplast Omp85 proteins change orientation during evolution. *Proceedings of the National Academy of Sciences of the United States of America* **2011,** *108* (33), 13841-13846.

14. GENTLE, I. E.; BURRI, L.; LITHGOW, T., Molecular architecture and function of the Omp85 family of proteins. *Molecular Microbiology* **2005,** *58* (5), 1216-1225.

15. SON, S. Y.; MA, J.; KONDOU, Y.; YOSHIMURA, M.; YAMASHITA, E.; TSUKIHARA, T., Structure of human monoamine oxidase A at 2.2-A resolution: the control of opening the entry for substrates/inhibitors. *Proceedings of the National Academy of Sciences of the United States of America* **2008,** *105* (15), 5739-5744.

16. ESTEBAN, O.; BERNAL, R. A.; DONOHOE, M.; VIDELER, H.; SHARON, M.; ROBINSON, C. V.; STOCK, D., Stoichiometry and localization of the stator subunits

E and G in Thermus thermophilus H+-ATPase/synthase. *Journal of Biological Chemistry* **2008,** *283* (5), 2595-2603.

17. ZHOU, M.; MORGNER, N.; BARRERA, N. P.; POLITIS, A.; ISAACSON, S. C.; MATAK-VINKOVIĆ, D.; MURATA, T.; BERNAL, R. A.; STOCK, D.; ROBINSON, C. V., Mass spectrometry of intact V-type ATPases reveals bound lipids and the effects of nucleotide binding. *Science* **2011,** *334*, 380-385.

18. GU, Y. H.; LI, H. Y.; DONG, H. H.; ZENG, Y.; ZHANG, Z. Y.; PATERSON, N. G.; STANSFELD, P. J.; WANG, Z. S.; ZHANG, Y. Z.; WANG, W. J.; DONG, C. J., Structural basis of outer membrane protein insertion by the BAM complex. *Nature* **2016,** *531* (7592), 64-69.

19. HAN, L.; ZHENG, J. G.; WANG, Y.; YANG, X.; LIU, Y. Q.; SUN, C. Q.; CAO, B. H.; ZHOU, H. Z.; NI, D. C.; LOU, J. Z.; ZHAO, Y. F.; HUANG, Y. H., Structure of the BAM complex and its implications for biogenesis of outer-membrane proteins. *Nature Structural and Molecular Biology* **2016,** *23* (3), 192-196.

20. PAUTSCH, A.; SCHULZ, G. E., High-resolution structure of the OmpA membrane domain. *Journal of Molecular Biology* **2000,** *298* (2), 273-282.

21. ALMÉN, M. S.; NORDSTRÖM, K. J. V.; FREDRIKSSON, R.; SCHIÖTH, H. B., Mapping the human membrane proteome: a majority of the human membrane proteins can be classified according to function and evolutionary origin. *BMC Biology* **2009,** *7*, 50-50.

22. ARINAMINPATHY, Y.; KHURANA, E.; ENGELMAN, D. M.; GERSTEIN, M. B., Computational analysis of membrane proteins: the largest class of drug targets. *Drug Discovery Today* **2009,** *14* (23-24), 1130-1135.

23. DORSAM, R. T.; GUTKIND, J. S., G-protein-coupled receptors and cancer. *Nature Reviews Cancer* **2007,** *7* (2), 79-94.

24. BOWIE, J. U., Membrane proteins: a new method enters the fold. *Proceedings of the National Academy of Sciences of the United States of America* **2004,** *101* (12), 3995-3996.

25. WHITE, S. H.; WIMLEY, W. C., Membrane protein folding and stability: Physical principles. *Annual Review of Biophysics and Biomolecular Structure* **1999,** *28*, 319-365.

26. POPOT, J. L.; ENGELMAN, D. M., Helical membrane protein folding, stability, and evolution. *Annual Review of Biochemistry* **2000,** *69*, 881-922.

27. OTZEN, D. E.; ANDERSEN, K. K., Folding of outer membrane proteins. *Archives of Biochemistry and Biophysics* **2013,** *531* (1-2), 34-43.

28. AHN, V. E.; LO, E. I.; ENGEL, C. K.; CHEN, L.; HWANG, P. M.; KAY, L. E.; BISHOP, R. E.; PRIVÉ, G. G., A hydrocarbon ruler measures palmitate in the enzymatic acylation of endotoxin. *The EMBO Journal* **2004,** *23* (15), 2931-2941.

29. KRAMER, R. A.; ZANDWIJKEN, D.; EGMOND, M. R.; DEKKER, N., In vitro folding, purification and characterization of Escherichia coli outer membrane protease ompT. *European Journal of Biochemistry / FEBS* **2000,** *267* (3), 885-893.

30. VANDEPUTTE-RUTTEN, L.; KRAMER, R. A.; KROON, J.; DEKKER, N.; EGMOND, M. R.; GROS, P., Crystal structure of the outer membrane protease OmpT from

Escherichia coli suggests a novel catalytic site. *The EMBO Journal* **2001,** *20* (18), 5033-5039.

31. HOUSDEN, N. G.; WOJDYLA, J. A.; KORCZYNSKA, J.; GRISHKOVSKAYA, I.; KIRKPATRICK, N.; BRZOZOWSKI, A. M.; KLEANTHOUS, C., Directed epitope delivery across the Escherichia coli outer membrane through the porin OmpF. *Proceedings of the National Academy of Sciences of the United States of America* **2010,** *107* (50), 21412-21417.

32. CHIMENTO, D. P.; MOHANTY, A. K.; KADNER, R. J.; WIENER, M. C., Substrate-induced transmembrane signaling in the cobalamin transporter BtuB. *Nature Structural Biology* **2003,** *10* (5), 394-401.

33. POPOT, J.-L., Amphipols, nanodiscs, and fluorinated surfactants: three nonconventional approaches to studying membrane proteins in aqueous solutions. *Annual Review of Biochemistry* **2010,** *79*, 737-775.

34. RUIZ, N.; KAHNE, D.; SILHAVY, T. J., Advances in understanding bacterial outer-membrane biogenesis. *Nature Reviews Microbiology* **2006,** *4* (1), 57-66.

35. FERGUSON, A. D.; HOFMANN, E.; COULTON, J. W.; DIEDERICHS, K.; WELTE, W., Siderophore-mediated iron transport: Crystal structure of FhuA with bound lipopolysaccharide. *Science* **1998,** *282* (5397), 2215-2220.

36. FERGUSON, A. D.; WELTE, W.; HOFMANN, E.; LINDNER, B.; HOLST, O.; COULTON, J. W.; DIEDERICHS, K., A conserved structural motif for lipopolysaccharide recognition by procaryotic and eucaryotic proteins. *Structure with Folding and Design* **2000,** *8* (6), 585-592.

37. BISHOP, R. E., Structural biology of membrane-intrinsic beta-barrel enzymes: Sentinels of the bacterial outer membrane. *Biochimica et Biophysica Acta (BBA) - Biomembranes* **2008,** *1778* (9), 1881-1896.

38. MCCARTER, J. D.; STEPHENS, D.; SHOEMAKER, K.; ROSENBERG, S.; KIRSCH, J. F.; GEORGIOU, G., Substrate Specificity of the Escherichia coli Outer Membrane Protease OmpT. *Journal of Bacteriology* **2004,** *186* (17), 5919-5925.

39. GUO, L.; LIM, K. B.; PODUJE, C. M.; DANIEL, M.; GUNN, J. S.; HACKETT, M.; MILLER, S. I., Lipid A acetylation and bacterial resistance against vertebrate antimicrobial peptides. *Cell* **1998,** *95*, 189-198.

40. HUYSMANS, G. H. M.; RADFORD, S. E.; BROCKWELL, D. J.; BALDWIN, S. A., The N-terminal helix is a post-assembly clamp in the bacterial outer membrane protein PagP. *Journal of Molecular Biology* **2007,** *373* (3), 529-540.

41. MCMORRAN, L. M.; BARTLETT, A. I.; HUYSMANS, G. H. M.; RADFORD, S. E.; BROCKWELL, D. J., Dissecting the Effects of Periplasmic Chaperones on the In Vitro Folding of the Outer Membrane Protein PagP. *Journal of Molecular Biology* **2013,** *425* (17), 3178-3191.

42. KOEBNIK, R.; LOCHER, K. P.; VAN GELDER, P., Structure and function of bacterial outer membrane proteins: barrels in a nutshell. *Molecular Microbiology* **2000,** *37* (2), 239-253.

43. PRIVE, G. G., Detergents for the stabilization and crystallization of membrane proteins. *Methods* **2007,** *41* (4), 388-397.

44. GARAVITO, R. M.; FERGUSON-MILLER, S., Detergents as tools in membrane biochemistry. *Journal of Biological Chemistry* **2001,** *276* (35), 32403-32406.

45. SEDDON, A. M.; CURNOW, P.; BOOTH, P. J., Membrane proteins, lipids and detergents: not just a soap opera. *Biochimica et Biophysica Acta (BBA)* **2004,** *1666* (1-2), 105-117.

46. RIGAUD, J. L.; PITARD, B.; LEVY, D., Reconstitution of membrane proteins into liposomes: application to energy-transducing membrane proteins. *Biochimica et Biophysica Acta (BBA)* **1995,** *1231* (3), 223-246.

47. RIGAUD, J. L.; LEVY, D., Reconstitution of membrane proteins into liposomes. *Methods in Enzymology* **2003,** *372*, 65-86.

48. BAYBURT, T. H.; SLIGAR, S. G., Membrane protein assembly into Nanodiscs. *FEBS Letters* **2010,** *584* (9), 1721-1727.

49. HAGN, F.; ETZKORN, M.; RASCHLE, T.; WAGNER, G., Optimized phospholipid bilayer nanodiscs facilitate high-resolution structure determination of membrane proteins. *Journal of the American Chemical Society* **2013,** *135* (5), 1919-1925.

50. MARTY, M. T.; ZHANG, H.; CUI, W.; GROSS, M. L.; SLIGAR, S. G., Interpretation and deconvolution of nanodisc native mass spectra. *Journal of the American Society for Mass Spectrometry* **2014,** *25* (2), 269-277.

51. JUSTESEN, B. H.; LAURSEN, T.; WEBER, G.; FUGLSANG, A. T.; MØLLER, B. L.; GÜNTHER POMORSKI, T., Isolation of Monodisperse Nanodisc-Reconstituted Membrane Proteins Using Free Flow Electrophoresis. *Analytical Chemistry* **2013,** *1*, 58-61.

52. LY, S.; BOURGUET, F.; FISCHER, NICHOLAS O.; LAU, EDMOND Y.; COLEMAN, MATTHEW A.; LAURENCE, TED A., Quantifying Interactions of a Membrane Protein Embedded in a Lipid Nanodisc using Fluorescence Correlation Spectroscopy. *Biophysical Journal* **2014,** *106* (2), L05-L08.

53. MARTY, M. T.; ZHANG, H.; CUI, W.; BLANKENSHIP, R. E.; GROSS, M. L.; SLIGAR, S. G., Native mass spectrometry characterization of intact nanodisc lipoprotein complexes. *Analytical Chemistry* **2012,** *84* (21), 8957-8960.

54. MCKIBBIN, C.; FARMER, N. A.; JEANS, C.; REEVES, P. J.; KHORANA, H. G.; WALLACE, B. A.; EDWARDS, P. C.; VILLA, C.; BOOTH, P. J., Opsin stability and folding: modulation by phospholipid bicelles. *Journal of Molecular Biology* **2007,** *374* (5), 1319-1332.

55. MILLS, A.; LE, H.-T.; COULTON, J. W.; DUONG, F., FhuA interactions in a detergent-free nanodisc environment. *Biochimica et Biophysica Acta (BBA)* **2014,** *1838* (1), 364-371.

56. MORGAN, C. R.; HEBLING, C. M.; RAND, K. D.; STAFFORD, D. W.; JORGENSON, J. W.; ENGEN, J. R., Conformational transitions in the membrane scaffold protein of phospholipid bilayer nanodiscs. *Molecular & Cellular Proteomics* **2011,** *10* (9).

57. RASMUSSEN, S. G.; CHOI, H. J.; ROSENBAUM, D. M.; KOBILKA, T. S.; THIAN, F. S.; EDWARDS, P. C.; BURGHAMMER, M.; RATNALA, V. R.; SANISHVILI, R.; FISCHETTI, R. F.; SCHERTLER, G. F.; WEIS, W. I.; KOBILKA, B. K., Crystal structure of the

human beta2 adrenergic G-protein-coupled receptor. *Nature* **2007,** *450* (7168), 383-387.

58. POPOT, J. L.; ALTHOFF, T.; BAGNARD, D.; BANÈRES, J. L.; BAZZACCO, P.; BILLON-DENIS, E.; CATOIRE, L. J.; CHAMPEIL, P.; CHARVOLIN, D.; COCCO, M. J.; CRÉMEL, G.; DAHMANE, T.; DE LA MAZA, L. M.; EBEL, C.; GABEL, F.; GIUSTI, F.; GOHON, Y.; GOORMAGHTIGH, E.; GUITTET, E.; KLEINSCHMIDT, J. H.; KÜHLBRANDT, W.; LE BON, C.; MARTINEZ, K. L.; PICARD, M.; PUCCI, B.; SACHS, J. N.; TRIBET, C.; VAN HEIJENOORT, C.; WIEN, F.; ZITO, F.; ZOONENS, M., Amphipols: from A to Z. *Annual Review of Biophysics* **2011,** *40*, 379-408.

59. ZOONENS, M.; POPOT, J.-L., Amphipols for each season. *The Journal of Membrane Biology* **2014,** *247* (9-10), 759-796.

60. POCANSCHI, C. L.; POPOT, J.-L.; KLEINSCHMIDT, J. H., Folding and stability of outer membrane protein A (OmpA) from Escherichia coli in an amphipathic polymer, amphipol A8-35. *European Biophysics Journal* **2013,** *42*, 103-118.

61. GORZELLE, B. M.; HOFFMAN, A. K.; KEYES, M. H.; GRAY, D. N.; RAY, D. G.; SANDERS, C. R., Amphipols can support the activity of a membrane enzyme. *Journal of the American Chemical Society* **2002,** *124* (39), 11594-11595.

62. GOHON, Y.; DAHMANE, T.; RUIGROK, R. W. H.; SCHUCK, P.; CHARVOLIN, D.; RAPPAPORT, F.; TIMMINS, P.; ENGELMAN, D. M.; TRIBET, C.; POPOT, J.-L.; EBEL, C., Bacteriorhodopsin/amphipol complexes: structural and functional properties. *Biophysical Journal* **2008,** *94* (9), 3523-3537.

63. BECHARA, C.; BOLBACH, G.; BAZZACO, P.; SHARMA, K. S.; DURAND, G.; POPOT, J.-L.; ZITO, F.; SAGAN, S., MALDI-TOF mass spectrometry analysis of amphipol-trapped membrane proteins. *Analytical Chemistry* **2012,** *84* (14), 6128-6135.

64. PERLMUTTER, J. D.; POPOT, J.-L.; SACHS, J. N., Molecular dynamics simulations of a membrane protein/amphipol complex. *The Journal of Membrane Biology* **2014,** *247* (9-10), 883-895.

65. TRIBET, C.; AUDEBERT, R.; POPOT, J.-L., Amphipols : Polymers that keep membrane proteins soluble in aqueous solution. *Biochemistry* **1996,** *93*, 15047-15050.

66. GIUSTI, F.; RIEGER, J.; CATOIRE, L. J.; QIAN, S.; CALABRESE, A. N.; WATKINSON, T. G.; CASIRAGHI, M.; RADFORD, S. E.; ASHCROFT, A. E.; POPOT, J.-L., Synthesis, characterization and applications of a perdeuterated amphipol. *Journal of Membrane Biology* **2014,** *247* (9-10), 909-924.

67. GOHON, Y.; GIUSTI, F.; PRATA, C.; CHARVOLIN, D.; TIMMINS, P.; EBEL, C.; TRIBET, C.; POPOT, J.-L., Well-defined nanoparticles formed by hydrophobic assembly of a short and polydisperse random terpolymer, amphipol A8-35. *Langmuir* **2006,** *22* (3), 1281-1290.

68. ETZKORN, M.; RASCHLE, T.; HAGN, F.; GELEV, V.; RICE, A. J.; WALZ, T.; WAGNER, G., Cell-free expressed bacteriorhodopsin in different soluble membrane mimetics: biophysical properties and NMR accessibility. *Structure* **2013,** *21* (3), 394-401.

69. KNOWLES, T. J.; FINKA, R.; SMITH, C.; LIN, Y. P.; DAFFORN, T.; OVERDUIN, M., Membrane Proteins Solubilized Intact in Lipid Containing Nanoparticles

Bounded by Styrene Maleic Acid Copolymer. *Journal of the American Chemical Society* **2009,** *131* (22), 7484-+.

70. LEE, S. C.; KNOWLES, T. J.; POSTIS, V. L. G.; JAMSHAD, M.; PARSLOW, R. A.; LIN, Y. P.; GOLDMAN, A.; SRIDHAR, P.; OVERDUIN, M.; MUENCH, S. P.; DAFFORN, T. R., A method for detergent-free isolation of membrane proteins in their local lipid environment. *Nature Protocols* **2016,** *11* (7), 1149-1162.

71. DISCHER, D. E.; AHMED, F., Polymersomes. *Annual Review of Biomedical Engineering* **2006,** *8*, 323-341.

72. LEE, J. S.; FEIJEN, J., Polymersomes for drug delivery: design, formation and characterization. *Journal of Controlled Release* **2012,** *161* (2), 473-483.

73. CATOIRE, L. J.; DAMIAN, M.; GIUSTI, F.; MARTIN, A. E.; HEIJENOORT, C. V.; POPOT, J. L.; GUITTET, R.; BAN??RES, J. L., Structure of a GPCR ligand in its receptor-bound state: Leukotriene B4 adopts a highly constrained conformation when associated to human BLT2. *Journal of the American Chemical Society* **2010,** *132* (26), 9049-9057.

74. CVETKOV, T. L.; HUYNH, K. W.; COHEN, M. R.; MOISEENKOVA-BELL, V. Y., Molecular architecture and subunit organization of TRPA1 ion channel revealed by electron microscopy. *Journal of Biological Chemistry* **2011,** *286* (44), 38168-38176.

75. LENEY, A. C.; MCMORRAN, L. M.; RADFORD, S. E.; ASHCROFT, A. E., Amphipathic Polymers Enable the Study of Functional Membrane Proteins in the Gas Phase. *Analytical Chemistry* **2012,** *84*, 9841-9847.

76. ZOONENS, M.; CATOIRE, L. J.; GIUSTI, F.; POPOT, J.-L., NMR study of a membrane protein in detergent-free aqueous solution. *Proceedings of the National Academy of Sciences of the United States of America* **2005,** *102* (25), 8893-8898.

77. ZOONENS, M.; GIUSTI, F.; ZITO, F.; POPOT, J.-L., Dynamics of Membrane Protein / Amphipol Association Studied by Fo ¨ rster Resonance Energy Transfer : Implications for in Vitro Studies of Amphipol-Stabilized Membrane Proteins †. *Biochemistry* **2007,** *46*, 10392-10404.

78. CATOIRE, L. J.; ZOONENS, M.; VAN HEIJENOORT, C.; GIUSTI, F.; POPOT, J. L.; GUITTET, E., Inter- and intramolecular contacts in a membrane protein/surfactant complex observed by heteronuclear dipole-to-dipole cross-relaxation. *Journal of Magnetic Resonance* **2009,** *197* (1), 91-95.

79. CAO, E.; LIAO, M.; CHENG, Y.; JULIUS, D., TRPV1 structures in distinct conformations reveal activation mechanisms. *Nature* **2013,** *504* (7478), 113-118.

80. LIAO, M.; CAO, E.; JULIUS, D.; CHENG, Y., Structure of the TRPV1 ion channel determined by electron cryo-microscopy. *Nature* **2013,** *504* (7478), 107-112.

81. DE HOFFMAN, E.; STROOBANT, V., *Mass Spectrometry: Principles and Applications*. 2007.

82. KARAS, M.; BACHMANN, D.; BAHR, U.; HILLENKAMP, F., Marix-Assisted Ultraviolet Laser Desorption of Non-Volatile Compounds. *International Journal of Mass Spectrometry and Ion Processes* **1987,** *78*, 53-68.

83. KARAS, M.; HILLENKAMP, F., Laser Desorption Ionization of Proteins with Molecular Masses Exceeding 10 000 Daltons. *Analytical Chemistry* **1988,** *60* (20), 2299-2301.

84. CHEN, F.; GERBER, S.; HEUSER, K.; KORKHOV, V. M.; LIZAK, C.; MIREKU, S.; LOCHER, K. P.; ZENOBI, R., High-Mass Matrix-Assisted Laser Desorption Ionization-Mass Spectrometry of Integral Membrane Proteins and Their Complexes. *Analytical Chemistry* **2013**.

85. ZENOBI, R.; KNOCHENMUSS, R., Ion Formation in MALDI Mass Spectrometry. *Mass Spectrometry Reviews* **1999,** *17*, 337-366.

86. DOLE, M., Molecular Beams of Macroions. *Journal of Chemical Physics* **1968,** *49* (5), 2240-2240.

87. FENN, J. B.; MANN, M.; MENG, C. K.; WONG, S. F.; CRAIG, M.; MENG, C. K. A. I.; MANN, M.; WHITEHOUSE, C. M., Electrospray Ionization of Large for Mass Spectrometry Biomolecules. *Science* **1989,** *246*, 64-71.

88. KONERMANN, L.; AHADI, E.; RODRIGUEZ, A. D.; VAHIDI, S., Unravelling the Mechanism of Electrospray Ionisation. *Analytical Chemistry* **2013,** *85*, 2-9.

89. KEBARLE, P.; TANG, L., From Ions in Solution to Ions in the Gas Phase - The Mechanism of Electrospray Mass Spectrometry. *Analytical Chemistry* **1993,** *65* (22), 972A-986A.

90. WILM, M.; MANN, M., Analytical properties of the nanoelectrospray ion source. *Analytical Chemistry* **1996,** *68* (1), 1-8.

91. CHOWDHURY, S. K.; KATTE, V.; CHAIT, B. T., Probing Conformational Changes in Proteins by Mass Spectrometry. *Journal of the American Chemical Society* **1990,** *112*, 9012-9013.

92. SMITH, D. P.; KNAPMAN, T. W.; CAMPUZANO, I.; MALHAM, R. W.; BERRYMAN, J. T.; RADFORD, S. E.; ASHCROFT, A. E., Deciphering drift time measurements from travelling wave ion mobility spectrometry-mass spectrometry studies. *European Journal of Mass Spectrometry* **2009,** *15* (2), 113-130.

93. UETRECHT, C.; ROSE, R. J.; VAN DUIJN, E.; LORENZEN, K.; HECK, A. J. R., Ion mobility mass spectrometry of proteins and protein assemblies. *Chemical Society Reviews* **2010,** *39* (5), 1633-1655.

94. SEO, J.; HOFFMANN, W.; WARNKE, S.; BOWERS, M. T.; PAGEL, K.; VON HELDEN, G., Retention of Native Protein Structures in the Absence of Solvent: A Coupled Ion Mobility and Spectroscopic Study. *Angew Chem Int Ed Engl* **2016,** *55* (45), 14173-14176.

95. SEO, J.; HOFFMANN, W.; WARNKE, S.; HUANG, X.; GEWINNER, S.; SCHÖLLKOPF, W.; BOWERS, M. T.; VON HELDEN, G.; PAGEL, K., An infrared spectroscopy approach to follow β-sheet formation in peptide amyloid assemblies. *Nat Chem* **2016,** *advance online publication*.

96. SIUZDAK, G.; BOTHNER, B.; YEAGER, M.; BRUGIDOU, C.; FAUQUET, C. M.; HOEY, K.; CHANG, C. M., Mass spectrometry and viral analysis. *Chem Biol* **1996,** *3* (1), 45-48.

97. WILEY, W. C.; MCLAREN, I. H., Time-of-Flight Mass Spectrometer with Improved Resolution. *Review of Scientific Instruments* **1955,** *26* (12), 1150-1150.

98. VESTAL, M. L.; JUHASZ, P.; MARTIN, S. A., Delayed Extraction Matrix-Assisted Laser-Desorption Time-of-Flight Mass-Spectrometry. *Rapid Communications in Mass Spectrometry* **1995,** *9* (11), 1044-1050.

99. MAMYRIN, B. A., Laser assisted reflectron time-of-flight mass spectrometry. *International Journal of Mass Spectrometry and Ion Processes* **1994,** *131*, 1-19.

100. DODONOV, A.; KOZLOVSKI, V.; SOULIMENKOV, I.; RAZNIKOV, V.; LOBODA, A.; ZHEN, Z.; HORWATH, T.; WOLLNIK, H., High-resolution electrospray ionization orthogonal-injection time- of-flight mass spectrometer. *European Journal of Mass Spectrometry* **2000,** *6* (1), 481-481.

101. PAUL, W.; STEINWEDEL, H., *Ein Neues Massenspektrometer Ohne Magnetfeld. *Zeitschrift Fur Naturforschung Section a-a Journal of Physical Sciences* **1953,** *8* (7), 448-450.

102. MILLER, P. E.; DENTON, M. B., The quadrupole mass filter: Basic operating concepts. *Journal of Chemical Education* **1986,** *63* (7), 617-622.

103. CECH, N. B.; ENKE, C. G., Practical implications of some recent studies in electrospray ionization fundamentals. *Mass Spectrometry Reviews* **2002,** *20* (6), 362-387.

104. KOPPENAAL, D. W.; BARINAGA, C. J.; DENTON, M. B.; SPERLINE, R. P.; HIEFTJE, G. M.; SCHILLING, G. D.; ANDRADE, F. J.; BARNES, J. H., MS detectors. *Analytical Chemistry* **2005,** *77* (21), 418-427.

105. SHVARTSBURG, A. A.; SMITH, R. D., Fundamentals of traveling wave ion mobility spectrometry. *Analytical Chemistry* **2008,** *80* (24), 9689-9699.

106. BUSH, M. F.; HALL, Z.; GILES, K.; HOYES, J.; ROBINSON, C. V.; RUOTOLO, B. T., Collision cross sections of proteins and their complexes: a calibration framework and database for gas-phase structural biology. *Analytical Chemistry* **2010,** *82* (22), 9557-9565.

107. KANU, A. B.; DWIVEDI, P.; TAM, M.; MATZ, L.; JR, H. H. H., Ion mobility–mass spectrometry. *Journal of Mass Spectrometry* **2008,** *43*, 1-22.

108. CLEMMER, D. E.; HUDGINS, R. R.; JARROLD, M. F., Naked Protein Conformations - Cytochrome-C in the Gas-Phase. *Journal of the American Chemical Society* **1995,** *117* (40), 10141-10142.

109. GILES, K.; PRINGLE, S. D.; WORTHINGTON, K. R.; LITTLE, D.; WILDGOOSE, J. L.; BATEMAN, R. H., Applications of a travelling wave-based radio-frequency-only stacked ring ion guide. *Rapid Communications in Mass Spectrometry* **2004,** *18* (20), 2401-2414.

110. PRINGLE, S. D.; GILES, K.; WILDGOOSE, J. L.; WILLIAMS, J. P.; SLADE, S. E.; THALASSINOS, K.; BATEMAN, R. H.; BOWERS, M. T.; SCRIVENS, J. H., An investigation of the mobility separation of some peptide and protein ions using a new hybrid quadrupole/travelling wave IMS/oa-ToF instrument. *International Journal of Mass Spectrometry* **2007,** *261* (1), 1-12.

111. RUOTOLO, B. T.; BENESCH, J. L. P.; SANDERCOCK, A. M.; HYUNG, S.-J.; ROBINSON, C. V., Ion mobility-mass spectrometry analysis of large protein complexes. *Nature Protocols* **2008,** *3* (7), 1139-1152.

112. BLEIHOLDER, C.; WYTTENBACH, T.; BOWERS, M. T., A novel projection approximation algorithm for the fast and accurate computation of molecular collision cross sections (I). Method. *International Journal of Mass Spectrometry* **2011,** *308* (1), 1-10.

113. MESLEH, M. F.; HUNTER, J. M.; SHVARTSBURG, A. A.; SCHATZ, G. C.; JARROLD, M. F., Structural Information from Ion Mobility Measurements: Effects of the Long-Range Potential. *Journal of Physical Chemistry* **1996,** *3654* (96), 16082-16086.

114. SHVARTSBURG, A. A.; JARROLD, M. F., An exact hard-spheres scattering model for the mobilities of polyatomic ions. *Chemical Physical Letters* **1996,** *261*, 86-91.

115. WYTTENBACH, T.; VON HELDEN, G.; BATKA, J. J.; CARLAT, D.; BOWERS, M. T., Effect of the long-range potential on ion mobility measurements. *Journal of the American Society for Mass Spectrometry* **1997,** *8* (3), 275-282.

116. HOPFGARTNER, G.; HUSSER, C.; ZELL, M., Rapid screening and characterization of drug metabolites using a new quadrupole-linear ion trap mass spectrometer. *Journal of Mass Spectrometry* **2003,** *38* (2), 138-150.

117. MANN, M.; HENDRICKSON, R. C.; PANDEY, A., Analysis of proteins and proteomes by mass spectrometry. *Annual Review of Biochemistry* **2001,** *70*, 437-473.

118. BORYSIK, A. J.; HEWITT, D. J.; ROBINSON, C. V., Detergent release prolongs the lifetime of native-like membrane protein conformations in the gas-phase. *Journal of the American Chemical Society* **2013,** *135* (16), 6078-6083.

119. STEEN, H.; KUSTER, B.; MANN, M., Quadrupole time-of-flight versus triple-quadrupole mass spectrometry for the determination of phosphopeptides by precursor ion scanning. *Journal of Mass Spectrometry* **2001,** *36* (7), 782-790.

120. LANGE, V.; PICOTTI, P.; DOMON, B.; AEBERSOLD, R., Selected reaction monitoring for quantitative proteomics: a tutorial. *Molecular Systems Biology* **2008,** *4*.

121. YOST, R. A.; ENKE, C. G., Triple Quadrupole Mass-Spectrometry for Direct Mixture Analysis and Structure Elucidation. *Analytical Chemistry* **1979,** *51* (12), 1251-&.

122. YOST, R. A.; ENKE, C. G., Direct Mixture Analysis by Triple Quadrupole Mass-Spectrometry. *Abstracts of Papers of the American Chemical Society* **1979,** (Sep), 98-98.

123. HAN, X. M.; ASLANIAN, A.; YATES, J. R., Mass spectrometry for proteomics. *Current Opinion in Chemical Biology* **2008,** *12* (5), 483-490.

124. WYSOCKI, V. H.; RESING, K. A.; ZHANG, Q. F.; CHENG, G. L., Mass spectrometry of peptides and proteins. *Methods* **2005,** *35* (3), 211-222.

125. ZHANG, Y. Y.; FONSLOW, B. R.; SHAN, B.; BAEK, M. C.; YATES, J. R., Protein Analysis by Shotgun/Bottom-up Proteomics. *Chemical Reviews* **2013,** *113* (4), 2343-2394.

126. ZHONG, Y.; HAN, L.; RUOTOLO, B. T., Collisional and Coulombic Unfolding of Gas-Phase Proteins: High Correlation to Their Domain Structures in Solution. *Angewandte Chemie (International ed. in English)* **2014**, 1-5.

127. VERSLUIS, C.; HECK, A. J. R., Gas-phase dissociation of hemoglobin. *International Journal of Mass Spectrometry* **2001,** *210-211*, 637-649.

128. STEEN, H.; KUSTER, B.; FERNANDEZ, M.; PANDEY, A.; MANN, M., Detection of tyrosine phosphorylated peptides by precursor ion scanning quadrupole TOF mass spectrometry in positive ion mode. *Analytical Chemistry* **2001,** *73* (7), 1440-1448.

129. FERGUSON, P. L.; PAN, J.; WILSON, D. J.; DEMPSEY, B.; LAJOIE, G.; SHILTON, B.; KONERMANN, L., Hydrogen/deuterium scrambling during quadrupole time-of-flight MS/MS analysis of a zinc-binding protein domain. *Analytical Chemistry* **2007,** *79* (1), 153-160.

130. JORGENSEN, T. J. D., Collisional Activation by MALDI Tandem Time-of-flight Mass Spectrometry Induces Intramolecular Migration of Amide Hydrogens in Protonated Peptides. *Molecular & Cellular Proteomics* **2005,** *4* (12), 1910-1919.

131. HO, C.; YIN, S.; PENG, I.; LOO, J. A.; BEAUCHAMP, J. L., Investigation of the mechanism of electron capture and electron transfer dissociation of peptides with a covalently attached free radical hydrogen atom scavenger. *International Journal of Mass Spectrometry* **2015,** *390*, 49-55.

132. SOHN, C. H.; CHUNG, C. K.; YIN, S.; RAMACHANDRAN, P.; JOSEPH, A., Probing the Mechanism of Electron Capture and Electron Transfer Dissociation Using Tags with Variable Electron Affinity. *Journal of the the American Chemical Society* **2009,** *131* (15), 5444-5459.

133. SYKA, J. E.; COON, J. J.; SCHROEDER, M. J.; SHABANOWITZ, J.; HUNT, D. F., Peptide and protein sequence analysis by electron transfer dissociation mass spectrometry. *Proceedings of the National Academy of Sciences of the United States of America* **2004,** *101* (26), 9528-9533.

134. ABZALIMOV, R. R.; KAPLAN, D. A.; EASTERLING, M. L.; KALTASHOV, I. A., Protein conformations can be probed in top-down HDX MS experiments utilizing electron transfer dissociation of protein ions without hydrogen scrambling. *Journal of the American Society for Mass Spectrometry* **2010,** *20* (8), 1514-1517.

135. KONIJNENBERG, A.; BANNWARTH, L.; YILMAZ, D.; KOÇER, A.; VENIEN-BRYAN, C.; SOBOTT, F., Top-down mass spectrometry of intact membrane protein complexes reveals oligomeric state and sequence information in a single experiment. *Protein Science* **2015,** *24* (8), 1292-1300.

136. ZHANG, H.; CUI, W.; GROSS, M. L., Mass spectrometry for the biophysical characterization of therapeutic monoclonal antibodies. *FEBS Letters* **2014,** *588* (2), 308-317.

137. SOBOTT, F.; WATT, S. J.; SMITH, J.; EDELMANN, M. J.; KRAMER, H. B.; KESSLER, B. M., Comparison of CID versus ETD based MS/MS fragmentation for the analysis of protein ubiquitination. *Journal of the American Society for Mass Spectrometry* **2009,** *20* (9), 1652-1659.

138. RAND, K. D.; ZEHL, M.; JENSEN, O. N.; JØRGENSEN, T. J. D.; M, D.-O., ac research Protein Hydrogen Exchange Measured at Single-Residue Resolution by Electron Transfer Dissociation Mass Spectrometry. *Analytical Chemistry* **2009,** *81* (14), 5577-5584.

139. KAN, Z.-Y.; WALTERS, B. T.; MAYNE, L.; ENGLANDER, S. W., Protein hydrogen exchange at residue resolution by proteolytic fragmentation mass spectrometry analysis. *Proceedings of the National Academy of Sciences of the United States of America* **2013,** *110* (41), 16438-16443.

140. BARRERA, N. P.; DI BARTOLO, N.; BOOTH, P. J.; ROBINSON, C. V., Micelles protect membrane complexes from solution to vacuum. *Science* **2008,** *321*, 243-246.

141. LAGANOWSKY, A.; READING, E.; HOPPER, J. T. S.; ROBINSON, C. V., Mass spectrometry of intact membrane protein complexes. *Nature Protocols* **2013,** *8* (4), 639-651.

142. MORGNER, N.; MONTENEGRO, F.; BARRERA, N. P.; ROBINSON, C. V., Mass spectrometry--from peripheral proteins to membrane motors. *Journal of Molecular Biology* **2012,** *423* (1), 1-13.

143. BOHRER, B. C.; MERENBLOOM, S. I.; KOENIGER, S. L.; HILDERBRAND, A. E.; CLEMMER, D. E., Biomolecule analysis by ion mobility spectrometry. *Annual Review of Analytical Chemistry* **2008,** *1*, 293-327.

144. KONIJNENBERG, A.; BUTTERER, A.; SOBOTT, F., Native ion mobility-mass spectrometry and related methods in structural biology. *Biochimica et Biophysica Acta (BBA)* **2012**.

145. MARCOUX, J.; WANG, S. C.; POLITIS, A.; READING, E.; MA, J.; BIGGIN, P. C.; ZHOU, M., Mass spectrometry reveals synergistic effects of nucleotides , lipids , and drugs binding to a multidrug resistance efflux pump. *Proceedings of the National Academy of Sciences of the United States of America* **2013,** *110* (24), 9704-9709.

146. ILAG, L. L.; UBARRETXENA-BELANDIA, I.; TATE, C. G.; ROBINSON, C. V., Drug binding revealed by tandem mass spectrometry of a protein-micelle complex. *Journal of the American Chemical Society* **2004,** *126* (44), 14362-14363.

147. BARRERA, N. P.; ROBINSON, C. V., Advances in the mass spectrometry of membrane proteins: from individual proteins to intact complexes. *Annual Review of Biochemistry* **2011,** *80*, 247-271.

148. LENGQVIST, J.; SVENSSON, R.; EVERGREN, E.; MORGENSTERN, R.; GRIFFITHS, W. J., Observation of an intact noncovalent homotrimer of detergent-solubilized rat microsomal glutathione transferase-1 by electrospray mass spectrometry. *Journal of Biological Chemistry* **2004,** *279* (14), 13311-13316.

149. BARRERA, N. P.; ISAACSON, S. C.; ZHOU, M.; BAVRO, V. N.; WELCH, A.; SCHAEDLER, T. A.; SEEGER, M. A.; MIGUEL, R. N.; KORKHOV, V. M.; VAN VEEN, H. W.; VENTER, H.; WALMSLEY, A. R.; TATE, C. G.; ROBINSON, C. V., Mass spectrometry of membrane transporters reveals subunit stoichiometry and interactions. *Nature Methods* **2009,** *6* (8), 585-587.

150. WANG, S. C.; POLITIS, A.; DI BARTOLO, N.; BAVRO, V. N.; TUCKER, S. J.; BOOTH, P. J.; BARRERA, N. P.; ROBINSON, C. V., Ion mobility mass spectrometry of two tetrameric membrane protein complexes reveals compact structures and

differences in stability and packing. *Journal of the American Chemical Society* **2010,** *132* (44), 15468-15470.

151. KONIJNENBERG, A.; YILMAZ, D.; INGÓLFSSON, H. I.; DIMITROVA, A.; MARRINK, S. J.; LI, Z.; VÉNIEN-BRYAN, C.; SOBOTT, F.; KOÇER, A., Global structural changes of an ion channel during its gating are followed by ion mobility mass spectrometry. *Proceedings of the National Academy of Sciences of the United States of America* **2014,** *111* (48), 17170-17175.

152. GAULT, J.; DONLAN, J. A. C.; LIKO, I.; HOPPER, J. T. S.; GUPTA, K.; HOUSDEN, N. G.; STRUWE, W. B.; MARTY, M. T.; MIZE, T.; BECHARA, C.; ZHU, Y.; WU, B.; KLEANTHOUS, C.; BELOV, M.; DAMOC, E.; MAKAROV, A.; ROBINSON, C. V., High-resolution mass spectrometry of small molecules bound to membrane proteins. *Nature Methods* **2016**, 1-9.

153. LAGANOWSKY, A.; READING, E.; ALLISON, T. M.; ULMSCHNEIDER, M. B.; DEGIACOMI, M. T.; BALDWIN, A. J.; ROBINSON, C. V., Membrane proteins bind lipids selectively to modulate their structure and function. *Nature* **2014,** *510* (7503), 172-175.

154. MARCOUX, J.; ROBINSON, C. V., Twenty years of gas phase structural biology. *Structure* **2013,** *21* (9), 1541-1550.

155. BECHARA, C.; ROBINSON, C. V., Different Modes of Lipid Binding to Membrane Proteins Probed by Mass Spectrometry. *Journal of the American Chemical Society* **2015**.

156. READING, E.; LIKO, I.; ALLISON, T. M.; BENESCH, J. L. P.; LAGANOWSKY, A.; ROBINSON, C. V., The Role of the Detergent Micelle in Preserving the Structure of Membrane Proteins in the Gas Phase. *Angewandte Chemie (International ed. in English)* **2015**, 1-6.

157. READING, E.; WALTON, T. A.; LIKO, I.; MARTY, M. T.; LAGANOWSKY, A.; REES, D. C.; ROBINSON, C. V., The Effect of Detergent, Temperature, and Lipid on the Oligomeric State of MscL Constructs: Insights from Mass Spectrometry. *Chemistry and Biology* **2015,** *22* (5), 593-603.

158. ROUSE, SARAH L.; MARCOUX, J.; ROBINSON, CAROL V.; SANSOM, MARK S. P., Dodecyl Maltoside Protects Membrane Proteins In Vacuo. *Biophysical Journal* **2013,** *105* (3), 648-656.

159. HOPPER, J. T. S.; YU, Y. T.-C.; LI, D.; RAYMOND, A.; BOSTOCK, M.; LIKO, I.; MIKHAILOV, V.; LAGANOWSKY, A.; BENESCH, J. L. P.; CAFFREY, M.; NIETLISPACH, D.; ROBINSON, C. V., Detergent-free mass spectrometry of membrane protein complexes. *Nature Methods* **2013**, 1-6.

160. HEALTHCARE, G., *Hydrophobic Interaction Chromatography and Reverse Phase Chromatography - Principles and methods*. 2006.

161. SCHMIDT, A.; GEHLENBORG, N.; BODENMILLER, B.; MUELLER, L. N.; CAMPBELL, D.; MUELLER, M.; AEBERSOLD, R.; DOMON, B., An Integrated, Directed Mass Spectrometric Approach for In-depth Characterization of Complex Peptide Mixtures. *Molecular & Cellular Proteomics* **2008,** *7* (11), 2138-2150.

162. PLUMB, R. S.; JOHNSON, K. A.; RAINVILLE, P.; SMITH, B. W.; WILSON, I. D.; CASTRO-PEREZ, J. M.; NICHOLSON, J. K., UPLC/MSE; a new approach for

generating molecular fragment information for biomarker structure elucidation (vol 20, pg 1989, 2006). *Rapid Communications in Mass Spectrometry* **2006,** *20* (14), 2234-2234.

163. GAU, B. C.; CHEN, J.; GROSS, M. L., Fast photochemical oxidation of proteins for comparing solvent-accessibility changes accompanying protein folding: data processing and application to barstar. *Biochimica et Biophysica Acta (BBA)* **2013,** *1834* (6), 1230-1238.

164. GAU, B. C.; SHARP, J. S.; REMPEL, D. L.; GROSS, M. L., Fast photochemical oxidation of protein footprints faster than protein unfolding. *Analytical Chemistry* **2009,** *81* (16), 6563-6571.

165. XU, G.; CHANCE, M. R., Hydroxyl radical-mediated modification of proteins as probes for structural proteomics. *Chemical Reviews* **2007,** *107* (8), 3514-3543.

166. HAMBLY, D. M.; GROSS, M. L., Laser flash photolysis of hydrogen peroxide to oxidize protein solvent-accessible residues on the microsecond timescale. *Journal of the American Society for Mass Spectrometry* **2005,** *16* (12), 2057-2063.

167. JONES, L. M.; B SPERRY, J.; A CARROLL, J.; GROSS, M. L., Fast photochemical oxidation of proteins for epitope mapping. *Analytical Chemistry* **2011,** *83* (20), 7657-7661.

168. ZHANG, Y.; REMPEL, D. L.; ZHANG, H.; GROSS, M. L., An Improved Fast Photochemical Oxidation of Proteins (FPOP) Platform for Protein Therapeutics. *Journal of the American Society for Mass Spectrometry* **2015,** *26* (3), 526-529.

169. CALABRESE, A. N.; AULT, J. R.; RADFORD, S. E.; ASHCROFT, A. E., Using hydroxyl radical footprinting to explore the free energy landscape of protein folding. *Methods* **2015,** *89*, 38-44.

170. NIU, B.; ZHANG, H.; GIBLIN, D.; REMPEL, D. L.; GROSS, M. L., Dosimetry determines the initial OH radical concentration in fast photochemical oxidation of proteins (FPOP). *Journal of the American Society for Mass Spectrometry* **2015,** *26* (5), 843-846.

171. VAHIDI, S.; KONERMANN, L., Probing the Time Scale of FPOP (Fast Photochemical Oxidation of Proteins): Radical Reactions Extend Over Tens of Milliseconds. *Journal of the American Society for Mass Spectrometry* **2016,** *27* (7), 1156-1164.

172. ESPINO, J. A.; MALI, V. S.; JONES, L. M., In Cell Footprinting Coupled with Mass Spectrometry for the Structural Analysis of Proteins in Live Cells. *Analytical Chemistry* **2015,** *87* (15), 7971-7978.

173. WU, L.; LAPIDUS, L. J., Combining ultrarapid mixing with photochemical oxidation to probe protein folding. *Analytical Chemistry* **2013,** *85* (10), 4920-4924.

174. FARROKHI, V.; BAJRAMI, B.; NEMATI, R.; MCSHANE, A. J.; RUECKERT, F.; WELLS, B.; YAO, X., Development of Structural Marker Peptides for Cystic Fibrosis Transmembrane Conductance Regulator in Cell Plasma Membrane by Reversed-Footprinting Mass Spectrometry. *Analytical Chemistry* **2015,** *87* (17), 8603-8607.

175. YAN, Y.; CHEN, G.; WEI, H.; HUANG, R. Y. C.; MO, J.; REMPEL, D. L.; TYMIAK, A. A.; GROSS, M. L., Fast photochemical oxidation of proteins (FPOP) maps the epitope

of EGFR binding to adnectin. *Journal of the American Society for Mass Spectrometry* **2014,** *25* (12), 2084-2092.

176. HEINKEL, F.; GSPONER, J. R., Determination of Protein Folding Intermediate Structures Consistent with Data from Oxidative Footprinting Mass Spectrometry. *Journal of Molecular Biology* **2016,** *428* (2), 365-371.

177. PAN, Y.; BROWN, L.; KONERMANN, L., Mapping the structure of an integral membrane protein under semi-denaturing conditions by laser-induced oxidative labeling and mass spectrometry. *Journal of Molecular Biology* **2009,** *394* (5), 968-981.

178. PAN, Y.; PIYADASA, H.; O'NEIL, J. D.; KONERMANN, L., Conformational dynamics of a membrane transport protein probed by H/D exchange and covalent labeling: the glycerol facilitator. *Journal of Molecular Biology* **2012,** *416* (3), 400-413.

179. PAN, Y.; BROWN, L.; KONERMANN, L., Site-directed mutagenesis combined with oxidative methionine labeling for probing structural transitions of a membrane protein by mass spectrometry. *Journal of the American Society for Mass Spectrometry* **2010,** *21* (11), 1947-1956.

180. LU, Y.; ZHANG, H.; NIEDZWIEDZKI, D. M.; JIANG, J.; BLANKENSHIP, R. E.; GROSS, M. L., Fast photochemical oxidation of proteins (FPOP) maps the topology of intrinsic membrane proteins: light-harvesting complex 2 (LH2) in a Nanodisc. *Analytical Chemistry* **2016**.

181. HOOFNAGLE, A. N.; RESING, K. A.; AHN, N. G., Protein analysis by hydrogen exchange mass spectrometry. *Annual Review of Biophysics and Biomolecular Structure* **2003,** *32*, 1-25.

182. KONERMANN, L.; PAN, J.; LIU, Y. H., Hydrogen exchange mass spectrometry for studying protein structure and dynamics. *Chemical Society Reviews* **2011,** *40* (3), 1224-1234.

183. WALES, T. E.; ENGEN, J. R., Hydrogen exchange mass spectrometry for the analysis of protein dynamics. *Mass Spectrometry Reviews* **2006,** *25* (1), 158-170.

184. KATTA, V.; CHAIT, B. T., Hydrogen-Deuterium Exchange Electrospray-Ionization Mass-Spectrometry - a Method for Probing Protein Conformational-Changes in Solution. *Journal of the American Chemical Society* **1993,** *115* (14), 6317-6321.

185. ENGLANDER, S. W.; SOSNICK, T. R.; ENGLANDER, J. J.; MAYNE, L., Mechanisms and uses of hydrogen exchange. *Current Opinion in Structural Biology* **1996,** *6* (1), 18-23.

186. KONERMANN, L.; SIMMONS, D. A., Protein-folding kinetics and mechanisms studied by pulse-labeling and mass spectrometry. *Mass Spectrometry Reviews* **2003,** *22* (1), 1-26.

187. CHALLIS, B. C.; LONG, F. A., Acid- and Base-Catalyzed Hydrogen Exchange in Methyl-Substituted Indoles. *Journal of the American Chemical Society* **1963,** *85* (16), 2524-&.

188. VANWIJNE.WT; VANWIJNE.M; STEINBER.H; DEBOER, T. J., Base Catalysed Hydrogen Exchange in Cyclopropylcyanide. *Tetrahedron* **1967,** *23* (9), 3763-&.

189. BAI, Y.; MILNE, J. S.; MAYNE, L.; ENGLANDER, S. W., Primary structure effects on peptide group hydrogen exchange. *Proteins* **1993,** *17* (2), 75-86.

190. MOLDAY, R. S.; ENGLANDER, S. W.; KALLEN, R. G., Primary structure effects on peptide group hydrogen exchange. *Biochemistry* **1972,** *11* (2), 150-158.

191. MOLDAY, R. S.; KALLEN, R. G., Substituent effects on amide hydrogen exchange rates in aqueous solution. *Journal of the American Chemical Society* **1972,** (14), 6739-6745.

192. WALTERS, B. T.; RICCIUTI, A.; MAYNE, L.; ENGLANDER, S. W., Minimizing Back Exchange in the Hydrogen Exchange-Mass Spectrometry Experiment. *Journal of the American Society for Mass Spectrometry* **2012,** *23* (12), 2132-2139.

193. PAN, Y.; BROWN, L.; KONERMANN, L., Hydrogen exchange mass spectrometry of bacteriorhodopsin reveals light-induced changes in the structural dynamics of a biomolecular machine. *Journal of the American Chemical Society* **2011,** *133* (50), 20237-20244.

194. MEHMOOD, S.; DOMENE, C.; FOREST, E.; JAULT, J.-M., Dynamics of a bacterial multidrug ABC transporter in the inward- and outward-facing conformations. *Proceedings of the National Academy of Sciences of the United States of America* **2012,** *109* (27), 10832-10836.

195. LI, J.; RODNIN, M. V.; LADOKHIN, A. S.; GROSS, M. L., Hydrogen-deuterium exchange and mass spectrometry reveal the pH-dependent conformational changes of diphtheria toxin T domain. *Biochemistry* **2014,** *53* (43), 6849-6856.

196. LODOWSKI, D. T.; PALCZEWSKI, K.; MIYAGI, M., Conformational changes in the g protein-coupled receptor rhodopsin revealed by histidine hydrogen-deuterium exchange. *Biochemistry* **2010,** *49* (44), 9425-9427.

197. REY, M.; MAN, P.; CLEMENCON, B.; TREZEGUET, V.; BRANDOLIN, G.; FOREST, E.; PELOSI, L., Conformational dynamics of the bovine mitochondrial ADP/ATP carrier isoform 1 revealed by hydrogen/deuterium exchange coupled to mass spectrometry. *Journal of Biological Chemistry* **2010,** *285* (45), 34981-34990.

198. REY, M.; FOREST, E.; PELOSI, L., Exploring the conformational dynamics of the bovine ADP/ATP carrier in mitochondria. *Biochemistry* **2012,** *51* (48), 9727-9735.

199. ZHANG, X.; CHIEN, E. Y. T.; CHALMERS, M. J.; PASCAL, B. D.; GATCHALIAN, J.; STEVENS, R. C.; GRIFFIN, P. R., Dynamics of the beta2-adrenergic G-protein coupled receptor revealed by hydrogen-deuterium exchange. *Analytical Chemistry* **2010,** *82* (3), 1100-1118.

200. KHANAL, A.; PAN, Y.; BROWN, L. S.; KONERMANN, L., Pulsed hydrogen/deuterium exchange mass spectrometry for time-resolved membrane protein folding studies. *Journal of Mass Spectrometry* **2012,** *47* (12), 1620-1626.

201. HUYSMANS, G. H. M.; RADFORD, S. E.; BALDWIN, S. A.; BROCKWELL, D. J., Malleability of the folding mechanism of the outer membrane protein PagP: parallel pathways and the effect of membrane elasticity. *Journal of Molecular Biology* **2012,** *416* (3), 453-464.

202. Clemmer Group Cross Sections Database - http://www.indiana.edu/~clemmer/Research/Cross%20Section%20Database/cs_database.php.

203. SHVARTSBURG, A. A.; MASHKEVICH, S. V.; BAKER, E. S.; SMITH, R. D., Optimization of algorithms for ion mobility calculations. *Journal of Physical Chemistry A* **2007,** *111* (10), 2002-2010.

204. MA, B.; ZHANG, K. Z.; HENDRIE, C.; LIANG, C. Z.; LI, M.; DOHERTY-KIRBY, A.; LAJOIE, G., PEAKS: powerful software for peptide de novo sequencing by tandem mass spectrometry. *Rapid Communications in Mass Spectrometry* **2003,** *17* (20), 2337-2342.

205. CONSORTIUM", T. U., UniProt: a hub for protein information. *Nucleic Acids Res* **2014,** *43*, D204-D212.

206. CALABRESE, A. N.; WATKINSON, T. G.; HENDERSON, P. J. F.; RADFORD, S. E.; ASHCROFT, A. E., Amphipols outperform dodecylmaltoside micelles in stabilizing membrane protein structure in the gas phase. *Analytical Chemistry* **2015,** *87* (2), 1118-1126.

207. WATKINSON, T. G.; CALABRESE, A. N.; GIUSTI, F.; ZOONENS, M.; RADFORD, S. E.; ASHCROFT, A. E., Systematic analysis of the use of amphipathic polymers for studies of outer membrane proteins using mass spectrometry. *International Journal of Mass Spectrometry* **2015,** *391*, 54-61.

208. POCANSCHI, C. L.; DAHMANE, T.; GOHON, Y.; RAPPAPORT, F.; APELL, H.-J.; KLEINSCHMIDT, J. H.; POPOT, J.-L., Amphipathic polymers: tools to fold integral membrane proteins to their active form. *Biochemistry* **2006,** *45* (47), 13954-13961.

209. POPOT, J. L.; BERRY, E. A.; CHARVOLIN, D.; CREUZENET, C.; EBEL, C.; ENGELMAN, D. M.; FL**?**TENMEYER, M.; GIUSTI, F.; GOHON, Y.; HERV**?**, P.; HONG, Q.; LAKEY, J. H.; LEONARD, K.; SHUMAN, H. A.; TIMMINS, P.; WARSCHAWSKI, D. E.; ZITO, F.; ZOONENS, M.; PUCCI, B.; TRIBET, C., Amphipols: polymeric surfactants for membrane biology research. *Cellular and Molecular Life Sciences* **2003,** *60* (8), 1559-1574.

210. HERNÁNDEZ, H.; ROBINSON, C. V., Determining the stoichiometry and interactions of macromolecular assemblies from mass spectrometry. *Nature Protocols* **2007,** *2* (3), 715-726.

211. WATKINSON, T. G.; CALABRESE, A. N.; AULT, J. R.; RADFORD, S. E.; ASHCROFT, A. E., FPOP-LC-MS/MS Suggests Differences in Interaction Sites of Amphipols and Detergents with Outer Membrane Proteins. *Journal of the American Society for Mass Spectrometry* **2016**, 35-40.

212. FINDLAY, H. E.; RUTHERFORD, N. G.; HENDERSON, P. J. F.; BOOTH, P. J., Unfolding free energy of a two-domain transmembrane sugar transport protein. *Proceedings of the National Academy of Sciences of the United States of America* **2010,** *107* (43), 18451-18456.

213. VENTER, H.; ASHCROFT, A. E.; KEEN, J. N.; HENDERSON, P. J. F.; HERBERT, R. B., Molecular dissection of membrane-transport proteins: mass spectrometry and sequence determination of the galactose-H+ symport protein, GalP, of

Escherichia coli and quantitative assay of the incorporation of [ring-2-C-13]histidine and (NH3)-N-15. *Biochemical Journal* **2002,** *363*, 243-252.

214. JONES, L. N.; BALDWIN, S. A.; HENDERSON, P. J. F.; ASHCROFT, A. E., Defining topological features of membrane proteins by nanoelectrospray ionisation mass spectrometry. *Rapid Communications in Mass Spectrometry* **2010,** *24* (3), 276-284.

215. SUN, L. F.; ZENG, X.; YAN, C. Y.; SUN, X. Y.; GONG, X. Q.; RAO, Y.; YAN, N. E., Crystal structure of a bacterial homologue of glucose transporters GLUT1-4. *Nature* **2012,** *490* (7420), 361-366.

216. KHAN, M. A.; NEALE, C.; MICHAUX, C.; POMES, R.; PRIVE, G. G.; WOODY, R. W.; BISHOP, R. E., Gauging a hydrocarbon ruler by an intrinsic exciton probe. *Biochemistry* **2007,** *46* (15), 4565-4579.

217. BORYSIK, A. J.; ROBINSON, C. V., The 'sticky business' of cleaning gas-phase membrane proteins: a detergent oriented perspective. *Physical Chemistry Chemical Physics* **2012,** *14* (42), 14439-14449.

218. ZHANG, H.; GAU, B. C.; JONES, L. M.; VIDASKY, I.; GROSS, M. L., Fast Photochemical Oxidation of Proteins (FPOP) for Comparing Structures of Protein/Ligand Complexes: The Calmodulin- peptide Model System. *Analytical Chemistry* **2011,** *83* (1), 311-318.

219. PLUMB, R. S.; JOHNSON, K. A.; RAINVILLE, P.; SMITH, B. W.; WILSON, I. D.; CASTRO-PEREZ, J. M.; NICHOLSON, J. K., UPLC/MSE; a new approach for generating molecular fragment information for biomarker structure elucidation. *Rapid Communications in Mass Spectrometry* **2006,** *20* (13), 1989-1994.

220. MAURYA, S. R.; CHATURVEDI, D.; MAHALAKSHMI, R., Modulating lipid dynamics and membrane fluidity to drive rapid folding of a transmembrane barrel. *Scientific Reports* **2013,** *3* (1989), 1-6.

221. PAN, Y.; KONERMANN, L., Membrane protein structural insights from chemical labeling and mass spectrometry. *The Analyst* **2010,** *135* (6), 1191-1200.

222. HUYSMANS, G. H. M.; BALDWIN, S. A.; BROCKWELL, D. J.; RADFORD, S. E., The transition state for folding of an outer membrane protein. *Proceedings of the National Academy of Sciences of the United States of America* **2010,** *107* (9), 4099-4104.

223. CATOIRE, L. J.; ZOONENS, M.; VAN HEIJENOORT, C.; GIUSTI, F.; GUITTET, E.; POPOT, J. L., Solution NMR mapping of water-accessible residues in the transmembrane beta-barrel of OmpX. *European Biophysics Journal with Biophysics Letters* **2010,** *39* (4), 623-630.

224. ALTHOFF, T.; MILLS, D. J.; POPOT, J.-L.; KÜHLBRANDT, W., Arrangement of electron transport chain components in bovine mitochondrial supercomplex I1III2IV1. *The EMBO Journal* **2011,** *30* (22), 4652-4664.

225. KOSHY, S. S.; EYLES, S. J.; WEIS, R. M.; THOMPSON, L. K., Hydrogen Exchange Mass Spectrometry of Functional Membrane-Bound Chemotaxis Receptor Complexes. *Biochemistry* **2013**.